

Identification of substandard and falsified vaccines using spectroscopic techniques and machine learning algorithms

Megan Watson

A thesis submitted in partial fulfilment of the requirements of Liverpool
John Moores University for the degree of Master of Philosophy

September 2024

Abstract

Covid-19 is a novel coronavirus first noted in 2019. Accumulating over 775 million cases and 7.1 million deaths worldwide, vaccination was presented as the most effective solution for Covid-19 related harm reduction. However, the accelerated development and limited availability of Covid-19 vaccines opened a gap in the market for the emergence of substandard and falsified (SF) vaccines. SF Covid-19 vaccines were seized around the world, with impacts on public health and the economy. Traditional analytical techniques are costly and require specialist training, as well as sophisticated laboratory environments.

This thesis evaluated the application of vibrational spectroscopic techniques, specifically ATR-FTIR, Raman, and SERS, for the rapid, cost-effective, and robust analysis of Covid-19 vaccines and the identification of SF vaccines. The study focused on the use of both laboratory-based and portable handheld instruments, assessing their potential for both laboratory and field-based vaccine authentication.

The ATR-FTIR method was optimised using a Perkin Elmer Spectrum Two FTIR spectrometer with an ATR diamond accessory. It was applied to Covid-19 vaccines, comprising DNA-based, mRNA-based, and live attenuated formulations. The method was effective in characterising vaccine brands, yielding high-quality spectra and achieving excellent results in vaccine identification. Key spectral features, including nucleic acid-specific bands, were identified, allowing for clear discrimination between vaccine brands. A classification model, specifically KNN, achieved 99.7% accuracy in classifying vaccine brands, demonstrating ATR-FTIR's potential for semi-automated vaccine authentication.

Raman and SERS methods were optimised using the Metrohm MIRA XTR DS handheld Raman spectrometer. Despite positive results in vaccine characterisation, the performance of SERS was variable, with lower enhancement factors observed in the final study compared to the pilot study. Vaccine degradation over time and changes in colloidal silver substrates were cited as contributing factors. Nonetheless, classification models achieved 100% accuracy, precision, and recall, indicating strong potential for SF vaccine detection with continued method development.

Raman microscopy, performed using the Horiba XPlora™ PLUS, demonstrated excellent potential for Covid-19 vaccine identification, particularly in samples with minimal fluorescence interference. However, the presence of fluorescence in most spectra limited the method's reliability, highlighting the need for further method optimisation and larger datasets.

Overall, ATR-FTIR was identified as the most robust and effective technique for rapid, non-destructive vaccine analysis, while Raman and SERS showed promise but required further refinement. This research supports the use of ATR-FTIR combined with machine learning as a powerful tool for Covid-19 vaccine authentication and the detection of SF vaccines.

Thesis dedications

First and foremost, I would like to thank my supervisors, Dr Sulaf Assi, Dr Jason Birkett, Dr Iftikhar Khan and Professor Dhiya Al-Jumeily OBE for their ongoing support and encouragement throughout this project. Their expertise and training have expanded my knowledge, developed my skills and improved my confidence overall. In particular, I would like to express my gratitude to my lead supervisor, Sulaf Assi for providing me with exceptional support and guidance throughout this journey, truly exceeding what was expected. I could not imagine undertaking this journey without your guidance and am especially grateful.

I would also like to thank my family, and my partner Sam for their support and generosity over the last few years throughout changes in my circumstances. This challenging journey would not have been possible with your personal support.

Finally, I would like to extend a big thank you to my colleagues Megan Wilson and Dr Matthew Harper for their continued support and advice throughout the project, especially Dr Harper for his invaluable machine-learning insights. It has been a pleasure to work alongside you both.

Acknowledgement

I would like to thank the NHS Central Liverpool Primary Care Network, especially Dr David Lewis, Jackie Szynalski and Cath Kitchen. Also, thanks to Professor Gillian Hutcheon, Dr Alan Simms and Mr Geoff Henshaw for further supporting with facilitating sampling for the study. Thanks to Nour Al-Kak from the Lebanese University for Supporting with assessing Spectral Quality.

Table of Contents

Abstract	2
Thesis dedications.....	4
Acknowledgement.....	5
List of Figures.....	11
List of Tables	21
List of Equations.....	25
1. INTRODUCTION.....	26
1.1 Medicine Counterfeiting	26
1.1.1 Prevalence and profiles of counterfeit medical products	27
1.1.2 Substandard and falsified Covid-19 vaccines.....	31
1.2 Identification by conventional techniques	32
1.2.1 Principles of conventional analytical techniques	33
1.2.2 Authentication by conventional analytical techniques.....	36
1.3 Principles of spectroscopic techniques	37
1.3.1 Principles of attenuated total reflectance-Fourier transform infrared spectroscopy.....	37
1.3.2 Identification of anti-infectives by ATR-FTIR spectroscopy.....	38
1.3.3 Principles of Raman spectroscopy	39
1.3.4 Identification of anti-infectives by Raman spectroscopy.....	44
1.4 Gaps in research	45
1.5 Rationale	45

1.6 Aim and Objectives	47
1.7 Thesis Structure	48
2. AUTHENTICATION OF COVID-19 VACCINES USING PORTABLE ATTENUATED TOTAL REFLECTANCE-FOURIER TRANSFORM INFRARED SPECTROSCOPY	50
2.1 Introduction	50
2.2 Experimental.....	54
2.2.1 Materials.....	54
2.2.2 Instrumentation	57
2.2.3 Methods	57
2.2.4 Spectral Treatment and qualitative analysis	58
2.3 Results and Discussion	66
2.3.1 IR activity of vaccines and their constituents.....	66
2.3.2 Spectral Quality.....	70
2.3.3 Authentication of vaccines by ATR-FTIR spectroscopy	90
2.3.4 Vaccine Classification.....	96
2.4 Conclusion.....	99
3. AUTHENTICATION OF TRADITIONAL AND NOVEL ANTI-INFECTIVES USING HANDHELD SURFACE-ENHANCED RAMAN SPECTROSCOPY.....	101
3.1 Introduction	101
3.2 Experimental.....	103
3.2.1 Materials.....	103

3.2.2 Instrumentation	103
3.2.3 Methods	105
.....	107
3.2.4 Spectral treatment and qualitative analysis	107
3.3 Pilot Study	117
3.3.1 Aim	117
3.3.2. Experimental	117
3.3.3 Results and Discussion	119
3.4 Conclusion of the pilot study	125
3.4 Results and Discussion	125
3.4.1.1 Raman activity of vaccines.....	125
3.4.1.2 Spectral quality.....	139
3.4.1.3 Authentication of Covid-19 vaccines by handheld Raman Spectroscopy	149
3.4.1.4 Vaccine Classification.....	154
3.4.1.5 Conclusion.....	167
4. AUTHENTICATION OF COVID-19 VACCINES USING RAMAN MICROSCOPY	170
4.1 Introduction.....	170
4.2 Experimental.....	173
4.2.1 Materials.....	173
4.2.2 Instrumentation	173

4.2.3 Methods	175
4.2.4 Spectral treatment and qualitative analysis	176
4.3 Results and Discussion	176
4.3.1 Raman activity of vaccines.....	176
4.3.2 Spectral quality.....	188
4.3.3 Authentication of Covid-19 Vaccines by Raman microscopy.....	191
4.4 Conclusion.....	203
CHAPTER 5. CONCLUSIONS AND FUTURE WORK.....	205
5.1 Conclusions	205
5.2 Outcomes of thesis results/contribution to knowledge	211
5.3 Limitations	214
5.4 Further research	215
References.....	217
Appendices	250
Appendix I. Details of Covid-19 vaccine samples obtained for the study (manufacturer redacted)	251
Appendix II. Risk Assessment	455
Appendix III. Standard Operating Procedures.....	477
PerkinElmer Spectrum Two ATR-FTIR spectrometer.....	477
Operating Procedure for Metrohm MIRA XTR DS handheld Raman spectrometer	480

List of Figures

Figure 2.1. PerkinElmer SpectrumTwo FTIR spectrometer equipped with ATR diamond holder	57
Figure 2.2 Mean spectra of a) brand 1 vaccine LJMUCV459 b) brand 2 vaccine LJMUCV367 c) brand 3 vaccine LJMUCV1421 and c) brand 4 vaccine LJMUCV1422 measured using the PerkinElmer Spectrum Two FTIR spectrometer equipped with ATR diamond holder.....	68
Figure 2.3. PC scores plot of Covid-19 Vaccine brands 1 (red), 2 (blue), 3 (green) and 4 (pink) measured using the PerkinElmer SpectrumTwo FTIR spectrometer equipped with ATR diamond holder across a range of 450-4000 cm^{-1}	90
Figure 2.4. PC1 loading plot of vaccine brands 1, 2, 3 and 4 across a wavenumber range of 450-4000 cm^{-1}	91
Figure 2.5 PC2 loading plot of vaccine brands 1, 2, 3 and 4 across a wavenumber range of 450-4000 cm^{-1}	91
Figure 2.6 PC scores plot of Covid-19 Vaccine brands 1 (red), 2 (blue), 3 (green) and 4 (pink) measured using the PerkinElmer SpectrumTwo FTIR spectrometer equipped with ATR diamond holder across a range of 450-1850 cm^{-1}	92
Figure 2.7 PC1 loading plot of vaccine brands 1, 2, 3 and 4 across a wavenumber range of 450-1850 cm^{-1}	93
Figure 2.8 PC scores plot of Covid-19 Vaccine brands 1 (red), 2 (blue), 3 (green) and 4 (pink) measured using the PerkinElmer SpectrumTwo FTIR spectrometer equipped with ATR diamond holder across a range of 2500-4000 cm^{-1}	94
Figure 2.9 PC1 loading plot of vaccine brands 1, 2, 3 and 4 across a wavenumber range of 2500-4000 cm^{-1}	94

Figure 2.10 Confusion matrix for Ensemble subspace K-nearest neighbour classification model 6-fold validation trained using Matlab 2023b classification learner and spectral dataset from vaccine brands 1, 2, 3 and 4	96
Figure 2.11 AUC-ROC curve for the test dataset of Ensemble subspace K-nearest neighbour classification model carried out on vaccine brands 1 (blue), 2 (red), 3 (yellow) and 4 (purple).....	98
Figure 3.1 Metrohm MIRA XTR DS handheld Raman Spectrometer equipped with 785nm laser and orbital raster scattering	104
Figure 3.2 ThermoScientific Silver nanoparticles used for SERS sample formulation	106
Figure 3.3 SERS samples made with 500µl Vaccine, 500µl Silver nanoparticles and 10µl 1M KBr	107
Figure 3.4 Process of hydroxylamine hydrochloride reduced-silver colloid formulation for SERS	118
Figure 3.5 Stacked spectra of DNA based vaccine LJMUCV722 (blue), hydroxylamine reduced-silver colloid (red) and SERS spectra of LJMUCV722 (black) measured using the Metrohm MIRA XTR DS handheld Raman spectrometer equipped with 785nm laser and orbital raster scattering	120
Figure 3.6 Conventional Raman spectra of a) Bovine globulin, b) Calcium phosphate, c) Cholesterol, d) Citric acid, e) DSPC, f) Linoleic acid, g) mPEGDMG2), h) mPEGDTA2K, i) PEG4000, j) Polysorbate80, k) Sodium citrate monobasic, l) and m) Sucrose measured using the Metrohm MIRA XTR DS handheld Raman spectrometer equipped with 785nm laser and orbital raster scattering across a range of 400-2300 cm^{-1}	120

Figure 3.7 Correlation plot of Raman spectra of Bovine globulin (1-3), Calcium phosphate (4-6), Cholesterol (7-9), Citric acid (10-12), DSPC (13-15), Linoleic acid (16-18), mPEGDMG2K (19-21), mPEGDTA2K (22-24), PEG4000 (25-27), Polysorbate80 (28-30), Sodium citrate monobasic (31-33), and Sucrose (34-36) measured using the Metrohm MIRA XTR DS handheld Raman spectrometer equipped with 785nm laser and orbital raster scattering across a range of 400-2300 cm^{-1} 123

Figure 3.8 Correlation plot of Brand 1 vaccine spectra (1-68) measured using the Metrohm MIRA XTR DS handheld Raman spectrometer equipped with 785nm laser and orbital raster scattering across a range of 400-2300 cm^{-1} 124

Figure 3.9 PC Scores plot of all Brand 1 vaccines measured using the Metrohm MIRA XTR DS handheld Raman spectrometer equipped with 785nm laser and orbital raster scattering across a range of 400-2300 cm^{-1} 124

Figure 3.10 Untreated conventional Raman spectra of brand 1 vaccines a) LJMUCV661 b) LJMUCV664 c) LJMUCV665 d) LJMUCV667 measured using the Metrohm MIRA XTR DS handheld Raman spectrometer equipped with orbital raster scattering across 400-2300 cm^{-1} 127

Figure 3.11 Baselined conventional Raman spectra of brand 1 vaccines a) LJMUCV661 b) LJMUCV664 c) LJMUCV665 d) LJMUCV667 measured using the Metrohm MIRA XTR DS handheld Raman spectrometer equipped with orbital raster scattering across 400-2300 cm^{-1} 127

Figure 3.12 Untreated conventional Raman spectra of brand 2 vaccines a) LJMUCV355 b) LJMUCV356 c) LJMUCV357 d) LJMUCV358 measured using the Metrohm MIRA XTR DS handheld Raman spectrometer equipped with orbital raster scattering across 400-2300 cm^{-1}

Figure 3.13 Baselined conventional Raman spectra of brand 2 vaccines a) LJMUCV355 b) LJMUCV356 c) LJMUCV357 d) LJMUCV358 measured using the Metrohm MIRA XTR DS handheld Raman spectrometer equipped with orbital raster scattering across 400-2300 cm^{-1} 129

Figure 3.14 Untreated conventional Raman spectra of brand 3 vaccines a) LJMUCV1400 b) LJMUCV1401 c) LJMUCV1403 d) LJMUCV1404 measured using the Metrohm MIRA XTR DS handheld Raman spectrometer equipped with orbital raster scattering across 400-2300 cm^{-1} 131

Figure 3.15 Baselined conventional Raman spectra of brand 3 vaccines a) LJMUCV1400 b) LJMUCV1401 c) LJMUCV1403 d) LJMUCV1404 measured using the Metrohm MIRA XTR DS handheld Raman spectrometer equipped with orbital raster scattering across 400-2300 cm^{-1} 131

Figure 3.16 Baselined conventional Raman spectra of excipients a) Bovine Globulin b) DHA c) DNA from salmon testes and d) DSPC816_94_4 measured using the Metrohm MIRA XTR DS handheld Raman spectrometer equipped with orbital raster scattering across 400-2300 cm^{-1} 132

Figure 3.17 Baselined conventional Raman spectra of excipients e) HUO f) Linoleic Acid g) mPEG_DMG_2K and h) mPEG_DTA_2K measured using the Metrohm MIRA XTR DS handheld Raman spectrometer equipped with orbital raster scattering across 400-2300 cm^{-1} 132

Figure 3.18 Stacked spectra of vaccine excipients bovine globulin (blue), DHA (orange), DSPC816_94_4 (yellow), HUO (purple), mPEG_DMG_2K (light blue), mPEG_DTA_2K (dark red), brand 1 vaccine LJMUCV661 (bold blue), brand 2 vaccine LJMUCV355 (bold red), and brand 3 vaccine LJMUCV1400 (bold black)..... 133

Figure 3.19 Baseline conventional Raman spectra of purified RNA (black), and DNA from salmon testes measured using the Metrohm MIRA XTR DS handheld Raman spectrometer equipped with orbital raster scattering across 400-2300 cm^{-1} 134

Figure 3.20 Stacked baseline spectra of brand 1 vaccine LJMUCV661 measured as received (black) and with the addition of silver nanoparticles + 1M KBr aggregating agent (red) using the Metrohm MIRA XTR DS handheld Raman spectrometer equipped with orbital raster scattering across 400-2300 cm^{-1} 136

Figure 3.21 Stacked baseline spectra of brand 2 vaccine LJMUCV355 measured as received (black) and with the addition of silver nanoparticles + 1M KBr aggregating agent (red) using the Metrohm MIRA XTR DS handheld Raman spectrometer equipped with orbital raster scattering across 400-2300 cm^{-1} 137

Figure 3.22 Stacked baseline spectra of brand 3 vaccine LJMUCV1374 measured as received (black) and with the addition of silver nanoparticles + 1M KBr aggregating agent (red) using the Metrohm MIRA XTR DS handheld raman spectrometer equipped with orbital raster scattering across 400-2300 cm^{-1} 139

Figure 3.23 2D PC Scores plot of Brand 1 (red), Brand 2 (blue), and Brand 3 (green) vaccines measured using the Metrohm MIRA XTR DS handheld Raman spectrometer equipped with 785nm laser and orbital raster scattering across a range of 400-2300 cm^{-1} 151

Figure 3.24 2D PC Scores plot of Brand 1 (red), Brand 2 (blue), and Brand 3 (green) vaccines measured using the Metrohm MIRA XTR DS handheld Raman spectrometer equipped with 785nm laser and orbital raster scattering across a range of 400-2300 cm^{-1} 151

Figure 3.25 2D PC Scores plot of the SERS Brand 1 (red), Brand 2 (blue), and Brand 3 (green) vaccines measured with the addition of the silver nanoparticles and 1M KBr

aggregating salt using the Metrohm MIRA XTR DS handheld Raman spectrometer equipped with 785nm laser and orbital raster scattering across a range of 400-2300cm⁻¹ 152

Figure 3.26 3D PC Scores plot of the SERS Brand 1 (red), Brand 2 (blue), and Brand 3 (green) vaccines measured with the addition of the silver nanoparticles and 1M KBr aggregating salt using the Metrohm MIRA XTR DS handheld Raman spectrometer equipped with 785nm laser and orbital raster scattering across a range of 400-2300cm⁻¹ 153

Figure 3.27 Confusion matrix for Ensemble subspace K-nearest neighbour classification 10-fold validation model trained using Matlab 2023a classification learner and conventional Raman spectral dataset from vaccine brands 1, 2 and 3 measured using the Metrohm MIRA XTR DS handheld Raman spectrometer..... 157

Figure 3.28 AUC-ROC curve for 10-fold validation of Ensemble subspace K-nearest neighbour classification model carried out on Raman spectral dataset of vaccine brands 1 (blue), 2 (red), and 3 (yellow) measured on the Metrohm MIRA XTR DS handheld Raman spectrometer 158

Figure 3.29 Confusion matrix for ensemble subspace discriminant classification 10-fold validation model trained using Matlab 2023a classification learner and SERS dataset from vaccine brands 1, 2 and 3 measured using the Metrohm MIRA XTR DS handheld Raman spectrometer 162

Figure 3.30 Confusion matrix for linear discriminant classification 10-fold validation model trained using Matlab 2023a classification learner and SERS dataset from vaccine brands 1, 2 and 3 measured using the Metrohm MIRA XTR DS handheld Raman spectrometer..... 163

Figure 3.31 Confusion matrix for weighted KNN classification 10-fold validation model trained using Matlab 2023a classification learner and SERS dataset from vaccine brands 1, 2 and 3 measured using the Metrohm MIRA XTR DS handheld Raman spectrometer	164
Figure 3.32 AUC-ROC curve for 10-fold validation of ensemble subspace discriminant classification model carried out on SERS dataset of vaccine brands 1 (blue), 2 (red), and 3 (yellow) measured on the Metrohm MIRA XTR DS handheld Raman spectrometer	165
Figure 3.33 AUC-ROC curve for 10-fold validation of linear discriminant classification model carried out on SERS dataset of vaccine brands 1 (blue), 2 (red), and 3 (yellow) measured on the Metrohm MIRA XTR DS handheld Raman spectrometer	166
Figure 3.34 AUC-ROC curve for 10-fold validation of linear discriminant classification model carried out on SERS dataset of vaccine brands 1 (blue), 2 (red), and 3 (yellow) measured on the Metrohm MIRA XTR DS handheld Raman spectrometer	167
Figure 4.1 Horiba XploRA™ PLUS equipped with 532 nm laser attached to PC with Horiba's LabSpec 6 V6.6.7.2 spectroscopy suite open	174
Figure 4.2 Conventional Raman spectra of brand 2 vaccine LJMUCV965 measured using the Horiba XploRA™ PLUS Raman microscope equipped with 532 nm laser and x10 objective lens at 600 grating and 10% filter across 25-4000cm ⁻¹	185
Figure 4.3 Conventional Raman spectra of brand 1 vaccine LJMUCV672 measured using the Horiba XploRA™ PLUS Raman microscope equipped with 532 nm laser and x10 objective lens at 600 grating and 10% filter across 25-4000 cm ⁻¹	185
Figure 4.4 Conventional Raman spectra of brand 1 vaccine LJMUCV601 measured using the Horiba XploRA™ PLUS Raman microscope equipped with 532 nm laser and x100 objective lens at 1200 grating and 10% filter across 25-4000 cm ⁻¹	186

Figure 4.5 Conventional Raman spectra of brand 2 vaccine LJMUCV148 measured using the Horiba XploRA™ PLUS Raman microscope equipped with 532 nm laser and x100 objective lens at 1200 grating and 10% filter across 25-4000 cm⁻¹..... 186

Figure 4.6 Stacked spectra of brand 2 vaccine LJMUCV159 measured using conventional Raman (black) and SERS (red) using the Horiba XploRA™ PLUS equipped with 532 nm laser and x100 objective..... 187

Figure 4.7 Stacked spectra of brand 2 vaccine LJMUCV151 measured using conventional Raman (black) and SERS (red) using the Horiba XploRA™ PLUS equipped with 532 nm laser and x100 objective..... 188

Figure 4.8 PC scores plot of conventional Raman vaccine samples measured using the Horiba XploRA™ PLUS Raman microscope-spectrometer equipped with 532 nm laser and x10 objective across 25-4000 cm⁻¹ where PC1 = 98.1% and PC2 = 1.7 % 193

Figure 4.9 PC scores plot with equal frequency ellipsis of conventional Raman vaccine samples measured using the Horiba XploRA™ PLUS Raman microscope-spectrometer equipped with 532 nm laser and x10 objective across 25-4000 cm⁻¹ where PC1 = 98.1% and PC2 = 1.7 % 193

Figure 4.10 PC1 loading graph of conventional Raman vaccine samples measured using the Horiba XploRA™ PLUS Raman microscope-spectrometer equipped with 532 nm laser and x10 objective across 25-4000 cm⁻¹ 194

Figure 4.11 PC2 loading graph of conventional Raman vaccine samples measured using the Horiba XploRA™ PLUS Raman microscope-spectrometer equipped with 532 nm laser and x10 objective across 25-4000 cm⁻¹ 194

Figure 4.12 PC scores plot of conventional Raman vaccine samples measured using the Horiba XploRA™ PLUS Raman microscope-spectrometer equipped with 532 nm

laser and x100 objective across 25-4000 cm^{-1} where PC1 = 77.1% and PC2 = 20.5%	196
Figure 4.13 PC1 loading graph of conventional Raman vaccine samples measured using the Horiba XploRA™ PLUS Raman microscope-spectrometer equipped with 532 nm laser and x100 objective across 25-4000 cm^{-1}	196
Figure 4.14 PC2 loading graph of conventional Raman vaccine samples measured using the Horiba XploRA™ PLUS Raman microscope-spectrometer equipped with 532 nm laser and x100 objective across 25-4000 cm^{-1}	197
Figure 4.15 Microscope image of brand 2 vaccine SERSLJMUCV159 acquired using the Horiba XploRA™ PLUS Raman microscope-spectrometer equipped with 532 nm laser and x10 objective (left) and x100 objective (right)	197
Figure 4.16 Stacked spectra of brand 3 vaccine LJMUCV1390 (blue) and brand 2 vaccine LJMUCV151 (red) measured using the Horiba XploRA™ PLUS Raman microscope-spectrometer equipped with 532 nm laser and x100 objective across 25-4000 cm^{-1}	198
Figure 4.17 PC scores plot of conventional Raman vaccine samples measured using the Horiba XploRA™ PLUS Raman microscope-spectrometer equipped with 532 nm laser and x100 objective, with one sample measured at x10 objective across 25-4000 cm^{-1} where PC1 = 90.2% and PC2 = 9.2%	199
Figure 4.18 PC1 loading graph of conventional Raman vaccine samples measured using the Horiba XploRA™ PLUS Raman microscope-spectrometer equipped with 532 nm laser and x100 objective, with one sample measured at x10 objective across 25-4000 cm^{-1}	199
Figure 4.19 PC2 loading graph of conventional Raman vaccine samples measured using the Horiba XploRA™ PLUS Raman microscope-spectrometer equipped with	

532 nm laser and x100 objective, with one sample measured at x10 objective across 25-4000 cm^{-1} 200

Figure 4.20 CWS of conventional Raman spectra of brand 1 vaccines (1-6) and brand 2 vaccines (7-15) measured using the Horiba XploRA™ PLUS equipped with 532nm laser and x10 objective where dark blue colour represents a minimum r value of 0.75 and a dark yellow colour represents a maximum r value of 0.9999. In between the r values 0.0.77 – 0.82 correspond to light blue colour, r value of 0.83 – 0.87 correspond to cyan colour, 0.88 – 0.92 correspond to green, 0.93 – 0.97 correspond to greenish yellow colour and 0.98 – 0.99 correspond to orange colour. 201

Figure 4.21 CWS of conventional Raman spectra of brand 3 vaccines (1-2), brand 2 vaccines (3-8, 11) and brand 1 vaccine (9-10) measured using the Horiba XploRA™ PLUS equipped with 532nm laser and x100 objective where dark blue colour represents a minimum r value of 0.75 and a dark yellow colour represents a maximum r value of 0.9999. In between the r values 0.0.77 – 0.82 correspond to light blue colour, r value of 0.83 – 0.87 correspond to cyan colour, 0.88 – 0.92 correspond to green, 0.93 – 0.97 correspond to greenish yellow colour and 0.98 – 0.99 correspond to orange colour. 202

List of Tables

Table 1.1 Key differences between reflection and absorption in ATR-FTIR spectroscopy	Error! Bookmark not defined.
Table 2.1. Details of Covid-19 vaccine brands obtained from the NHS Central Liverpool Primary Care Network and Lebanese/Iraqi hospitals for use in this study.....	55
Table 2.2. Details of common vaccine excipients obtained from chemical suppliers for use in the procedure.....	56
Table 2.3. Spectral quality parameters of the vaccine excipients measured using the PerkinElmer SpectrumTwo FTIR spectrometer equipped with ATR diamond holder	66
Table 2.4. Values for spectral quality parameters of average spectra of each brand 1 vaccine measured using the PerkinElmer SpectrumTwo FTIR spectrometer equipped with ATR diamond holder	71
Table 2.5 Values for spectral quality parameters of average spectra of each brand 2 vaccine measured using the PerkinElmer SpectrumTwo FTIR spectrometer equipped with ATR diamond holder	78
Table 2.6. Values for spectral quality parameters of average spectra of each brand 3 vaccine measured using the PerkinElmer SpectrumTwo FTIR spectrometer equipped with ATR diamond holder	86
Table 2.7. Values for spectral quality parameters of average spectra of each brand 4 vaccine measured using the PerkinElmer SpectrumTwo FTIR spectrometer equipped with ATR diamond holder	88
Table 2.8. Accuracy, precision, recall, specificity and F1-score of Ensemble subspace KNN classification model for vaccine brands 1-4 and overall.....	97
Table 3.1. Handheld Raman instrument specifications.....	103

Table 3.2. Custom operating procedures stored on the Metrohm MIRA XTR DS handheld Raman Spectrometer	105
Table 3.3. Model type and hyperparameters of the classification models trained on the conventional Raman spectral dataset using Matlab 2023a classification learner ...	108
Table 3.4 Model type and hyperparameters of the classification models trained on the surface-enhanced Raman spectral dataset using Matlab 2023a classification learner	113
Table 3.5 Values for spectral quality parameters of Brand 1 standard and surface-enhanced average spectra measured using the Metrohm MIRA XTR DS handheld Raman Spectrometer equipped with orbital raster scattering across 400-2300 cm^{-1}	142
Table 3.6 Values for spectral quality parameters of Brand 2 standard and surface-enhanced average spectra measured using the Metrohm MIRA XTR DS handheld Raman Spectrometer equipped with orbital raster scattering across 400-2300 cm^{-1}	144
Table 3.7 Values for spectral quality parameters of Brand 3 standard and surface-enhanced average spectra measured using the Metrohm MIRA XTR DS handheld Raman Spectrometer equipped with orbital raster scattering across 400-2300 cm^{-1}	147
Table 3.8 Average values of spectral quality parameters for standard and surface-enhanced Raman spectra by brand, measured using the Metrohm MIRA XTR DS handheld Raman Spectrometer equipped with orbital raster scattering across a range of 400-2300 cm^{-1}	149

Table 3.9 Model number, type, and accuracy of the validation and test runs for each of the classification models trained on the conventional Raman dataset using Matlab 2023a classification learner tool	154
Table 3.10 Accuracy, precision, recall, specificity and F1-score of Ensemble subspace KNN 10-fold cross validation classification model for vaccine brands 1-3 and overall	158
Table 3.11 Model number, type, and accuracy of the validation and test runs for each of the classification models trained on the SERS dataset using Matlab 2023a classification learner tool	160
Table 4.1 Horiba XploRA™ PLUS specifications from manufacturers website (Horiba Scientific, 2024).....	174
Table 4.2 Measurement parameters of settings groups 1, 2, 3, and 4 for samples measured using the Horiba XploRA™ PLUS	175
Table 4.3 Raman band position, physical origin and literature references for the discernible bands in the conventional Raman spectrum of brand 1 vaccine LJMUCV601 measured using the Horiba XploRA™ PLUS Raman Microscope using the x100 objective	180
Table 4.4 Raman band position, physical origin and literature references for the discernible bands in the conventional Raman spectrum of brand 1 vaccine LJMUCV601 measured using the Horiba XploRA™ PLUS Raman Microscope using the x100 objective	183
Table 4.5 Spectral quality of conventional Raman active vaccines measured using the Horiba XploRA™ PLUS Raman microscope-spectrometer equipped with 532 nm laser	189

Table 4.6 Spectral quality of surface-enhanced Raman active vaccines measured using the Horiba XploRA™ PLUS Raman microscope-spectrometer equipped with 532nm laser	191
---	-----

List of Equations

Equation 2.1 Signal to noise ratio based on absorbance and standard deviation at a maximum peak (Adams, 2007).....	59
Equation 2.2 Correlation coefficient based on momentum product (Brereton, 2006)	59
Equation 2.3 Mathematical equation of PCA (Beattie and Esmonde-White, 2021) ..	61
Equation 2.4 Formula for Euclidean distance between two points p and q in a d-dimensional space (Short and Fukunaga, 1981).....	62
Equation 2.5 Formula for Accuracy calculation from confusion matrix (Agarwal et al., 2021).....	63
Equation 2.6 Formula for Precision calculation from confusion matrix (Davis and Goadrich, 2006)	63
Equation 2.7 Formula for Recall calculation from confusion matrix (Davis and Goadrich, 2006)	64
Equation 2.8 Formula for Specificity calculation from confusion matrix (Davis and Goadrich, 2006)	64
Equation 2.9 Formula for F1 Score calculation from confusion matrix (Agarwal et al., 2021).....	65
Equation 2.10 Calculation of AUC (Rakotomamonjy, 2004)	65

1. INTRODUCTION

1.1 Medicine Counterfeiting

Medicine counterfeiting is a serious global issue requiring urgent attention, driven by sophisticated networks of manufacturing and distribution that are deeply embedded in industrial organised crime. Countries around the world have their own definitions of what constitutes a counterfeit medicine and so there is no global consensus on what the term truly represents. 'Counterfeit' medicines are referred to as a number of adjacent terms by regulatory institutions worldwide, including spurious, substandard, falsified and falsely labelled medicines. This presents difficulties in both the identification of 'counterfeit' medicines, and the prosecution of those responsible for their presence in the global market. The European Medicines Agency (EMA) defines counterfeit medicine as "a medicine made by someone other than the genuine manufacturer, by copying or imitating an original product without authority or rights. Counterfeit medicines infringe trademark law" (European Medicines Agency, 2024). The MHRA describes falsified medicinal products as any medicinal product with a false representation of:

- its identity, including its packaging and labelling, its name or its composition (other than any unintentional quality defect) as regards any of its ingredients including excipients and the strength of those ingredients
- its source, including its manufacturer, its country of manufacturing, its country of origin or its marketing authorisation holder, or
- its history, including the records and documents relating to the distribution channels used (The Human Medicines Regulations, 2013).

The World Health Organisation (WHO) uses the terms substandard and falsified (SF) medicines and defines them as follows:

Substandard – “also called ‘out of specification’, these are authorised medical products that fail to meet either their quality standards or specifications, or both”.

Falsified – “medical products that deliberately/fraudulently misrepresent their identity, composition or source”.

The WHO also refers to unregistered/unlicensed medicines which they define as “medical products that have not undergone evaluation and/or approval by the National or Regional Regulatory Authority for the market in which they are marketed/distributed or used, subject to permitted conditions under national or regional regulation and legislation.” (World Health Organization, 2018)

For continuity, this thesis will refer to any medicinal products that fall into the aforementioned categories under the umbrella term of substandard and falsified, according to the World Health Organisation’s definitions.

1.1.1 Prevalence and profiles of counterfeit medical products

The WHO estimated in 2017 that 10.5% of medicines worldwide are substandard or falsified, this figure increases to 13.6% in LMICs (Ozawa et al., 2018; World Health Organisation, 2017). The fraudulent sales market from Asia to South-East Asia and Africa alone is estimated to be worth \$1.6 billion per year (United Nations Office on Drugs and Crime (UNODC), 2010). In 2012, 64% of anti-malarial medication in Nigeria was substandard and falsified (Economist, 2012).

The circulation of SF medicines has a number of severe implications on not only public health but also on economic growth and engagement in research and development (R&D). The global intellectual property market is valued at over \$180 billion dollars, with the economic value of counterfeiting and piracy estimated at up to \$4.2 trillion in 2022. Intellectual-property intensive industries account for approximately 26% of employment in the EU and supports over 45 million jobs in the U.S. and lost \$225 to \$600 billion annually due to counterfeit goods, according to the United States Chamber of Commerce (Eser, 2024; World Intellectual Property Organisation (WIPO), 2024). Economic loss in intellectual property intensive industries de-incentivises financial investment and engagement in R&D (Blackstone, Fuhr, Jr and Pociask, 2014).

Consumer consumption of substandard and falsified medicines holds dire consequences on public health related to treatment ineffectiveness and adverse effects. This can lead to loss of confidence in medical products, healthcare providers and healthcare systems (World Health Organisation, 2018). SF medical products may contain no active ingredient, the incorrect active ingredient or the correct active ingredient in the wrong concentration or volume. SF medicines can pose a significant threat to public health with some SF medicines found to contain toxic constituents or dangerous levels of Active Pharmaceutical Ingredient (API).

Between November 2008 and February 2009, a total of 84 children in Nigeria died from acute kidney failure as a result of ingesting teething syrup contaminated with diethylene glycol (Akuse et al., 2012). The product was licensed and registered with the Nigerian authority and the contamination was found to originate as a result of deliberate fraud by a chemical supplier in Lagos (Abubukar et al., 2009). This was not the first instance where substandard products instigated a tragedy. A similar incident occurred almost 20 years earlier where 47 children died at Jos University Teaching

Hospital in Nigeria following the ingestion of diethylene glycol adulterated paracetamol syrup between June and September 1990 (Okuonghae et al., 1992).

Falsified medicines are often difficult to detect. They are, by nature, designed to mimic the formulation of the genuine product, meaning SF medical products can go undetected and enter the pharmaceutical supply chain. In 2008, investigation of an outbreak of allergic-like reactions in patients who had received intravenous heparin (a blood thinner) during dialysis revealed that a toxic adulterant called over-sulphated chondroitin sulphate (OSCS) had been introduced during manufacture in China. The chemical structure of OSCS was so closely related to heparin that it had gone undetected before making it to patients (Centers for Disease Control and Prevention (CDC), 2021; Kishimoto et al., 2008; U.S Government Accountability Office, 2022).

Between 2012 and 2013, the FDA announced a total of three times that SF cancer medication bevacizumab (Avastin®, Genentech, USA) had been detected in the United States. The SF medicines allegedly arrived in the United States from overseas suppliers through illegal channels approved for use in Turkey but not the United States. The SF medicines in this latter incident contained none of the API and had been distributed to 48 states (Cuomo and Mackey, 2014; Mackey et al., 2015).

In 2002, criminals in Florida created high dose Epogen and Procrit (injectable anaemia drug) through relabelling 110,000 vials of low-dose Epogen. In this case, SF Epogen had successfully circulated through registered and unregistered brokers before reaching a national wholesaler. Patients suffered severe side-effects and ineffective dosage of life-preserving medicine (Thompson, 2003; Young, 2004).

Numerous preventative measures and global task forces/programmes have been established in recent years in an attempt to mitigate the prevalence and risks

associated with SF medicines worldwide. INTERPOL's Illicit Goods and Global Health Programme (IGGH) involves a collaborative effort from member countries to improve global cooperation and support legal enforcement capabilities in pharmaceutical crime. The programme aims to dismantle criminal networks and reduce risk to public health through:

“Collecting data and disseminating intelligence (e.g. analytical reports and threat assessments);”

“Coordinating transnational law enforcement operations;”

“Supporting multi-agency task forces to improve cooperation between police, customs, regulatory bodies and the private sector;”

“Raising public awareness of pharmaceutical crime and helping consumers to make informed choices.” (INTERPOL, 2022)

Operation Pangea has been tackling the trafficking of SF pharmaceuticals sold online since 2008. It also focuses on raising awareness of consumers of the risks associated with the unregulated purchase of pharmaceuticals online. Operation Pangea XIV facilitated the seizure of an estimated \$23,414,483 worth of illicit pharmaceutical products. 113,020 unregulated pharmaceutical marketing websites were removed (INTERPOL, 2022). Within the framework of operation Pangea, a regional ‘action against tramadol trafficking’ task force was established in 2020 to support investigations between source and destination countries to address tramadol trafficking across Africa (INTERPOL, 2022).

Operation Afya is an INTERPOL-led setup which targets organised crime in the manufacture and distribution of SF medicines in South Africa. INTERPOL's operation Heera aims to control the same across Western-Africa (INTERPOL, 2022).

The Qanoon initiative launched in 2015 aims to respond to the threat posed to public health in the Middle East and North Africa by pharmaceutical crime. Operation Qanoon led to the seizure of 63,418 facemasks in Jordan and 85,000 other Covid-19 related medical products in Qatar in 2020 amidst the ongoing pandemic (INTERPOL, 2022).

Operation Vigilant Interdiction (OVI) was established in 2020 as a response to emerging Covid-19 pandemic-exploiting crimes. Operation Flash – Illicit pharmaceutical products in Africa were found between INTERPOL and AFRIPOL in 2021 to target SF and illicit vaccines and medical products across Africa (INTERPOL, 2022).

1.1.2 Substandard and falsified Covid-19 vaccines

The Covid-19 pandemic instigated an eruption of pandemic-exploiting criminal activity including the production of SF healthcare products such as face masks, disinfectant spray and hand sanitiser. More concerning, with desperation for population immunity increasing and limited production of vaccines, came the emergence of substandard and falsified Covid-19 vaccines into global markets. SF medicines have always posed a threat to public health, and the Covid-19 pandemic brought about a surge in black market vaccine sales. SF covid-19 vaccines of various manufacturers were distributed, seized, or administered to patients in countries around the world, ranging from lower- and middle-income countries (LMICs) to developed countries with well-established governing bodies and regulatory agencies. This issue is particularly prevalent in LMICs where vaccine access is limited and only 4% of the population were fully vaccinated by the end of 2021 (Amnesty International, 2022; Gurgula and McDonagh, 2023).

A dozen people in Mumbai and Kolkata were prosecuted for their involvement in inauthentic “vaccination drives” in May and June of 2021 where around 500 people were administered falsified versions of Covishield (India’s product name for the ChAdOx1 nCoV-19 vaccine) (Mateen, 2021). Over 3000 falsified doses of China’s domestically produced Covid-19 vaccines were seized across the country including Beijing, Shanghai and Shandong in 2021. Falsified vaccines contained no API and vials had been filled with saline solution instead (Reuters, 2021). Falsified versions of the ChAdOx1 nCoV-19 vaccine were reported in Iran where used and discarded vials of the genuine product had been illicitly refilled and returned to the supply chain (World Health Organisation (WHO), 2021). Falsified Pfizer BioNTech vaccines were also identified in Iran where product labels and artwork were inconsistent with the regulated artwork of the genuine product, and expiry date was falsified and inconsistent with the genuine batch number listed on the label (World Health Organisation (WHO), 2021b). Further falsified Pfizer BioNTech vaccines were identified in Poland and Mexico where labels had been falsified and product had been substituted for an anti-wrinkle treatment (BBC News, 2021). SF covid-19 vaccines were also seized in South Africa, Uganda, and Myanmar throughout 2021 (World Health Organisation (WHO), 2021a).

1.2 Identification by conventional techniques

The first step in the detection of SF medicines is examination of physical appearance, primary and secondary packaging and patient information leaflets against genuine regulated artwork. As SF medicines become more sophisticated, chemical analysis must be used to establish the identity of suspected products. This is mostly performed using high-performance liquid chromatography (HPLC), widely regarded as the industry ‘gold standard’ analytical method in pharmaceutical and drug analysis. Less

sophisticated 'in-field' methods such as colorimetry or thin layer chromatography (TLC) have been applied. Advanced laboratory techniques including mass spectrometry and nuclear magnetic resonance (NMR) spectroscopy have also been utilised (Holzgrabe, 2018). These conventional analytical techniques allow quantitative determination of API, excipients and impurities. This facilitates the detection of low-quality medical products, including substandard and falsified medicines.

1.2.1 Principles of conventional analytical techniques

HPLC works by separating compounds based on their distribution between a stationary phase and a mobile phase. The stationary phase consists of small particles packed in a column, which interact with the analytes while they move through the mobile phase, typically a liquid solvent or a mixture. Variations in how strongly the compounds interact with the stationary phase results in different retention times, enabling effective separation. HPLC components include the solvent delivery system; injector; column; detector and data acquisition system. The retention of a drug in a given eluent is expressed by retention time or volume, dependent on flow rate, column length and diameter.

Modern HPLC techniques became available in 1969 but were not widely accepted in the industry until years later (Bidlingmeyer, 1993, pp.1–27). Now that quantitative HPLC instruments are readily available, their commercial uses in pharmaceutical analysis can be fully appreciated. Significant developments have been made in the last decade in terms of chromatographic methods and instrumentation. Improved resolution and separation of complex mixtures has resulted from the use of increased mobile phase temperatures, closely condensed particles (<2 µm) and silica-based

monolithic supports. Liquid chromatography is a popular technique in biological, forensic and pharmaceutical applications due to its resolving power, speed, low detection levels and separation of a wide range of sample types. It is commonly utilised for the characterisation of metabolites, assays of APIs, impurities and excipients, purification of synthetic/natural products and in pharmacokinetic/pharmacodynamic studies. In recent years, HPLC has been developed through high-speed separation, micro-HPLC, automation and hyphenated techniques.

Despite being regarded as the 'gold standard' in pharmaceutical analysis, HPLC has its disadvantages. The equipment and maintenance can be costly, limiting accessibility in some laboratories, especially in LMICs (S. Kulkarni and S. Palled, 2024). The technique is complex and requires specialist training, and method development and optimisation can be time-consuming (Pham-Tuan et al., 2003). The use of solvents holds potential environmental implications (Napolitano-Tabares et al., 2021) and there is potential for contamination if systems are not maintained properly (Yamagaki and Yamazaki, 2020). HPLC is generally unsuitable for samples of a large volume which can restrict its application, and sensitivity to variations in temperature, pressure, or flow rates can impact the reproducibility of results (Barwick, 1999; Mitra, 2003).

TLC is a chromatographic technique used to separate and analyse compounds. The technique uses a thin layer of adsorbent material such as silica gel on an inert surface (e.g. glass/plastic/aluminium) as the stationary phase. Similarly to HPLC, a solvent is used as the mobile phase, moving through the stationary phase via capillary action. Polarity and solubility of the chemical compounds in the sample influences their interaction with both phases as the mobile phase ascends the stationary phase. Compounds with an affinity for the mobile phase travel further than those attracted to the stationary phase. The retention factor (R_f) value represents the ratio of distance

travelled by the compound against the solvent front which is characteristic of a certain compound and can be used for identification (Sherma and Fried, 2003, pp.1–62). TLC is valued for its simplicity, speed and cost-effectiveness. However, TLC is qualitative in nature and does not provide quantitative results unless in conjunction with other techniques. TLC has limited resolution capabilities: the separation seen is less effective than other chromatographic techniques like HPLC, compounds with similar properties may not separate well leading to overlapping spots and misleading results. The technique involves manual spotting which introduces potential for variability and human error, and the process is generally less sensitive than other chromatographic techniques (Poole, 2003).

NMR spectroscopy is a powerful analytical technique used to analyse the properties of chemical compounds and to determine their structure. Certain nuclei, such as hydrogen-1 (^1H) or carbon-13 (^{13}C) possess an intrinsic form of angular momentum called 'spin' which creates a magnetic moment. A strong magnet is used to create a uniform magnetic field, when nuclei are placed in this magnetic field, they align with or against the field, creating different energy states. The application of radiofrequency (RF) radiation to the sample initiates transitions between these energy states (Ionin, 2012, pp.2–7). Different compounds have characteristic frequencies at which these transitions occur. Variations known as 'chemical shifts' are produced dependent on the environment around the nucleus which affects its resonant frequency. These shifts provide information on molecular structure and are measured in parts per million (ppm). The resulting NMR spectrum displays bands corresponding to specific nuclei, which in turn provides information on the chemical structure of the sample of interest (Macomber, 1998; Rule and Hitchens, 2006).

1.2.2 Authentication by conventional analytical techniques

Researchers from the Artemisinin-based Combination Therapy (ACT) Consortium at the London School of Hygiene and Tropical Medicine successfully employed the use of HPLC in a rigorous analysis of antimalarial drug quality conducted in Cambodia and Tanzania (ACT Consortium Drug Quality Project Team and the IMPACT2 Study Team, 2015; Yeung et al., 2015). The technique was used for the quantitative analysis of API, but researchers acknowledged the study was costly (London School of Hygiene & Tropical Medicine, 2015).

HPLC/mass spectrometry were used in a collaborative study between police, criminal analysts, chemists, palynologists and health workers under INTERPOL and the Western Pacific World Health Organisation Regional Office to determine the source of falsified artesunate (an antimalarial) in South East Asia in 2008 (Newton et al., 2008).

The Tanzanian Food and Drugs Authority has pilot-tested the use of the Minilab[®] (a ready-to-use TLC kit from the German Pharma Health Fund) for the screening of antimicrobials, antimalarials and antiretrovirals. It offered benefits in terms of speed and cost-effectiveness but was only able to detect grossly substandard or falsified samples. They concluded that the technique should only be used in conjunction with other robust, laboratory-based techniques (Risha et al., 2008).

In 2015, NMR spectroscopy of hydrogen (¹H) and phosphorous (³¹P) atoms in anti-leishmanial medication miltefosine in Bangladesh was used to identify the generic version as falsified, and not constituted of the correct API (Kaur et al., 2015).

1.3 Principles of spectroscopic techniques

1.3.1 Principles of attenuated total reflectance-Fourier transform infrared spectroscopy

Attenuated Total Reflectance-Fourier Transform Infrared (ATR-FTIR) spectroscopy is a powerful analytical technique used to identify chemical substances through measurement of their infrared (IR) absorption. ATR-FTIR spectroscopy utilises the mid-infrared region ($400 - 4000 \text{ cm}^{-1}$) which encompasses the fundamental vibrational modes of most organic molecules. This range is useful in the identification of functional groups, chemical bonds and molecular structures. ATR-FTIR measures the vibrational frequencies of bonds in a sample upon interaction and excitation when exposed to infrared radiation. Different molecules absorb and reflect specific frequencies of radiation, initiating the vibration of its chemical bonds (stretching/bending/twisting) (Stuart, 2004, pp.1–13). Each type of chemical bond absorbs IR radiation at a characteristic frequency, producing a 'fingerprint' spectrum for the sample (Stuart, 2004, pp.1–13). In ATR-FTIR, the sample is placed directly on a high-refractive-index crystal (e.g. zinc selenide or diamond). IR radiation penetrates the crystal at a specific angle and undergoes total internal reflection at the interface between crystal and sample (Coates, 2000).

Alongside reflection within the crystal, IR radiation creates an evanescent wave that extends beyond the crystal's surface into the sample and is absorbed based on the chemical composition of the sample (Smith, 2011). This larger depth penetration holds advantages in terms of determination of API homogeneity (Kaur et al., 2010). ATR-FTIR is often non-destructive, making it useful for applications such as forensic science where sample integrity is important (Sharma and Singh, 2020). It is a versatile technique, able to be used for characterisation of organic compounds, polymers, biological tissues, inorganic materials and surface contaminants (Stuart, 2004b,

pp.71–186). ATR-FTIR can be especially useful in the analysis of opaque or highly absorbent samples that may be difficult to analyse using traditional transmission FTIR (Liu and Kazarian, 2022). Minimal sample preparation is required as samples can be placed directly on the crystal, allowing straightforward analysis of solids, creams and liquids (Chophi, Sharma and Singh, 2019; Orphanou et al., 2015; Sharma et al., 2019; Sharma, Bhardwaj and Kumar, 2019; Williamson, Raeva and Almirall, 2016). As the radiation reacts with both the surface and interior of the sample, the technique can be well suited to the analysis of thin films and surface properties of samples (Müller et al., 2014). ATR-FTIR spectroscopy also has capabilities for quantitative analysis (Céline et al., 2014; Pizzo et al., 2015; Wojciechowski et al., 1998). However, IR spectroscopy is sensitive to OH bonding, making it prone to interference from water bands within liquid samples. The technique has a limited penetration depth: ATR only analyses a thin layer of the sample so is less effective in analysis of bulk materials. The ATR crystal can also be sensitive to damage from hard or reactive samples (Zhu, Chen and Qin, 2011). Since the technique is reliant on direct contact between the sample and the crystal, through-packaging screening is not possible.

1.3.2 Identification of anti-infectives by ATR-FTIR spectroscopy

ATR-FTIR has been employed as an analytical tool in the identification of SF medicines in recent years, most popularly in the identification of falsified sildenafil tablets (Coelho Neto and Lisboa, 2017; Custers et al., 2015; Lawson, Ogwu and Tanna, 2014; Ortiz et al., 2013).

Mittal, Sharma and Rathore proposed an ATR-FTIR spectroscopy-based workflow for the identification of SF antibiotics in 2021. The method combined the use of ATR-FTIR

in the mid-infrared region with chemometrics for characterisation of the chemical structure of 27 antibiotics with classification accuracies of over 87.3%. The dataset consisted of anti-infective tablets and capsules (Mittal, Sharma and Rathore, 2021).

FTIR spectroscopy has also been used in manufacturing functions to evaluate the applied virus medium volume during sample filling for detection of vaccine doses in freeze dried, live attenuated vaccine formulations (Hansen et al., 2015).

Over the last decade, several developments have been made in the use of ATR-FTIR spectroscopy for rapid screening of suspected SF medicines including anti-diabetics (Farouk, Moussa and Azzazy, 2011) and generic painkillers (Lawson, Ogwu and Tanna, 2018) with the FDA developing a handheld instrument for identification of tablets and capsules (Platek, Ranieri and Batson, 2016).

ATR-FTIR has been used in the analysis of the immune response triggered after vaccination with the Covid-19 vaccine (Mata-Miranda et al., 2024; Vazquez-Zapien et al., 2022) as well as in disease recognition itself (Calvo-Gomez et al., 2022; Garrone Barauna et al., 2021).

1.3.3 Principles of Raman spectroscopy

Raman spectroscopy is a vibrational spectroscopic technique that provides information about molecular vibrations, rotational and low-frequency modes. It is based on the inelastic scattering of light, where photons interact with molecular vibrations causing a shift in energy. When a monochromatic source of radiation interacts with a sample, most photons are scattered elastically (Rayleigh scattering), but some scatters inelastically (Raman scattering), this creates the Raman shift. This shift is attributed to specific molecular vibrational modes, which allows the

identification of chemical structure and molecular interactions. Each molecule has a unique Raman spectrum which acts as a molecular 'fingerprint' (Bruker, 2024).

Raman microscopy operates on the same foundational principles as Raman spectroscopy to identify chemical compounds within a sample. It utilises a laser that is directed at the target analyte, illuminating the sample. During this interaction, the laser light is scattered from the sample's surface, resulting in either Rayleigh or Raman scattering. Raman microscopy specifically focuses on Raman scattering for chemical analysis, which involves inelastic scattering where the frequency and wavelength of the scattered light differ from those of the incident laser. The incident laser may either gain or lose energy through interactions with photons, resulting in inelastic scattering characterised by Stokes (energy loss) and Anti-Stokes (energy gain) lines (Deluca et al., 2023). Stokes lines, originating from the ground state and being more prevalent at room temperature, have higher intensity and are therefore preferred in Raman spectroscopy (McCreery, 2000). The scattered light is collected to generate a spectrum unique to the chemical composition of the sample, serving as a 'chemical fingerprint' for the identification, characterisation, and quantification of its chemical compounds (Bruker, 2024).

Raman spectroscopy and imaging provide a quantitative and non-invasive method for visualizing and characterising pharmaceuticals. Raman microscopes can capture spectra from small sample volumes. Key features of Raman microscopy relate to two optical aspects: the focusing of the laser on the sample and the collection of the scattered light (Turrell and Corset, 1996, pp.27). The scattered Raman photons are gathered in a 180° backscattering configuration, allowing for sample visualisation, radiation focusing, and spectrum collection.

In conventional Raman spectroscopy, the exciting laser beam is usually focused onto the sample using a lens of 10-30 cm, concentrating the laser into a focal cylinder to enhance Raman scattering intensity. Raman microscopy employs a confocal laser, which features include:

- **Spatial filtering** achieved through optical conjugation onto the sample via pinhole apertures used for illumination and detection.
- **Reduction of stray background light** from out-of-focus areas of the sample through spatial filtering, ensuring that the primary signal contribution comes from a specific layer of the sample.

By eliminating unfocused light, the spatial resolution of the images improves, particularly in Raman imaging where detailed chemical images are essential. The quality of the Raman spectra generated through the confocal pinhole is enhanced by reducing background fluorescence, negating the need for fluorescence mitigation through wavenumber optimisation. This is achieved through increased spatial resolution: by concentrating the laser light through a smaller aperture; thus, the excitation volume is limited to a small area. This means that only a small fraction of the sample is illuminated, which limits the overall fluorescence produced compared to a broader area. The small aperture acts as a spatial filter which only allows light from the focal point to reach the detector, this removes fluorescence emitted from regions outside the focal plane which could contribute to background noise (Berry, 2022). Confocal microscopy also facilitates selective focal plane analysis, allowing examination of light corresponding to different depths in the sample and enabling three-dimensional analysis. However, there are limitations to this technique, as the intense monochromatic radiation can potentially cause thermal degradation of the sample (Assi, 2024).

Raman spectroscopy presents many advantages:

- It is generally non-destructive, allowing for the analysis of delicate materials and applications in a forensic setting where sample integrity is important.
- Samples typically require little to no preparation, which is time and cost-effective, and reduces the introduction of contamination.
- Raman spectroscopy can be used on a wide range of materials, including solids, liquids and gases, including aqueous solutions without interference from water.
- Techniques such as Spatially offset Raman spectroscopy (SORS) enables the optical probing of analytes through light-obscuring surfaces for non-invasive chemical characterisation. This allows materials to be chemically identified while inside sealed coloured and opaque containers.
- Handheld systems allow the portable, on-site analysis of samples, aiding the identification of medicines in the field.

Raman microscopy presents several additional advantages:

- A straightforward 'point and shoot' method for chemical analysis and imaging.
- The capability to analyse extremely small samples (Bruker, 2024).
- The ability to examine molecules and cells in aqueous solutions, thanks to the weak Raman scattering of water (Matthäus et al., 2008).

Raman microscopy has found numerous clinical applications, including but not limited to quality control, failure analysis, tissue imaging, in vitro diagnosis, DNA/RNA analysis, metabolic profiling, single-cell analysis, and photodynamic therapy (Antonio and Schultz, 2013; Carey, 2006; Cavonius et al., 2015; Deluca et al., 2023; Downes, 2015; Fung and Shi, 2020; Huang et al., 2004; Ito, Koyama and Otsuka, 2010;

Matthäus et al., 2008; Pavićević et al., 2012; W John Wolfgang, 2005; Zhang et al., 2021).

Surface-Enhanced Raman Spectroscopy (SERS) is an advanced analytical technique that significantly enhances the Raman scattering signal of molecules adsorbed on rough metal surfaces or nanostructures. SERS relies on the basic principle of inelastic Raman scattering of photons upon exposure to a monochromatic light to produce a spectral fingerprint for each chemical species. The primary mechanism behind SERS is electromagnetic enhancement. When the laser interacts with the surface of colloidal metal (e.g. gold/silver), it induces collective oscillations of free electrons in the metal called surface plasmons. This causes a significant increase in the electric field around the metal surface, which in turn enhances the Raman scattering of molecules that are close to the surface. The enhancement observed is estimated to extend up to between 10^6 to 10^{10} . In addition to electromagnetic enhancement, charge is transferred between the metal and adsorbed molecules, increasing the polarisability and enhancing the Raman signal.

The efficacy of SERS is dependent on the roughness of the colloidal metal surface and the presence of nanoparticles. These structures create regions where the electromagnetic field is concentrated, enhancing Raman signals from molecules in these regions. For SERS to occur, the analyte must adsorb onto the metal surface, this can affect the enhancement factor. Different wavelengths may interact differently with surface plasmons, causing variation in SERS enhancement, so laser wavelength optimisation can improve the SERS signal. SERS holds potential as a high sensitivity and selectivity method of detection for specific molecules. The use of specific coatings or targeted nanoparticles can selectively enhance the signals of specific analytes, proving particularly useful in trace analysis.

1.3.4 Identification of anti-infectives by Raman spectroscopy

Raman spectroscopy and spectral library-based correlation methods have been utilised for the detection of single API falsified anti-infective products including antimalarial, antibiotic and antiviral tablets and capsules (Loethen et al., 2015).

Lawson and Rodriguez present the use of a so-called 'Raman Barcode' for SF drug detection by comparison of API reference spectrum against suspect SF drugs, with 100% accuracy in identification of simulated SF medicines (Lawson and Rodriguez, 2016).

A study in 2017 explored the use of portable Raman systems in the screening of unapproved anti-infectives including Acyclovir, Amoxicillin and Doxycycline Hyclate in aqueous solutions which demonstrated promising results in terms of qualitative analysis but limitations with respect to the quantitative analysis (Tondepu et al., 2017).

Raman spectroscopy and imaging has been used to study the effect of Covid-19 vaccines on human lung carcinoma cells (Abramczyk and Surmacki, 2023), as well as the identification of toxoid vaccine products (Silge et al., 2018).

Silge et al., speculated that "chemometrics assisted Raman spectroscopy might be an important tool to close the analytical gap of heterogeneous sample matrices or complex biologicals like the mRNA vaccine technology actual used to fight the SARS-CoV2 pandemic" (Silge et al., 2022).

1.4 Gaps in research

Considering the aforementioned studies, the application of vibrational spectroscopic techniques for the authentication of medicinal products and identification of SF anti-infectives is not a new concept. However, spectroscopic based identification studies focused on single API formulations of anti-infective tablets and capsules (especially antimalarials). While this knowledge is undeniably valuable, limited research into identification of novel anti-infective formulations (aqueous solutions and liquids) has been undertaken using these techniques, specifically biologic formulations which are notoriously unstable and subject to degradation under imperfect conditions or the passing of time. While Raman and infrared spectroscopy have both been utilised as a tool in the study of Covid-19 vaccine effects on cells and immune response, little research has been conducted on the use of these techniques for characterisation of the vaccines' formulation. Raman spectroscopy has previously proved to be successful in the identification of vaccine constituents and has been theorised as a potential tool for analysis of complex biologics such as the mRNA vaccine technology used in some brands of Covid-19 vaccine. With this in mind, and the prevalence of substandard and falsified Covid-19 vaccines in circulation, this thesis aims to address some of the limitations in existing literature by exploring the feasibility, robustness and accuracy of portable spectroscopic based methods for the authentication of genuine, and identification of SF novel vaccine formulations.

1.5 Rationale

Presently, SF medicines pose a severe threat to public health and infrastructure, including public confidence in healthcare providers alongside detrimental economic consequences. The circulation of substandard and falsified Covid-19 vaccines has

severe implications including but not limited to treatment ineffectiveness, sociological impact on public opinion, morbidities and co-morbidities associated with toxic/incorrect dosage of APIs, reduced population immunity and increased outreach of the virus. With over 776 million reported cases worldwide and 7.1 million deaths (as of 8th September 2024) (World Health Organisation (WHO), 2024), vaccination against the highly virulent and deadly virus is a critical first line of defence against its adverse effects. The introduction of SFCovid-19 vaccines into market weakens the efficacy of global vaccination programmes and increases the risk of infection to the public, especially those who are vulnerable or immunocompromised. Traditional techniques for the identification of SF vaccines are sophisticated and costly, requiring significant resources that are not always available in less-developed countries where the risk of exposure to SF medical products is significantly higher. Traditional techniques are often laboratory-based, requiring controlled conditions for effective analysis which may not always be accessible in LMICs. Thus, there is a requirement for robust, rapid and cost-effective analytical tools which can be used with limited training and in varying conditions/outside of a laboratory to reliably identify SF Covid-19 vaccines in LMICs to reduce the risk to public health. This thesis aims to present novel, portable and cost-effective techniques for the detection of SF Covid-19 vaccines and evaluate their potential application in the field, especially in LMICs.

At the time of the research, limited literature on the use of ATR-FTIR spectroscopy for the analysis of complex biologic formulations, especially aqueous solutions such as vaccines was available. In this sense, the research presented in this thesis on the use of portable ATR-FTIR spectroscopy for the identification of genuine and SF Covid-19 vaccines is novel and has not been explored before. In this sense, as a portable instrument the ATR-FTIR spectrometer can be moved and operated outside of a

laboratory environment, but does not offer the same versatility as the handheld Raman instrument. Specifically the PerkinElmer SpectrumTwo FTIR spectrometer offers robust portability options, making it ideal for use in both laboratory and remote testing environments (PerkinElmer, 2025). While Raman spectroscopy has been utilised in vaccine analysis previously, at the time of this research little to no literature existed on the use of SERS as a highly sensitive tool for the detection of genuine and SF nucleic acid based Covid-19 vaccines using a handheld system. While one paper was published in 2023 on a similar technique: the use of SORS in the detection of falsified Covid-19 vaccines (Mosca et al., 2023), this study did not explore the use of colloidal metal nanoparticles in Raman enhancement of vaccine signal. At the time of publication, the SERS research was already ongoing, with pilot study findings presented in January 2023 and published the same year (Watson et al., 2023).

1.6 Aim and Objectives

The present thesis developed and validated infrared and Raman spectroscopic techniques for authentication of Covid-19 vaccines.

The objectives of the thesis were:

Use portable ATR-FTIR spectroscopy for authentication of Covid-19 vaccines surpassing challenges related to water interference.

Compare handheld conventional versus surface enhanced Raman spectroscopic methods for identification DNA and mRNA in vaccines considering challenges in fluorescence and method sensitivity.

Explore the ability of confocal Raman microscopy for authentication of Covid-19 vaccines of different manufacturers in low doses.

Determine the performance of machine learning algorithms in classification of infrared and Raman spectroscopic data.

1.7 Thesis Structure

The thesis is composed of five chapters. Chapter 1 (this chapter) comprises the introduction to the study and the background in relation to the prevalence of medicine falsification and the associated harm on the economy and public health. Traditional analytical techniques currently employed in the fight against substandard and falsified medicines and their limitations are discussed, and the principles of spectroscopic methods presented throughout the following chapters are introduced.

Chapter 2 discusses the use of ATR-FTIR spectroscopy for rapid and non-destructive characterisation of Covid-19 vaccines and their constituents. This chapter details stages of the study from sample acquisition to data collection, processing and evaluation of accuracy and identification potential using machine learning algorithms (MLAs). The results and discussion evaluate the application of ATR-FTIR spectroscopy as a robust analytical tool for identification of SF Covid-19 vaccines.

Chapter 3 compares the use of handheld conventional and surface-enhanced Raman spectroscopy at 785 nm for the through-barrier analysis of Covid-19 vaccines. All stages of the study are explained including sample acquisition, data collection, spectral treatment and data processing and assessment of accuracy and identification potential using MLAs. The signal enhancement for vaccines measured using SERS is discussed and quantified. The results and discussion present the potential of SERS

as a portable, non-destructive technique for rapid, on-site detection of SF Covid-19 vaccines for utilisation in-field such as hospitals, border forcers and airports.

Chapter 4 evaluates the use of laboratory-based Raman spectroscopy-microscopy at 532 nm for the characterisation of Covid-19 vaccines. Data collection and spectral processing are discussed, as well as assessment of identification potential through MLAs. Enhancement of vaccine signal when measured using SERS is presented. The results and discussion outline the advantages of Raman microscopy over conventional spectroscopy and acknowledge the instrumental limitations associated with this method.

Chapter 5 presents the study's conclusion and future recommendations in detail. The overarching scope of the research is discussed in relation to the aims and objectives of the thesis and contribution to knowledge, including shortfalls is acknowledged and discussed.

2. AUTHENTICATION OF COVID-19 VACCINES USING PORTABLE ATTENUATED TOTAL REFLECTANCE-FOURIER TRANSFORM INFRARED SPECTROSCOPY

2.1 Introduction

Covid-19 is a novel coronavirus that emerged in December 2019 in Wuhan, China, quickly spreading worldwide to establish a global pandemic. The virus was named SARS-CoV-2, 2019-nCoV due to its high homology (~80%) to SARS-CoV. SARS-CoV which spread worldwide between 2002 and 2003 causing acute respiratory distress syndrome (ARDS) and high mortality. SARS-CoV-2, 2019nCoV (Covid-19) far surpassed the morbidity rates of its predecessor during its rapid circulation around the globe. A pandemic of this nature had not been seen since the severe acute respiratory syndrome (SARS) outbreak in 2002-2003, accumulating a total of 8,096 cases and 774 deaths across 28 countries (Cherry, 2004). To date, SARS-CoV-2 has collected over 775 million cases and over 7 million deaths across more than 220 countries (World Health Organisation, 2024). The reported short- and long-term effects of COVID-19 included multiple organ damage related to cardiovascular, endocrine, gastrointestinal, nervous and respiratory systems, as well as mortality (Ghasemiyeh and Mohammadi-Samani, 2020). More than 50 detrimental long-term effects of COVID-19 on multiple systems have been reported (Lopez-Leon et al., 2021). In the time since the height of the pandemic, persistent symptoms have been reported in patients post Covid-19 infection and recovery. The extended presence of symptoms such as fatigue, cough, breathlessness, palpitations and myalgia have now coined the term “long Covid” or “Post Covid Syndrome” (Raveendran, Jayadevan and

Sashidharan, 2021). The negative impact on public health caused by Covid-19 infection is not limited to the detrimental short-term effects; but, extends to a wider population suffering with the long-term effects of infection and recovery, with over 65 million individuals with long-Covid worldwide (Davis et al., 2023).

As a result of the fast-paced establishment of the pandemic, countries around the world battled to contain and control the spread of the unprecedented Covid-19 outbreak through the intense implementation of strategies such as quarantine, isolation, social distancing and contact tracing. These protocols gave little indication of the eradication of the virus in the foreseeable future and highlighted the need for a longer-term solutions. Vaccination has been presented as the most effective solution against the virulence of Covid-19 and the reduced transmission between individuals (Delany, Rappuoli and De Gregorio, 2014). Governments pushed to accelerate Covid-19 vaccines' development to achieve population immunity and reduce virus transmission. Accelerated Covid-19 vaccine development pushed 105 vaccines into clinical development with 18 approved for emergency use. Vaccines in development include whole virus (live attenuated or inactivated), protein-based, viral vector, and nucleic acid vaccines. Nucleic acid-based vaccines comprised of mRNA and DNA showed promise with regards to production speed and efficient provocation of immune responses (Roghayyeh Baghban, Abdolmajid Ghasemian and Mahmoodi, 2023). The Covid-19 vaccines are the first instance where a nucleic acid vaccine has been approved for use in public health programmes (Ndwandwe and Wiysonge, 2021). Most Covid-19 vaccine formulations mimic the mechanism of cellular infection: the spiked glycoprotein binds to its cellular receptor, where the viral genome is released and begins to replicate in the cytoplasm. In nucleic acid-based vaccines, lipid nanoparticles deliver the spike glycoprotein to the host immune system, triggering an immune

response (de Queiroz et al., 2020). The use of lipid-based nanoparticles improved the bioavailability of the vaccines (FDA, 2020).

The worldwide requisite for enhanced vaccination programs opened a gap in the market for the rise of substandard and falsified (SF) vaccines. The World Health Organisation (WHO) defines SF medicines as “authorised medical products that fail to meet either their quality standards or specifications, or both” and Falsified medicines as “medical products that deliberately/fraudulently misrepresent their identity, composition or source” this includes counterfeit medical products (WHO, 2018). Falsified Covid-19 vaccines were reported in many countries including Colombia, China, India, Mexico, Poland and South Africa. Police seized 400 vials, equal to 2,400 doses of fake Covid-19 vaccines from a warehouse in South Africa and over 3,000 from China in 2021 (INTERPOL, 2021). In Mumbai, over 2,053 people were given jabs of falsified Covid-19 vaccines across nine vaccination centres. One housing committee was scammed by falsified vaccines and another hospital was shut down for running a fake vaccination drive where several arrests were made. In Kolkata, 800 people were administered falsified Covid-19 vaccines suspected to be either expired vaccines, empty vials, saline water or amikacin (an antibiotic) (Mukherjee et al., 2021). The potential implications of receiving substandard or falsified vaccines are not limited to treatment ineffectiveness but can also induce long-term morbidities or lethal effects. Treatment inefficacy leads to reduced population immunity and increased transmission, therefore increased cases of both the initial infection, and long-Covid symptoms. The widespread implications of proliferation of substandard and falsified vaccines extend to public health, sociological and economical effects (Amankwah-Amoah, 2022).

The prevalence of SF vaccines, particularly those utilised in the extensive effort to control the Covid-19 pandemic highlights a need for further research and implementation of authentication and quality control procedures for vaccines used in public health programs - particularly in lower and middle income countries (LMICs) where it was estimated 1 in 10 medicinal products are substandard or falsified (World Health Organisation, 2017). The development of a standard vaccine authentication procedure to aid in the detection of SF Covid-19 vaccines involves the characterisation of both the vaccines' chemical constituents and their physical properties. Most traditional analytical methods (such as liquid chromatography) do not satisfy the aforementioned need for synchronous characterisation of both chemical and physical properties and are expensive, time consuming, and bulky systems that are inconvenient to move and operate. Therefore, traditionally samples must be transported to the analytical instrument or system for testing, delaying the receipt of test results and subsequent action, or treatment of affected patients.

Vibrational spectroscopy addresses the limitations of traditional techniques in its ability to provide rapid, non-destructive characterisation of physical and chemical properties medicinal products. Portable spectroscopic instruments allow on-site analysis and reporting, accelerating the process of SF medicine detection and resulting actions. Vibrational spectroscopy measures the oscillations of atoms in molecules upon exposure to a light source. The observation of vibrational transitions yields information about the molecular vibration energy levels, which in turn are related to molecular conformation, structure, intermolecular interaction and chemical bonding (Li and Church, 2014). Infrared spectroscopy utilises a polychromatic laser (multiple wavelengths) for characterisation in the fingerprint region of $450-4000\text{cm}^{-1}$. ATR-FTIR spectroscopy is now the most prevalent utilisation of mid-infrared (MIR) spectroscopy.

The ATR sampling method allows fast and robust sampling of solid and liquid samples, including viscous samples and pastes (Ramer and Lendl, 2013). Advances in the use of ATR-FTIR spectroscopy in recent years include application of the technique in biopharmaceutical (biologics) analysis including protein structure characterisation, quantification and imaging of tissues and cells.

As a result, this chapter focuses on the utilisation of portable ATR-FTIR spectroscopy as a robust, rapid and on-site authentication method to aid in the reduction of the prevalence and harm associated with SF Covid-19 vaccines.

2.2 Experimental

2.2.1 Materials

A total of 410 Covid-19 vaccine samples from four leading manufacturers were utilised for method optimisation and experimental procedures (Edouard Mathieu, 2020). Vaccine samples included four 'Brands' of different formulations; Brand 1 (DNA-based), Brand 2 (mRNA-based), Brand 3 (Vero-cell inactivated) and Brand 4 (mRNA-based) (Table 2.1). Brand 1 and 2 vaccines were obtained through the NHS Central Liverpool Primary Care Network and consisted of leftover product from reconstituted vials (in saline) after six doses had been distributed to patients, so that the remaining volume was insufficient for medical use (<0.45mL). Vaccines were collected from a collection site seven minutes away from the laboratory by car and the samples were transported in sealed containers maintained at a temperature of 2-8°C during the journey using ice packs. Brand 3 and 4 vaccine samples consisted of recently expired or end-of-life vaccine remainders and were obtained from Hospitals in Lebanon and Iraq and transported by air under the same conditions.

Table 2.1. Details of Covid-19 vaccine brands obtained from the NHS Central Liverpool Primary Care Network and Lebanese/Iraqi hospitals for use in this study

Brand	Type	N	Batch numbers	Form
1	DNA-based	176	Redacted	Transparent liquid, Recombinant
2	mRNA-based	182	Redacted	White liquid, Suspension in 0.9% NaCl
3	Vero-cell inactivated	54	Redacted	Transparent liquid
4	mRNA-based	7	Redacted	White liquid

¹

¹ N = number of samples

Table 2.2. Details of common vaccine excipients obtained from chemical suppliers for use in the procedure

Excipient	CAS number	Form
RNA Standard	73049-77-1	white powder
DNA Standard	68938-01-2	transparent liquid
mPEG_DMG_2K	160743_62_4	frozen powder
mPEG_DTA_2K	1849616_42_7	frozen powder
DSPC	816_94_4	frozen powder
Linoleic Acid	60-33-3	transparent liquid
DHA	2036272_55_4	transparent liquid
Hemoglobin	9008-02-0	dark red metallic powder
L_Isoleucine	73-32-5	chilled white powder
L_Alanine	56-41-7	clear crystalline powder
Glycogen from bovine liver	9005-79-2	chilled white powder
β lactoglobulin (bovine milk)	9066-45-9	Clear crystalline powder
Polysorbate 80	9005-65-6	Yellow viscous liquid
RNA Sodium Salt from Yeast	73049-77-1	pale powder
Cholesterol	57-88-5	white powder
Sucrose	57-50-1	white powder
Citric Acid	77-92-9	crystalline powder
Calcium Phosphate	7758-87-4	fine white powder
Sodium Citrate monobasic	18996-35-5	crystalline powder
PEG 4000	25322-68-3	White solid
DNA from salmon testes	438545-06-3	white powder

2.2.2 Instrumentation

Measurements were taken on the PerkinElmer SpectrumTwo FTIR Spectrometer equipped with ATR diamond holder (Figure 2.1). The instrument was connected to a computer with PerkinElmer's SpectrumIR software for spectral visualisation.



Figure 2.1. PerkinElmer SpectrumTwo FTIR spectrometer equipped with ATR diamond holder

2.2.3 Methods

For vaccine measurement, liquid samples were defrosted, and a small volume of product (> 0.1 mL) was carefully dropped onto the diamond holder using a needle and syringe. It is noteworthy to mention that each vaccine droplet initially required 45 minutes – 1 hour to dry prior to measurement, otherwise water bands obscured the vaccines' spectra. Careful reduction of sample volume reduced this drying time to 20

– 45 minutes in some samples. A minimum of three spectra were taken from each vaccine sample, after the point of evaporation such is that three spectra were obtained from each sample that were reflective of the vaccines' characteristics without interference from water. Liquid excipients were syringed onto the diamond holder, powdered excipients were carefully placed onto the diamond holder using a small spatula. Each spectrum was the sum of 16 scans over a wavenumber range of 450-4000 cm^{-1} with a spectral resolution of 4 cm^{-1} . PerkinElmer's Spectrum IR software allowed real-time visualisation of spectra during measurement (Figure 2.1), spectra were then exported as .csv files to external software for spectral analysis and machine learning algorithm application.

2.2.4 Spectral Treatment and qualitative analysis

Spectra were exported to Matlab 2023a software, no pre-treatment methods were applied. For evaluation of identification potential, qualitative analysis methods were employed. This included the application of the following MLAs: correlation in wavelength space (CWS) and principal component analysis (PCA). Multiple classification models were trained using the vaccine dataset and Matlab2023a classification learner including Ensemble subspace K-Nearest Neighbour (KNN). An Area Under the Curve of the Receiver Operating Characteristic (AUC-ROC) curve was applied to evaluate the separation capacity of the model.

Spectral quality was assessed considering the following parameters: number of bands (N), maximum band intensity/position, range and signal to noise ratio (SNR) (equation 2.1.) (Adams, 2007; Assi and Fortunato, 2017). These parameters were considered to establish samples as of strong, medium or weak IR activity.

$$SNR = \frac{\text{mean}}{\text{standard deviation}} \text{ of three spectra at maximum peak}$$

Equation 2.1 Signal to noise ratio based on absorbance and standard deviation at a maximum peak (Adams, 2007)

CWS was employed to assess spectral similarity between a test spectrum (A) and reference spectrum (B). Similarity was demonstrated by a correlation coefficient value (r-value) greater than or equal to 0.95 obtained between the test spectrum and reference spectrum.

$$r_p = \frac{\sum(A_i - \bar{A})(B_i - \bar{B})}{\sqrt{\sum(A_i - \bar{A})^2 \sum(B_i - \bar{B})^2}}$$

Equation 2.2 Correlation coefficient based on momentum product (Brereton, 2006)

Where, r_p is the correlation coefficient value corresponding to the momentum product,

A_i is the test spectrum of A,

B_i is the reference spectrum B and is the average spectrum of B.

Theoretically, an r-value of -1 obtained between two spectra represents complete dissimilarity, whereas an r-value of +1 indicates two identical spectra. Variation in sample concentrations and therefore signal intensity meant that the likelihood of achieving an r-value of +1 between two vaccine samples of the same brand was highly unlikely, and so the threshold of 0.95 was employed to indicate sufficient similarity between two vaccines of the same composition. This threshold allowed for variance in absorbance values obtained between samples of the same brand, but not spectral

characteristics such as band position. Therefore, in theory, an r-value of 0.95 or above indicates two spectra are from the same brand.

Principal component analysis (PCA) was applied to the multidimensional dataset as an unsupervised machine learning technique. PCA identifies recurring patterns in the data with minimal loss of information to simplify complex spectral datasets into comprehensible information (Beattie and Esmonde-White, 2021).

PCA reduces the matrix's dimensionality to two subspaces – scores and loading and was therefore able to classify the spectral data. The scores showed the distribution of different vaccine brands in the dataset in a multidimensional space. Scores were used for the identification of clusters and patterns within the dataset, therefore able to distinguish between clusters representative of different vaccine brands.

“The PC (loadings) are by definition hidden, repeated and uncorrelated spectral shapes that linearly combine to generate the observed spectra” (Beattie and Esmonde-White, 2021). The loadings highlight significant absorbance values that correspond to specific functional groups within the vaccines' composition. PCA organises the scores in terms of magnitude and prevalence, with the early PCs holding the largest volume of information, usually corresponding to chemical features (e.g., physical properties or concentration). The first and second dimensions (PC1 and PC2) provide explanation for the highest variance and second highest variance, PC3 for the third highest variance and so on. If PC1 and PC2 showed contribution to over 95% of the variance observed, the following PCs were disregarded as their contribution to the variance of the overall dataset was negligible. The focus of the research was to ascertain the chemical and physical properties of the vaccines, primarily demonstrated by the earlier PCs (Beattie and Esmonde-White, 2021).

$$X = T \cdot P + q$$

Equation 2.3 Mathematical equation of PCA (Beattie and Esmonde-White, 2021)

Where, X is the original data matrix (m x P),

T is representative of the scores (m x n),

P represents the loading (n x p) and is representative of the residuals (m x p).

Type I and II errors were identified and consolidated to evaluate the performance of PCA. Type I errors (false negatives) occurred when scores of the same vaccine brand were not clustered together, whereas Type II errors (false positives) occurred when scores of one vaccine brand were clustered with the scores of a different brand. For example, a brand 1 vaccine clustered with the brand 2 group.

Classification tools were used to assess the identification potential and separation capacity of the method. Classification algorithms used comprised supervised machine learning techniques where samples were distributed into different classes based on various features. The algorithms were 'supervised' because the model is initially provided with the identity of the data it is classifying and predicting. Various classification models were trained on the vaccine dataset using the Matlab r2023a classification learner toolbox. This involved feeding the whole spectral dataset into the classification learner toolbox and allowing each model to be trained using a 6-fold validation. The classification learner was provided with the following information: brand identity of each spectrum, and absorbance value at each wavenumber from 450-4000 cm^{-1} . The classification models then used this information to predict vaccine brand from each spectrum based on their spectral characteristics at each wavenumber. A

randomly assigned 20% of the dataset was set aside by the classification learner for capability testing and to check for data overfitting of the model. Classification models were preliminarily chosen based on the automated accuracy calculation of the 6-fold validation training data provided by Matlab.

An 'Ensemble subspace K-nearest neighbour (KNN)' classification model showed the highest percentage accuracy across the 6-fold validation runs. Multiple neural network models also demonstrated high accuracy for brand prediction based on the training data.

KNN is a supervised learning classifier, which is non-parametric and makes classifications or predictions about the grouping of an individual data point based on proximity by a distance metric. By considering its K closest neighbours in the training dataset, KNN predicts the label or value of a new data point. As its non-parametric, no underlying assumptions are made based on the distribution of data (Zhang, 2016). Euclidean distance is the most popular distance parameter and is used as the default metric by Matlab classification learner for KNN based classification. It is a measure of the true distance between two points in Euclidean space (equation 2.4.).

$$d(p, q) = \sqrt{\sum_{i=1}^d (q_i - p_i)^2}$$

Equation 2.4 Formula for Euclidean distance between two points p and q in a d-dimensional space (Short and Fukunaga, 1981)

Where p_i and q_i are the i^{th} coordinates of p and q, respectively.

KNN based ensemble methods minimise the effect of outliers by identifying a set of datapoints in the given feature space that are nearest to an unseen observation in order to predict its response by using majority voting (Ali et al., 2022).

Matlab's classification learner tool was used to generate a classification matrix for both training and test datasets. This presents the data as a matrix where x = predicted class, and y = true class, allowing the visualisation of Type I and II errors (false positives and negatives) and calculation of model evaluation metrics based on correct and incorrect class predictions. For evaluation of the Ensemble subspace KNN classification model, the following metrics were considered: Accuracy, Precision, Recall, Specificity and F1 Score (Agarwal et al., 2021).

$$Accuracy = \frac{TN + TP}{TN + FP + TP + FN}$$

Equation 2.5 Formula for Accuracy calculation from confusion matrix (Agarwal et al., 2021)

Where TP is the number of true positive classifications

TN is the number of true negative classifications

FP is the number of false positive classifications

FN is the number of false negative classifications

$$Precision = \frac{TP}{TP + FP}$$

Equation 2.6 Formula for Precision calculation from confusion matrix (Davis and Goadrich, 2006)

Where TP is the number of true positive classifications

TN is the number of true negative classifications

FP is the number of false positive classifications

FN is the number of false negative classifications

$$\text{Recall} = \frac{TP}{TP + FN}$$

Equation 2.7 Formula for Recall calculation from confusion matrix (Davis and Goadrich, 2006)

Where TP is the number of true positive classifications

TN is the number of true negative classifications

FP is the number of false positive classifications

FN is the number of false negative classifications

$$\text{Specificity} = \frac{TN}{TN + FP}$$

Equation 2.8 Formula for Specificity calculation from confusion matrix (Davis and Goadrich, 2006)

Where TP is the number of true positive classifications

TN is the number of true negative classifications

FP is the number of false positive classifications

FN is the number of false negative classifications

$$F1\ Score = 2 \left(\frac{Precision \times Recall}{Precision + Recall} \right)$$

Equation 2.9 Formula for F1 Score calculation from confusion matrix (Agarwal et al., 2021)

Area under the receiver operator characteristic (AUC-ROC) curve was used to evaluate the performance and separation capacity of the classification model, where AUC represents the measure of separability and ROC is a probability curve (Bradley, 1997). Using an AUC-ROC curve for evaluation of the multi-class model involved using a “one vs all” methodology where an ROC was generated for each vaccine brand against the remaining classes. An AUC value of 1 or close to 1 demonstrates excellent separation capability of the model, while an AUC of approximately 0.5 indicates that the model possesses no discrimination capacity in distinguishing between positive and negative class.

$$AUC = \frac{\sum_{i=1}^{n^+} \sum_{j=1}^{n^-} 1_{f(x_i^+) > f(x_j^-)}}{mn}$$

Equation 2.10 Calculation of AUC (Rakotomamonjy, 2004)

Where $f(\cdot)$ is denoted as the scoring function,

x^+ and x^- respectively denote the positive and negative samples

n^+ and n^- are respectively the number of positive and negative examples

1_{π} is defined to be 1 if the predicate π holds and 0 otherwise

2.3 Results and Discussion

2.3.1 IR activity of vaccines and their constituents

The interpretation of IR spectra encompasses the consideration of numerous factors beyond the chemical structure. IR spectra are sensitive to both the physical properties of a sample and its moisture content. IR spectroscopy is sensitive to hydrogen bonding; samples with a high-water content may present increased interference in their spectra from OH bonds in the sample (Chen et al., 2004). These factors were taken into consideration when interpreting the IR spectra of the vaccines and their corresponding excipients.

IR spectra of isolated DNA and RNA sodium samples were collected for evaluation of the nucleic acid-based vaccines. Samples demonstrated a maximum absorbance of 0.1903 and 0.3983 absorbance units across a wavenumber range of 450-4000 cm^{-1} for the DNA and RNA standards respectively (Table 2.3).

Table 2.3. Spectral quality parameters of the vaccine excipients measured using the PerkinElmer SpectrumTwo FTIR spectrometer equipped with ATR diamond holder

Sample	N	Max Peak Position (cm^{-1})	Max Absorbance (absorbance units)	SNR*
Excipient 1	2	456	0.52	249.6
Excipient 2	59	1055	0.15	87.5
Excipient 3 (nanoparticle)	18	1733	0.23	2003.7

Excipient 4 (nanoparticle)	50	2917	0.10	105.5
Excipient 5 (nanoparticle)	22	2924	0.23	3971
Excipient 6 (nanoparticle)	25	1103	0.68	88.5
Excipient 7 (nanoparticle)	26	1102	0.47	155.4
Excipient 8 (nanoparticle)	24	1097	0.56	60.9
Excipient 9	26	1095	0.34	212.7
RNA	33	464	0.40	302.8
Excipient 10	38	1092	0.22	240.5
Excipient 11	48	988	0.28	82.9
DNA	30	1644	0.19	82.3

2

² * at maximum peak position
N = number of bands

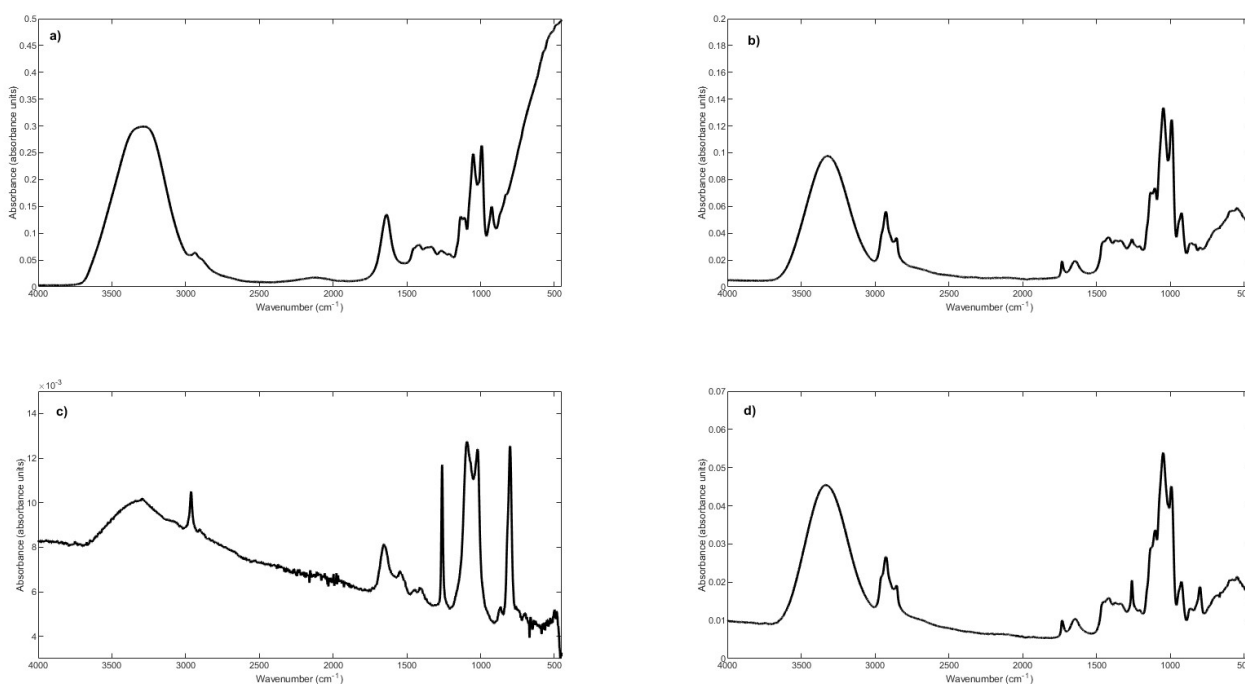


Figure 2.2 Mean spectra of a) brand 1 vaccine LJMUCV459 b) brand 2 vaccine LJMUCV367 c) brand 3 vaccine LJMUCV1421 and d) brand 4 vaccine LJMUCV1422 measured using the PerkinElmer Spectrum Two FTIR spectrometer equipped with ATR diamond holder

The ATR-FTIR spectra of DNA showed characteristic bands corresponding to phosphate groups at 1083 (strong symmetric PO_4^- stretching), 1235 (strong asymmetric PO_4^- stretching), 962 and 1049 cm^{-1} (strong C-O-P stretching), as well as O-P-O stretching at 780 and 828 cm^{-1} (weak asymmetric), respectively. Characteristic bands at 1635 (OH bending in plane), 934 (weak stretching of C-C ring), 640 (C-O-C rocking), 1299 and 1453 cm^{-1} (CH_2 wagging and bending in plane) were observed. Nitrogenous groups were observed at 1516 and 1532 cm^{-1} (NH in-plane bending), as well as at 3281 (NH_2 bound asymmetric stretching) and 1644 cm^{-1} (C=N of purine and pyrimidine bases) (Zhizhina and Oleinik, 1972).

Brand 1 vaccines shared significant bands corresponding to the characteristic bands of the isolated DNA spectra. These included bands at 1042 (strong C-O-P stretching), 1456 (CH₂ in-plane bending), and 923 cm⁻¹ (medium stretching of C-C ring). The nitrogenous groups observed in the DNA spectra were also observed in the vaccine spectra at 3282 (NH₂ bound asymmetric stretching) and 1640 cm⁻¹ (C=N of purine and pyrimidine bases). Bands observed between 1400-2932 cm⁻¹ could correspond to various mechanisms of CH stretching. Further characteristic bands of DNA were identified exclusively in the Brand 1 vaccine spectra: bands at 832, 1110 and 1133 cm⁻¹ (C-O of deoxyribose ring), and 1209, 1267 and 1331 cm⁻¹ (C-NH₂) (Zhizhina and Oleinik, 1972).

The ATR-FTIR spectra of RNA sodium shared similar characteristic bands with the isolated DNA including phosphate groups at 1089 (strong symmetric PO₄⁻ stretching), 1221 (strong asymmetric PO₄⁻ stretching), 931, 1022 and 1055 cm⁻¹ (C-O-P stretching). Further similar characteristic bands at 1636 (OH in-plane bending), 915 (weak stretching of C-C ring), and 624 cm⁻¹ (C-O-C rocking) were observed. The nitrogenous bands present in DNA were also present in the RNA spectra at 1380 (NH out-of-plane bending), 2849 (weak NH stretching), 1363 (NH₂ out-of-plane bending) and 1562 cm⁻¹ (NH₂ in-plane bending). Various CH vibrations were observed at 798 (=C-H out-of-plane bending), 1463 (CH₃ in-plane bending) and 1437 cm⁻¹ (C-H in-plane bending). Bands at 831, 1106 and 1131 could result from C-C groups and bands at 953 and 984 cm⁻¹ corresponded to weak stretching of the C-O-C bond. An additional OH stretching band was identified at 3351 cm⁻¹ (Zhizhina and Oleinik, 1972).

The ATR-FTIR spectra of the Brand 2 vaccines showed similarities between the RNA sodium spectra, including bands at 926 and 1050 (weak and strong C-O-P stretching), 1735 (OH in-plane bending), 1456 (CH₃ in-plane bending) and 1423 cm⁻¹ (C-H in-

plane bending). The vaccine spectra showed similar bands to RNA at 832 and 1136 cm^{-1} . Characteristic nitrogenous bands were again observed at 1263 (NH bending out-of-plane), 2853 (NH stretching), 1376 (NH_2 bending out of plane), 1648 (C=N of purine and pyrimidine bases), 1209 and 1238 (weak stretching of C-NH₂). Stretching of the C-O-C ring was seen at 994 cm^{-1} as well as various CH vibrations at 799 (out-of-plane bending), 2925 (CH stretching), and C-C stretching at 832 and 1136 cm^{-1} . An additional OH stretching band was observed at 3337 cm^{-1} (Zhizhina and Oleinik, 1972). This band is key to distinguishing between the two nucleic acid-based vaccines. The OH stretching band exclusively present at 3351 and 3337 cm^{-1} in the RNA sodium and Brand 2 vaccine spectra is attributed to the additional hydroxyl group present in the ribose molecule of RNA and absent in the deoxyribose molecule of DNA.

Brand 3 vaccine spectra showed some similarities to the brand 1 and 2 vaccines including bands at 628 cm^{-1} (C-O-C rocking), 1068 cm^{-1} (C-O-P stretching), 1262 cm^{-1} (C-NH₂), 1649 cm^{-1} (C=N stretching) and 3306 cm^{-1} (OH stretching). Brand 4 spectra showed distinct similarities to the brand 2 vaccines, with all bands observed corresponding to bands observed in the brand 2 vaccine spectra.

2.3.2 Spectral Quality

Spectral quality showed strong IR activity for the majority of the brand 1 and 2 vaccine samples, demonstrated by the numerous absorption bands, maximum absorbance and high SNR values. Brand 1 obtained an average of 25 bands per spectra in comparison to 22, 9 and 19 for brands 2, 3 and 4 respectively (Table 2.4). The main excipients analysed showed between 18 and 59 absorption bands. The main excipients had a maxima absorbance ranging between 0.1458-0.6827 absorbance units. Nanoparticle-based excipient number 4 showed weaker IR activity, with a

maximum absorbance of 0.0975 absorbance units. However, signal intensity was not the only indicator of spectral quality, high SNR values were obtained for the brand 1 vaccine samples, ranging from 8.74 to 3919.9, with an average of 397.1. Brand 2 vaccines demonstrated weaker IR activity with an absorbance maxima of 0.1503 absorbance units, however, these samples obtained an average SNR of 1068.1.

Table 2.4. Values for spectral quality parameters of average spectra of each brand 1 vaccine measured using the PerkinElmer SpectrumTwo FTIR spectrometer equipped with ATR diamond holder

Vaccine	Brand	N	Max Peak Position (cm ⁻¹)	Max Absorbance (absorbance units)	SNR*	IR activity
LJMUCVIR460	1	25	982	0.78	671	strong
LJMUCVIR461	1	26	984	0.79	2105	strong
LJMUCVIR463	1	25	984	0.78	433	strong
LJMUCVIR464	1	25	984	0.79	381	strong
LJMUCVIR465	1	26	985	0.74	46	strong
LJMUCVIR466	1	24	984	0.80	258	strong
LJMUCVIR467	1	26	984	0.80	352	strong
LJMUCVIR468	1	25	985	0.73	234	strong
LJMUCVIR469	1	25	984	0.77	325	strong
LJMUCVIR472	1	25	985	0.77	954	strong
LJMUCVIR473	1	27	986	0.67	145	strong
LJMUCVIR474	1	25	984	0.78	847	strong

LJMUCVIR475	1	24	985	0.72	188	strong
LJMUCVIR477	1	26	984	0.68	366	strong
LJMUCVIR478	1	25	986	0.64	64	strong
LJMUCVIR499	1	24	986	0.70	183	strong
LJMUCVIR500	1	24	986	0.81	336	strong
LJMUCVIR501	1	25	986	0.73	80	strong
LJMUCVIR502	1	24	986	0.66	84	strong
LJMUCVIR503	1	25	985	0.76	658	strong
LJMUCVIR504	1	25	985	0.79	1092	strong
LJMUCVIR505	1	24	985	0.75	62	strong
LJMUCVIR506	1	25	985	0.79	1187	strong
LJMUCVIR507	1	24	984	0.78	154	strong
LJMUCVIR508	1	24	985	0.83	1019	strong
LJMUCVIR509	1	24	988	0.57	46	strong
LJMUCVIR510	1	24	984	0.77	600	strong
LJMUCVIR511	1	23	985	0.71	115	strong
LJMUCVIR512	1	24	985	0.76	792	strong
LJMUCVIR513	1	23	984	0.78	667	strong
LJMUCVIR514	1	26	984	0.80	1743	strong
LJMUCVIR515	1	24	988	0.52	13	strong
LJMUCVIR556	1	25	984	0.81	1841	strong
LJMUCVIR557	1	23	985	0.76	142	strong
LJMUCVIR558	1	23	985	0.77	344	strong
LJMUCVIR559	1	24	985	0.77	766	strong

LJMUCVIR560	1	23	985	0.74	83	strong
LJMUCVIR561	1	24	986	0.66	214	strong
LJMUCVIR562	1	25	986	0.72	68	strong
LJMUCVIR563	1	24	985	0.79	1342	strong
LJMUCVIR564	1	23	986	0.71	17	strong
LJMUCVIR565	1	25	984	0.76	250	strong
LJMUCVIR566	1	25	984	0.79	1447	strong
LJMUCVIR568	1	25	984	0.76	105	strong
LJMUCVIR569	1	25	984	0.78	315	strong
LJMUCVIR570	1	25	985	0.76	897	strong
LJMUCVIR571	1	24	986	0.74	160	strong
LJMUCVIR572	1	26	985	0.74	773	strong
LJMUCVIR573	1	24	984	0.78	931	strong
LJMUCVIR574	1	24	985	0.74	149	strong
LJMUCVIR575	1	24	985	0.75	35	strong
LJMUCVIR656	1	24	985	0.79	241	strong
LJMUCVIR658	1	23	984	0.80	241	strong
LJMUCVIR659	1	24	984	0.80	715	strong
LJMUCVIR660	1	23	985	0.78	66	strong
LJMUCVIR661	1	23	985	0.78	165	strong
LJMUCVIR662	1	23	986	0.69	114	strong
LJMUCVIR663	1	23	985	0.76	217	strong
LJMUCVIR664	1	24	984	0.82	1105	strong
LJMUCVIR665	1	24	984	0.79	457	strong

LJMUCVIR666	1	24	985	0.78	465	strong
LJMUCVIR667	1	24	985	0.77	315	strong
LJMUCVIR668	1	25	984	0.79	448	strong
LJMUCVIR669	1	23	986	0.72	87	strong
LJMUCVIR670	1	24	984	0.81	725	strong
LJMUCVIR673	1	25	984	0.78	307	strong
LJMUCVIR674	1	25	985	0.79	402	strong
LJMUCVIR675	1	24	984	0.81	570	strong
LJMUCVIR676	1	25	985	0.77	366	strong
LJMUCVIR677	1	25	985	0.72	96	strong
LJMUCVIR678	1	25	984	0.79	825	strong
LJMUCVIR679	1	24	985	0.79	421	strong
LJMUCVIR680	1	25	984	0.78	70	strong
LJMUCVIR681	1	25	986	0.70	305	strong
LJMUCVIR682	1	24	985	0.81	1665	strong
LJMUCVIR683	1	24	985	0.77	122	strong
LJMUCVIR684	1	24	985	0.74	95	strong
LJMUCVIR685	1	24	987	0.64	19	strong
LJMUCVIR686	1	26	986	0.71	18	strong
LJMUCVIR687	1	25	984	0.80	574	strong
LJMUCVIR688	1	25	986	0.73	54	strong
LJMUCVIR689	1	26	985	0.77	172	strong
LJMUCVIR690	1	25	986	0.74	26	strong
LJMUCVIR691	1	25	984	0.80	1474	strong

LJMUCVIR692	1	25	985	0.78	221	strong
LJMUCVIR693	1	25	985	0.72	52	strong
LJMUCVIR694	1	25	984	0.81	1063	strong
LJMUCVIR695	1	26	985	0.77	300	strong
LJMUCVIR696	1	25	984	0.77	91	strong
LJMUCVIR697	1	25	986	0.68	9	strong
LJMUCVIR699	1	25	984	0.80	1267	strong
LJMUCVIR700	1	26	985	0.77	239	strong
LJMUCVIR701	1	25	986	0.71	19	strong
LJMUCVIR702	1	24	984	0.83	67	strong
LJMUCVIR703	1	25	985	0.78	165	strong
LJMUCVIR704	1	24	983	0.82	201	strong
LJMUCVIR705	1	24	986	0.68	50	strong
LJMUCVIR706	1	25	985	0.74	78	strong
LJMUCVIR707	1	24	984	0.80	267	strong
LJMUCVIR708	1	26	985	0.74	25	strong
LJMUCVIR709	1	25	985	0.75	55	strong
LJMUCVIR710	1	23	984	0.81	383	strong
LJMUCVIR711	1	25	984	0.82	3920	strong
LJMUCVIR712	1	25	984	0.77	144	strong
LJMUCVIR713	1	24	984	0.81	135	strong
LJMUCVIR714	1	25	985	0.72	183	strong
LJMUCVIR715	1	25	984	0.81	622	strong
LJMUCVIR716	1	25	985	0.75	37	strong

LJMUCVIR717	1	25	985	0.72	129	strong
LJMUCVIR718	1	24	984	0.82	395	strong
LJMUCVIR719	1	25	985	0.75	50	strong
LJMUCVIR720	1	25	985	0.72	80	strong
LJMUCVIR722	1	25	984	0.76	202	strong
LJMUCVIR723	1	25	984	0.76	181	strong
LJMUCVIR724	1	25	986	0.74	118	strong
LJMUCVIR725	1	24	984	0.73	69	strong
LJMUCVIR726	1	24	984	0.81	21	strong
LJMUCVIR727	1	25	984	0.78	42	strong
LJMUCVIR728	1	24	986	0.74	695	strong
LJMUCVIR729	1	24	986	0.70	73	strong
LJMUCVIR730	1	24	985	0.78	80	strong
LJMUCVIR731	1	25	985	0.75	103	strong
LJMUCVIR732	1	24	985	0.71	361	strong
LJMUCVIR733	1	25	985	0.72	54	strong
LJMUCVIR734	1	24	984	0.78	108	strong
LJMUCVIR735	1	25	985	0.78	777	strong
LJMUCVIR736	1	25	986	0.71	10	strong
LJMUCVIR737	1	25	986	0.73	82	strong
LJMUCVIR738	1	25	985	0.78	254	strong
LJMUCVIR739	1	25	985	0.77	67	strong
LJMUCVIR740	1	25	985	0.75	136	strong
LJMUCVIR741	1	24	984	0.81	1052	strong

LJMUCVIR742	1	25	985	0.78	315	strong
LJMUCVIR743	1	25	985	0.74	132	strong
LJMUCVIR744	1	24	985	0.71	341	strong
LJMUCVIR745	1	25	985	0.67	288	strong
LJMUCVIR746	1	25	984	0.79	528	strong
LJMUCVIR747	1	25	986	0.76	144	strong
LJMUCVIR748	1	24	985	0.80	671	strong
LJMUCVIR750	1	25	985	0.80	673	strong
LJMUCVIR751	1	24	985	0.77	415	strong
LJMUCVIR753	1	24	984	0.81	2221	strong
LJMUCVIR754	1	24	984	0.80	181	strong
LJMUCVIR755	1	25	984	0.79	119	strong
LJMUCVIR756	1	24	985	0.76	280	strong
LJMUCVIR757	1	25	984	0.78	252	strong
LJMUCVIR758	1	25	985	0.75	391	strong
LJMUCVIR759	1	24	985	0.75	554	strong
LJMUCVIR760	1	24	985	0.54	245	strong
LJMUCVIR761	1	24	985	0.78	259	strong
LJMUCVIR762	1	24	985	0.77	171	strong
LJMUCVIR763	1	25	985	0.76	103	strong
LJMUCVIR764	1	25	985	0.71	130	strong
LJMUCVIR765	1	25	985	0.79	173	strong
LJMUCVIR767	1	25	985	0.74	147	strong
LJMUCVIR768	1	25	985	0.78	372	strong

LJMUCVIR769	1	24	985	0.62	197	strong
LJMUCVIR770	1	24	985	0.75	93	strong
LJMUCVIR771	1	24	984	0.81	444	strong
LJMUCVIR772	1	23	988	0.58	59	strong
LJMUCVIR773	1	24	985	0.79	353	strong
LJMUCVIR774	1	25	985	0.78	324	strong

Table 2.5 Values for spectral quality parameters of average spectra of each brand 2 vaccine measured using the PerkinElmer SpectrumTwo FTIR spectrometer equipped with ATR diamond holder

Vaccine	Brand	N	Max peak position (cm ⁻¹)	Max absorbance (absorbance units)	SNR*	IR activity
LJMUCVIR365	2	25	1049	0.05	336	medium
LJMUCVIR366	2	23	1051	0.07	1236	medium
LJMUCVIR367	2	24	1048	0.13	1071	strong
LJMUCVIR368	2	24	1049	0.12	118	medium
LJMUCVIR370	2	23	1051	0.06	957	medium
LJMUCVIR371	2	24	1052	0.06	627	medium
LJMUCVIR372	2	23	1051	0.06	395	medium
LJMUCVIR373	2	21	1051	0.04	656	medium
LJMUCVIR824	2	23	1049	0.05	929	medium
LJMUCVIR839	2	22	1049	0.04	699	medium

LJMUCVIR858	2	22	1047	0.07	1177	medium
LJMUCVIR867	2	23	1048	0.04	761	medium
LJMUCVIR875	2	25	1046	0.18	1781	medium
LJMUCVIR883	2	22	1048	0.12	2109	medium
LJMUCVIR886	2	23	1050	0.03	446	medium
LJMUCVIR898	2	23	1048	0.06	626	medium
LJMUCVIR899	2	22	1049	0.06	1066	medium
LJMUCVIR978	2	22	1051	0.05	834	medium
LJMUCVIR997	2	23	1050	0.05	829	medium
LJMUCVIR998	2	22	1048	0.06	995	medium
LJMUCVIR999	2	25	1049	0.15	306	medium
LJMUCVIR1000	2	24	1050	0.04	662	medium
LJMUCVIR1001	2	23	1051	0.04	647	medium
LJMUCVIR1002	2	24	1050	0.04	387	medium
LJMUCVIR1003	2	22	1050	0.05	872	medium
LJMUCVIR1004	2	24	1050	0.06	994	medium
LJMUCVIR1005	2	22	1051	0.04	609	medium
LJMUCVIR1007	2	22	1051	0.04	607	medium
LJMUCVIR1008	2	22	1051	0.03	449	medium
LJMUCVIR1009	2	25	1050	0.06	1075	medium
LJMUCVIR1010	2	23	1051	0.04	745	medium
LJMUCVIR1011	2	23	986	0.62	259	medium
LJMUCVIR1012	2	22	1048	0.18	1793	medium
LJMUCVIR1013	2	21	1051	0.06	978	medium

LJMUCVIR1014	2	24	1049	0.04	712	medium
LJMUCVIR1142	2	22	1050	0.10	1669	medium
LJMUCVIR1178	2	21	1049	0.14	1195	medium
LJMUCVIR1207	2	23	1049	0.13	733	medium
LJMUCVIR1209	2	22	1048	0.23	1482	medium
LJMUCVIR1215	2	23	1049	0.08	1472	medium
LJMUCVIR1219	2	23	987	0.56	521	medium
LJMUCVIR990	2	25	1049	0.06	409	medium
LJMUCVIR991	2	23	1051	0.06	995	medium
LJMUCVIR992	2	27	1051	0.02	418	medium
LJMUCVIR993	2	26	1050	0.06	482	medium
LJMUCVIR994	2	26	1050	0.05	790	medium
LJMUCVIR995	2	23	1050	0.05	833	medium
LJMUCVIR996	2	22	1050	0.04	704	medium
LJMUCVIR980	2	22	1049	0.05	850	medium
LJMUCVIR981	2	24	1049	0.03	592	medium
LJMUCVIR982	2	23	1049	0.05	876	medium
LJMUCVIR983	2	23	1049	0.04	697	medium
LJMUCVIR984	2	22	1050	0.03	528	medium
LJMUCVIR985	2	23	1049	0.05	822	medium
LJMUCVIR986	2	21	1052	0.02	375	medium
LJMUCVIR987	2	20	1050	0.03	532	medium
LJMUCVIR988	2	20	1049	0.07	1126	medium
LJMUCVIR989	2	22	987	0.59	121	medium

LJMUCVIR979	2	20	1051	0.03	567	medium
LJMUCVIR908	2	22	1049	0.07	1262	medium
LJMUCVIR912	2	23	1052	0.07	1225	medium
LJMUCVIR919	2	23	1050	0.03	576	medium
LJMUCVIR920	2	23	1049	0.05	470	medium
LJMUCVIR925	2	24	1050	0.03	460	medium
LJMUCVIR929	2	24	1048	0.04	643	medium
LJMUCVIR930	2	23	1050	0.05	917	medium
LJMUCVIR931	2	23	1050	0.02	430	medium
LJMUCVIR932	2	23	1050	0.05	826	medium
LJMUCVIR933	2	23	1051	0.04	676	medium
LJMUCVIR934	2	23	1050	0.03	473	medium
LJMUCVIR935	2	21	1047	0.05	816	medium
LJMUCVIR936	2	23	1051	0.05	905	medium
LJMUCVIR937	2	23	1051	0.06	1004	medium
LJMUCVIR938	2	22	1049	0.07	715	medium
LJMUCVIR939	2	23	3333	0.13	0.87	strong
LJMUCVIR940	2	21	988	0.53	178	medium
LJMUCVIR941	2	22	1048	0.06	998	medium
LJMUCVIR942	2	23	3340	0.02	275	medium
LJMUCVIR943	2	22	1052	0.05	857	medium
LJMUCVIR944	2	21	1050	0.05	782	medium
LJMUCVIR945	2	21	1051	0.03	533	medium
LJMUCVIR946	2	21	1048	0.02	394	medium

LJMUCVIR947	2	21	1051	0.04	730	medium
LJMUCVIR948	2	21	1050	0.09	994	medium
LJMUCVIR953	2	23	1049	0.03	477	medium
LJMUCVIR954	2	22	1048	0.04	755	medium
LJMUCVIR955	2	22	1048	0.07	699	medium
LJMUCVIR956	2	24	1049	0.04	668	medium
LJMUCVIR957	2	22	987	0.55	350	medium
LJMUCVIR958	2	23	1050	0.03	586	medium
LJMUCVIR959	2	22	1049	0.07	573	medium
LJMUCVIR960	2	23	1049	0.05	786	medium
LJMUCVIR961	2	23	1051	0.03	487	medium
LJMUCVIR962	2	21	1049	0.10	1809	medium
LJMUCVIR963	2	21	987	0.55	441	medium
LJMUCVIR964	2	22	1046	0.06	1061	medium
LJMUCVIR965	2	22	1049	0.05	926	medium
LJMUCVIR966	2	23	1048	0.04	330	medium
LJMUCVIR967	2	21	988	0.56	2419	medium
LJMUCVIR968	2	23	1048	0.03	515	medium
LJMUCVIR969	2	23	1048	0.03	443	medium
LJMUCVIR970	2	22	1051	0.07	1288	medium
LJMUCVIR971	2	22	1050	0.05	793	medium
LJMUCVIR972	2	22	1049	0.10	29	medium
LJMUCVIR973	2	22	1050	0.05	803	medium
LJMUCVIR974	2	22	1050	0.05	848	medium

LJMUCVIR975	2	21	1050	0.05	917	medium
LJMUCVIR976	2	24	1050	0.04	729	medium
LJMUCVIR977	2	24	1050	0.03	468	medium
LJMUCVIR950	2	22	1049	0.08	1460	medium
LJMUCVIR951	2	23	3333	0.13	0.83	medium
LJMUCVIR952	2	22	1050	0.05	917	medium
LJMUCVIR1226	2	22	1049	0.07	1284	medium
LJMUCVIR1228	2	22	1050	0.08	1363	medium
LJMUCVIR1238	2	23	1049	0.06	993	medium
LJMUCVIR1241	2	23	3333	0.12	0.80	medium
LJMUCVIR1242	2	21	986	0.62	1021	medium
LJMUCVIR1244	2	21	988	0.55	1078	medium
LJMUCVIR1245	2	21	986	0.57	1363	medium
LJMUCVIR1251	2	22	1049	0.13	853	medium
LJMUCVIR1253	2	22	1051	0.08	1466	medium
LJMUCVIR1256	2	21	988	0.54	1054	medium
LJMUCVIR1258	2	21	987	0.58	109	medium
LJMUCVIR1270	2	21	1048	0.25	2200	medium
LJMUCVIR1276	2	22	1051	0.07	1201	medium
LJMUCVIR1277	2	23	1050	0.07	564	medium
LJMUCVIR1278	2	22	1049	0.09	945	medium
LJMUCVIR1279	2	23	1049	0.10	486	medium
LJMUCVIR1280	2	23	1049	0.05	844	medium
LJMUCVIR1281	2	23	1050	0.04	357	medium

LJMUCVIR1282	2	22	1049	0.11	178	strong
LJMUCVIR1283	2	23	1050	0.03	327	medium
LJMUCVIR1284	2	23	1049	0.09	1066	medium
LJMUCVIR1285	2	24	1048	0.23	268	strong
LJMUCVIR1286	2	23	1047	0.05	932	medium
LJMUCVIR1287	2	22	1048	0.09	366	medium
LJMUCVIR1288	2	23	1049	0.05	359	medium
LJMUCVIR1289	2	23	1049	0.05	487	medium
LJMUCVIR1290	2	22	1048	0.04	243	medium
LJMUCVIR1291	2	22	1050	0.03	598	medium
LJMUCVIR1292	2	22	1049	0.06	999	medium
LJMUCVIR1293	2	23	1051	0.06	1242	medium
LJMUCVIR1294	2	22	1052	0.07	490	medium
LJMUCVIR1295	2	22	1050	0.04	4	medium
LJMUCVIR1296	2	23	1050	0.04	633	medium
LJMUCVIR1297	2	22	1049	0.09	101	medium
LJMUCVIR1298	2	22	1049	0.07	1141	medium
LJMUCVIR1299	2	21	1051	0.03	462	medium
LJMUCVIR1300	2	23	3352	0.06	3	medium
LJMUCVIR1301	2	23	1050	0.03	472	medium
LJMUCVIR1302	2	23	1050	0.05	845	medium
LJMUCVIR1303	2	22	1049	0.04	748	medium
LJMUCVIR1304	2	22	1050	0.05	869	medium
LJMUCVIR1305	2	23	1050	0.05	905	medium

LJMUCVIR1306	2	23	1048	0.06	1030	medium
LJMUCVIR1307	2	23	1049	0.06	30	medium
LJMUCVIR1308	2	21	1049	0.07	1253	medium
LJMUCVIR1309	2	23	1049	0.05	1001	medium
LJMUCVIR1310	2	22	1049	0.08	1457	medium
LJMUCVIR1311	2	21	1048	0.11	1868	medium
LJMUCVIR1312	2	21	1048	0.05	876	medium
LJMUCVIR1313	2	22	1049	0.05	968	medium
LJMUCVIR1314	2	21	1050	0.06	1014	medium
LJMUCVIR1315	2	21	1050	0.08	256	medium
LJMUCVIR1316	2	21	1051	0.04	673	medium
LJMUCVIR1350	2	22	2923	0.03	456	medium
LJMUCVIR1354	2	20	1055	0.06	1047	medium
LJMUCVIR1355	2	20	1100	0.02	285	medium
LJMUCVIR135	2	21	986	0.61	118	strong
LJMUCVIR1366	2	20	2922	0.01	6x10 ¹⁵	medium
LJMUCVIR1367	2	21	1055	0.04	169	medium
LJMUCVIR1368	2	21	1051	0.07	1236	medium
LJMUCVIR1369	2	21	1056	0.03	66	medium
LJMUCVIR1370	2	22	1055	0.04	641	medium

Table 2.6. Values for spectral quality parameters of average spectra of each brand 3 vaccine measured using the PerkinElmer SpectrumTwo FTIR spectrometer equipped with ATR diamond holder

Vaccine	Brand	N	Max Peak Position (cm ⁻¹)	Max Absorbance (absorbance units)	SNR*	IR activity
LJMUCVIR1348	3	9	1092	0.016	174	weak
LJMUCVIR1349	3	11	477	0.021	109	weak
LJMUCVIR1352	3	10	1091	0.019	400	weak
LJMUCVIR1353	3	8	476	0.032	46	weak
LJMUCVIR1356	3	9	1081	0.018	381	weak
LJMUCVIR1357	3	10	1073	0.010	203	weak
LJMUCVIR1358	3	13	475	0.025	311	weak
LJMUCVIR1359	3	14	1090	0.027	110	weak
LJMUCVIR1360	3	14	1090	0.022	150	weak
LJMUCVIR1362	3	11	1083	0.025	300	weak
LJMUCVIR1363	3	8	476	0.055	444	weak
LJMUCVIR1364	3	10	1074	0.016	337	weak
LJMUCVIR1365	3	10	1090	0.020	250	weak
LJMUCVIR1371	3	11	1087	0.009	110	weak
LJMUCVIR1372	3	9	3306	0.013	267	weak
LJMUCVIR1374	3	8	799	0.012	147	weak
LJMUCVIR1375	3	10	1069	0.009	201	weak

LJMUCVIR1376	3	7	1024	0.002	35	weak
LJMUCVIR1378	3	4	1068	0.001	27	weak
LJMUCVIR1379	3	7	1072	0.005	99	weak
LJMUCVIR1381	3	5	1074	0.008	162	weak
LJMUCVIR1387	3	3	1081	0.002	52	weak
LJMUCVIR1389	3	7	799	0.003	31	weak
LJMUCVIR1390	3	10	1086	0.002	39	weak
LJMUCVIR1392	3	7	798	0.003	71	weak
LJMUCVIR1393	3	12	1084	0.016	347	weak
LJMUCVIR1394	3	10	1072	0.009	64	weak
LJMUCVIR1396	3	9	1069	0.007	152	weak
LJMUCVIR1397	3	8	1073	0.008	168	weak
LJMUCVIR1398	3	7	3356	0.006	14	weak
LJMUCVIR1399	3	9	1073	0.006	131	weak
LJMUCVIR1400	3	6	1070	0.005	101	weak
LJMUCVIR1401	3	6	2920	0.012	243	weak
LJMUCVIR1403	3	7	800	0.005	101	weak
LJMUCVIR1404	3	8	3376	0.010	3	weak
LJMUCVIR1405	3	6	1083	0.005	59	weak
LJMUCVIR1406	3	8	3362	0.016	30	weak
LJMUCVIR1407	3	7	1067	0.012	245	weak
LJMUCVIR1408	3	4	796	0.001	18	weak
LJMUCVIR1409	3	8	3357	0.015	23	weak
LJMUCVIR1410	3	13	484	0.025	34	weak

LJMUCVIR1411	3	6	1073	0.006	118	weak
LJMUCVIR1412	3	10	3324	0.011	74	weak
LJMUCVIR1413	3	9	799	0.010	204	weak
LJMUCVIR1414	3	4	1064	0.003	54	weak
LJMUCVIR1415	3	7	1090	0.008	177	weak
LJMUCVIR1416	3	6	799	0.013	34	weak
LJMUCVIR1417	3	13	2981	0.018	10	weak
LJMUCVIR1418	3	8	1066	0.010	211	weak
LJMUCVIR1419	3	9	1060	0.014	276	weak
LJMUCVIR1420	3	9	1073	0.010	213	weak
LJMUCVIR1421	3	8	1090	0.013	270	weak

Table 2.7. Values for spectral quality parameters of average spectra of each brand 4 vaccine measured using the PerkinElmer SpectrumTwo FTIR spectrometer equipped with ATR diamond holder

Brand	N	Max peak position (cm ⁻¹)	Max absorbance (absorbance units)	SNR*	IR activity
LJMUCVIR1422	18	1049	0.05	1108	medium
LJMUCVIR1424	19	1049	0.03	196	medium
LJMUCVIR1425	19	1049	0.06	248	medium
LJMUCVIR1426	19	1048	0.03	223	medium
LJMUCVIR1427	20	1047	0.08	961	medium
LJMUCVIR1428	19	1020	0.07	653	medium

³ * at maximum peak position
N = number of bands

2.3.3 Authentication of vaccines by ATR-FTIR spectroscopy

For vaccine authentication, unsupervised clustering was applied to the vaccine and their constituents' spectra using PCA. Type I and II errors were used to evaluate the accuracy of the clustering. Type I errors were observed when the PC scores of a vaccine brand were clustered away from the majority of that brand. Type II errors were observed when the PC scores of a vaccine brand were clustered with the PC scores of another brand.

Three unsupervised clustering models were applied across three different wavenumber ranges to assess the variance at different regions:

- The full range of 450-4000 cm^{-1}
- 450 – 1850 cm^{-1}
- 2500 – 4000 cm^{-1}

No significant bands were observed in the vaccine spectra between 1850 – 2000 cm^{-1} so this range was not included.

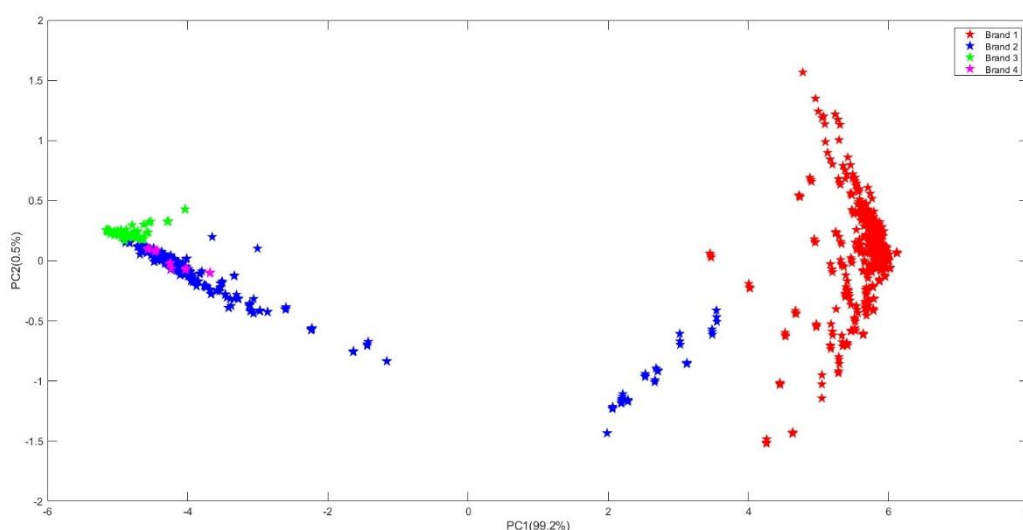


Figure 2.3. PC scores plot of Covid-19 Vaccine brands 1 (red), 2 (blue), 3 (green) and 4 (pink) measured using the PerkinElmer SpectrumTwo FTIR spectrometer equipped with ATR diamond holder across a range of 450-4000 cm^{-1}

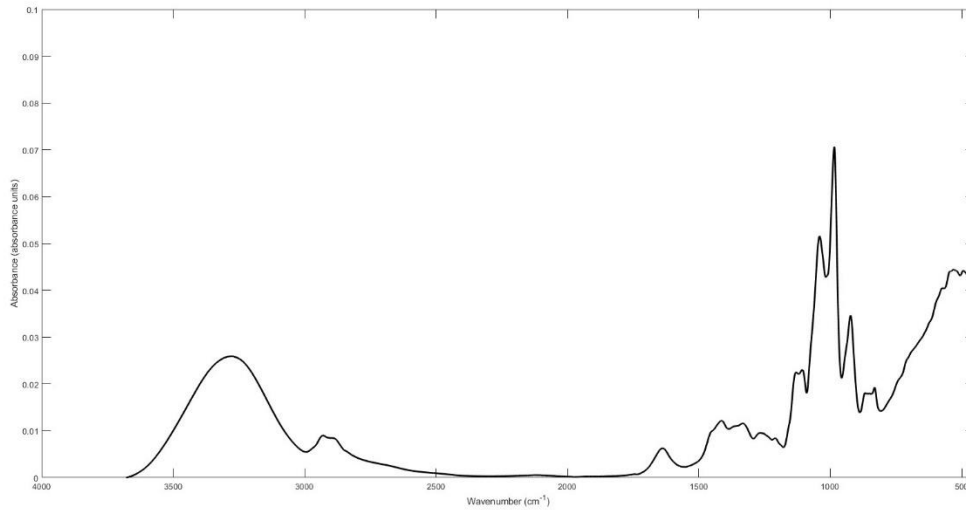


Figure 2.4. PC1 loading plot of vaccine brands 1, 2, 3 and 4 across a wavenumber range of 450-4000 cm^{-1}

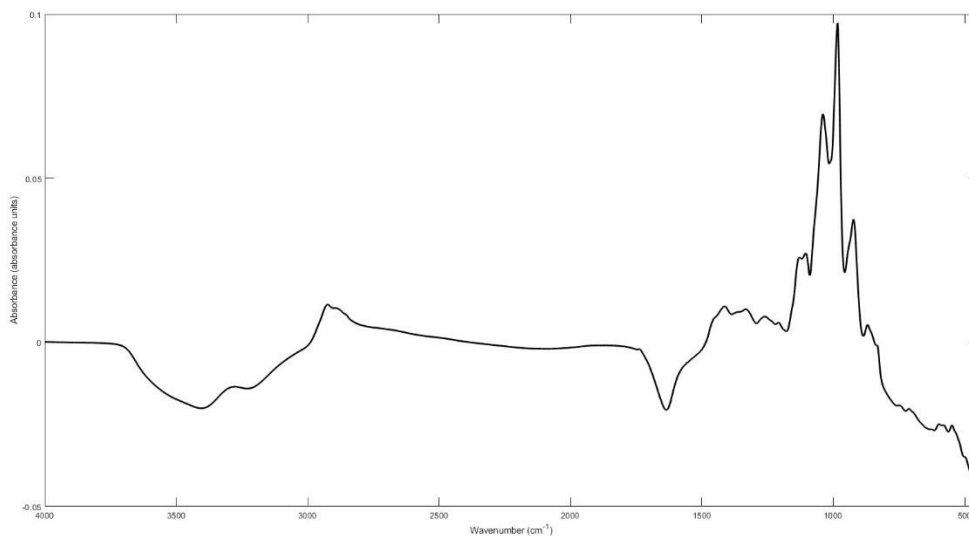


Figure 2.5 PC2 loading plot of vaccine brands 1, 2, 3 and 4 across a wavenumber range of 450-4000 cm^{-1}

Figure 2.3 shows the PC scores plot of the four vaccine brands across the full range of 450-4000 cm^{-1} . Brands 1 and 2 showed high contribution to the variance demonstrated by their spatial position at PC1 that reflected 99.2% of the variance

observed (Figure 2.3). Examination of PC1 loading (Figure 2.4) showed significant bands from both of the nucleic acids measured. PC2 loading showed other spectral bands that contributed to only 0.5% of the variance in the data (Figure 2.5). The PCA scores plot showed four main populations, with the mRNA-based brand 4 vaccines clustered with the brand 2 mRNA-based vaccines, these vaccines are manufactured by the same license holder and clustered together due to their spectral similarities and formulation. Brand 1 DNA-based vaccines clustered separately with some Type II errors observed for brand 2 vaccines which were clustered nearby. No Type I or II error was observed between brands 3 and 4. Errors observed for brand 2 vaccine spectra are attributed to variation in absorbance values within that dataset rather than band position, samples received were of low volume (< 0.45ml) and reconstituted in saline for measurement which further reduced the concentration and signal intensity.

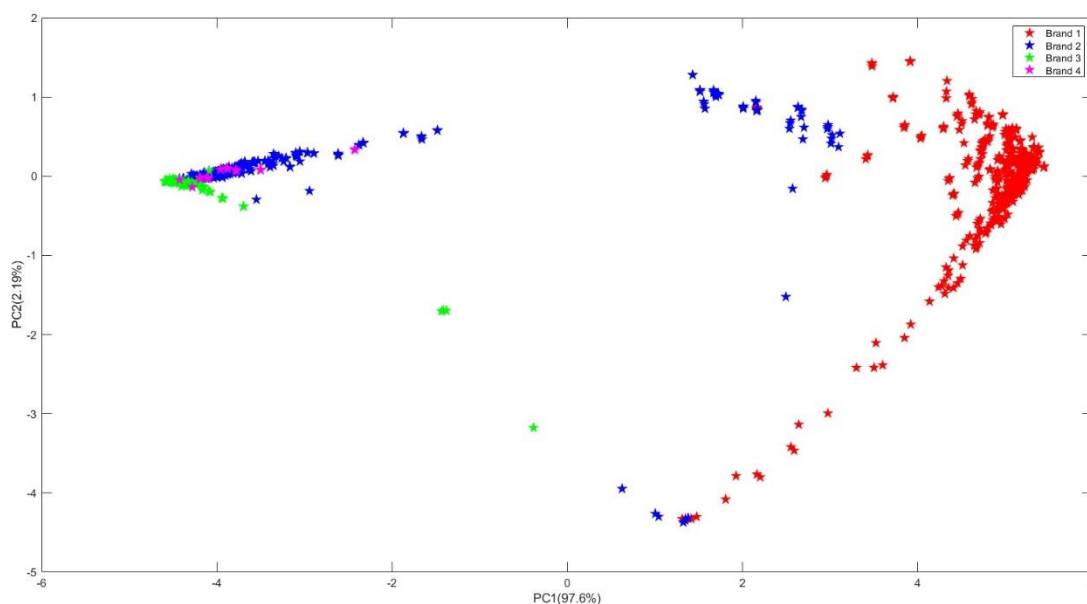


Figure 2.6 PC scores plot of Covid-19 Vaccine brands 1 (red), 2 (blue), 3 (green) and 4 (pink) measured using the PerkinElmer SpectrumTwo FTIR spectrometer equipped with ATR diamond holder across a range of 450-1850 cm^{-1}

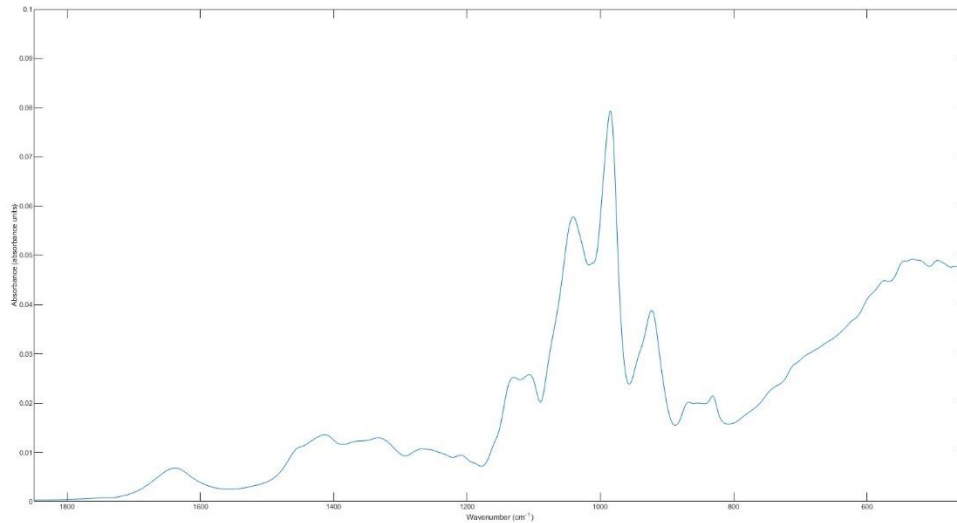


Figure 2.7 PC1 loading plot of vaccine brands 1, 2, 3 and 4 across a wavenumber range of 450-1850 cm^{-1}

Figure 2.6 shows the PC scores plot of the four vaccine brands across a shorter wave of 450-1850 cm^{-1} . Brand 1 showed the highest contribution to the variance demonstrated by its spatial position at PC1 which contributed to 97.6% of the variance. PC1 loading (Figure 2.7) showed significant bands observed in the nucleic acid-based vaccine spectra. PC2 loading showed other bands that only contributed to 2.19% of the variance. Increased type II errors were observed between brand 1 and 2 vaccines in the 450-1850 cm^{-1} range where scores overlapped, indicating spectral similarities between the brands in this region. Type I errors were observed for brand 3 vaccines where scores were clustered away from their major population, this suggests more significant variation in brand 3 spectra in this range.

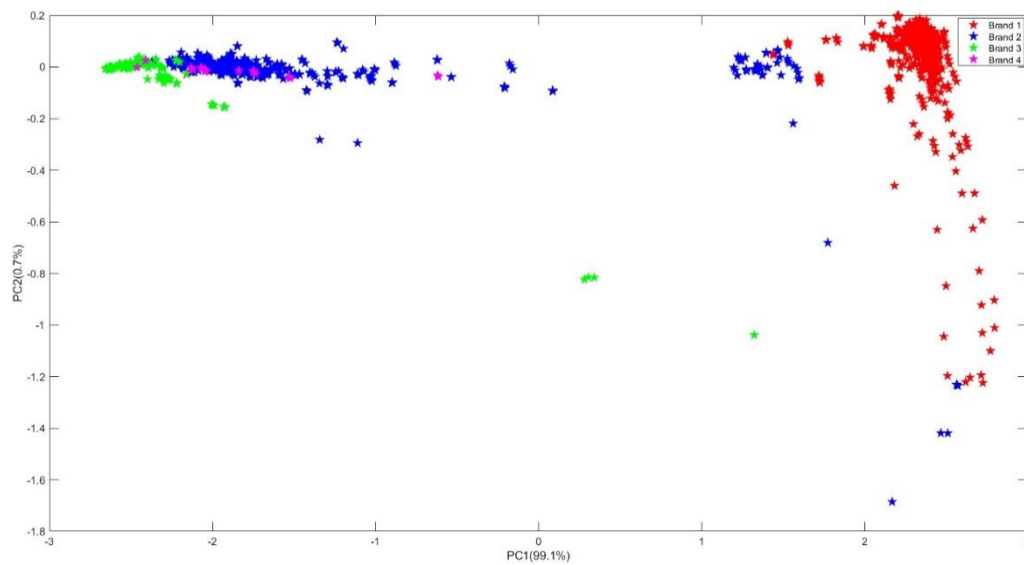


Figure 2.8 PC scores plot of Covid-19 Vaccine brands 1 (red), 2 (blue), 3 (green) and 4 (pink) measured using the PerkinElmer SpectrumTwo FTIR spectrometer equipped with ATR diamond holder across a range of 2500-4000 cm^{-1}

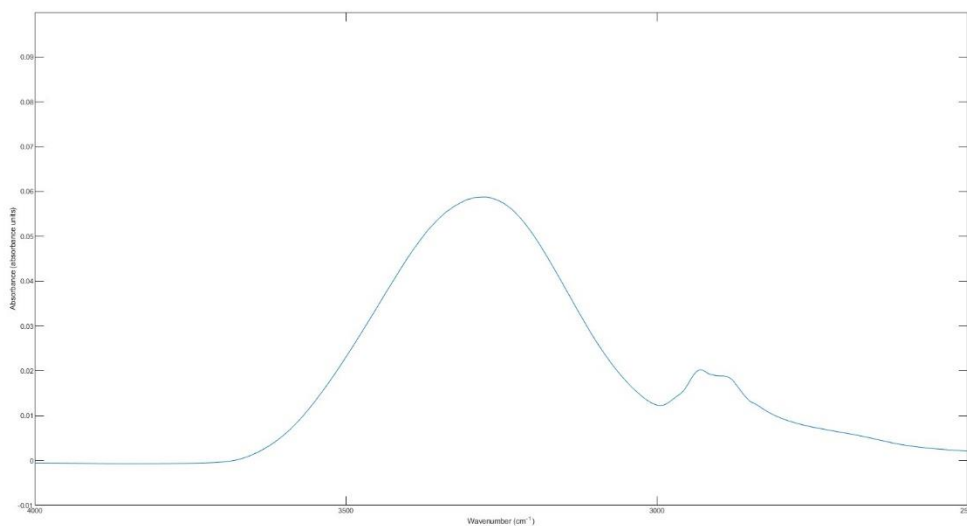


Figure 2.9 PC1 loading plot of vaccine brands 1, 2, 3 and 4 across a wavenumber range of 2500-4000 cm^{-1}

Figure 2.8 shows the PC scores plot of the four vaccine brands in the range of 2500-4000 cm^{-1} . Brand 1 showed the greatest contribution to variance in the dataset again demonstrated by its spatial position at PC1 which accounted for 99.1% of variance. PC1 loading showed significant contribution from the RNA sodium spectra and mRNA-based vaccines including the OH stretching band around 3350 cm^{-1} and NH stretching around 2850 cm^{-1} . The PC scores plot showed more distinct clustering than the 450-1850 cm^{-1} range with brand 1 and 2 vaccines clustered together more tightly. Type II errors were still observed for both brands respectively, with overlap between the scores of both brand 1 and 2 vaccines on the model. Type II errors were observed for the brand 4 vaccines, which scores were entirely clustered with the scores of the brand 2 vaccines, indicating the physiochemical similarities between the two lies in the 2500-4000 cm^{-1} region. Type I error was encountered in the brand 3 vaccines again with a small population clustered away from the main group. Overall, the 450-4000 cm^{-1} range obtained the least type I and II errors and most distinct clustering, indicating a preferable wavenumber range for separation capacity and identification potential.

2.3.4 Vaccine Classification

Model 2.24

True Class	Brand 1	422	2	
	Brand 2	1	436	
	Brand 3	1	128	1
	Brand 4	1	1	15
	Brand 1	Brand 2	Brand 3	Brand 4
	Predicted Class			

Figure 2.10 Confusion matrix for Ensemble subspace K-nearest neighbour classification model 6-fold validation trained using Matlab 2023b classification learner and spectral dataset from vaccine brands 1, 2, 3 and 4

Supervised machine learning techniques were used to establish the identification potential of the method. An Ensemble subspace KNN classification model was trained using Matlab 2023b classification learner tool. The model was trained using 80% of

the spectral dataset with an unseen 20% allocated as a test dataset to evaluate the model for overfitting (Ying, 2019). The training dataset was divided into four ‘classes’ – brands 1, 2, 3 and 4 and classes were predicted based on absorbance values at each data point across a range of 450-4000cm⁻¹. Figure 2.10 shows the confusion matrix for the 6-fold validation dataset which obtained an accuracy of 99.3%. One Type I error and 2 Type II errors were observed for brand 1 vaccines (Figure 2.10). Brands 2 and 4 obtained type I and II errors against each other (Figure 2.10), attributed to their significantly similar spectral qualities resulting from their common constituent nucleic acid, excipients and manufacturer. Liquid vaccine samples that were not allowed sufficient time to dry on the detector experienced spectral interference from a broad OH stretching band that obscured the vaccines’ signal at around 3000cm⁻¹ regardless of brand. Spectra that were entirely inhibited by the presence of this water band appeared almost identical, resulting in misclassification amongst these samples. Hence, the optimal method is to allow sufficient time for evaporation of sample moisture content prior to measurement.

Table 2.8. Accuracy, precision, recall, specificity and F1-score of Ensemble subspace KNN classification model for vaccine brands 1-4 and overall

Brand	Accuracy (%)	Precision (%)	Recall (%)	Specificity (%)	F1-Score
1	99.7	99.8	99.5	99.8	0.997
2	99.7	99.5	99.8	99.7	0.997
3	99.5	97.7	98.5	99.7	0.981
4	99.7	93.8	88.2	99.9	0.909
Overall	99.7	97.7	96.5	99.8	0.971

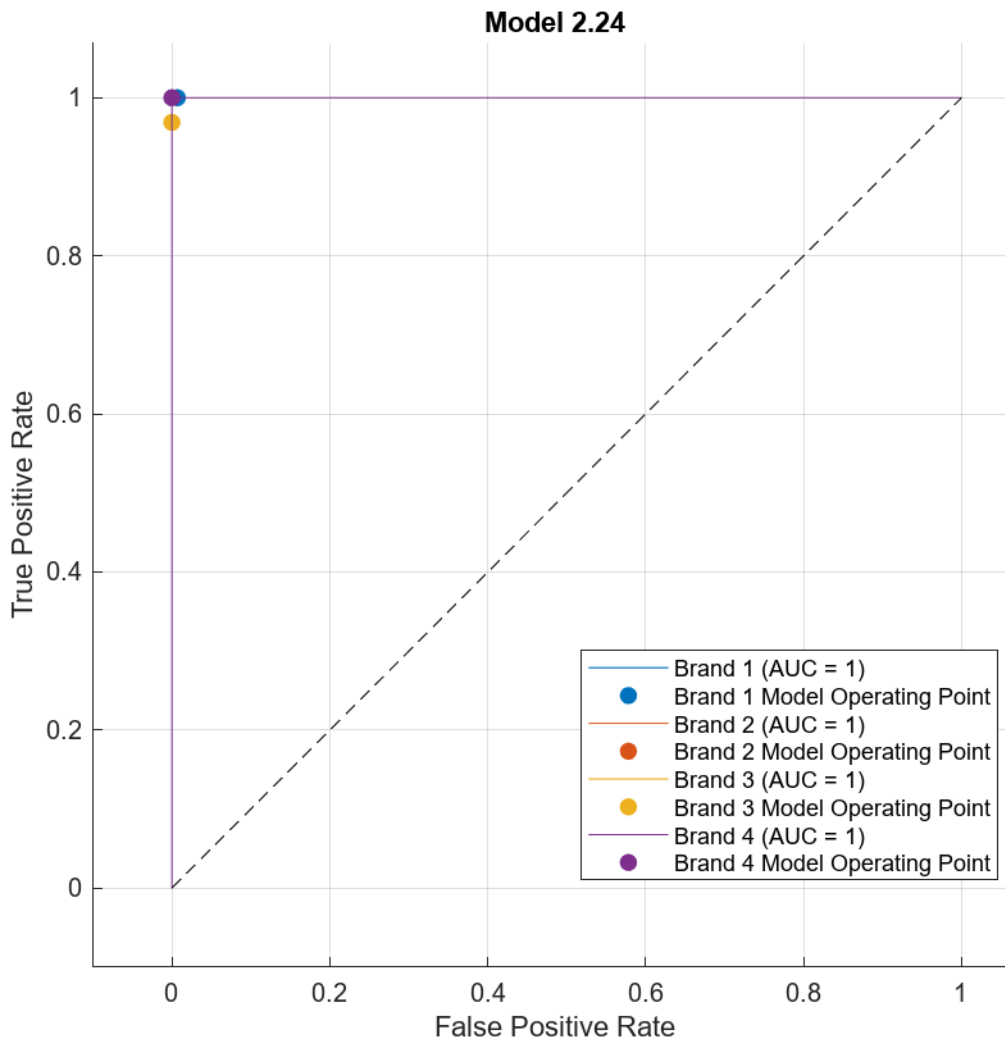


Figure 2.11 AUC-ROC curve for the test dataset of Ensemble subspace K-nearest neighbour classification model carried out on vaccine brands 1 (blue), 2 (red), 3 (yellow) and 4 (purple)

An AUC-ROC curve was used to evaluate the separation capacity of the model. The ROC curve maps the relationship between true positive rate (TPR) and true negative rate (TNR) (precision/recall) and the AUC is the area under the curve, which represents the ability of the model to distinguish between classes correctly. An AUC value of 1 indicates perfect separation capacity of the model with no errors made between class distinction. An AUC-ROC curve was drawn from both the 6-fold validation dataset and the 20% test dataset, to evaluate the separation capacity of the model when presented with unsupervised learning.

Figure 2.11 shows the AUC-ROC curve for the results of the Ensemble subspace KNN classification model trained on the 6-fold validation dataset and then tested on the allocated test dataset. The AUC value for every class (brand) in this test was 1, demonstrating the potential of the model to distinguish between vaccine classes with no errors.

2.4 Conclusion

In conclusion, this chapter demonstrates the effectiveness of ATR-FTIR spectroscopy as a valuable tool for the authentication of Covid-19 vaccines. The vaccine spectra featured bands corresponding to their component nucleic acids and were discriminable by their constituent-specific bands. Spectral quality showed strong IR activity in terms of number of bands and SNR for the majority of the measured vaccines. Clustering based on PCA showed accuracy in differentiating between vaccine brands, and this was further demonstrated by the performance of the Ensemble subspace KNN classification model, which yielded 99.7% accuracy in characterisation of vaccine class based on spectral properties. KNN outperformed PCA, especially considering the imbalance of brand representation in the data; however, considering this application in a real-life scenario, future work could involve data augmentation techniques for balancing the dataset. The AUC-ROC curve showed perfect separation capacity for the model indicating a potential for the use of MLAs in conjunction with portable ATR-FTIR spectroscopy as a robust, reliable and semi-automated process of vaccine authentication in the future. By leveraging MLAs and ATR-FTIR spectroscopy, this technology plays a crucial role in mitigating the prevalence and risks associated with SF vaccines, especially in lower- and middle-

income countries where the impact of substandard vaccines is more pronounced. The combination of these advanced techniques provides a powerful tool for ensuring the authenticity of vaccines.

3. AUTHENTICATION OF TRADITIONAL AND NOVEL ANTI- INFECTIVES USING HANDHELD SURFACE-ENHANCED RAMAN SPECTROSCOPY

3.1 Introduction

As discussed in section 2.1, Covid-19 is a novel coronavirus that established a global pandemic in 2019 causing millions of fatalities. Accelerated vaccination programmes successfully achieved population immunity and reduced the transmission of the virus. Nowadays, its virulence is controlled through regular vaccination programmes similar to the influenza vaccination drives. However, the success of these vaccination programmes is threatened by the prevalence of substandard and falsified (SF) Covid-19 vaccines, particularly in lower and middle-income countries (LMICs).

SF vaccines, particularly those being used in such a large-scale effort to control the virus highlights a need for implementation of an authentication and quality control procedure for vaccines in public supply. The development of a vaccine identification method to aid in the detection of SF products involves the characterisation of both the vaccines' chemical constituents and their physical properties. Most traditional analytical methods (such as liquid chromatography) do not satisfy the aforementioned need for synchronous characterisation of both chemical and physical properties and are also expensive and time consuming. Vibrational spectroscopy addresses the limitations of traditional techniques in its ability to provide rapid, non-destructive characterisation of physical and chemical properties of samples. This study focuses on the application of handheld Raman spectroscopy for the authentication of Covid-19 vaccines.

Raman spectroscopy measures the oscillations of atoms in molecules upon exposure to a monochromatic light source. The observation of the vibrational transitions yields information about the molecular vibrational energy levels, which in turn are related to molecular conformation, structure, intermolecular interaction and chemical bonding (Li and Church, 2014)

Raman spectroscopic techniques are based on the interaction of light with a sample. Raman uses monochromatic light (single wavelength) and is effective for the analysis of drugs and active pharmaceutical ingredients (APIs) in pharmaceutical products. Raman spectroscopy is particularly successful in the identification of C-C bonds and carbonyl groups. Raman spectroscopy has been applied previously for analysis of drugs, pharmaceuticals and food products (Assi et al., 2020).

Yet, the sensitivity of Raman spectroscopy has always been a challenge where the detection limit of a drug/API has been high (above 5% m/m or m/v in most cases). To address this limitation, surface enhanced Raman spectroscopy (SERS) has emerged and that involves enhancing the Raman signal of trace analyte by about 1000,000 times. SERS was first discovered when the Raman spectra of pyridine on roughened silver was first observed in 1974 (Fleischmann, Hendra and McQuillan, 1974), although at the time this was not attributed to any novel or enhanced effects. Further development and application of these findings (Jeanmaire and Van Duyne, 1977), has sparked significant interest in and use of SERS for applications such as single molecule detection (Almehmadi et al., 2019), and sensing and imaging (Kneipp, 2022). Fundamentally, **“SERS is a way to significantly increase the signal from the weak yet structurally rich technique of Raman scattering”** (Sharma et al., 2012). SERS allows enhancement of the Raman signal intensity of a molecule through its adsorption on a colloidal surface such as silver or gold nanostructure. This adsorption quenches

fluorescence, addressing fluorescence interference in conventional Raman spectra alongside sensitivity issues (Shan et al., 2017).

3.2 Experimental

3.2.1 Materials

Brands 1 and 2 Covid-19 vaccine samples were obtained through the NHS Central Liverpool Primary Care Network as outlined in section 2.2.1, brand 3 vaccines were obtained from hospitals in Lebanon and Iraq.

A total of 64 vaccines from three brands were measured using the Metrohm MIRA XTR handheld Raman spectrometer. Brand 1 (n=20), brand 2 (n=23) and brand 3 (n=21).

3.2.2 Instrumentation

Measurements were taken using the Metrohm MIRA XTR DS handheld Raman Spectrometer, the specifications are detailed in Table 3.1.

Table 3.1. Handheld Raman instrument specifications

Instrument	MIRA XTR DS handheld Raman Spectrometer
Manufacturer	Metrohm
Laser Wavelength(s)	785 nm \pm 0.5 nm
Maximum Laser Power	\leq 100 mW, 50 mW at sample, five adjustable laser powers down to 10 mW
Spectral Range	400 – 2300 cm^{-1}
Modes of Operation	Handheld

Technique(s)	XTR Algorithm, Orbital Raster Scan (ORS™) technology
---------------------	---

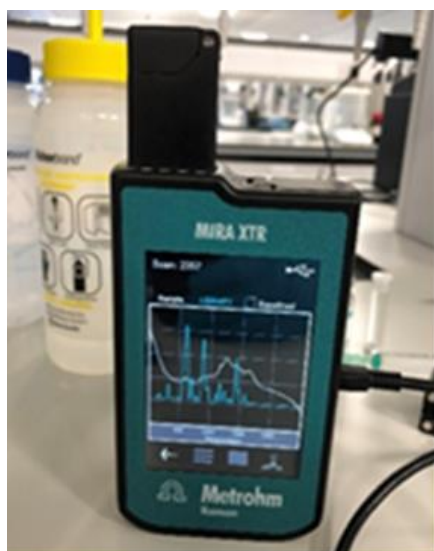


Figure 3.1 Metrohm MIRA XTR DS handheld Raman Spectrometer equipped with 785nm laser and orbital raster scattering

Measurements were taken using the Metrohm MIRA XTR DS handheld Raman spectrometer using the vial holder attachment (Figure 3.1). The instrument was equipped with a 785 nm wavelength laser and orbital raster scattering function. Measurements were taken across a range of 400 - 2300 cm^{-1} . Spectra were visualised in real-time on the instrument screen and saved to the device for export to a computer using Metrohm's MIRA Cal software. Metrohm's XTR algorithm is designed to pull Raman data out of fluorescent backgrounds and allows generation of baseline spectra through their MIRA Cal Software. The MIRA XTR allows customisation of measurement protocol parameters including laser power, average scans, integration time and XTR application. A variety of custom measurement procedures were trialled to assess spectral quality as detailed below:

Table 3.2. Custom operating procedures stored on the Metrohm MIRA XTR DS handheld Raman Spectrometer

Procedure	Laser Power (mW)	Averages	Integration time (s)	XTR
Default	Auto	Auto	Auto	Every Scan
MRW LJMU	02	05	Auto	Every Scan
MRW LJMU 2	01	10	Auto	Every Scan
MRW LJMU 3	05	10	0.20	Off
MRW LJMU 4	05	10	Auto	Every Scan
Preset 1	05	01	2	Auto
Preset 2	Auto	Auto	Auto	Never
SA off XTR on max	05	05	Auto	Every Scan

3.2.3 Methods

Surface and sample holder

Various surfaces and sample holders for measurement of SERS samples were trialled, including filter paper, aluminium foil, glass slides and glass vials. 1-2 drops of sample were applied to filter paper, glass slides and small pieces of aluminium foil and allowed to dry at room temperature for 1-4 hours. Samples dried on substrate were measured using the pointer attachments of the instrument. Samples in glass vials were measured using the instrument's vial holder attachment.

Surface-enhanced Raman Spectroscopy

For SERS analysis, samples were measured with the addition of ThermoScientific 10 nm, 0.02 mg/ml silver nanoparticles (CAS: 7440-22-4) (Figure 3.2) and 1M KBr Aggregating agent (Kimani, Lanzarotta and Batson, 2020). SERS formulations were made using 500 μ l vaccine with the addition of 500 μ l silver nanoparticles and 10 μ l 1M KBr aggregating salt vortexed for 30 s in 2 ml VWR glass vials (Figure 3.3). Samples were measured through glass vials using the vial holder and pointer attachments for the instrument, a minimum of three scans were taken per vial across the wavenumber ranges specified in table 3.1. SERS formulations were mixed prior to drying on substrate for measurement.



Figure 3.2 ThermoScientific Silver nanoparticles used for SERS sample formulation



Figure 3.3 SERS samples made with 500 μ l Vaccine, 500 μ l Silver nanoparticles and 10 μ l 1M KBr

3.2.4 Spectral treatment and qualitative analysis

Spectra were exported as .csv files into Matlab 2023a software. Samples measured using the Metrohm MIRA XTR handheld Raman spectrometer were pre-treated in Metrohm's MIRA Cal DS software using their XTR baseline algorithm and both standard and baselined spectra were exported for analysis.

For evaluation of identification potential, machine learning algorithms (MLAs) including CWS (equation 2.2) and PCA (equation 2.3) were applied to the spectral datasets as detailed in section 2.2.4. 33 classification models ranging from simple decision trees to neural networks were trained on both the conventional (table 3.3) and SERS (table 3.4) datasets using Matlab 2023a classification learner to identify the highest accuracy automated identification method for Covid-19 vaccine brand. Confusion matrices were produced for each classification model visualising the frequency of true and false class predictions. A true positive is obtained when the actual classification is positive, and the predicted classification is positive. A true negative is obtained when the actual

classification is negative, and the predicted classification is negative. A false positive is obtained when the actual classification is negative, and the predicted classification is positive (Type I error). A false negative is observed when the actual classification is positive, and the predicted classification is negative (Type II error). The frequency of true positives, true negatives, false positives and false negatives were used to generate performance evaluation metrics for each model as detailed in section 2.2.4. Accuracy (equation 2.5), precision (equation 2.6), recall (equation 2.7), specificity (equation 2.8) and F1-score (equation 2.9) were calculated to evaluate the identification potential of the model. An AUC-ROC curve (equation 2.10) was produced as described in section 2.2.4 for each dataset to assess the separation capacity of the highest accuracy models. Spectral quality was assessed considering the parameters specified in section 2.2.4. These parameters were used to establish the samples as strong, medium or weak Raman intensity.

Table 3.3. Model type and hyperparameters of the classification models trained on the conventional Raman spectral dataset using Matlab 2023a classification learner

Model Number	Model Type	Hyperparameters
1	Tree	Maximum number of splits: 100; Split criterion: Gini's diversity index; Surrogate decision splits: Off
2.01	Tree	Maximum number of splits: 100; Split criterion: Gini's diversity index; Surrogate decision splits: Off
2.02	Tree	Maximum number of splits: 20; Split criterion: Gini's diversity index; Surrogate decision splits: Off

2.03	Tree	Maximum number of splits: 4; Split criterion: Gini's diversity index; Surrogate decision splits: Off
2.04	Discriminant	Covariance structure: Full
2.05	Discriminant	Covariance structure: Full
2.06	Efficient Logistic Regression	Learner: Logistic regression; Solver: Auto; Regularization: Auto; Regularisation strength (Lambda): Auto; Relative coefficient tolerance (Beta tolerance): 0.0001; Multiclass coding: One-vs-One
2.07	Efficient Linear SVM	Learner: SVM; Solver: Auto; Regularisation: Auto; Regularisation strength (Lambda): Auto; Relative coefficient tolerance (Beta tolerance): 0.0001; Multiclass coding: One-vs-One
2.08	Naive Bayes	Distribution name for numeric predictors: Gaussian; Distribution name for categorical predictors: Not Applicable
2.09	Naive Bayes	Distribution name for numeric predictors: Kernel; Distribution name for categorical predictors: Not Applicable; Kernel type: Gaussian; Support: Unbounded; Standardise data: No
2.10	SVM	Kernel function: Linear; Kernel scale: Automatic; Box constraint level: 1; Multiclass coding: One-vs-One; Standardise data: Yes

2.11	SVM	Kernel function: Quadratic; Kernel scale: Automatic; Box constraint level: 1; Multiclass coding: One-vs-One; Standardise data: Yes
2.12	SVM	Kernel function: Cubic; Kernel scale: Automatic; Box constraint level: 1; Multiclass coding: One-vs-One; Standardise data: Yes
2.13	SVM	Kernel function: Gaussian; Kernel scale: 11; Box constraint level: 1; Multiclass coding: One-vs-One; Standardise data: Yes
2.14	SVM	Kernel function: Gaussian; Kernel scale: 44; Box constraint level: 1; Multiclass coding: One-vs-One; Standardise data: Yes
2.15	SVM	Kernel function: Gaussian; Kernel scale: 170; Box constraint level: 1; Multiclass coding: One-vs-One; Standardise data: Yes
2.16	KNN	Number of neighbours: 1; Distance metric: Euclidean; Distance weight: Equal; Standardise data: Yes
2.17	KNN	Number of neighbours: 10; Distance metric: Euclidean; Distance weight: Equal; Standardise data: Yes
2.18	KNN	Number of neighbours: 100; Distance metric: Euclidean; Distance weight: Equal; Standardise data: Yes
2.19	KNN	Number of neighbours: 10; Distance metric: Cosine; Distance weight: Equal; Standardise data: Yes
2.20	KNN	Number of neighbours: 10; Distance metric: Minkowski (cubic); Distance weight: Equal; Standardise data: Yes

2.21	KNN	Number of neighbours: 10; Distance metric: Euclidean; Distance weight: Squared inverse; Standardise data: Yes
2.22	Ensemble	Ensemble method: AdaBoost; Learner type: Decision tree; Maximum number of splits: 20; Number of learners: 30; Learning rate: 0.1; Number of predictors to sample: Select All
2.23	Ensemble	Ensemble method: Bag; Learner type: Decision tree; Maximum number of splits: 153; Number of learners: 30; Number of predictors to sample: Select All
2.24	Ensemble	Ensemble method: Subspace; Learner type: Discriminant; Number of learners: 30; Subspace dimension: 951
2.25	Ensemble	Ensemble method: Subspace; Learner type: Nearest neighbours; Number of learners: 30; Subspace dimension: 951
2.26	Ensemble	Ensemble method: RUSBoost; Learner type: Decision tree; Maximum number of splits: 20; Number of learners: 30; Learning rate: 0.1; Number of predictors to sample: Select All
2.27	Neural Network	Number of fully connected layers: 1; First layer size: 10; Activation: ReLU; Iteration limit: 1000; Regularisation strength (Lambda): 0; Standardise data: Yes
2.28	Neural Network	Number of fully connected layers: 1; First layer size: 25; Activation: ReLU; Iteration limit: 1000; Regularisation strength (Lambda): 0; Standardise data: Yes

2.29	Neural Network	Number of fully connected layers: 1; First layer size: 100; Activation: ReLU; Iteration limit: 1000; Regularisation strength (Lambda): 0; Standardise data: Yes
2.30	Neural Network	Number of fully connected layers: 2; First layer size: 10; Second layer size: 10; Activation: ReLU; Iteration limit: 1000; Regularisation strength (Lambda): 0; Standardise data: Yes
2.31	Neural Network	Number of fully connected layers: 3; First layer size: 10; Second layer size: 10; Third layer size: 10; Activation: ReLU; Iteration limit: 1000; Regularisation strength (Lambda): 0; Standardise data: Yes
2.32	Kernel	Learner: SVM; Number of expansion dimensions: Auto; Regularisation strength (Lambda): Auto; Kernel scale: Auto; Multiclass coding: One-vs-One; Standardise data: No; Iteration limit: 1000
2.33	Kernel	Learner: Logistic Regression; Number of expansion dimensions: Auto; Regularisation strength (Lambda): Auto; Kernel scale: Auto; Multiclass coding: One-vs-One; Standardise data: No; Iteration limit: 1000

Table 3.4 Model type and hyperparameters of the classification models trained on the surface-enhanced Raman spectral dataset using Matlab 2023a classification learner

Model Number	Model Type	Hyperparameters
3.01	Tree	Maximum number of splits: 100; Split criterion: Gini's diversity index; Surrogate decision splits: Off
3.02	Tree	Maximum number of splits: 20; Split criterion: Gini's diversity index; Surrogate decision splits: Off
3.03	Tree	Maximum number of splits: 4; Split criterion: Gini's diversity index; Surrogate decision splits: Off
3.04	Discriminant	Covariance structure: Full
3.05	Discriminant	Covariance structure: Full
3.06	Efficient Logistic Regression	Learner: Logistic regression; Solver: Auto; Regularisation: Auto; Regularisation strength (Lambda): Auto; Relative coefficient tolerance (Beta tolerance): 0.0001; Multiclass coding: One-vs-One
3.07	Efficient Linear SVM	Learner: SVM; Solver: Auto; Regularization: Auto; Regularisation strength (Lambda): Auto; Relative coefficient tolerance (Beta tolerance): 0.0001; Multiclass coding: One-vs-One
3.08	Naive Bayes	Distribution name for numeric predictors: Gaussian; Distribution name for categorical predictors: Not Applicable
3.09	Naive Bayes	Distribution name for numeric predictors: Kernel; Distribution name for categorical predictors: Not

		Applicable; Kernel type: Gaussian; Support: Unbounded; Standardise data: Yes
3.1	SVM	Kernel function: Linear; Kernel scale: Automatic; Box constraint level: 1; Multiclass coding: One-vs-One; Standardise data: Yes
3.11	SVM	Kernel function: Quadratic; Kernel scale: Automatic; Box constraint level: 1; Multiclass coding: One-vs-One; Standardise data: Yes
3.12	SVM	Kernel function: Cubic; Kernel scale: Automatic; Box constraint level: 1; Multiclass coding: One-vs-One; Standardise data: Yes
3.13	SVM	Kernel function: Gaussian; Kernel scale: 11; Box constraint level: 1; Multiclass coding: One-vs-One; Standardise data: Yes
3.14	SVM	Kernel function: Gaussian; Kernel scale: 44; Box constraint level: 1; Multiclass coding: One-vs-One; Standardise data: Yes
3.15	SVM	Kernel function: Gaussian; Kernel scale: 170; Box constraint level: 1; Multiclass coding: One-vs-One; Standardise data: Yes
3.16	KNN	Number of neighbours: 1; Distance metric: Euclidean; Distance weight: Equal; Standardise data: Yes
3.17	KNN	Number of neighbours: 10; Distance metric: Euclidean; Distance weight: Equal; Standardise data: Yes

3.18	KNN	Number of neighbours: 100; Distance metric: Euclidean; Distance weight: Equal; Standardise data: Yes
3.19	KNN	Number of neighbours: 10; Distance metric: Cosine; Distance weight: Equal; Standardise data: Yes
3.2	KNN	Number of neighbours: 10; Distance metric: Minkowski (cubic); Distance weight: Equal; Standardise data: Yes
3.21	KNN	Number of neighbours: 10; Distance metric: Euclidean; Distance weight: Squared inverse; Standardise data: Yes
3.22	Ensemble	Ensemble method: AdaBoost; Learner type: Decision tree; Maximum number of splits: 20; Number of learners: 30; Learning rate: 0.1; Number of predictors to sample: Select All
3.23	Ensemble	Ensemble method: Bag; Learner type: Decision tree; Maximum number of splits: 153; Number of learners: 30; Number of predictors to sample: Select All
3.24	Ensemble	Ensemble method: Subspace; Learner type: Discriminant; Number of learners: 30; Subspace dimension: 951
3.25	Ensemble	Ensemble method: Subspace; Learner type: Nearest neighbours; Number of learners: 30; Subspace dimension: 951
3.26	Ensemble	Ensemble method: RUSBoost; Learner type: Decision tree; Maximum number of splits: 20; Number of learners: 30; Learning rate: 0.1; Number of predictors to sample: Select All

3.27	Neural Network	Number of fully connected layers: 1; First layer size: 10; Activation: ReLU; Iteration limit: 1000; Regularization strength (Lambda): 0; Standardise data: Yes
3.28	Neural Network	Number of fully connected layers: 1; First layer size: 25; Activation: ReLU; Iteration limit: 1000; Regularisation strength (Lambda): 0; Standardise data: Yes
3.29	Neural Network	Number of fully connected layers: 1; First layer size: 100; Activation: ReLU; Iteration limit: 1000; Regularisation strength (Lambda): 0; Standardise data: Yes
3.3	Neural Network	Number of fully connected layers: 2; First layer size: 10; Second layer size: 10; Activation: ReLU; Iteration limit: 1000; Regularisation strength (Lambda): 0; Standardise data: Yes
3.31	Neural Network	Number of fully connected layers: 3; First layer size: 10; Second layer size: 10; Third layer size: 10; Activation: ReLU; Iteration limit: 1000; Regularisation strength (Lambda): 0; Standardise data: Yes
3.32	Kernel	Learner: SVM; Number of expansion dimensions: Auto; Regularisation strength (Lambda): Auto; Kernel scale: Auto; Multiclass coding: One-vs-One; Standardise data: Yes; Iteration limit: 1000
3.33	Kernel	Learner: Logistic Regression; Number of expansion dimensions: Auto; Regularisation strength (Lambda): Auto; Kernel scale: Auto; Multiclass coding: One-vs-One; Standardise data: Yes; Iteration limit: 1000

3.3 Pilot Study

3.3.1 Aim

The Pilot Study provided a proof of concept regarding SERS for authenticating Covid-19 vaccines.

3.3.2. Experimental

3.3.2.1 Materials

Covid-19 vaccine samples were obtained through the NHS Central Liverpool Primary Care Network as outlined in section 2.2.1 and consisted of Brand 1 (DNA-based) and Brand 2 (mRNA-based). A total of 46 vaccine samples were used in this pilot study.

3.3.2.2 Procedure

Measurements were taken using the Metrohm MIRA XTR DS handheld Raman spectrometer as detailed in section 3.2.2 (Figure 3.1).



Figure 3.4 Process of hydroxylamine hydrochloride reduced-silver colloid formulation for SERS

An optimisation study was conducted using 20 vaccine samples for SERS colloid and aggregating agent optimisation. For Raman analysis, vaccines were defrosted and measured in 2 ml glass vials (VWR) with the addition of a hydroxylamine reduced-silver colloid and potassium bromide (KBr) aggregating agent for SERS. The hydroxylamine reduced-silver colloid (Figure 3.4) was formulated according to the method set out by Leopold and Lendl (Leopold and Lendl, 2003). The KBr aggregating agent was utilised in accordance with a method developed for the detecting trace level opioids by SERS with handheld devices (Kimani, Lanzarotta and Batson, 2020). Three scans were taken per vial over a wavenumber range of 400 - 2200 cm^{-1} with 785 nm laser wavelength and 5 mW laser output. Excipients were measured as received in 2 ml glass vials using the Metrohm vial attachment for the Raman system and using the same settings as the previous vaccines.

3.3.2.3 Qualitative analysis

Spectra were exported from the MIRA Cal software into Matlab 2021b. Data analysis involved the assessment of spectral quality and the identification potential of SERS for Covid-19 vaccines. Spectral quality was assessed considering the parameters outlined in section 2.2.4. Identification potential was assessed through the application of supervised machine learning techniques including PCA and CWS as described in section 2.2.4.

3.3.3 Results and Discussion

The overall results proved that Raman spectroscopy was well-suitable for identifying Covid-19 vaccines. Raman spectra showed key features corresponding to DNA, mRNA and other Raman active excipients in the vaccines. The wavelength of the laser impacted the Raman activity varied between individual vaccines and that was related to the stability of the vaccines under the laser light. However, key bands to constituents were common across each brand where the noise level introduced variation alongside the intensity. Intensity variation is expected considering that the Raman signal is cumulative.

3.3.3.1 Spectral Interpretation

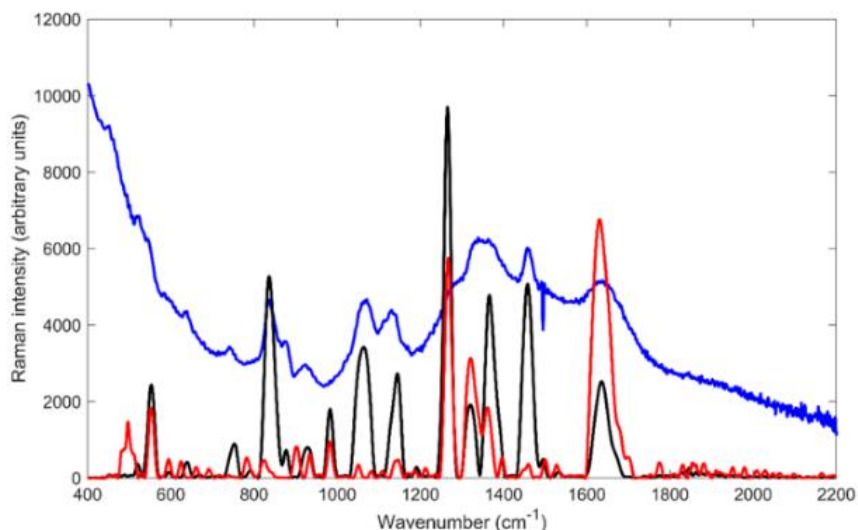


Figure 3.5 Stacked spectra of DNA based vaccine LJMUCV722 (blue), hydroxylamine reduced-silver colloid (red) and SERS spectra of LJMUCV722 (black) measured using the Metrohm MIRA XTR DS handheld Raman spectrometer equipped with 785nm laser and orbital raster scattering

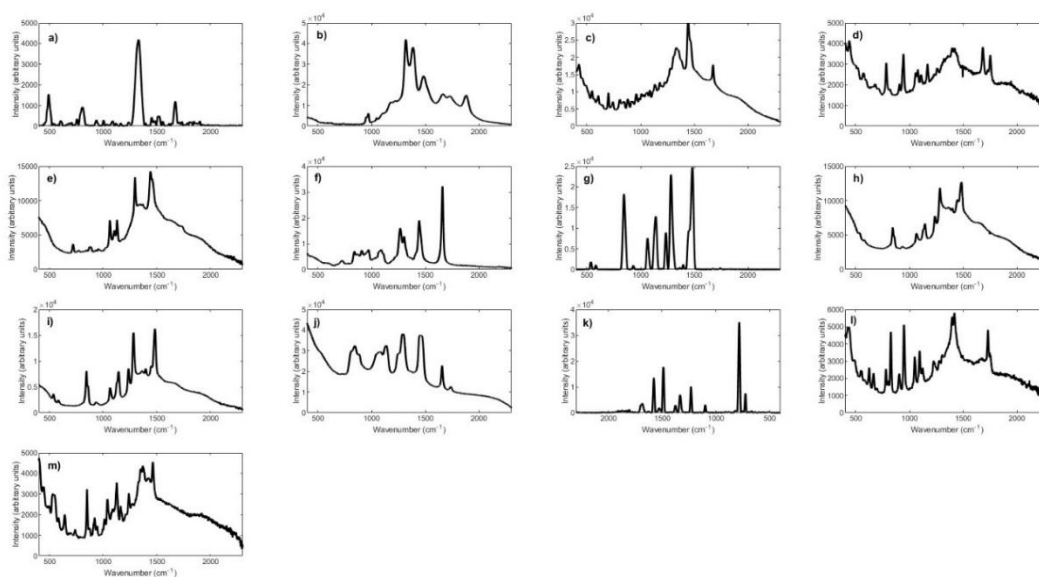


Figure 3.6 Conventional Raman spectra of a) Bovine globulin, b) Calcium phosphate, c) Cholesterol, d) Citric acid, e) DSPC, f) Linoleic acid, g) mPEGDMG2, h) mPEGDTA2K, i) PEG4000, j) Polysorbate80, k) Sodium citrate monobasic, l) and m) Sucrose measured using the Metrohm MIRA XTR DS handheld Raman spectrometer equipped with 785nm laser and orbital raster scattering across a range of 400-2300 cm^{-1}

Raman spectroscopy was applied to a smaller sample of 26 of the DNA based vaccines. In this respect, conventional Raman (CR) showed weak signal for the vaccine that was masked by the fluorescence attributed to water and excipients in the vaccine formulation. The excipients had varying Raman activity that depended on their chemical characteristics, hence, the excipients that were not Raman active constituted the majority of the formulation. However, when SERS was applied, enhancement was seen specifically for the bands at 757, 836, 1061, 1145, 1322, 1365, 1455 and 1640 cm^{-1} (Figure 3.5). Due to the fluorescence of the vaccine, it was not possible to estimate the degree of enhancement but based on the literature the enhancement could extend up to 10^6 (Graham and Goodacre, 2008). Considering the possibility of the SERS method causing a band shift of up to 15 cm^{-1} (Leonard et al., 2017), the key bands identified on the SERSLJMUCV722 spectra could be associated with known DNA characteristic Raman bands. The band at 836 cm^{-1} could be attributed to phosphodiester asymmetric stretching observed in Raman DNA spectra, the band at 1061 cm^{-1} could also be attributed to PO_4^- stretching modes in DNA. The strong band at 1365 cm^{-1} is characteristic of the ring vibration of guanine. Bands observed at 757 and 1090 cm^{-1} are attributed to vibrations of the DNA backbone (Benevides and Thomas, 1983). However, further SERS analysis of DNA standards and comparison against existing literature is required to further confirm these attributions. The excipients measured showed variable Raman activity with variable maximum intensity ranging between 5,000 and 50,000 arbitrary units (Figure 3.6).

3.3.3.2 Correlation in Wavenumber Space and Principal Component Analysis

Figure 3.8 shows the PC scores plot for all the Brand 1 vaccines measured in the study. The first three PCs contributed to 84.4% of the variance among the data. The PCA scores plot showed three groups, with two groups clustered away from the main volume of the vaccines including LJMUCV718, LJMUCV721, LJMUCV736, LJMUCV716 and LJMUCV743. All the aforementioned vaccines were DNA-based so the variance is not attributed to instability of the RNA molecule. It is more likely that this variance is influenced by either the dilution of the vaccine prior to measurement, or by the interaction between the nanoparticle-based colloid and the sample. The hydroxylamine hydrochloride reduced-silver colloid can be subject to degradation after time or upon exposure to light, variation in the stability of the colloid across different days of measurement could account for the variance between vaccine samples. The correlation map for the vaccine spectra showed strong identification potential where all the vaccine samples showed a perfect match ($r=1$) against themselves (Figure 3.9).

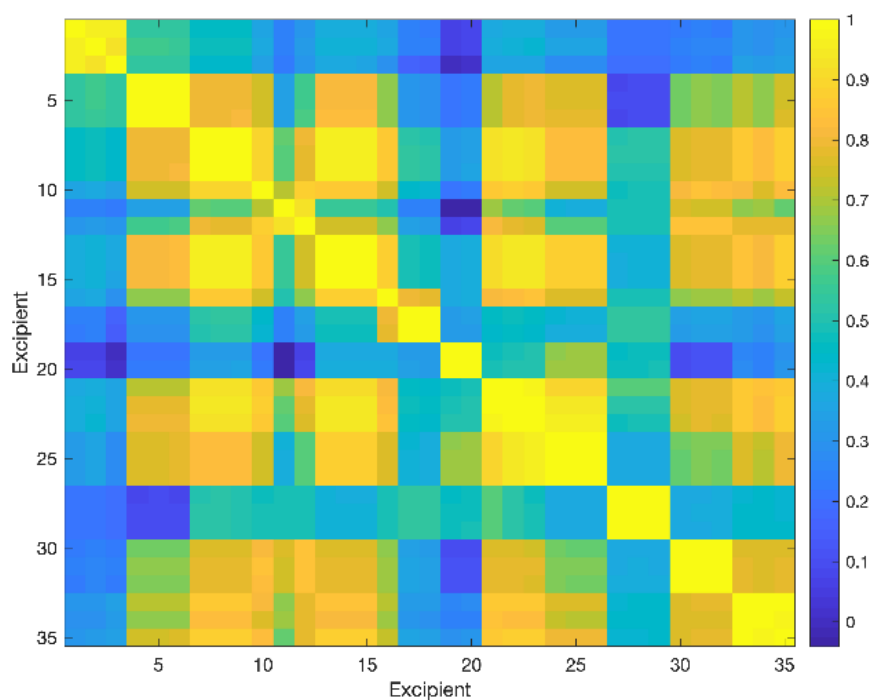


Figure 3.7 Correlation plot of Raman spectra of Bovine globulin (1-3), Calcium phosphate (4-6), Cholesterol (7-9), Citric acid (10-12), DSPC (13-15), Linoleic acid (16-18), mPEGDMG2K (19-21), mPEGDTA2K (22-24), PEG4000 (25-27), Polysorbate80 (28-30), Sodium citrate monobasic (31-33), and Sucrose (34-36) measured using the Metrohm MIRA XTR DS handheld Raman spectrometer equipped with 785nm laser and orbital raster scattering across a range of 400-2300 cm^{-1}

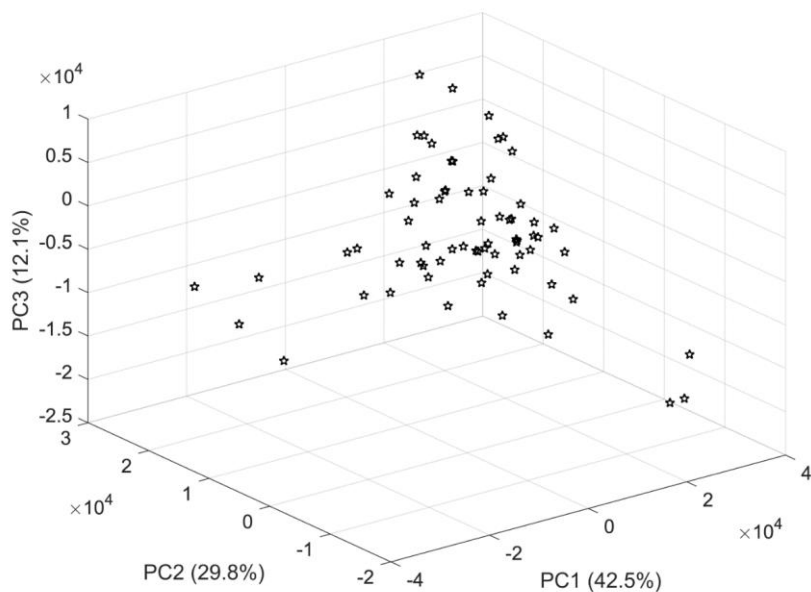


Figure 3.9 PC Scores plot of all Brand 1 vaccines measured using the Metrohm MIRA XTR DS handheld Raman spectrometer equipped with 785nm laser and orbital raster scattering across a range of 400-2300 cm^{-1}

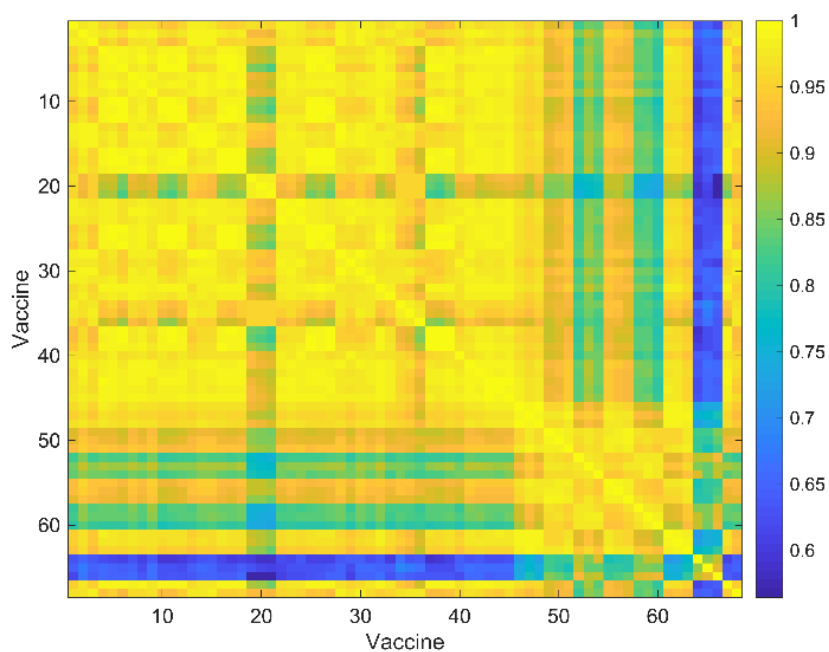


Figure 3.8 Correlation plot of Brand 1 vaccine spectra (1-68) measured using the Metrohm MIRA XTR DS handheld Raman spectrometer equipped with 785nm laser and orbital raster scattering across a range of 400-2300 cm^{-1}

3.4 Conclusion of the pilot study

SERS proved to be an effective method of vaccine identification in comparison to CR spectroscopy which was limited due to the sensitivity of the handheld instrument and the fluorescence of the vaccines' formulation. However, due to variance observed in PC scores of vaccines' SERS spectra, further investigation is required to examine the stability of the nucleic acids in the vaccines, the colloid nanoparticle stability, and the influence of sample dilution on measurement. SERS showed strong identification potential for both vaccines and their excipients, further work involving the optimisation of SERS parameters was necessary as well as additional spectral interpretation alongside nucleic acid standards and existing literature to confirm SERS as a prospective technique for vaccine authentication.

3.4 Results and Discussion

3.4.1.1 Raman activity of vaccines

Spectral interpretation was carried out to assess the Raman activity and signature of each of the vaccine samples. Figure 3.10 shows the untreated conventional Raman spectra of brand 1 vaccines LJMUCV661, LJMUCV664, LJMUCV665 and LJMUCV667, measured using the Metrohm MIRA XTR handheld Raman instrument. Figure 3.11 shows the baseline conventional Raman spectra of the brand 1 vaccines, treated using Metrohm's MIRA Cal DS software. All brand 1 spectra showed consistencies in the appearance of characteristic bands of DNA Raman spectra at around 750, 836, 875, 918, 999, 1066, 1132, 1296, 1337, 1357, 1460 and 1632 cm^{-1} .

Sharp bands at around 836 cm^{-1} could be attributed to phosphodiester asymmetric stretching observed in Raman DNA spectra. Bands at 1066 cm^{-1} could also be attributed to PO_4^- stretching modes or PO_2^- stretching of the backbone. Further bands observed between 750 and 1066 cm^{-1} are attributed to vibrations of the DNA backbone (Benevides and Thomas, 1983). A weak peak between 633 and 655 cm^{-1} in all brand 1 spectra is attributed to the ring breathing mode of guanine (Gearheart, Ploehn and Murphy, 2001; Ni, Sheng and Cotton, 1990). Peaks between 729 and 743 cm^{-1} correspond to the nucleic acid base adenine, while the bands at 787 cm^{-1} are characteristic of bases thymine and cytosine (Barhoumi et al., 2008). Some bands such as that observed at a broad peak around 1365 cm^{-1} could correspond to the ring vibration of guanine, although the exact determination of these peak positions is limited due to obscurity from the fluorescence of the vaccines' formulation. Peaks between 1328 and 1357 cm^{-1} correspond to adenine bases, although these bands also appear broad due to fluorescence interference and so exact quantification of this peak position in each spectrum is not possible. A sharp peak at around 1460 cm^{-1} is characteristic of adenine, thymine and cytosine bases. Bands at 1573 cm^{-1} correspond with the ring stretching or N_6H_2 deformation of adenine (Gearheart, Ploehn and Murphy, 2001; Otto et al., 1986). Significant fluorescence was observed between 1800 and 2300 cm^{-1} , limiting the identification of any discernible bands.

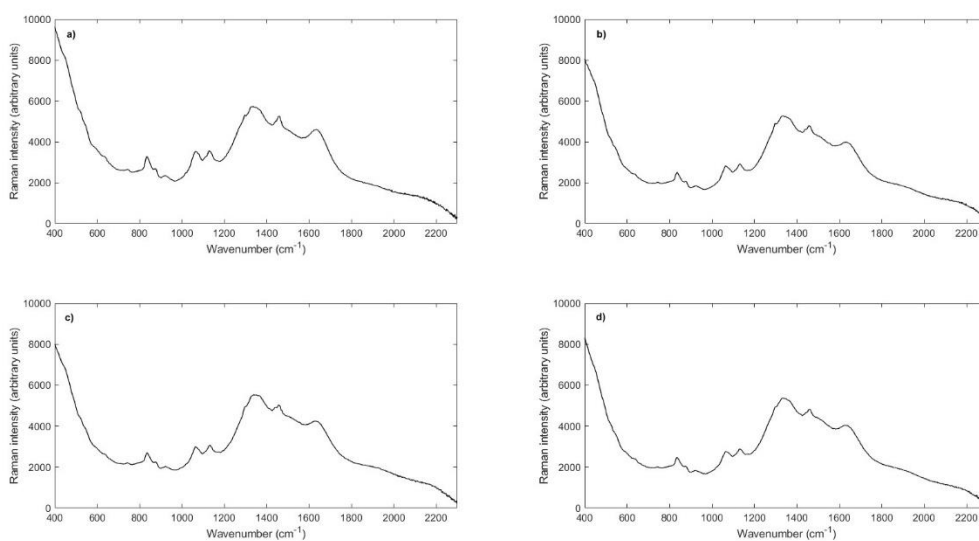


Figure 3.10 Untreated conventional Raman spectra of brand 1 vaccines a) LJMUCV661 b) LJMUCV664 c) LJMUCV665 d) LJMUCV667 measured using the Metrohm MIRA XTR DS handheld Raman spectrometer equipped with orbital raster scattering across $400\text{-}2300\text{ cm}^{-1}$

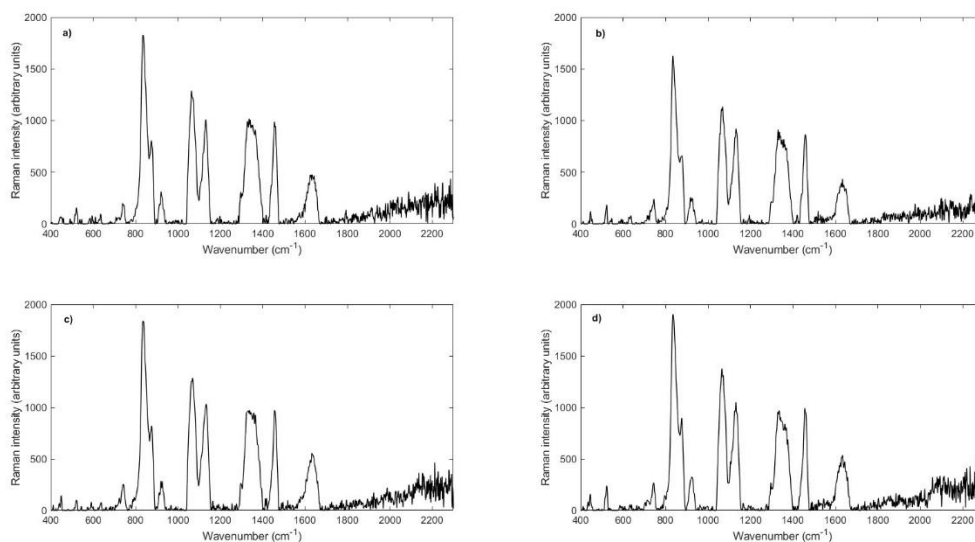


Figure 3.11 Baselined conventional Raman spectra of brand 1 vaccines a) LJMUCV661 b) LJMUCV664 c) LJMUCV665 d) LJMUCV667 measured using the Metrohm MIRA XTR DS handheld Raman spectrometer equipped with orbital raster scattering across $400\text{-}2300\text{ cm}^{-1}$

Figure 3.12 shows the untreated conventional Raman spectra of brand 2 vaccines LJMUCV355, LJMUCV356, LJMUCV357 and LJMUCV358 measured using the Metrohm MIRA XTR handheld Raman instrument. Figure 3.13 shows the baseline conventional Raman spectra of the brand 2 vaccines, treated using Metrohm's MIRA Cal DS software. The brand 2 spectra shared characteristic nucleic acid bands with the brand 1 spectra including those at 837, 1065, 1129, 1295, 1331, 1350, 1461 and 1635 cm^{-1} . The peak at 837 cm^{-1} corresponds with phosphodiester asymmetric stretching of the sugar-phosphate backbone. Peaks at 1065 cm^{-1} could also be attributed to PO_4^- stretching modes or PO_2^- stretching of the backbone. Weak peaks at around 639 cm^{-1} in all brand 2 spectra are attributed to the ring breathing mode of guanine (Gearheart, Ploehn and Murphy, 2001; Ni, Sheng and Cotton, 1990). Peaks between 729 and 743 cm^{-1} correspond to the nucleic acid base adenine (Barhoumi et al., 2008), while bands observed between 777 and 800 correspond to the nitrogenous uracil base found exclusively in RNA. Bands such as that observed at 1331 cm^{-1} could correspond to the ring vibration of guanine, and peaks at 1350 cm^{-1} correspond to adenine bases, the area underlying these peaks appears broad due to fluorescence. A sharp peak at around 1460 cm^{-1} could be characteristic of adenine and cytosine bases. In addition to the bands between 777 and 800 cm^{-1} , RNA specific peaks at 1233 cm^{-1} correspond to ring modes of uracil bases (Desai et al., 2020; Gong et al., 2009). A strong peak at 1295 and 1635 cm^{-1} demonstrates the presence of proteins, corresponding to amide I and III bonds (De Gelder et al., 2007). Bands observed between 1900 and 2300 cm^{-1} were not positively distinguishable due to heavy interference from fluorescence in this region. The brand 2 vaccine spectra featured

bands between 406 and 443 cm^{-1} corresponding to out-of-plane ring, and C=O deformations of uracil and cytosine found in aqueous RNA (Thomas, 1970).

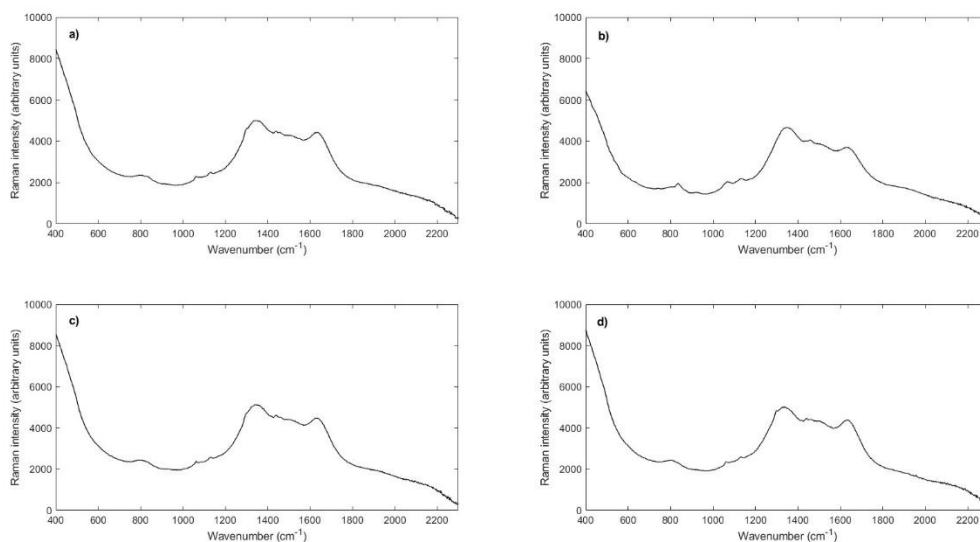


Figure 3.12 Untreated conventional Raman spectra of brand 2 vaccines a) LJMUCV355 b) LJMUCV356 c) LJMUCV357 d) LJMUCV358 measured using the Metrohm MIRA XTR DS handheld Raman spectrometer equipped with orbital raster scattering across 400-2300 cm^{-1}

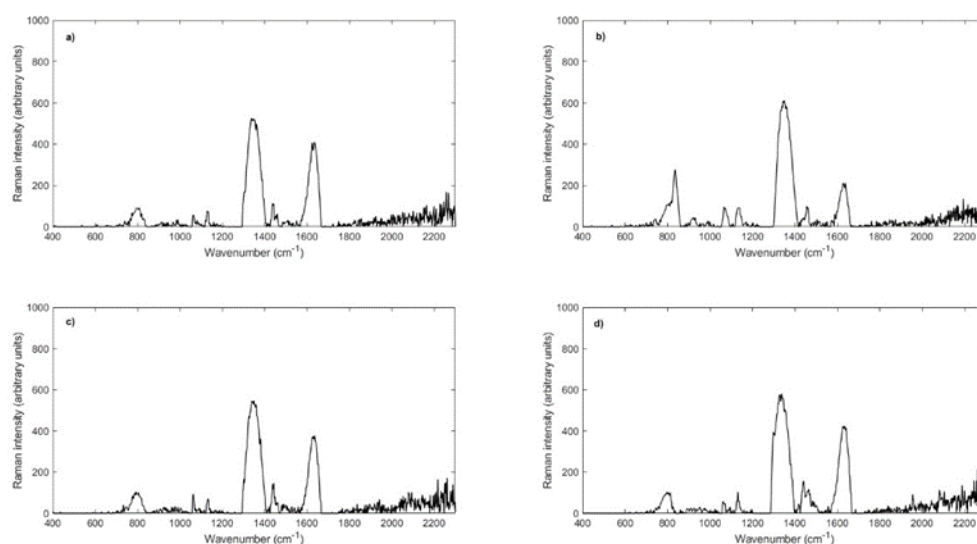


Figure 3.13 Baselined conventional Raman spectra of brand 2 vaccines a) LJMUCV355 b) LJMUCV356 c) LJMUCV357 d) LJMUCV358 measured using the Metrohm MIRA XTR DS handheld Raman spectrometer equipped with orbital raster scattering across 400-2300 cm^{-1}

Figure 3.14 shows the untreated conventional Raman spectra of brand 3 vaccines LJMUCV1400, LJMUCV1401, LJMUCV1403 and LJMUCV1404 measured using the Metrohm MIRA XTR DS handheld Raman spectrometer. Figure 3.15 shows the baseline conventional Raman spectra of the brand 3 vaccines, treated using Metrohm's MIRA Cal DS spectral visualisation and treatment software. The brand 3 vaccines showed spectral similarities to the DNA-based brand 1 vaccines, attributed to the viral DNA of the live-attenuated inactivated formulation of the brand 3 vaccines. Brand 3 vaccine spectra showed prominent peaks at around 615, 680-695, 806, 819, 1066, 1129, 1225, 1297-1311, 1324-1343, 1444, 1588 and 1631 cm^{-1} . Characteristic DNA bands observed included those at 1066 cm^{-1} (PO_4^- stretching modes or PO_2^- stretching of the backbone), 1297-1311 and 1631 cm^{-1} (amide I and III bonds in proteins), 1324-1343 cm^{-1} (adenine bases), 1444 cm^{-1} (adenine, thymine and cytosine bases), and 1588 cm^{-1} (ring stretching or N6H2 deformation of adenine) (Benevides and Thomas, 1983; De Gelder et al., 2007; Gearheart, Ploehn and Murphy, 2001; Otto et al., 1986; Thomas, 1970).

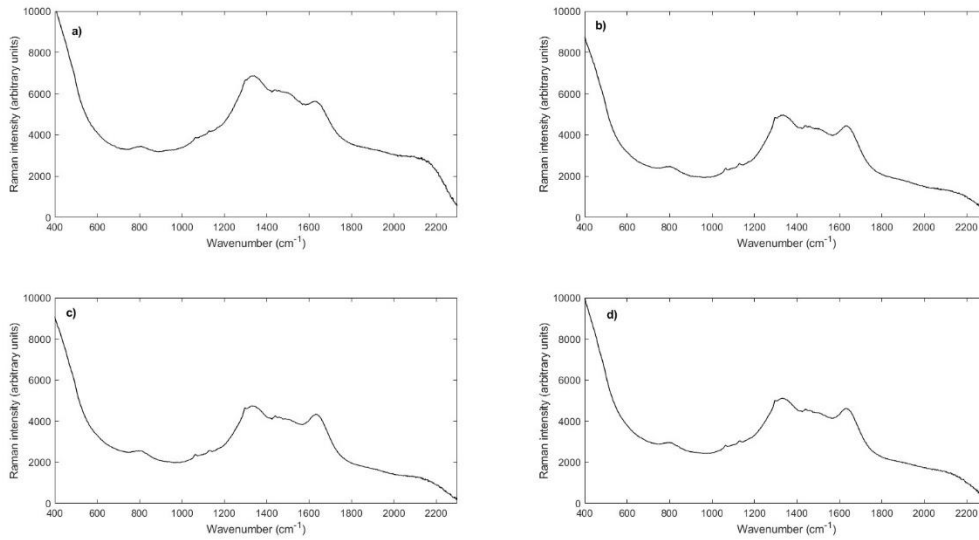


Figure 3.14 Untreated conventional Raman spectra of brand 3 vaccines a) LJMUCV1400 b) LJMUCV1401 c) LJMUCV1403 d) LJMUCV1404 measured using the Metrohm MIRA XTR DS handheld Raman spectrometer equipped with orbital raster scattering across 400-2300 cm^{-1}

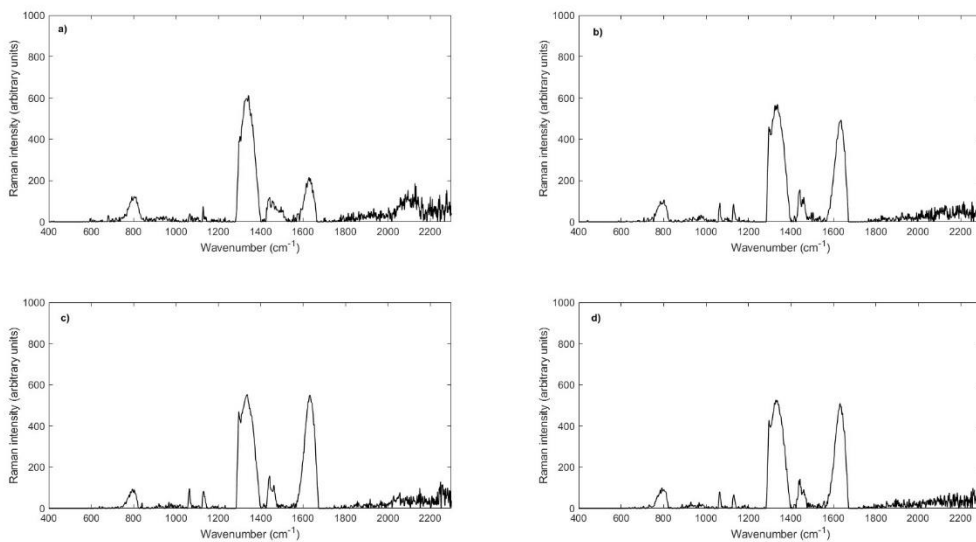


Figure 3.15 Baselined conventional Raman spectra of brand 3 vaccines a) LJMUCV1400 b) LJMUCV1401 c) LJMUCV1403 d) LJMUCV1404 measured using the Metrohm MIRA XTR DS handheld Raman spectrometer equipped with orbital raster scattering across 400-2300 cm^{-1}

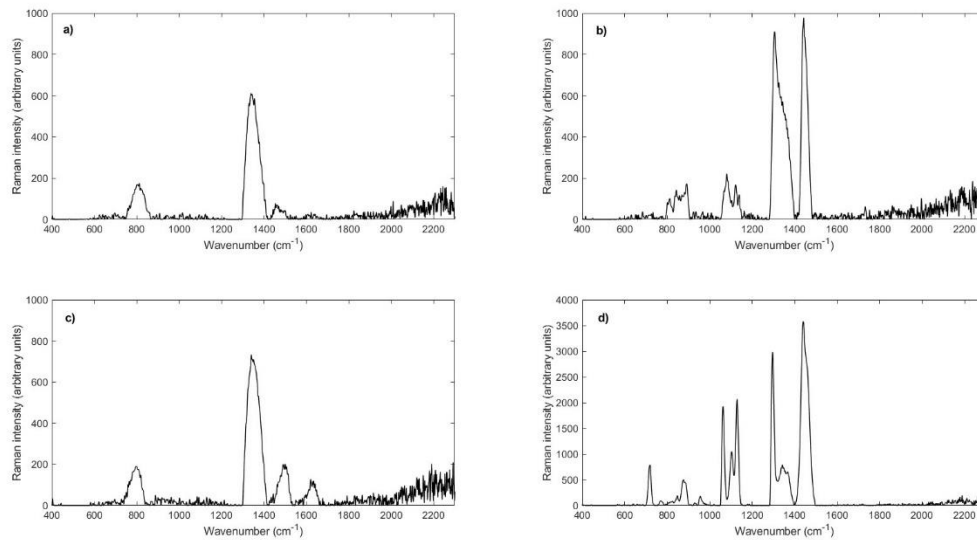


Figure 3.16 Baselined conventional Raman spectra of excipients a) Bovine Globulin b) DHA c) DNA from salmon testes and d) DSPC816_94_4 measured using the Metrohm MIRA XTR DS handheld Raman spectrometer equipped with orbital raster scattering across 400-2300 cm^{-1}

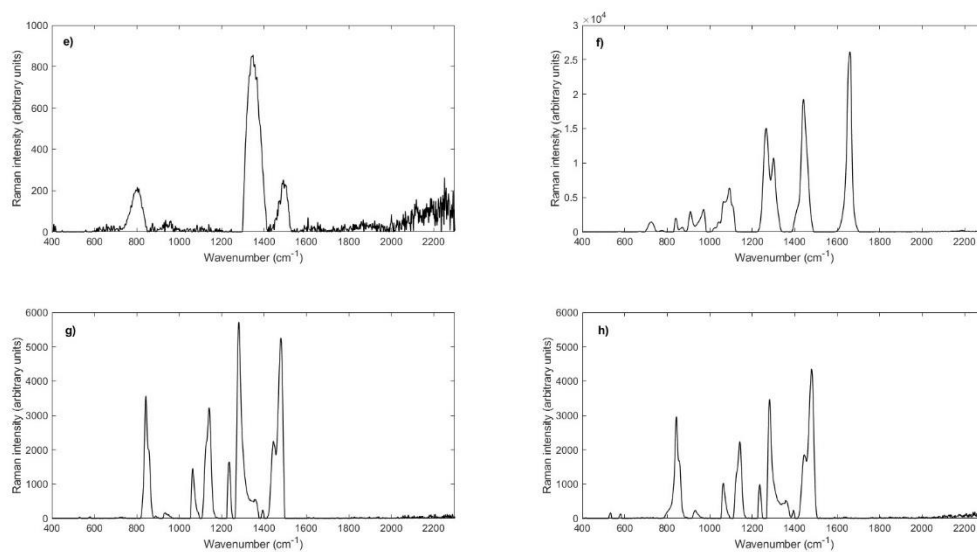


Figure 3.17 Baselined conventional Raman spectra of excipients e) HUO f) Linoleic Acid g) mPEG_DMG_2K and h) mPEG_DTA_2K measured using the Metrohm MIRA XTR DS handheld Raman spectrometer equipped with orbital raster scattering across 400-2300 cm^{-1}

Figure 3.18 shows the stacked spectra of the measured excipients against a brand 1, 2 and 3 vaccines. Spectral similarities between the excipients and the vaccine spectra can be drawn, most notably in the band position of the PEGylated lipid nanoparticles: mPEG_DMG_2K and mPEG_DTA_2K. Noteworthy bands include those at 840 cm^{-1} , 1140 cm^{-1} , 1300 cm^{-1} and 1440 cm^{-1} observed in the spectra of the aforementioned PEGylated lipids nanoparticles and DHA, alongside the three vaccine brands. Spectral contribution from the remaining excipients was difficult to identify due to fluorescence in the vaccines' spectra obscuring the exact peak positions in these regions, notably the $1500\text{--}1800\text{ cm}^{-1}$ range. Overall, the measured nucleic acids, and the PEGylated lipid excipients demonstrated the highest contribution to the spectral characteristics observed in all three vaccine brands spectra.

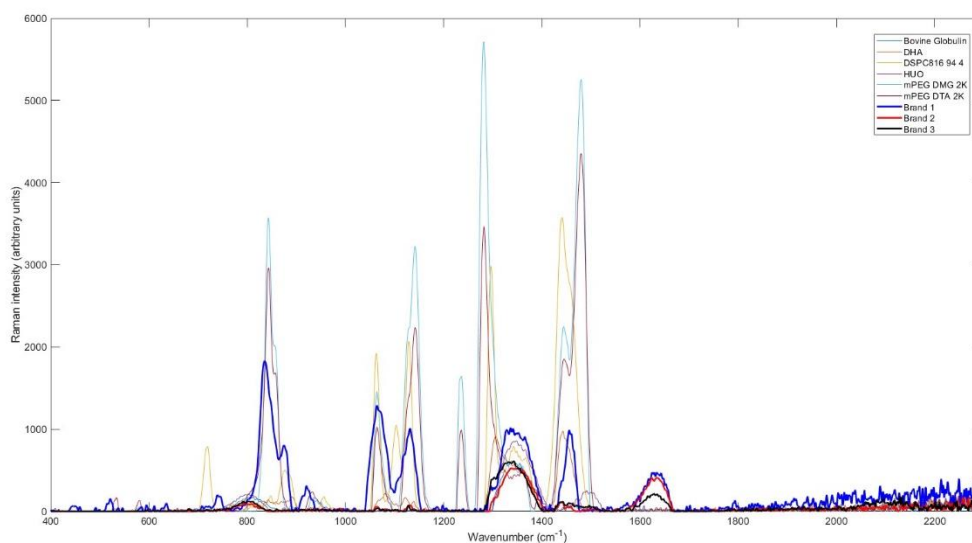


Figure 3.18 Stacked spectra of vaccine excipients bovine globulin (blue), DHA (orange), DSPC816_94_4 (yellow), HUO (purple), mPEG_DMG_2K (light blue), mPEG_DTA_2K (dark red), brand 1 vaccine LJMUCV661 (bold blue), brand 2 vaccine LJMUCV355 (bold red), and brand 3 vaccine LJMUCV1400 (bold black)

Figure 3.19 shows the baseline conventional Raman spectra of purified RNA (black) and DNA from salmon testes (blue) measured using the Metrohm MIRA XTR DS handheld Raman instrument. The CR spectra of DNA from salmon testes showed characteristic nucleic acid bands observed in the spectra of brand 1 and 3 covid-19 vaccines. The DNA CR spectra showed prominent peaks at 780 and 800 cm^{-1} which are characteristic of bases thymine and cytosine, while peaks between 1340 and 1352 cm^{-1} correspond to adenine bases. The peak at around 1490 cm^{-1} is characteristic of adenine, thymine and cytosine bases (Barhoumi et al., 2008), and peaks at 1635 are attributed to amide III protein bonding (De Gelder et al., 2007). The CR spectra of purified RNA also demonstrated similarities to the brand 2 mRNA-based vaccine spectra, including bands at 794 cm^{-1} corresponding to nitrogenous base uracil (Desai et al., 2020; Gong et al., 2009). A weak band at 403 cm^{-1} corresponds to out-of-plane ring, and C=O deformations of uracil and cytosine (Thomas, 1970).

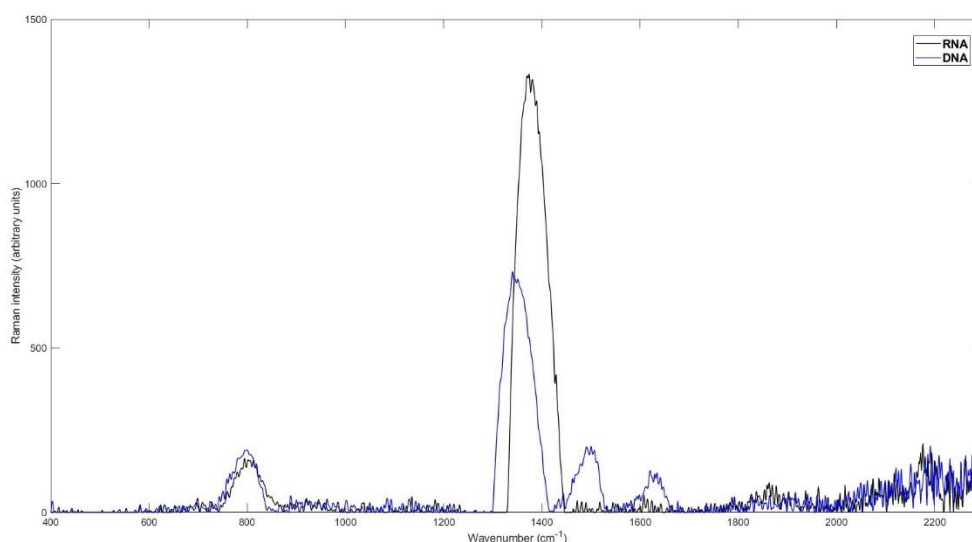


Figure 3.19 Baseline conventional Raman spectra of purified RNA (black), and DNA from salmon testes measured using the Metrohm MIRA XTR DS handheld Raman spectrometer equipped with orbital raster scattering across 400-2300 cm^{-1}

Figure 3.20 shows the stacked spectra of brand 1 vaccine LJMUCV661 measured as standard (black), and with the addition of the ThermoScientific silver nanoparticles (red) and 1M KBr aggregating salt (see section 3.2.3). Brand 1 vaccines showed reduced enhancement when measured with the addition of the silver colloid for all samples, the intensity between 400 cm^{-1} and 700 cm^{-1} was reduced so significantly that bands in this region were rendered indiscernible. However, the fluorescence quenching effects of SERS were demonstrated in the range of $1800 - 2300\text{ cm}^{-1}$, where fluorescence interference in the spectra was notably reduced. The poor enhancement observed for brand 1 vaccines' is likely attributed to the low sample concentrations. Brand 1 vaccine samples measured using conventional Raman had been previously diluted with 0.9% NaCl to support sample stability and to increase volume for repeated testing, as the initial volume received was insufficient. A small volume ($500\mu\text{l}$) of the diluted brand 1 vaccine samples was then further diluted with $500\mu\text{l}$ silver nanoparticles and $5\mu\text{l}$ 1M KBr for SERS measurement. The final concentration of the SERS vaccines sample is not possible to quantify, but as signal intensity is positively correlated with sample concentration, the poor enhancement observed in Figure 3.20 is attributed to insufficient sample concentration for SERS enhancement.

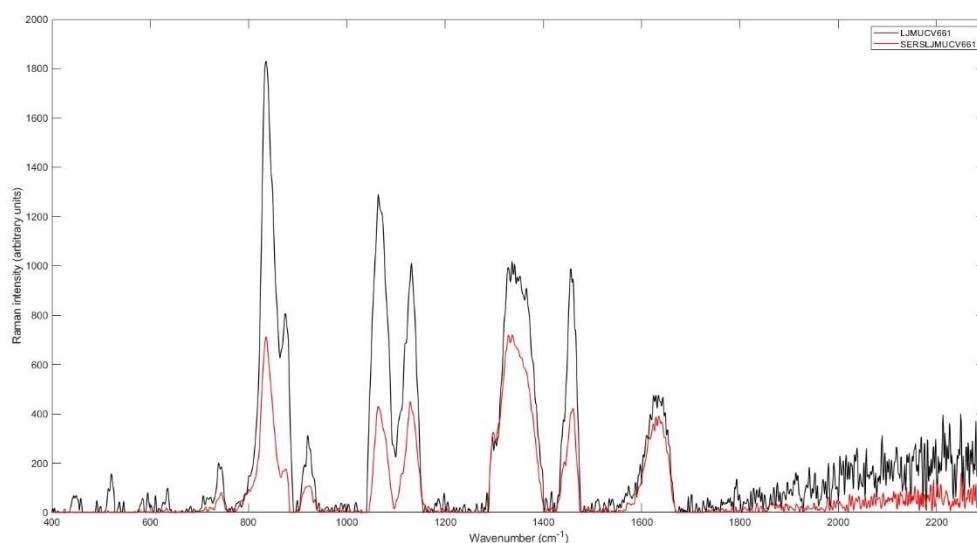


Figure 3.20 Stacked baseline spectra of brand 1 vaccine LJMUCV661 measured as received (black) and with the addition of silver nanoparticles + 1M KBr aggregating agent (red) using the Metrohm MIRA XTR DS handheld Raman spectrometer equipped with orbital raster scattering across 400-2300cm⁻¹

Figure 3.21 shows the stacked spectra of brand 2 vaccine LJMUCV355 measured as standard (black) and with the addition of the silver nanoparticles (red). Signal enhancement was seen, specifically for peaks at 785, 797, 808, 937, 1064, 1128, 1330, 1338, 1351, 1441 and 1459 cm⁻¹. The fluorescence quenching effects of the colloid were less notable in the 1800 – 2300 cm⁻¹ range of the brand 2 SERS vaccine spectra compared to the brand 1 SERS vaccine spectra. However, peak resolution was visibly improved throughout 850 – 1200 cm⁻¹ region. Enhancement however was inconsistent throughout the spectra, with bands at 1624 and 1636 cm⁻¹ showing reduced signal intensity for the SERS sample. This could again be attributed to the

low concentration of the vaccines used in the SERS sample formulation, or degradation in the formulation of the original sample over time.

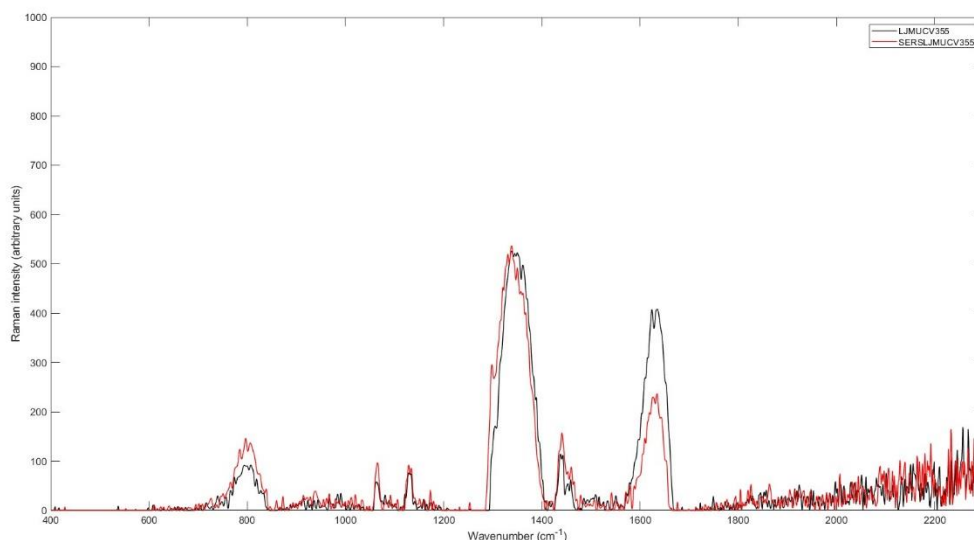


Figure 3.21 Stacked baseline spectra of brand 2 vaccine LJMUCV355 measured as received (black) and with the addition of silver nanoparticles + 1M KBr aggregating agent (red) using the Metrohm MIRA XTR DS handheld Raman spectrometer equipped with orbital raster scattering across 400-2300cm⁻¹

Figure 3.22 shows the stacked spectra of brand 3 vaccine LJMUCV1374 measured as standard (black) and with the addition of the silver nanoparticles and 1M KBr aggregating agent (red). Significant enhancement was seen for all of the brand 3 vaccine samples when measured with the addition of the colloid. Increased signal intensity was observed for peaks at 1297, 1303, 1314, 1324, 1338, 1362, 1415, 1443, 1571, 1628, 1634, 1779, 1795, 1805, and 1817 cm⁻¹. Fluorescence quenching effects of the colloid were particularly notable in the brand 3 SERS vaccine spectra, where bands otherwise obscured were able to be identified in the 1800-2300 cm⁻¹ region (Figure 3.22). While enhancement of signal intensity was not observed for bands in

the 750–1000 cm^{-1} range, peaks appeared significantly better resolved and the appearance of ‘broad’ peaks due to fluorescence reduced dramatically. It is noteworthy to mention that the brand 3 vaccines were obtained from an alternate source to the brand 1 and 2 vaccines, and were of sufficient volume for repeated testing, so were not diluted with 0.9% NaCl at receipt. Therefore, the concentration of the brand 3 vaccine samples added to the silver nanoparticles was significantly greater than that of the other two other vaccine brands. The successful signal enhancement of the more concentrated SERS vaccine formulations indicates that the SERS method described in this study can be used as an effective tool for spectral enhancement when used in conjunction with samples of sufficient concentration but is inhibited by the sensitivity of the instrument. Brand 1 and 2 vaccines were obtained for the pilot study in 2021, whereas brand 3 vaccines were obtained in 2023. All vaccines used in this study were measured between December 2023 and January 2024. Therefore, brand 1 and 2 vaccines were significantly more susceptible to degradation of their biological formulation in the time elapsed prior to their measurement. This is a particularly prominent limitation in measurement of brand 2 vaccines due to the instability and ultracold storage requirement of mRNA vaccines (Liu et al., 2022; Schoenmaker et al., 2021; Uddin and Roni, 2021).

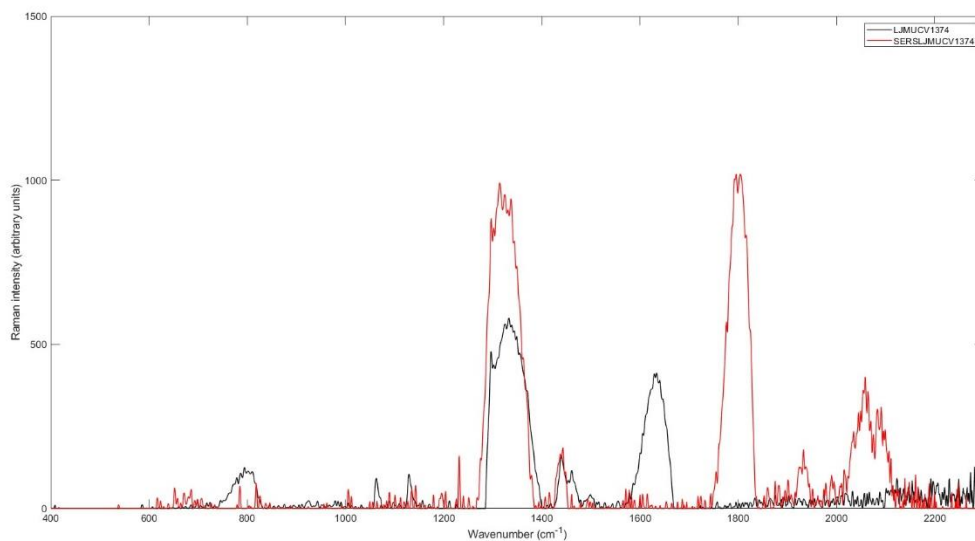


Figure 3.22 Stacked baseline spectra of brand 3 vaccine LJMUCV1374 measured as received (black) and with the addition of silver nanoparticles + 1M KBr aggregating agent (red) using the Metrohm MIRA XTR DS handheld Raman spectrometer equipped with orbital raster scattering across 400-2300cm⁻¹

3.4.1.2 Spectral quality

Spectral quality showed strong Raman scattering for the majority of the measured samples for brands 1, 2 and 3 vaccines based on their numerous bands, maximum intensity and signal-to-noise ratio (SNR). Standard brand 1 samples demonstrated an average of 18 bands in their spectra, with maximum baselined peak intensity ranging from 1216 to 2026 arbitrary units. SNR values for standard brand 1 vaccines ranged between 2 and 305, compared to a range of 51-1226 for surface-enhanced Raman samples (table 3.3). SERS brand 1 vaccines demonstrated less numerous absorption bands of 14 and maximum baselined peak intensity of 612-853 arbitrary units. Average maximum peak intensity for the untreated spectra reduced from 6808 to 6528 for standard brand 1 vaccines and surface-enhanced brand 1 vaccines, respectively

(table 3.6). However, SNR values increased significantly between standard and surface-enhanced Raman spectra. All SERS brand 1 vaccines showed a percentage increase in SNR compared to their conventional Raman counterparts of between 14% and 18617%. LJMUCV688 had a SNR of 3, and SERSLJMUCV688 obtained a SNR of 483, LJMUCV690 obtained a SNR of 7 compared to 1129 for SERSLJMUCV690. It is noteworthy that the maximum peak intensity was observed at an average of 835cm^{-1} for standard brand 1 vaccines, and 1339 cm^{-1} for the vaccines measured with the addition of silver nanoparticles and KBr aggregating agent.

Brand 2 vaccines showed overall weaker Raman scattering for the surface-enhanced samples in comparison to the vaccines measured as received, demonstrated by their reduced average maximum peak intensity for both baselined and untreated spectra. Brand 2 vaccine spectra consisted of 11 peaks on average, in comparison to 9 peaks in the surface-enhanced brand 2 spectra. Maximum peak intensity for the standard brand 2 vaccines ranged from 507 to 668 arbitrary units, and from 496 to 662 arbitrary units for the SERS samples (table 3.4). Standard brand 2 vaccines obtained SNR values of up to 977, compared to a maximum SNR of 397 for SERS samples. 9 samples of a total 23 brand 2 vaccines exhibited an increase in SNR when measured with the addition of silver nanoparticles and a KBr aggregating agent, with a maximum percentage increase of 1938% between LJMUCV403 and SERSLJMUCV403. Maximum peak position occurred on average at 1338 cm^{-1} and 1339 cm^{-1} for standard samples and surface enhanced samples, respectively.

Overall, brand 3 vaccines showed stronger Raman scattering when measured with the addition of silver nanoparticles and KBr aggregating agent, demonstrated by the enhancement of signal intensity for both baselined and untreated spectra. Five of the brand 3 samples showed higher SNR values for the SERS samples compared to the

conventional Raman samples, with percentage increases ranging from 27% to 498%. LJMUCV1405 obtained a SNR value of 7 compared to 39 for SERSLJMUCV1405. LJMUCV1403 obtained a SNR value of 147 compared to 267 for SERSLJMUCV1403. However, overall, the average SNR obtained for SERS brand 3 vaccines was reduced in comparison to the conventional brand 3 vaccines (table 3.6). Maximum peak intensity for brand 3 vaccines measured conventionally ranged from 515 to 611 arbitrary units in baselined spectra and from 679-1336 in the baselined spectra of SERS brand 3 vaccines. Standard brand 3 spectra demonstrated an average maximum peak intensity of 10959 arbitrary units in untreated spectra compared to 32130 for SERS brand 3 samples (table 3.6), indicating an average signal enhancement of 193% when measured with the addition of the silver nanoparticles and aggregating agent.

Overall, brand 1 and 2 vaccines showed poorer signal intensity and spectral quality for SERS samples in comparison to conventional Raman samples, demonstrated by reduced peak intensity for both treated and baselined spectra, and number of peaks. Brand 1 vaccines however demonstrated increased SNR values for SERS samples, indicating that although the addition of a colloid prior to measurement failed to enhance the signal intensity of the samples, SERS demonstrated potential in reducing spectral interference from sample fluorescence and noise in these cases. Brand 3 vaccines showed significant enhancement of signal intensity when measured with the addition of silver nanoparticles in comparison to conventional Raman vaccine samples. Brand 1 and 2 vaccines were diluted with 0.9% NaCl prior to measurement, and further diluted with silver nanoparticles and 1M KBr aggregating agent for SERS measurement. Brand 3 vaccines were measured as received without the addition of 0.9% NaCl for conventional Raman measurement. Brand 3 vaccines obtained

significantly higher maximum peak intensity in untreated spectra compared to brand 1 and 2 vaccines (table 3.6). Hence, the higher peak intensity observed for brand 3 vaccines could be attributed to the increased concentration of the undiluted vaccines, as drug concentration positively correlates with signal intensity in Raman spectroscopy (Elshout et al., 2011). The significantly weaker concentration of the diluted brand 1 and 2 vaccines could inhibit enhancement of the vaccines' signal when measured with the addition of the silver colloid. Previous studies of biologics using surface-enhanced Raman spectroscopy experienced signal intensity related limitations corresponding to low concentrations of samples (Clarke et al., 2005; Sackmann and Materny, 2006).

Table 3.5 Values for spectral quality parameters of Brand 1 standard and surface-enhanced average spectra measured using the Metrohm MIRA XTR DS handheld Raman Spectrometer equipped with orbital raster scattering across 400-2300 cm⁻¹

Vaccine	Brand	N	Maximum band position (cm⁻¹)	Baselined Max intensity (arbitrary units)	SNR*	Raman Scattering
LJMUCV661	1	17	835	1837	54	M
SERSLJMUCV661	1	16	834	785	97	S
LJMUCV664	1	17	836	2026	9	M
SERSLJMUCV664	1	15	1328	670	379	S
LJMUCV665	1	15	835	1937	3	W
SERSLJMUCV665	1	15	1338	724	80	M

LJMUCV667	1	17	834	2005	119	S
SERSLJMUCV667	1	13	1330	735	183	S
LJMUCV668	1	16	835	1527	4	W
SERSLJMUCV668	1	16	1352	612	195	M
LJMUCV670	1	19	838	1890	88	S
SERSLJMUCV670	1	14	1327	729	616	S
LJMUCV679	1	17	836	1216	24	M
SERSLJMUCV679	1	13	836	853	302	S
LJMUCV681	1	16	836	1478	3	W
SERSLJMUCV681	1	16	1347	692	240	S
LJMUCV683	1	18	835	1942	121	S
SERSLJMUCV683	1	15	834	852	138	S
LJMUCV687	1	19	835	1514	4	W
SERSLJMUCV687	1	13	1338	804	87	M
LJMUCV688	1	16	836	1508	3	W
SERSLJMUCV688	1	14	1356	720	483	S
LJMUCV690	1	21	835	1621	7	M
SERSLJMUCV690	1	14	1355	777	1129	S
LJMUCV691	1	17	835	1575	182	S
SERSLJMUCV691	1	16	1333	671	864	S
LJMUCV692	1	18	836	1410	9	M
SERSLJMUCV692	1	15	1356	656	233	S
LJMUCV694	1	19	834	1545	4	W
SERSLJMUCV694	1	15	1331	729	228	S

LJMUCV697	1	20	836	1750	306	S
SERSLJMUCV697	1	14	1342	690	350	S
LJMUCV702	1	19	836	1781	37	M
SERSLJMUCV702	1	13	1328	658	257	S
LJMUCV703	1	16	835	1367	3	W
SERSLJMUCV703	1	13	1340	684	52	M
LJMUCV704	1	17	835	1657	169	S
SERSLJMUCV704	1	13	1342	673	1226	S
LJMUCV705	1	18	835	1777	3	W
SERSLJMUCV705	1	15	1334	670	138	S

*at maximum band position, S=Strong, M=Medium, W=Weak

Table 3.6 Values for spectral quality parameters of Brand 2 standard and surface-enhanced average spectra measured using the Metrohm MIRA XTR DS handheld Raman Spectrometer equipped with orbital raster scattering across 400-2300 cm⁻¹

Vaccine	Brand	N	Maximum band position (cm⁻¹)	Baselined Max intensity (arbitrary units)	SNR*	Raman Scattering
LJMUCV355	2	11	1346	644	254	S
SERSLJMUCV355	2	10	1335	514	68	M
LJMUCV356	2	12	1347	592	143	S
SERSLJMUCV356	2	7	1335	629	104	S
LJMUCV357	2	12	1336	645	197	S

SERSLJMUCV357	2	9	1346	578	241	S
LJMUCV358	2	11	1326	588	978	S
SERSLJMUCV358	2	10	1325	625	36	M
LJMUCV359	2	11	1337	597	297	S
SERSLJMUCV359	2	7	1345	540	141	S
LJMUCV360	2	11	1338	598	122	S
SERSLJMUCV360	2	9	1346	563	202	S
LJMUCV361	2	10	1342	507	203	S
SERSLJMUCV361	2	10	1335	513	295	S
LJMUCV363	2	11	1350	648	152	S
SERSLJMUCV363	2	8	1340	563	229	S
LJMUCV364	2	10	1349	628	361	S
SERSLJMUCV364	2	8	1345	527	19	M
LJMUCV395	2	12	1341	539	224	S
SERSLJMUCV395	2	10	1354	497	252	S
LJMUCV396	2	12	1332	625	150	S
SERSLJMUCV396	2	10	1338	543	123	S
LJMUCV397	2	12	1341	614	174	S
SERSLJMUCV397	2	9	1328	496	52	M
LJMUCV398	2	10	1330	655	47	M
SERSLJMUCV398	2	7	1332	621	134	S
LJMUCV399	2	12	1331	633	8	W
SERSLJMUCV399	2	8	1338	544	98	M
LJMUCV400	2	10	1336	596	298	S

SERSLJMUCV400	2	10	1339	565	103	S
LJMUCV401	2	11	1337	668	29	M
SERSLJMUCV401	2	9	1347	580	22	M
LJMUCV402	2	12	1342	604	468	S
SERSLJMUCV402	2	7	1338	571	136	S
LJMUCV403	2	11	1331	617	19	M
SERSLJMUCV403	2	9	1336	618	397	S
LJMUCV404	2	11	1336	610	25	M
SERSLJMUCV404	2	9	1338	662	103	S
LJMUCV1287	2	11	1330	611	157	S
SERSLJMUCV1287	2	7	1340	512	116	S
LJMUCV1292	2	12	1336	609	193	S
SERSLJMUCV1292	2	10	1328	539	181	S
LJMUCV1296	2	9	1335	624	214	S
SERSLJMUCV1296	2	8	1340	554	50	M
LJMUCV1313	2	10	1345	538	385	S
SERSLJMUCV1313	2	9	1339	552	159	S

*at maximum band position, S=Strong, M=Medium, W=Weak

Table 3.7 Values for spectral quality parameters of Brand 3 standard and surface-enhanced average spectra measured using the Metrohm MIRA XTR DS handheld Raman Spectrometer equipped with orbital raster scattering across 400-2300 cm⁻¹

Vaccine	Brand	N	Maximum band position (cm⁻¹)	Baselined Max intensity (arbitrary units)	SNR*	Raman Scattering
LJMUCV1371	3	9	1327	573	611	S
SERSLJMUCV1371	3	4	1334	825	27	W
LJMUCV1373	3	10	1320	515	95	M
SERSLJMUCV1373	3	6	1802	1336	27	W
LJMUCV1374	3	11	1333	590	119	S
SERSLJMUCV1374	3	4	1312	1026	18	W
LJMUCV1375	3	10	1333	586	132	S
SERSLJMUCV1375	3	4	1334	832	42	W
LJMUCV1376	3	9	1333	559	70	M
SERSLJMUCV1376	3	5	1336	1059	22	W
LJMUCV1378	3	9	1337	559	84	M
SERSLJMUCV1378	3	5	1335	816	11	W
LJMUCV1381	3	11	1330	536	186	S
SERSLJMUCV1381	3	6	1335	929	86	M
LJMUCV1387	3	10	1336	605	35	M
SERSLJMUCV1387	3	4	1802	945	12	W

LJMUCV1389	3	10	1331	584	240	S
SERSLJMUCV1389	3	5	1335	869	28	M
LJMUCV1390	3	9	1329	546	341	S
SERSLJMUCV1390	3	4	1795	1113	14	W
LJMUCV1392	3	10	1329	579	134	S
SERSLJMUCV1392	3	4	1327	768	123	M
LJMUCV1394	3	10	1331	543	525	S
SERSLJMUCV1394	3	5	1354	870	12	W
LJMUCV1395	3	11	1332	588	353	S
SERSLJMUCV1395	3	5	1338	867	11	W
LJMUCV1396	3	9	1325	529	41	M
SERSLJMUCV1396	3	3	1332	748	5	W
LJMUCV1397	3	10	1328	611	260	S
SERSLJMUCV1397	3	3	1336	860	38	W
LJMUCV1399	3	9	1333	602	9	W
SERSLJMUCV1399	3	4	1340	679	26	W
LJMUCV1400	3	10	1338	604	2	W
SERSLJMUCV1400	3	5	1334	878	7	W
LJMUCV1401	3	10	1335	604	169	S
SERSLJMUCV1401	3	3	1335	856	37	W
LJMUCV1403	3	10	1335	566	147	M
SERSLJMUCV1403	3	4	1343	756	267	M
LJMUCV1404	3	11	1336	526	22	M
SERSLJMUCV1404	3	4	1340	871	28	W

LJMUCV1405	3	8	1354	532	7	W
SERSLJMUCV1405	3	4	1336	748	39	M

*at maximum band position, S=Strong, M=Medium, W=Weak

Table 3.8 Average values of spectral quality parameters for standard and surface-enhanced Raman spectra by brand, measured using the Metrohm MIRA XTR DS handheld Raman Spectrometer equipped with orbital raster scattering across a range of 400-2300 cm⁻¹

Vaccine Brand	N	Maximum band position (cm⁻¹)	Standard Max Intensity (arbitrary units)	Baselined Max Intensity (arbitrary units)	SNR*	Raman Scattering
1	18	835	6808	1668	58	S
1 (SERS)	14	1339	6528	719	364	S
2	11	1338	6203	608	222	S
2 (SERS)	9	1339	6096	561	142	M
3	10	1333	10959	568	171	S
3 (SERS)	4	1335	32130	888	42	M

*at maximum band position, S=Strong, M=Medium, W=Weak

3.4.1.3 Authentication of Covid-19 vaccines by handheld Raman Spectroscopy

For vaccine authentication, unsupervised clustering was applied to the vaccines' spectra using PCA as specified in section 2.3.3. The frequency of Type I and Type II

errors observed in the PC scores scatter plots were used for assessment of accuracy in clustering. Type I errors were observed where vaccine scores were clustered with the scores of a different vaccine brand. Type II errors were observed where the scores of a vaccine were clustered away from the majority of their representative brand.

Figures 3.23 and 3.24 show the PC scores plots of the conventional Raman vaccine spectra, brand 1 vaccines showed the highest contribution to the variance observed, demonstrated by their spatial position at PC1 which reflected 80.5% of the variance observed (Figure 3.23; Figure 3.24). Distinct clusters were able to be identified for all three brands of vaccines, however type I and type II errors were observed for all brands. Type II errors were observed for brand 1 vaccines where 5 of the vaccine scores were clustered with the majority of the brand 2 vaccines and 11 of the vaccine scores were clustered away from the majority of all vaccine scores (Figure 3.23). However, when plotted across three axis (Figure 3.24) distinct clustering for brand 1 vaccines was observed where no type I or type II errors occurred. Brand 2 vaccines showed significant overlap with the brand 3 vaccine scores in Figure 3.23 and Figure 3.24. One type I error was observed for brand 2 vaccines, where one score was clustered with the majority of brand 1 vaccine scores. Brand 3 showed the poorest clustering in both PCA models (Figure 3.23; Figure 3.24) where type I errors were observed when brand 3 scores were clustered with the majority of brand 1 vaccine scores. 14 type II errors were observed for brand 3 vaccines where scores were clustered away from the majority of the brand 3 vaccines. Two significant outliers were identified in the brand 3 vaccine spectra where scores were plotted a significant distance from the majority of the vaccines.

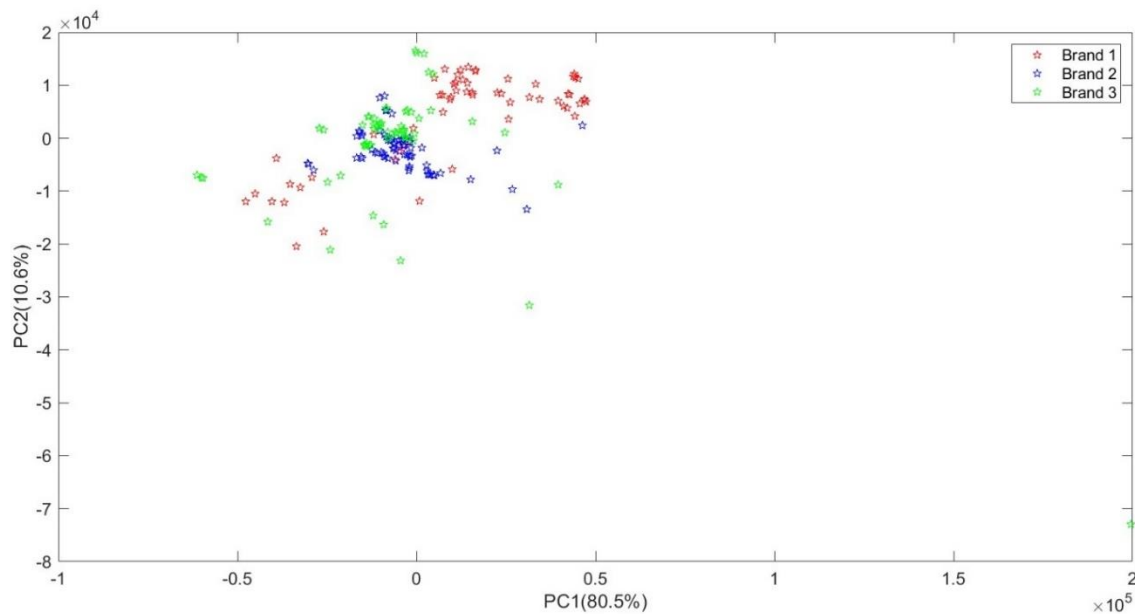


Figure 3.23 2D PC Scores plot of Brand 1 (red), Brand 2 (blue), and Brand 3 (green) vaccines measured using the Metrohm MIRA XTR DS handheld Raman spectrometer equipped with 785nm laser and orbital raster scattering across a range of $400\text{-}2300\text{cm}^{-1}$

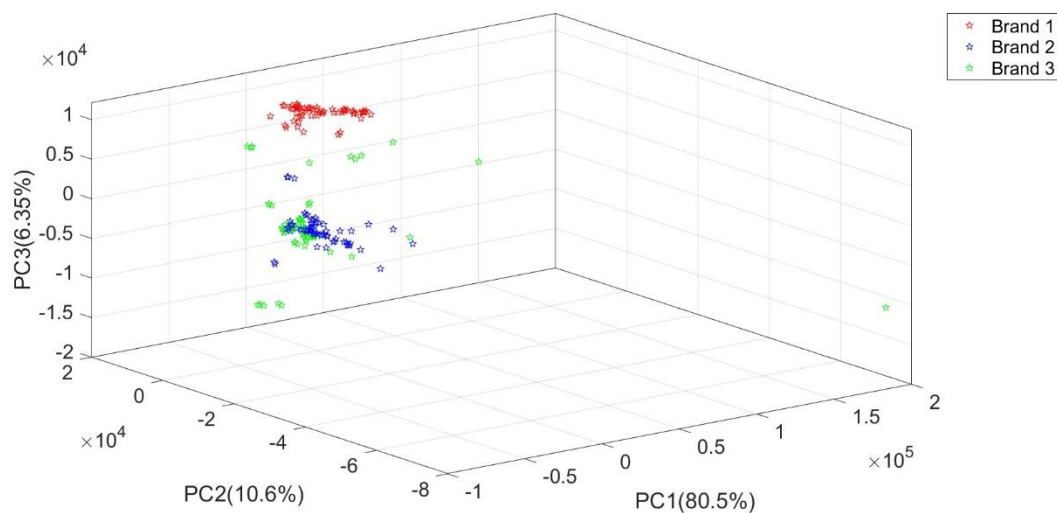


Figure 3.24 2D PC Scores plot of Brand 1 (red), Brand 2 (blue), and Brand 3 (green) vaccines measured using the Metrohm MIRA XTR DS handheld Raman spectrometer equipped with 785nm laser and orbital raster scattering across a range of $400\text{-}2300\text{cm}^{-1}$

Figure 3.25 and Figure 3.26 show the PC scores plot of the SERS vaccine spectra. Brand 3 vaccines showed the highest contribution to the variance observed in the vaccine spectra, demonstrated by the special position of the scores at PC1, which attributed to 98.9% of the variance. Distinct clustering was observed for the SERS brand 1 and 2 vaccine scores (Figure 3.25; Figure 3.26), where scores of the same vaccine were clustered closely together. Significant overlap between the brand 1 and 2 vaccines was observed, type I errors occurred for both brand 1 and 2 vaccines where scores of each brand were clustered with the majority of scores from the other. No distinct clustering was seen for the brand 3 vaccines, where all scores were plotted away from each other, and at distance from the other two vaccine brands' scores.

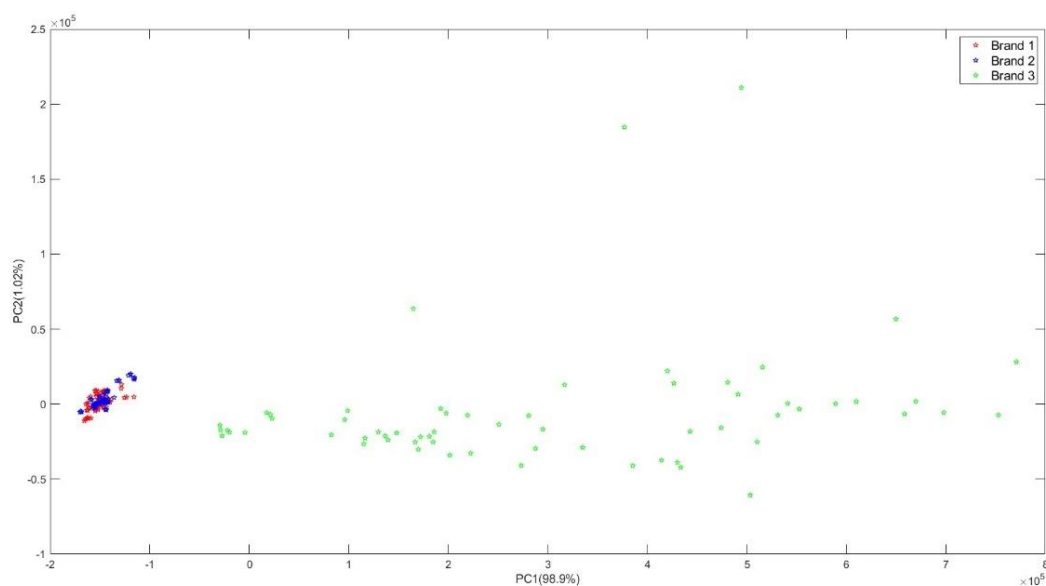


Figure 3.25 2D PC Scores plot of the SERS Brand 1 (red), Brand 2 (blue), and Brand 3 (green) vaccines measured with the addition of the silver nanoparticles and 1M KBr aggregating salt using the Metrohm MIRA XTR DS handheld Raman spectrometer equipped with 785nm laser and orbital raster scattering across a range of 400-2300 cm^{-1}

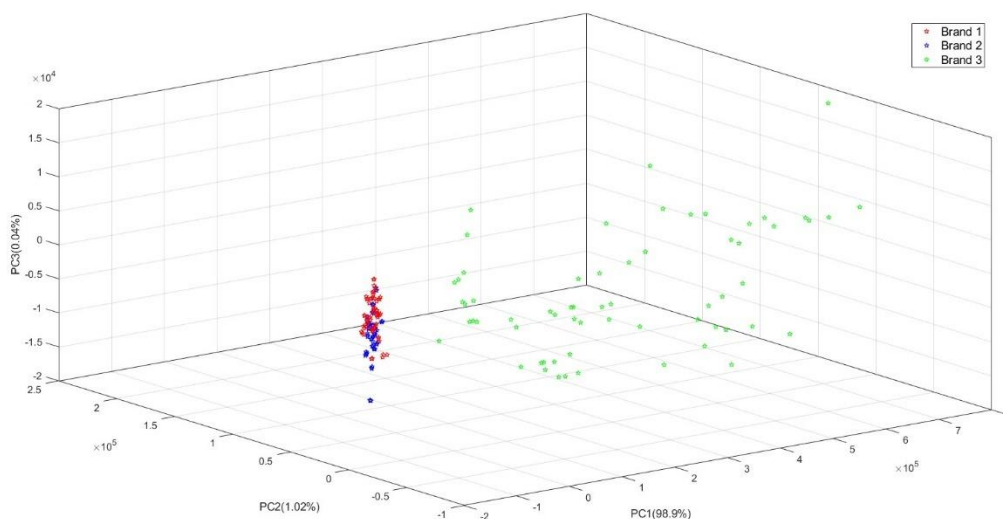


Figure 3.26 3D PC Scores plot of the SERS Brand 1 (red), Brand 2 (blue), and Brand 3 (green) vaccines measured with the addition of the silver nanoparticles and 1M KBr aggregating salt using the Metrohm MIRA XTR DS handheld Raman spectrometer equipped with 785nm laser and orbital raster scattering across a range of 400-2300 cm^{-1}

These results suggest that PCA is a poor indicator of identification potential in SERS vaccine spectra. Although distinct clustering was identified in the 3D PC scores model of the conventional Raman spectra of the covid-19 vaccines (Figure 3.24), type II errors were noted for the scores of the brand 3 vaccines. Significant variation in the brand 3 vaccine scores was seen in both the 2D and 3D PC scores plots of the SERS vaccine spectra, suggesting the SERS spectra of brand 3 lack consistency and reproducibility in comparison to the other two brands. Reproducibility has long been a limitation in SERS, especially colloidal SERS (Tantra, Brown and Milton, 2007). As the SERS enhancement scales with $|E/E_0|^4$, small changes in the in- and out-coupling or disconcertion in near-field enhancement (E/E_0) drastically alter SERS intensities (Le Ru and Etchegoin, 2006).

3.4.1.4 Vaccine Classification

Supervised machine learning techniques were applied to the spectral dataset for assessment of identification potential. A total of 33 classification models were trained on both the conventional Raman spectral dataset and the SERS vaccine dataset. For each model, 80% of the data was used to train a 10-fold cross validation model, with 20% allocated as a test dataset to prevent overfitting. The dataset was divided into three classes (brands) and the model predicted class based on Raman intensity at each data point across a range of 400-2300 cm^{-1} . Table 3.9 shows the accuracy for each model of the 10-fold cross validation and test runs. Matlab's classification learner tool highlighted model 2.25 – an ensemble subspace KNN classification model as the most accurate across both validation and test classifications.

Table 3.9 Model number, type, and accuracy of the validation and test runs for each of the classification models trained on the conventional Raman dataset using Matlab 2023a classification learner tool

Model Number	Model Type	Accuracy % (Validation)	Accuracy % (Test)
1	Tree	72.07792	65.78947
2.1	Tree	72.07792	65.78947
2.2	Tree	72.07792	65.78947
2.3	Tree	71.42857	65.78947
2.4	Discriminant	79.22078	78.94737
2.5	Discriminant	NaN	NaN
2.6	Efficient Logistic Regression	36.36364	52.63158
2.7	Efficient Linear SVM	62.98701	71.05263

2.8	Naive Bayes	68.18182	68.42105
2.9	Naive Bayes	67.53247	NaN
2.1	SVM	82.46753	86.84211
2.11	SVM	90.25974	94.73684
2.12	SVM	87.66234	94.73684
2.13	SVM	84.41558	89.47368
2.14	SVM	83.11688	89.47368
2.15	SVM	73.37662	73.68421
2.16	KNN	94.80519	92.10526
2.17	KNN	75.97403	76.31579
2.18	KNN	37.66234	47.36842
2.19	KNN	84.41558	86.84211
2.2	KNN	79.22078	76.31579
2.21	KNN	84.41558	89.47368
2.22	Ensemble	36.36364	34.21053
2.23	Ensemble	85.06494	78.94737
2.24	Ensemble	83.11688	84.21053
2.25	Ensemble	96.1039	94.73684
2.26	Ensemble	76.62338	78.94737
2.27	Neural Network	86.36364	78.94737
2.28	Neural Network	88.31169	97.36842
2.29	Neural Network	90.90909	92.10526
2.3	Neural Network	88.31169	92.10526
2.31	Neural Network	87.01299	86.84211

2.32	Kernel	91.55844	97.36842
2.33	Kernel	83.11688	84.21053

The ensemble subspace K-Nearest Neighbour (KNN) classification model was trained using Matlab 2023a classification learner. Figure 3.27 shows the confusion matrix for the 10-fold cross validation which obtained an accuracy of 96.1% and was identified by Matlab 2023a classification learner tool as the most effective classification model trained using the spectral dataset provided. Three type I errors were observed for brand 1 vaccines where vaccines of the other classes were falsely predicted as brand 1. Brand 2 vaccines expressed type I and type II errors against brands 1, 2 and 3 and brand 3 vaccines expressed type I and II errors against the other three classes. No brand 1 vaccines were falsely predicted as either of the other two brands, likely attributed to the difference in number of bands and signal intensity between the brand 1 vaccines and the rest of the dataset. Two brand 3 vaccines were falsely predicted to be brand 1, probably as a result of the similarities in their formulation and constituent nucleic acid. Table 3.8 shows the classification evaluation metrics for the ensemble subspace KNN classification model (Model 2.25) by brand, including accuracy, precision, recall, specificity and F1-score. Model 2.25 demonstrated excellent performance in terms of the aforementioned metrics, with an overall accuracy of 97.4% and an F1-score of 0.961 (Table 3.10).

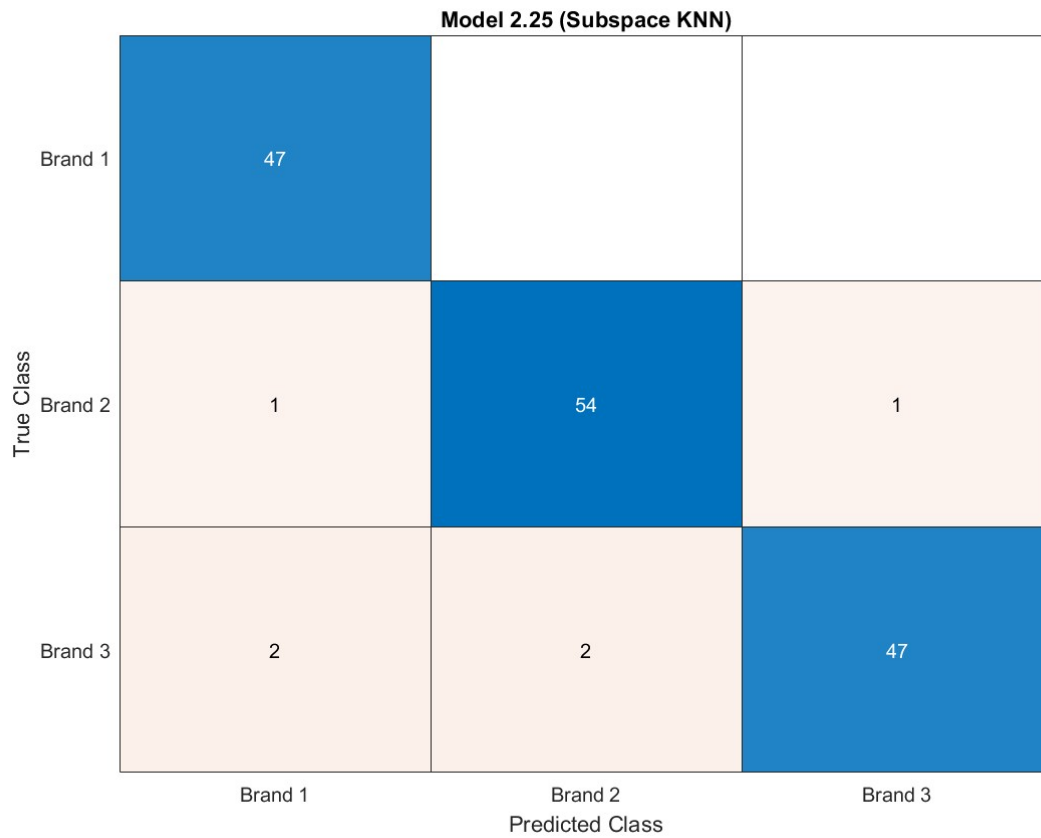


Figure 3.27 Confusion matrix for Ensemble subspace K-nearest neighbour classification 10-fold validation model trained using Matlab 2023a classification learner and conventional Raman spectral dataset from vaccine brands 1, 2 and 3 measured using the Metrohm MIRA XTR DS handheld Raman spectrometer

Table 3.10 Accuracy, precision, recall, specificity and F1-score of Ensemble subspace KNN 10-fold cross validation classification model for vaccine brands 1-3 and overall

Brand	Accuracy (%)	Precision (%)	Recall (%)	F1-Score	Specificity (%)
1	98.1	94.0	100.0	0.969	97.2
2	97.4	96.4	96.4	0.964	98.0
3	96.8	97.9	92.2	0.949	99.0
Overall	97.4	96.1	96.2	0.961	98.1

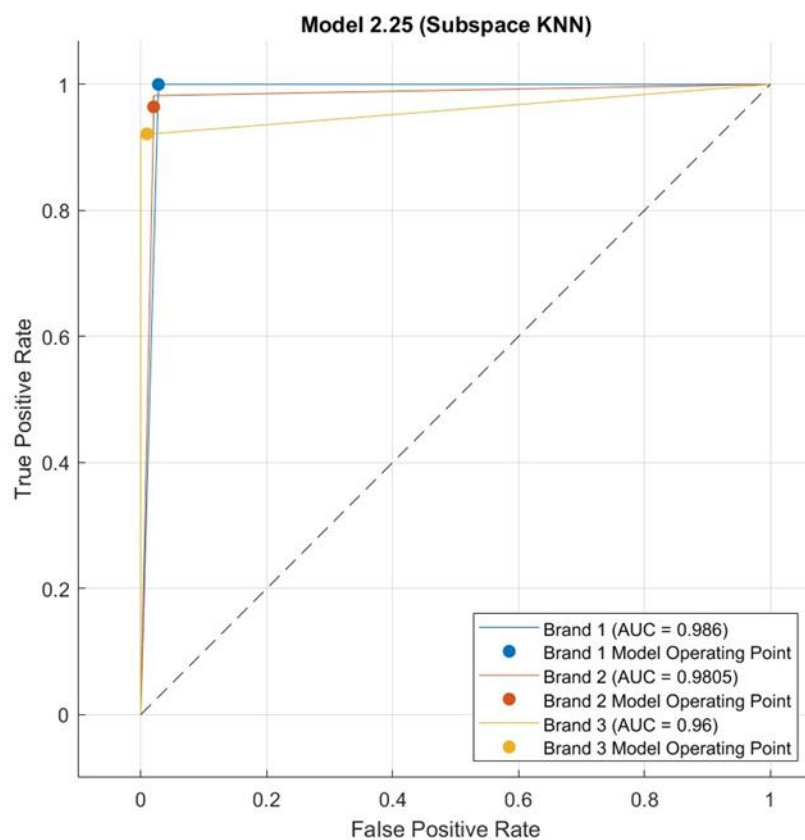


Figure 3.28 AUC-ROC curve for 10-fold validation of Ensemble subspace K-nearest neighbour classification model carried out on Raman spectral dataset of vaccine brands 1 (blue), 2 (red), and 3 (yellow) measured on the Metrohm MIRA XTR DS handheld Raman spectrometer

Figure 3.28 shows the AUC-ROC curve produced in Matlab 2023a Classification Learner tool for the 10-fold validation of the Raman spectral dataset. The AUC-ROC curve demonstrates the separation capacity of the model between the three different classes when presented with unsupervised machine learning. An AUC value of 1 demonstrates perfect separation capacity of the classification model with no errors observed between class categorisations. The results of the 10-fold validation of the Ensemble subspace K-nearest neighbour classification run obtained AUC values of 0.986, 0.9805 and 0.96 for brands 1, 2 and 3 respectively (Figure 3.28). AUC values of at least 0.80 are considered clinically useful with values over 0.90 considered to demonstrate an excellent measure of separability in models (Gardner and Greiner, 2006; Huang and Ling, 2005). Hence, with AUC values exceeding the lower threshold of acceptance, the ensemble subspace K-nearest neighbour exhibited potential as a reliable and accurate method of vaccine classification based on spectral characteristics.

Table 3.9 shows the accuracy for the 10-fold cross validation and 20% test classification models trained on the SERS vaccine spectral dataset using Matlab 2023a classification learner. The classification models executed on the SERS dataset outperformed the conventional Raman dataset in terms of accuracy across both the cross validation and test runs. 15 of the 33 SERS classification models obtained an accuracy of 100% for the test dataset, where all vaccine spectra were correctly predicted as their brand of origin.

Table 3.11 Model number, type, and accuracy of the validation and test runs for each of the classification models trained on the SERS dataset using Matlab 2023a classification learner tool

Model Number	Model Type	Accuracy % (Validation)	Accuracy % (Test)
3.01	Tree	94.80519	94.73684
3.02	Tree	94.80519	94.73684
3.03	Tree	94.80519	94.73684
3.04	Discriminant	100	100
3.05	Discriminant	NaN	NaN
3.06	Efficient Logistic Regression	68.18182	68.42105
3.07	Efficient Linear SVM	71.42857	65.78947
3.08	Naive Bayes	87.66234	84.21053
3.09	Naive Bayes	92.20779	94.73684
3.10	SVM	100	100
3.11	SVM	100	100
3.12	SVM	100	100
3.13	SVM	98.05195	94.73684
3.14	SVM	100	100
3.15	SVM	85.71429	86.84211
3.16	KNN	99.35065	100
3.17	KNN	94.80519	97.36842
3.18	KNN	57.79221	57.89474
3.19	KNN	96.1039	94.73684

3.20	KNN	92.85714	97.36842
3.21	KNN	100	100
3.22	Ensemble	36.36364	34.21053
3.23	Ensemble	94.15584	92.10526
3.24	Ensemble	100	100
3.25	Ensemble	99.35065	100
3.26	Ensemble	48.7013	92.10526
3.27	Neural Network	96.1039	100
3.28	Neural Network	100	100
3.29	Neural Network	100	100
3.30	Neural Network	99.35065	100
3.31	Neural Network	100	100
3.32	Kernel	99.35065	100
3.33	Kernel	98.05195	94.73684

Figure 3.29 shows an ensemble subspace discriminant classification 10-fold cross validation classification model trained using Matlab 2023a classification learner tool on the SERS vaccine dataset. This classification model (Model 3.24) was identified in the classification learner as obtaining an accuracy of 100% across validation and test runs. This demonstrates faultless performance of the model for vaccine brand prediction based on spectral characteristics across a range of 400-2300 cm^{-1} . Other classification models obtaining prediction accuracies of 100% include a linear discriminant-based model (Figure 3.30) and a weighted KNN based model (Figure 3.31).

Figures 3.32, Figure 3.33 and Figure 3.34 show the AUC-ROC curves for the ensemble subspace discriminant, linear discriminant and weighted KNN based classification models, respectively. All three models exhibited an AUC value of 1 for each vaccine brand, demonstrating the perfect separation capacity of the models.

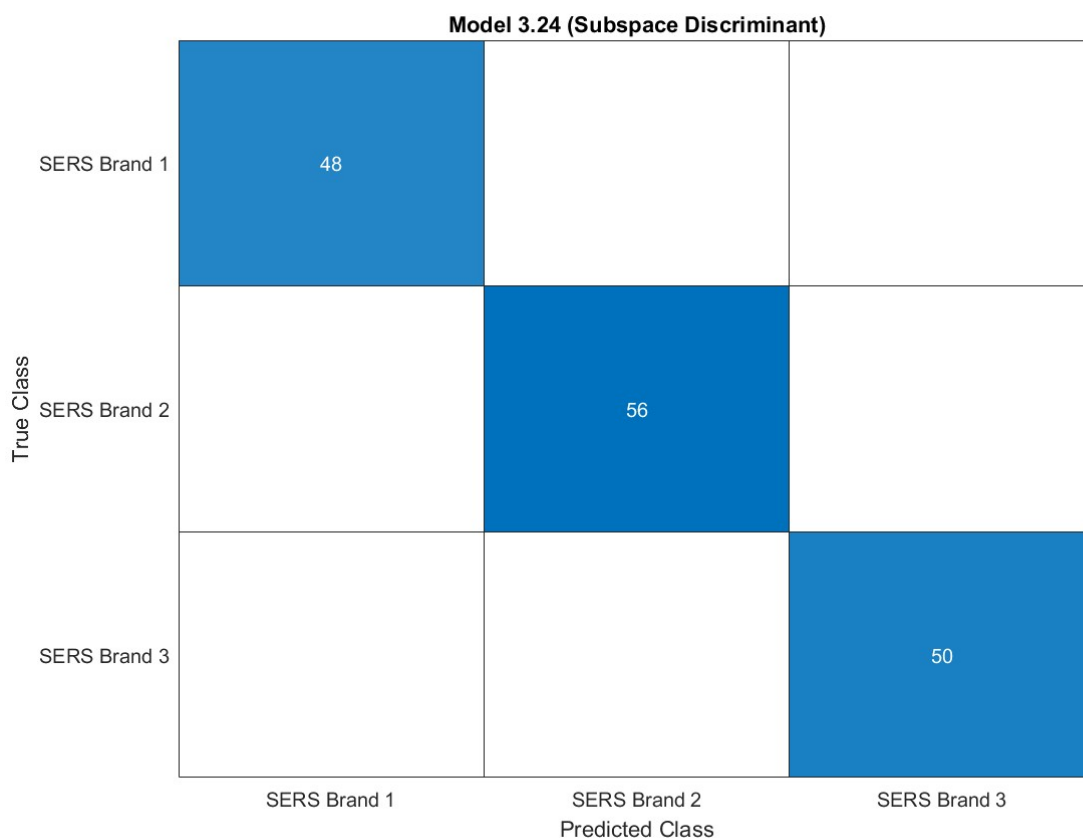


Figure 3.29 Confusion matrix for ensemble subspace discriminant classification 10-fold validation model trained using Matlab 2023a classification learner and SERS dataset from vaccine brands 1, 2 and 3 measured using the Metrohm MIRA XTR DS handheld Raman spectrometer

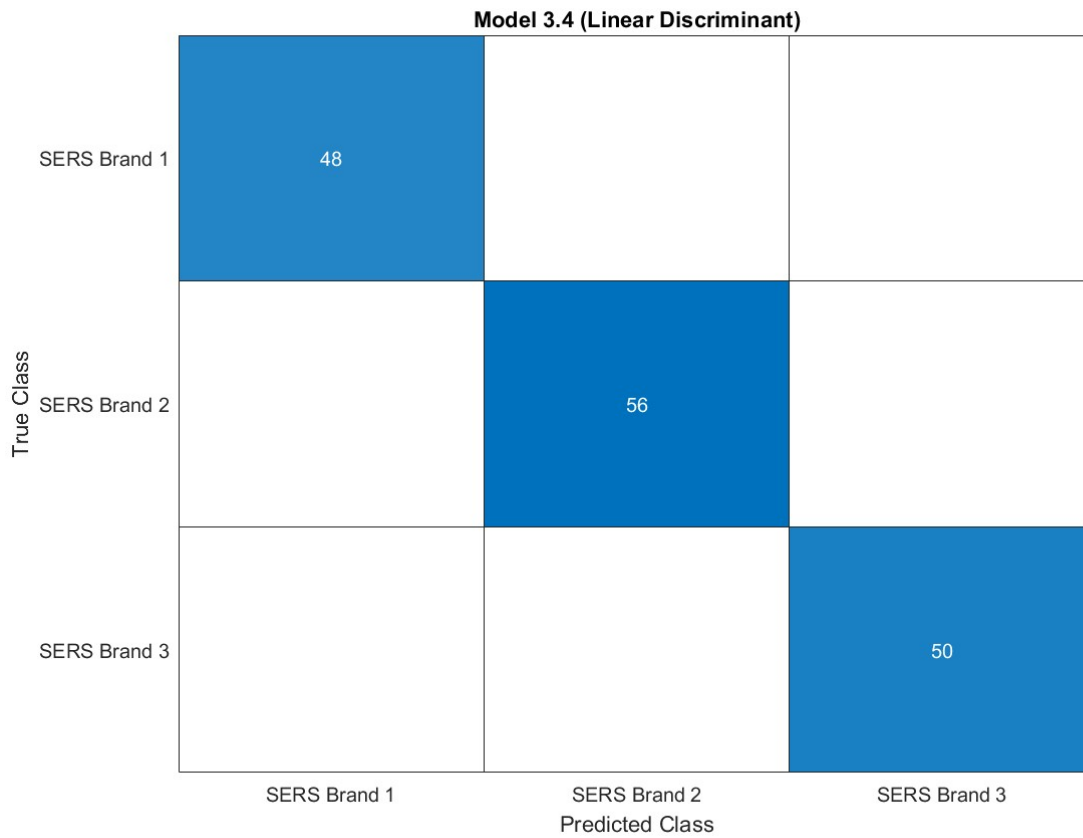


Figure 3.30 Confusion matrix for linear discriminant classification 10-fold validation model trained using Matlab 2023a classification learner and SERS dataset from vaccine brands 1, 2 and 3 measured using the Metrohm MIRA XTR DS handheld Raman spectrometer

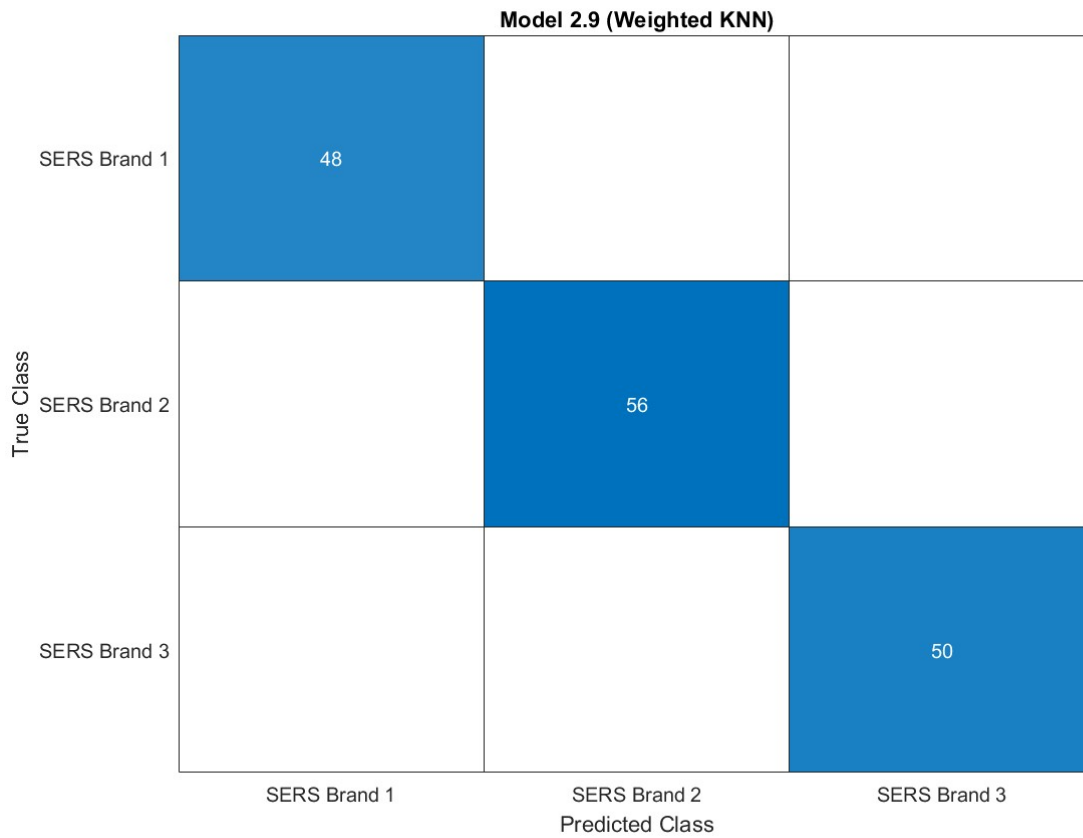


Figure 3.31 Confusion matrix for weighted KNN classification 10-fold validation model trained using Matlab 2023a classification learner and SERS dataset from vaccine brands 1, 2 and 3 measured using the Metrohm MIRA XTR DS handheld Raman spectrometer

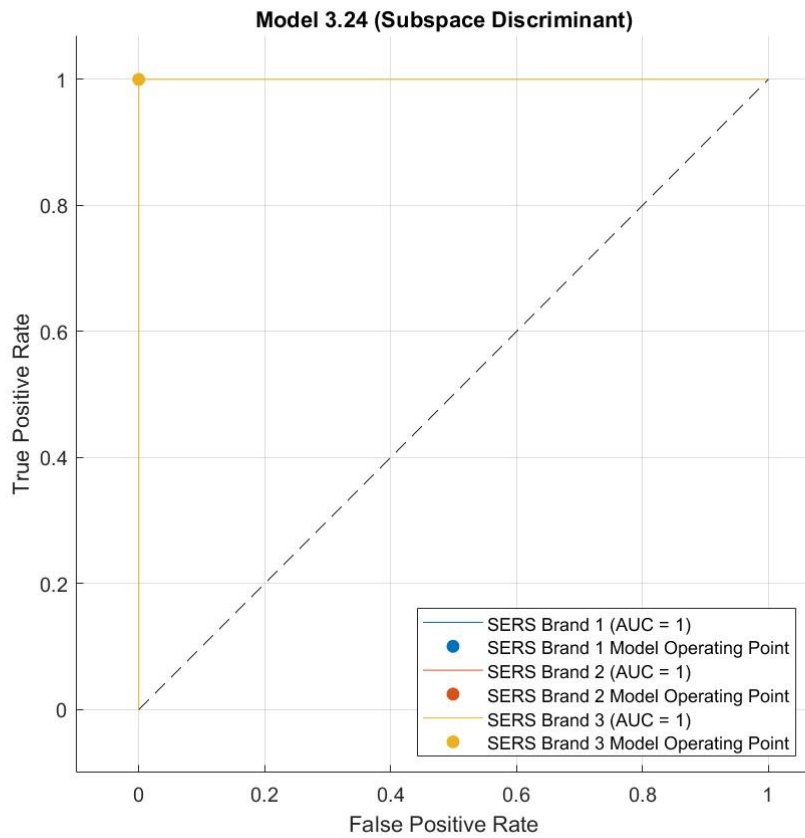


Figure 3.32 AUC-ROC curve for 10-fold validation of ensemble subspace discriminant classification model carried out on SERS dataset of vaccine brands 1 (blue), 2 (red), and 3 (yellow) measured on the Metrohm MIRA XTR DS handheld Raman spectrometer

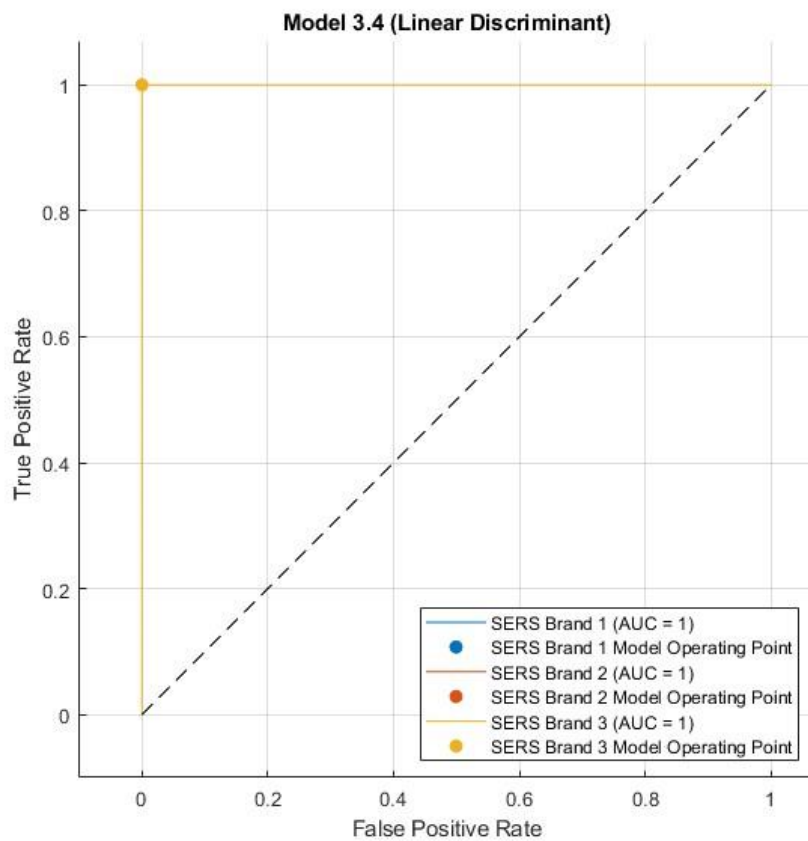


Figure 3.33 AUC-ROC curve for 10-fold validation of linear discriminant classification model carried out on SERS dataset of vaccine brands 1 (blue), 2 (red), and 3 (yellow) measured on the Metrohm MIRA XTR DS handheld Raman spectrometer

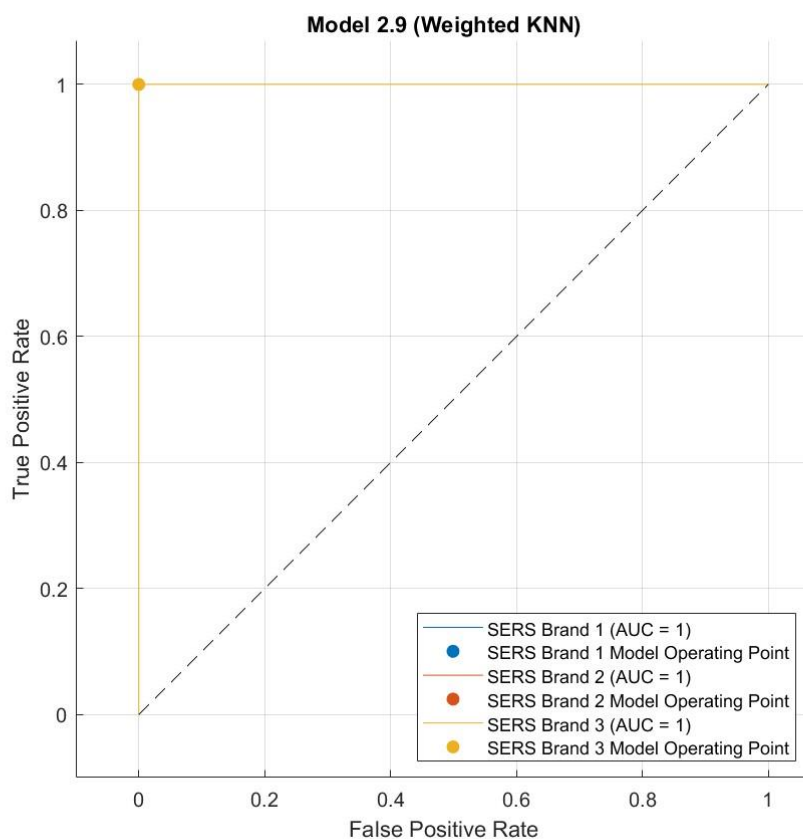


Figure 3.34 AUC-ROC curve for 10-fold validation of linear discriminant classification model carried out on SERS dataset of vaccine brands 1 (blue), 2 (red), and 3 (yellow) measured on the Metrohm MIRA XTR DS handheld Raman spectrometer

3.4.1.5 Conclusion

To conclude, this study highlights the potential of both conventional Raman spectroscopy and surface-enhanced Raman spectroscopy as effective analytical tools in the authentication of covid-19 vaccines. All three bands of vaccine spectra displayed bands corresponding to their constituent nucleic acids and their excipients. The DNA and mRNA lipid nanoparticle-based vaccines showed spectral similarities that could be attributed to the PEGylated lipid nanoparticles in their formulation. Vaccine spectra were able to be distinguished by formulation, based on nucleic acid specific peaks in

their spectra. mRNA based vaccines were able to be identified by the presence of nitrogenous uracil groups. Improved enhancement was seen for SERS in the pilot study in comparison to the overall study, suggesting that the greater concentration of vaccines used in the pilot study, alongside reduced storage time could be responsible for the favourable results. The hydroxylamine hydrochloride reduced-silver colloid could also be a favourable SERS substrate in comparison to the silver nanoparticles used in the final study. The addition of silver nanoparticles indicated potential for signal enhancement when SERS was applied to samples of a sufficient original concentration as demonstrated by signal intensity enhancement of up to 498% for the brand 3 vaccines. Repeated dilution of brand 1 and 2 samples could be responsible for the poor enhancement experienced when samples were measured with the addition of the colloid. Brand 1 and 2 vaccines were at greater risk of degradation due to storage conditions and time elapsed between sample receipt and measurement, especially for the brand 2 mRNA-based vaccines which formulation is notoriously unstable. Clustering based on PCA showed some accuracy in differentiating between the different vaccine brands for conventional Raman spectroscopy, but overlap between brand 1 and 2 vaccines, and significant variation between the brand 3 vaccines indicated poor repeatability of the method when SERS was applied. Classification models far outperformed PCA as a measure of identification potential, with multiple models producing 100% accuracy for brand prediction based on spectral characteristics across a range of 400-2300 cm^{-1} . In this sense, SERS outperformed conventional Raman, with linear discriminant, ensemble subspace discriminant and weighted KNN based classification models obtaining 100% accuracy, precision, recall, specificity and F1-score of 100% for both validation and test runs performed on the SERS data. Conventional Raman still produced high values of over 90% for each of

these evaluation metrics featured in its highest performing classification model – ensemble subspace KNN. AUC-ROC indicated promising results for the separation capacity of the ensemble subspace KNN classification model trained on the conventional Raman dataset, with AUC values of 0.986, 0.91 and 0.96 for brands 1, 2 and 3 respectively, suggesting excellent separation capacity of the model. The linear discriminant, ensemble subspace discriminant and weighted KNN based classification models trained on the SERS dataset produced AUC values of 1 for all three vaccine brands, demonstrating the perfect separation capacity of all three classification models. While these results indicate that SERS has a promising future as a valuable technique in the quality control of novel biologics, more extensive research is required to address the limitations of this study. Future work would involve the quantification of vaccine samples to establish an accepted limit of detection (LOD) for the handheld instrument, and further optimisation of the colloidal formulation, and measurement parameters. Repetition of this study on a larger sample size would allow for more representative PCA. However, the faultless results of the classification models, indicate potential in the use of portable SERS in conjunction with machine learning as a rapid, non-destructive, and accurate semi-automated technique for the authentication of covid-19 vaccines.

4. AUTHENTICATION OF COVID-19 VACCINES USING RAMAN MICROSCOPY

4.1 Introduction

Raman microscopy relies on the same principles as Raman spectroscopy for identification of chemical compounds in a sample of interest. A laser is directed at the analyte of interest, the sample is illuminated, where the laser interacts with it and light is scattered off the sample's surface – Rayleigh scattering or Raman scattering. Raman microscopy focuses on Raman scattering for chemical analysis at micro levels, this is inelastic scattering where the Raman scattered light is of a different frequency and wavelength to the original laser. The incident laser gains or loses energy through the interaction with photons, the inelastically scattered radiation is constituted by Anti-stokes (energy gain) or Stokes (energy loss) lines (Deluca et al., 2023). Stokes lines originate from the ground state and are more likely at room temperature, they also have a higher intensity, so therefore Stokes lines are used in Raman spectroscopy (McCreery, 2000). The scattered light is detected to produce a spectrum which is unique to the chemical composition of the sample, acting as a 'chemical fingerprint' which can be used for identification, characterisation and quantification of the chemical compounds (Bruker, 2024).

Raman microscopy offers the aforementioned advantages with ability to measure at microlevels. This is useful in case of biological samples where minute amount of sample is Raman active. Raman spectroscopy and imaging (Raman microscopy) can be used as a quantitative and non-invasive method of visualisation and

characterisation of pharmaceuticals. Raman spectra can be acquired from small volumes of sample through the utilisation of a Raman microscope. Characteristics of Raman microscopy are related to two optical considerations: the focusing of the incident laser excitation on the sample, and the collection of the scattered light (Turrell and Corset, 1996, pp.27).

Raman scattered photons are collected in a 180° backscattering configuration which allows viewing of the sample, focusing of radiation and collection of Raman spectra. Most commercial microscope systems increase axial resolution through confocal microscopy. Confocal points are defined as the point source, the in-focus sample location and the focused image of the sample point. Axial resolution is defined as the distance away from the focal plane in which the Raman intensity from the sample decreases to 50% of the in-focus intensity. Axial resolution can be estimated using the numerical aperture (NA) used in the microscope (Assi, 2024).

In conventional Raman spectroscopy, the exciting laser beam is focused on the sample usually using a 10-30 cm lens. The laser is concentrated in a focal cylinder (Ikeshoji and Sekine, 1977) which increases the intensity of Raman scattering. Raman microscopy utilises a confocal laser, the essential features of confocal microscopy include:

- Spatial filtering that occurs through optical conjugation onto the sample through the pinhole apertures used for sample illumination and detection.
- Stray background light originating from out-of-focus regions of the sample is attenuated by the aforementioned spatial filtering, so that the main contribution to the signal comes from a selective layer of sample.

By removing the unfocused light, the spatial resolution of imaging is improved, this is especially useful in Raman imaging where detailed chemical images are required. The quality of Raman spectra produced through the confocal pinhole is improved, by removing background light from fluorescence. This removes the need for fluorescence mitigation through wavenumber optimisation. Confocal microscopy also allows selectivity of focal plane, allowing the analysis of light corresponding to different depths within the sample, thus enabling 3-dimensional analysis of the sample of interest. There are limitations to this technique however, a high intensity of monochromatic radiation is focused on a selective area of the sample, exposing the sample to potential thermal degradation (Assi, 2024).

Raman microscopy offers several further advantages:

- A convenient 'point and shoot' approach to chemical analysis and imaging
- The ability to analyse exceptionally small samples (Bruker, 2024)
- Allows the examination of molecules and cells in aqueous solutions, due to the weak Raman scattering of water (Matthäus et al., 2008).

Raman microscopy has been utilised for many clinical applications, included but not limited to: quality control and failure analysis, tissue imaging, in vitro diagnosis, DNA/RNA analysis, metabolic accretions, single cell analysis and photodynamic therapy (Antonio and Schultz, 2013; Carey, 2006; Cavonius et al., 2015; Deluca et al., 2023; Downes, 2015; Fung and Shi, 2020; Huang et al., 2004; Ito, Koyama and Otsuka, 2010; Matthäus et al., 2008; Pavićević et al., 2012; W John Wolfgang, 2005; Zhang et al., 2021).

While previous studies have examined the use of Raman microscopy for studying the cellular effects of mRNA and DNA based vaccines, as well as viral characterisation,

no work has been conducted on the use of Raman microscopy for identification and characterisation of nucleic acid-based vaccines. In this sense, this study aims to address the gaps in existing literature by examining the utilisation of Raman microscopy as a tool for covid-19 vaccine control, to reduce the prevalence and harm associated with SF vaccines in circulation.

4.2 Experimental

4.2.1 Materials

Brands 1 and 2 covid-19 vaccines were obtained from the central Liverpool primary care network as outlined in section 2.2.1. Vaccines were of insufficient volume for clinical use after six or more doses had been administered to patients. Brand 1 and 2 vaccines were diluted with 0.9% NaCl upon receipt to improve stability and increase volume for repeated testing. Brand 3 vaccines were obtained from hospitals in Lebanon and Iraq.

4.2.2 Instrumentation

Measurements were taken using the Horiba XploRA™ PLUS – a MicroRaman Spectrometer/Confocal Raman Microscope (Figure 4.1). The Horiba XploRA™ PLUS includes up to three internal lasers in combination with 12 density filter levels and 4 gratings, allowing it to cover all UV-Vis range and perform Raman and Photoluminescence (PL) analysis. One 532 nm laser was available in this study. The confocal microscope allows both transmission and reflectance illumination to produce 2D and 3D images. Image focusing and spectral acquisition were conducted using Horiba's LabSpec 6 V6.6.2.7 spectroscopy suite.

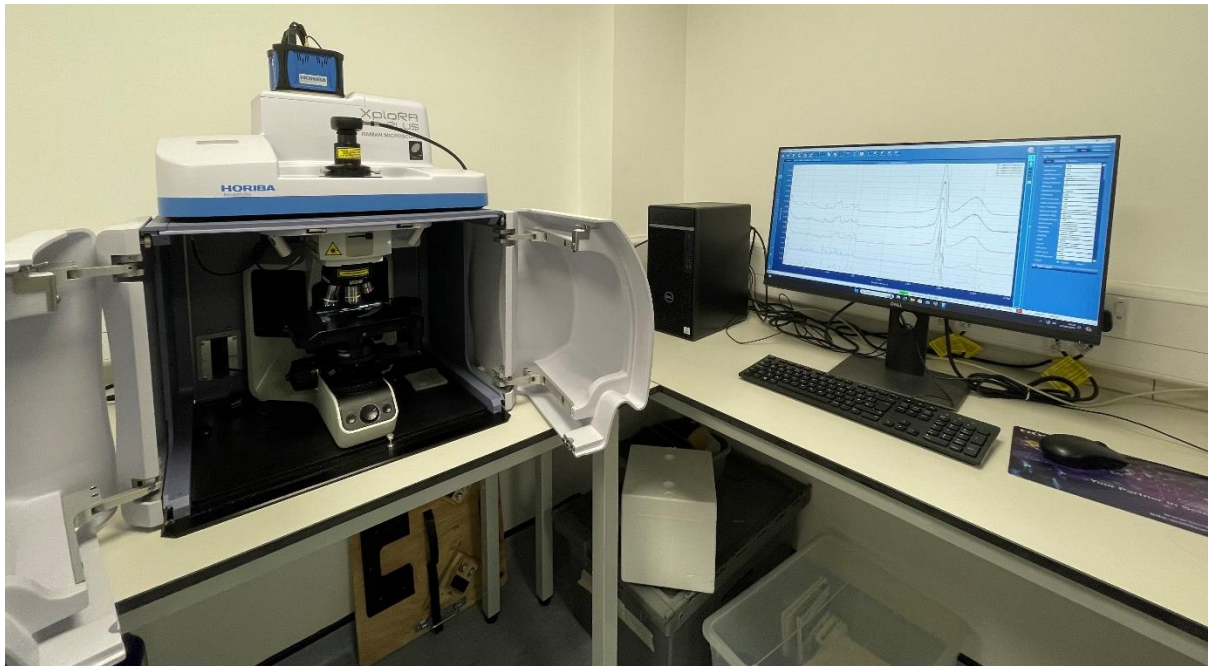


Figure 4.1 Horiba XploRA™ PLUS equipped with 532 nm laser attached to PC with Horiba's LabSpec 6 V6.6.7.2 spectroscopy suite open

Table 4.1 Horiba XploRA™ PLUS specifications from manufacturers website (Horiba Scientific, 2024)

Faster Raman SWIFT™ Imaging/ SWIFTXS (with EMCCD)	Yes, with XY stage
Confocal Imaging	0.5 µm XY
Routine operation automation	OneClick Auto
Full Microscope	Upright
Resolution	Standard + High
Multi-laser options	532, 638, 785 nm

4.2.3 Methods

A small volume (1 drop) of vaccine was syringed onto glass microscope slides and allowed to dry for 1-2 hours prior to measurement.

For SERS measurement, vaccine samples were prepared following the method outlined in chapter 3.2.3. 1 drop of SERS sample was added to a glass slide and allowed to dry for 1-2 hours in a fume hood with the light turned off to minimise light induced degradation of the photosensitive colloid (Grillet et al., 2013).

Samples were measured on the Horiba XploRA™ PLUS using four different categories of system settings, these were altered using Horiba's LabSpec 6 V6.6.2.7 spectroscopy suite. Spectra were acquired across a range of 25-400 cm⁻¹.

Table 4.2 Measurement parameters of settings groups 1, 2, 3, and 4 for samples measured using the Horiba XploRA™ PLUS

Setting	1	2	3	4
Objective	X10	X10	X100	X100
Laser	532 nm	532 nm	532 nm	532 nm
Acquisition Time (sec)	10	10	10	10
Accumulations	2	2	2	2
Grating	1200	600	1200	1200
Filter	25%	10%	25%	10%
Slit (µm)	100	100	100	100
Hole (µm)	100	100	100	100
Number of spectra acquired	20	21	18	8

4.2.4 Spectral treatment and qualitative analysis

Spectra were exported as .spc files through Horiba's LabSpec 6 V6.6.2.7 spectroscopy suite and imported into The Unscrambler software for qualitative analysis and the application of machine learning algorithms. The Unscrambler was used as opposed to Matlab 2024b software due to non-compatibility of the LabSpec 6 files with Matlab's software.

Spectra were divided into three categories for the application of MLA's: x10 objective, x100 objective and SERS x10 objective. PCA was applied to each of the datasets respectively using The Unscrambler software. Raw data was converted to.csv files using The Unscrambler and then imported into Matlab 2024b for application of CWS. For PCA and CWS algorithm equations, see section 2.2.4.

4.3 Results and Discussion

4.3.1 Raman activity of vaccines

It is noteworthy to mention that spectral acquisition was limited by a number of possible confounding factors including but not limited to the liquid pharmaceutical formulation; varying instrument performance under uncontrolled laboratory conditions; the availability of only one laser source; lack of motor stage that facilitates imaging; and no long working distance objective. The drying process itself held potential to inhibit spectral acquisition, although biopharmaceuticals are generally more stable in a dried state, the process of drying is known to cause damage to proteins in the liquid

formulations (Carpenter, Prestrelski and Arakawa, 1993; Griebenow and Klibanov, 1995; Prestrelski et al., 1993; Wang, 2000).

Vaccines showed varying Raman activity and spectral quality related to fluorescence in their spectra. Vaccines could be classified into three categories: Raman active with fluorescence (Figure 4.3); not Raman active with fluorescence (Figure 4.2); and Raman active without fluorescence (Figure 4.4). Conventional Raman spectra measured using the x10 objective saw increased interference from fluorescence of the vaccines' formulation. All of the spectra acquired using the x10 objective were classified as either Raman active with fluorescence or non-Raman active with fluorescence. Figure 4.2 shows the conventional Raman spectrum of brand 2 vaccine LJMUCV965 measured using the x10 objective where the vaccines' signal was entirely obscured by fluorescence. Figure 4.3 shows the conventional Raman spectrum of brand 1 vaccine LJMUCV672 measured using the x10 objective, where bands are distinguishable at 555, 786, 1094, and 2431 cm^{-1} but the majority of the vaccines' signal is obscured by fluorescence. Of the 10 vaccines measured using the x10 objective lens, 6 were categorised as Raman active with fluorescence and four were categorised as not Raman active with fluorescence interference. Spectra acquired using the x100 objective lens obtained higher signal quality and reduced fluorescence. In a sense, the confocal microscope acted in a fluorescence quenching function, as high intensity radiation was focused on a small region of the sample (St. Croix, Shand and Watkins, 2005). Vaccines measured using the x100 objective were classified as Raman active with no fluorescence or non-Raman active with fluorescence.

Figure 4.4 shows the Raman spectrum of brand 1 vaccine LJMUCV601 measured using the x100 objective. The spectrum of LJMUCV601 shows significantly improved signal quality and reduced fluorescence interference in comparison to the brand 1

vaccines measured using the x10 objective. Key bands corresponding to the vaccines' formulation were able to be identified between 600-3000 cm^{-1} . Bands corresponding with the protein content of the biologics formulation were observed at 870, 922, 1054, 1163 and 1460 and 2896 cm^{-1} associated with C-C stretching of hydroxyproline (Huang et al., 2003), C-C stretching in amino acids (Lau et al., 2003), C-O and C-N stretching in proteins (Chan et al., 2006), C=C stretching in lipids and C-C stretching in proteins (De Gelder et al., 2007; Katainen et al., 2007), CH_2/CH_3 deformation in protein, glycerol and saccharides (Lu et al., 2013), and sp^3 C-H stretching in lipids and proteins (Lazar, 2001), respectively. Bands associated with the nucleic acid content of the vaccines were observed at 1084, 1325 and 1376 cm^{-1} corresponding to O-P-O stretching in adenosine diphosphate nucleoside (Jenkins et al., 1999), CH_3CH_2 wagging in purine bases of DNA, and ring breathing in thymine, adenosine, and guanine of DNA bases (D'Amico et al., 2015) respectively.

Figure 4.5 shows the conventional Raman spectrum of brand 2 vaccine LJMUCV148 measured using the x100 objective. The spectrum of LJMUCV148 showed improved spectral quality and reduced fluorescence interference in comparison to the brand 2 vaccines measured using the x10 objective. Key bands corresponding to the vaccines' formulation were identified between 500 - 3000 cm^{-1} . Bands associated with the protein content of the vaccine formulation were observed at 523, 1411, and 1455 cm^{-1} corresponding to S-S disulfide stretch in proteins (Stone et al., 2002), C-H bending and C-N-C anti-symmetric stretching in dGTP COO^- stretching in F-glycoproteins (D'Amico et al., 2015; Lu et al., 2013) and CH_2 scissoring in lipids and proteins (Teh et al., 2008), respectively. Bands associated with the nucleic acid content of the vaccines' formulation were seen at 740, 1079, 1111, 1337, and 1364 cm^{-1} . Bands at 740 and 1079 cm^{-1} corresponded to ring breathing in RNA, and bases guanine, adenine and

cytosine in RNA (Dovbeshko et al., 2002; Lopes et al., 2012; Xu and Lu, 2005). Bands at 1111, 1337 and 1364 cm^{-1} corresponded to PO_2^- symmetrical stretching in RNA, ring stretching in adenosine triphosphate (ATP), and ring breathing in thymine, adenosine and guanine in RNA and DNA respectively (D'Amico et al., 2015; Krafft et al., 2005; Ochsenkühn et al., 2009; Ruokola et al., 2014). Bands associated with the lipid content of the vaccines were observed at 1064, 1455, 2910 and 2930 cm^{-1} corresponding to C-C stretching in phospholipids (Krafft et al., 2005), CH_2 scissoring in lipids and proteins (Teh et al., 2008), C-H bands of lipids (Kline and Treado, 1997), and CH_2 antisymmetric stretching in lipids (Krafft et al., 2005).

Bands related to amino acids were observed in both the vaccine brands spectra (table 4.3; table 4.4).

Figure 4.2 shows the conventional Raman spectrum of brand 2 vaccine LJMUCV965 measured using the Horiba XploRA™ instrument and x10 objective. LJMUCV965 was classified as non-Raman active with fluorescence. Significant interference from fluorescence was observed where no discernible bands were able to be positively identified in the vaccines' spectra.

Figure 4.3 shows the conventional Raman spectrum of brand 1 vaccine LJMUCV672 measured using the x10 objective. LJMUCV672 was classified as Raman active with fluorescence interference where bands were able to be identified between 300 – 2500 cm^{-1} associated with the nucleic acid and lipid content of the vaccine formulation. Bands observed in the 0-400 cm^{-1} range were not interpreted in this chapter as this range represents the far-infrared region which provides physical information rather than chemical (Sheppard, 1972). Bands observed over 3000 cm^{-1} could correspond

to aromatic CH bonds, CH stretching, OH stretching and NH stretching in alcohols, phenols, amines and amides (Brissette and C. Sandorfy, 1960).

Table 4.3 Raman band position, physical origin and literature references for the discernible bands in the conventional Raman spectrum of brand 1 vaccine LJMUCV601 measured using the Horiba XPlora™ PLUS Raman Microscope using the x100 objective

Band Position (cm ⁻¹)	Functional group	Reference
526	S-S disulfide stretch in proteins	(Stone et al., 2002)
641	C-C twisting mode in tyrosine	(Severcan and Haris, 2012, pp.12–52)(Stone et al., 2004)
698	C-S stretching in methionine	(Podstawka, Ozaki and Proniewicz, 2004)(Zhu et al., 2011)
737		
850	out-of-plane ring bending mode in tyrosine & O-P-O in adenosine triphosphate	(Bhaumik et al., 2014)(Li, Wurrey and Thomas, 1992)(Rimai et al., 1969)(Yu, Jo and D.C. O'Shea, 1973)
870	C-C stretching of hydroxyproline in proteins?	(Huang et al., 2003)

922	C-C stretching in amino acids	(Lau et al., 2003)
944	skeletal modes in polysaccharides?	(Shetty et al., 2006)
1013	ring breathing in benzene ring of tryptophan	(Combs et al., 2005)(Takeuchi, Nemoto and Harada, 1990)
1037	C-C-H bending in ribose ring of virus	(Hernández et al., 2013)(Hernández et al., 2015)
1054	C-O & C-N stretching in proteins	(Chan et al., 2006)
1084	O-P-O stretching in adenosine diphosphate nucleoside	(Jenkins et al., 1999)
1104	PO ₂ ⁻ symmetrical stretching in phosphatidylinositol	(Krafft et al., 2005)(Ruokola et al., 2014)
1126	Backbone C-C stretching in fatty acids, phosphatidylethanolamine and phosphatidylserine	(De Gelder et al., 2007)(Krafft et al., 2005)(Xu and Lu, 2005)
1163	C=C stretching in lipids and C-C stretching in proteins	(De Gelder et al., 2007)(Katainen et al., 2007)
1209	C-C stretching in phenol ring of phenylalanine	(Hernández et al., 2013)(Hernández et al., 2015)
1239	NH ₂ bending overlapping to amide III in N'-formylkynurenine	(Bieker and Schmidt, 1979)

1261	out-of-plane ring bending mode in tyrosine	(Hernández et al., 2015)
1325	CH ₃ CH ₂ wagging in purine bases of DNA	(Robichaux Viehovever et al., 2003)(Malini et al., 2006)
1349	Amide III in N-formal group, skeletal stretching in tryptophan benzene ring	(Bieker and Schmidt, 1979)(Combs et al., 2005)(Takeuchi, Nemoto and Harada, 1990)
1376	Ring breathing in thymine, adenosine, and guanine of DNA bases	(D'Amico et al., 2015)
1421	C-H bending & C-N-C anti symmetric stretch in dGTP, COO- stretching in F glycoproteins	(Krafft et al., 2005)(Malini et al., 2006)
1460	CH ₂ /CH ₃ deformation in proteins, glycerol & saccharides	(Lu et al., 2013)
2824	CH ₂ symmetric stretching in lipids	(Koljenović et al., 2005)
2896	sp ³ C-H stretching in lipids and proteins	(Lazar, 2001)
2913	CH bands of lipids	(Kline and Treado, 1997)
2942	CH ₂ antisymmetric stretching in lipids	
2972	CH ₃ antisymmetric stretching in lipids and fatty acids	
2984	Olefinic sp ² -CH ₂ stretching (only virus)	

Table 4.4 Raman band position, physical origin and literature references for the discernible bands in the conventional Raman spectrum of brand 1 vaccine LJMUCV601 measured using the Horiba XPlora™ PLUS Raman Microscope using the x100 objective

Band Position (cm ⁻¹)	Functional group	Reference
523	S-S disulfide stretch in proteins	(Stone et al., 2002)
607	steroid ring stretching in cholesterol	(Krafft et al., 2005)
637	C-C twisting mode in tyrosine	(Severcan and Haris, 2012, pp.12–52)(Stone et al., 2004)
703	C-S stretching in methionine	(Podstawka, Ozaki and Proniewicz, 2004)(Zhu et al., 2011)
740	Ring breathing in RNA	(Dovbeshko et al., 2002)(Lopes et al., 2012)
870	C-C stretching of hydroxyproline	(Huang et al., 2003)
924	C-C stretching in amino acids	(Lau et al., 2003)
993	CH ₃ rocking in tryptophan?	(Combs et al., 2005)
1064	C-C stretching in phospholipids	(Krafft et al., 2005)
1079	guanine, adenine and cytosine in RNA	(Xu and Lu, 2005)
1111	PO ₂ ⁻ symm stretching in RNA	(Krafft et al., 2005)(Ruokola et al., 2014)

1128	backbone C-C stretching in fatty acids	(De Gelder et al., 2007)(Krafft et al., 2005)(Xu and Lu, 2005)
1212	C-C stretching in the phenol ring of tyrosine	(Hernández et al., 2015)
1256	out-of-plane ring bending mode in tyrosine	(Hernández et al., 2015)
1276	Amide III in random coil	(Iconomidou et al., 2001)
1337	ring stretching in adenosine triphosphate?	(D'Amico et al., 2015)(Ochsenkühn et al., 2009)
1364	ring breathing in thymine, adenosine and guanine of RNA/DNA	(D'Amico et al., 2015)
1411	C-H bending & C-N-C anti-symm stretch in dGTP COO- stretching in F-glycoproteins	(D'Amico et al., 2015)(Lu et al., 2013)
1455	CH ₂ scissoring in lipids and proteins	(Teh et al., 2008)
1667	Amide I in β strand, C=C stretching in cholesterol	(Tuma and Thomas, 2001)(Tuma, 2005)
2910	CH bands of lipids	(Kline and Treado, 1997)
2930	CH ₂ antisymmetric stretching in lipids	(Krafft et al., 2005)

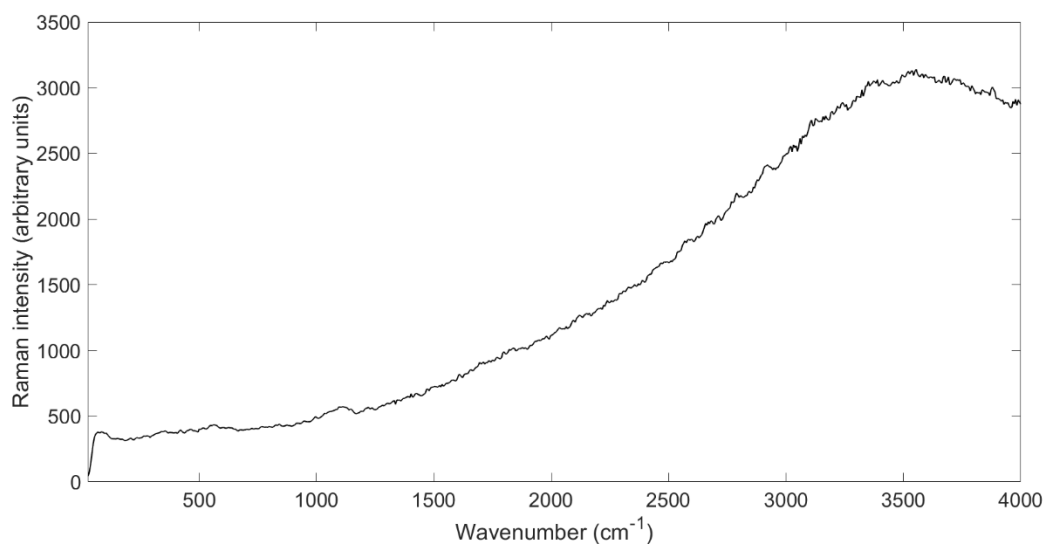


Figure 4.2 Conventional Raman spectra of brand 2 vaccine LJMUCV965 measured using the Horiba XploRA™ PLUS Raman microscope equipped with 532 nm laser and x10 objective lens at 600 grating and 10% filter across 25-4000cm⁻¹

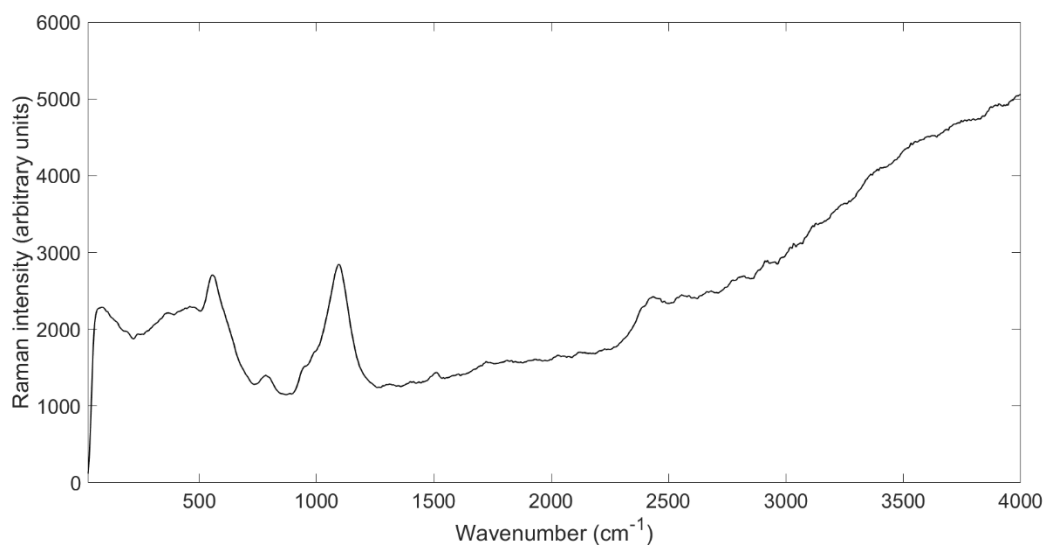


Figure 4.3 Conventional Raman spectra of brand 1 vaccine LJMUCV672 measured using the Horiba XploRA™ PLUS Raman microscope equipped with 532 nm laser and x10 objective lens at 600 grating and 10% filter across 25-4000 cm⁻¹

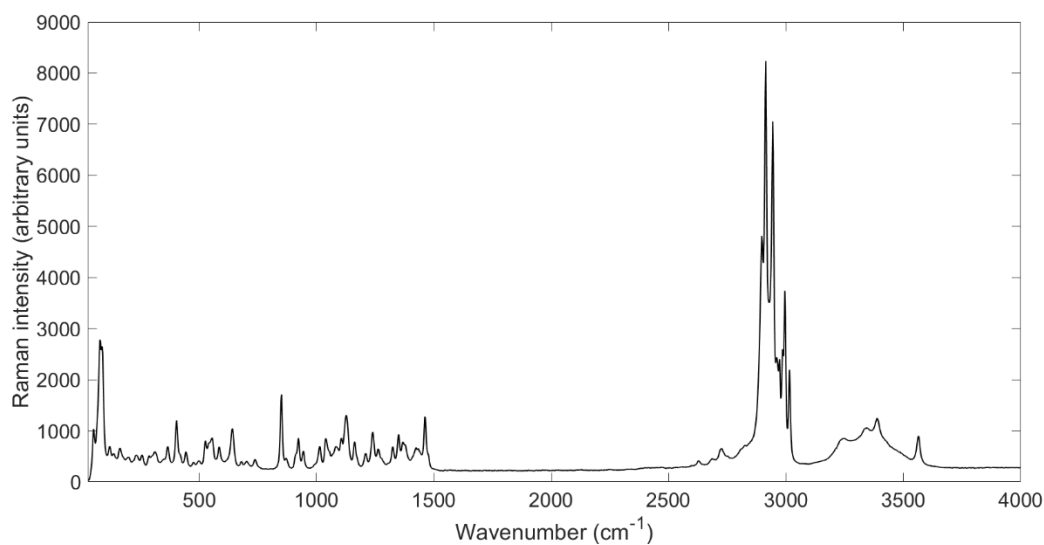


Figure 4.4 Conventional Raman spectra of brand 1 vaccine LJMUCV601 measured using the Horiba XploRA™ PLUS Raman microscope equipped with 532 nm laser and x100 objective lens at 1200 grating and 10% filter across 25-4000 cm^{-1}

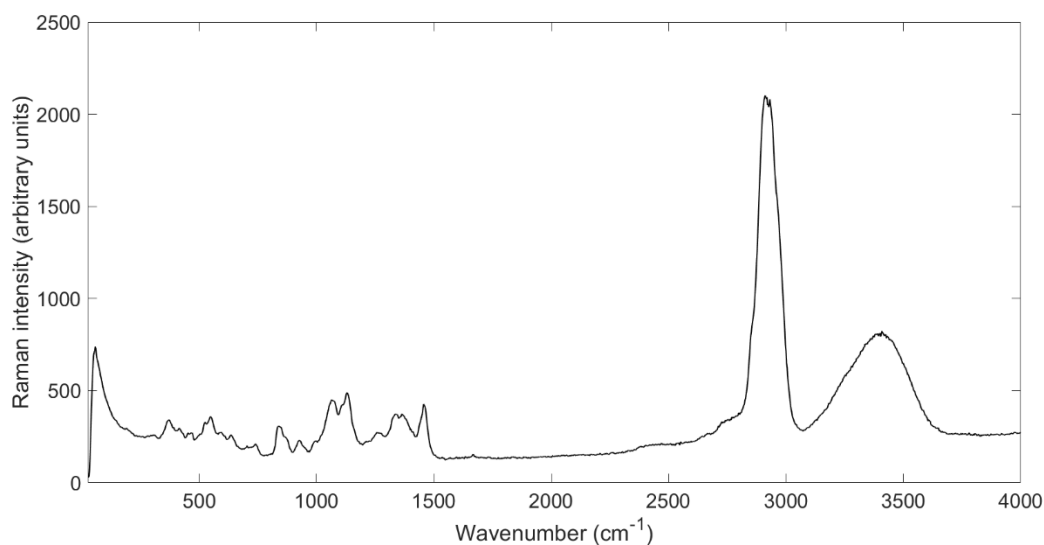


Figure 4.5 Conventional Raman spectra of brand 2 vaccine LJMUCV148 measured using the Horiba XploRA™ PLUS Raman microscope equipped with 532 nm laser and x100 objective lens at 1200 grating and 10% filter across 25-4000 cm^{-1}

Figure 4.6 shows the spectrum of brand 2 vaccine LJMUCV159 measured using conventional Raman (black) and with the addition of silver nanoparticles for SERS (red). Enhancement was seen for bands at 49, 150, 1308, 1595, 1883, and 2930. Figure 4.7 shows the stacked spectra of brand 2 vaccine LJMUCV152 measured using conventional Raman (black) and with the addition of silver nanoparticles (red). Significant enhancement of the signal was observed for the SERS measurement, however, the vaccines' spectra was heavily influenced by interference from fluorescence, for which enhancement was also seen. This indicated that while SERS was an effective tool for enhancement of vaccine signal, it did not discriminate between signal and fluorescence which could potentially inhibit the successful interpretation of the vaccine spectra.

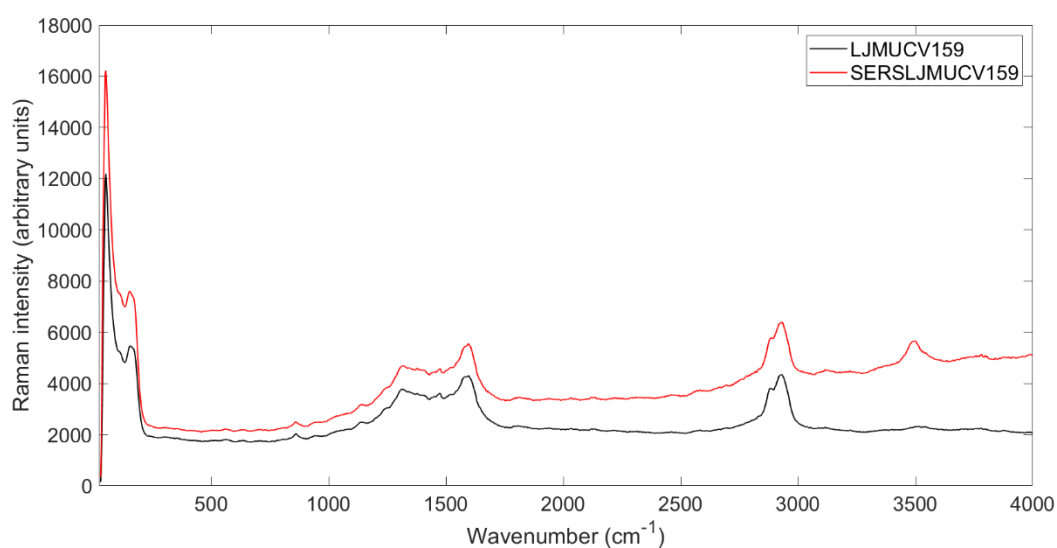


Figure 4.6 Stacked spectra of brand 2 vaccine LJMUCV159 measured using conventional Raman (black) and SERS (red) using the Horiba XploRA™ PLUS equipped with 532 nm laser and x100 objective

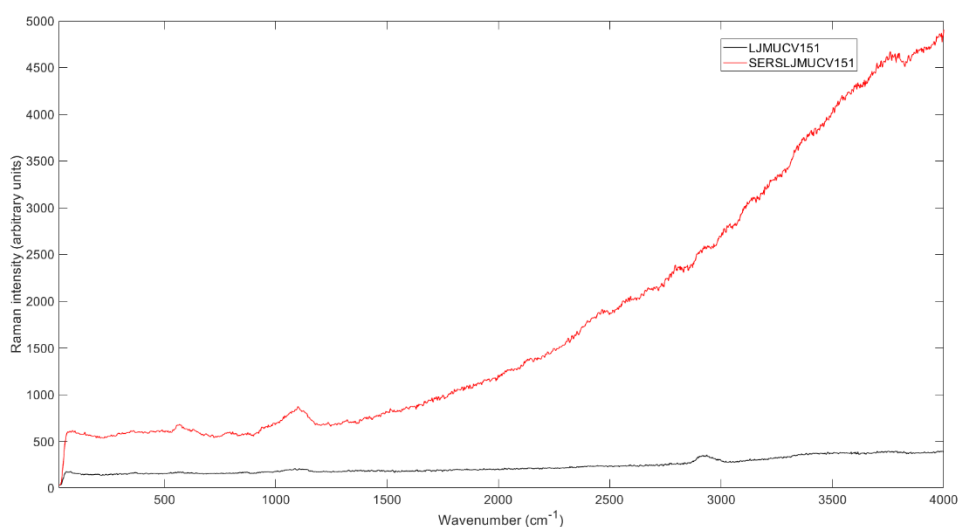


Figure 4.7 Stacked spectra of brand 2 vaccine LJMUCV151 measured using conventional Raman (black) and SERS (red) using the Horiba XploRA™ PLUS equipped with 532 nm laser and x100 objective

4.3.2 Spectral quality

Spectral quality showed varied results for the vaccines measured with the x10 and x100 objective. Table 4.5 shows the spectral quality of vaccines which spectra reflected that the samples were Raman active. Spectral quality was not assessed in spectra where samples were not Raman active and/or obscured by fluorescence. Vaccines measured using the x100 objective showed an average of 30 bands in their spectra, ranging from 4 to 59 (table 4.5). Vaccines measured using the x10 objective showed an average of 16 bands, ranging from 8 to 31 (table 4.5). Vaccines that were classified as Raman active with no fluorescence (LJMUCV601;LJMUCV691;LJMUCV148) demonstrated good spectral quality in terms of number of bands (N), maximum peak intensity and SNR with 59, 51 and 31 discernible bands in their spectra, respectively. LJMUCV601 and LJMUCV691

obtained maximum peak intensities of 8238 and 1278 cm^{-1} and SNR values of 34 and 32 respectively, in comparison to SNR values of between 1 and 4 for the other vaccines measured using the x100 objective. Most vaccines measured using the x10 objective were classified as Raman active, with fluorescence. However, vaccines measured using the x10 objective obtained higher maximum peak intensity with an average of 8020 arbitrary units in comparison to an average of 2444 arbitrary units for the x100 objective. Vaccines measured using the x10 objective also obtained a higher average SNR value than the x100 objective vaccines. This increased peak intensity was attributed to the high fluorescence observed in the spectra of the vaccines using the x10 objective. In this sense, traditional assessment of spectral quality through peak intensity and SNR falsely indicated that better spectral quality was observed for the vaccines measured using the x10 objective due to the influence of fluorescence on these parameters. This suggests that evaluation of spectral quality using this method is unreliable when performed on spectra that are significantly influenced by the interference of fluorescence.

Table 4.5 Spectral quality of conventional Raman active vaccines measured using the Horiba XploRA™ PLUS Raman microscope-spectrometer equipped with 532 nm laser

Vaccine	Brand	Objective	N	Maximum peak position (cm^{-1})	Maximum peak intensity (arbitrary units)	SNR*
LJMUCV601	1	100	59	2913	8238	34
LJMUCV662	1	10	31	3978	8019	3
LJMUCV663	1	10	32	3994	8559	21
LJMUCV672	1	10	12	3983	5042	55
LJMUCV691	1	100	51	2948	1278	32

LJMUCV148	2	100	31	2911	2101	4
LJMUCV151	2	100	7	2936	353	2
LJMUCV159	2	10	8	49	12196	2
LJMUCV930	2	10	12	3980	2948	2
LJMUCV957	2	10	12	3983	10796	45
LJMUCV964	2	10	8	3978	8584	70
LJMUCV1390	3	100	4	3899	255	1

*At maximum peak position, N = number of bands

Table 4.6 shows the spectral quality of SERS spectra acquired from vaccines that were Raman active. Surface-enhanced vaccine spectra obtained a higher average peak intensity of 12887 arbitrary units in comparison to 5697 arbitrary units for the conventional Raman spectra, demonstrating successful enhancement of the vaccines' signal when measured with the addition of the silver nanoparticles and 1M KBr. SERS vaccines measured using the x10 objective showed higher peak intensity than the vaccines measured using the x100 objective. However, these vaccines showed decreased number of bands in comparison to the vaccines measured using x100 objective, suggesting the enhancement of fluorescence as well as the vaccines' signal itself. SNR was not able to be calculated for SERSLJMUCV152 as only one spectrum was able to be acquired from the vaccine. Overall brand 1 showed stronger Raman activity in terms of number of bands.

Table 4.6 Spectral quality of surface-enhanced Raman active vaccines measured using the Horiba XploRA™ PLUS Raman microscope-spectrometer equipped with 532nm laser

Vaccine	Brand	Objective	N	Maximum peak position (cm ⁻¹)	Maximum peak intensity (arbitrary units)	SNR*
SERSLJMUCV152	2	100	21	54	4984	N/A
SERSLJMUCV159	2	10	8	49	16231	3
SERSLJMUCV717	1	100	9	3547	2116	13
SERSLJMUCV722	1	100	37	47	4116	1
SERSLJMUCV965	2	10	14	50	36989	2

*At maximum peak position, N = number of bands

4.3.3 Authentication of Covid-19 Vaccines by Raman microscopy

When PCA was applied to the vaccines measured with objective 10, six different clusters were obtained over the first two PC scores. In this respect, PC scores on PC1 and PC2 contributed to 98.1% and 1.7% respectively (Figure 4.8). Unlike PCA applied to FTIR spectra (Chapter 2.3.3), PCA applied to the Raman microscopy spectra showed clusters corresponding to the Raman activity of the vaccines rather than the brand of the vaccines. Hence, vaccines with stronger Raman activity were clustered on the right side of the PCA with the highest variance (Figure 4.8). In this respect, the PC scores with the highest variance corresponded to LJMUCV957 that was more Raman active than the other samples and less fluorescent. This was followed by LJMUCV662 and LJMUCV964. It is of note that these three vaccines were of two

manufacturers as such: LJMUCV662 was brand 1; while LJMUCV964 and LJMUCV957 were from brand 2. On the other hand, vaccines of weaker Raman activity were clustered to the left side of the PC scores plot and included LJMUCV672 (brand 1), LJMUCV965 (brand 2) and LJMUCV943 (brand 2). The aforementioned three vaccines showed high fluorescence which could be related to the interference from humidity, excipients and low concentration of Raman active constituents in the sample. Yet, it is significant that each vaccine was clustered separately, and no overlap was seen between scores of different vaccines though they had been collected in the same settings. This demonstrated accuracy in classifying products despite fluorescence. Moreover, the equal frequency ellipses applied to the vaccines confirmed their authenticity (Figure 4.9) where no score was seen outside the ellipse. To ensure the transparency of the PCA model, the PC1 loading plot showed eight key bands, mainly in the range of 25 to 1300 cm^{-1} (Figure 4.10). The highest two bands were seen at 553 and 1089 cm^{-1} and corresponded to O-P-O stretching in adenosine diphosphate nucleoside group. It is worth noting that these two bands were also significant on PC2 that showed a loading plot very similar to PC1 loading (Figure 4.11). Additional key bands were seen at 777 and 2426 cm^{-1} which corresponded to DNA phosphodiester stretching (Krafft et al., 2005).

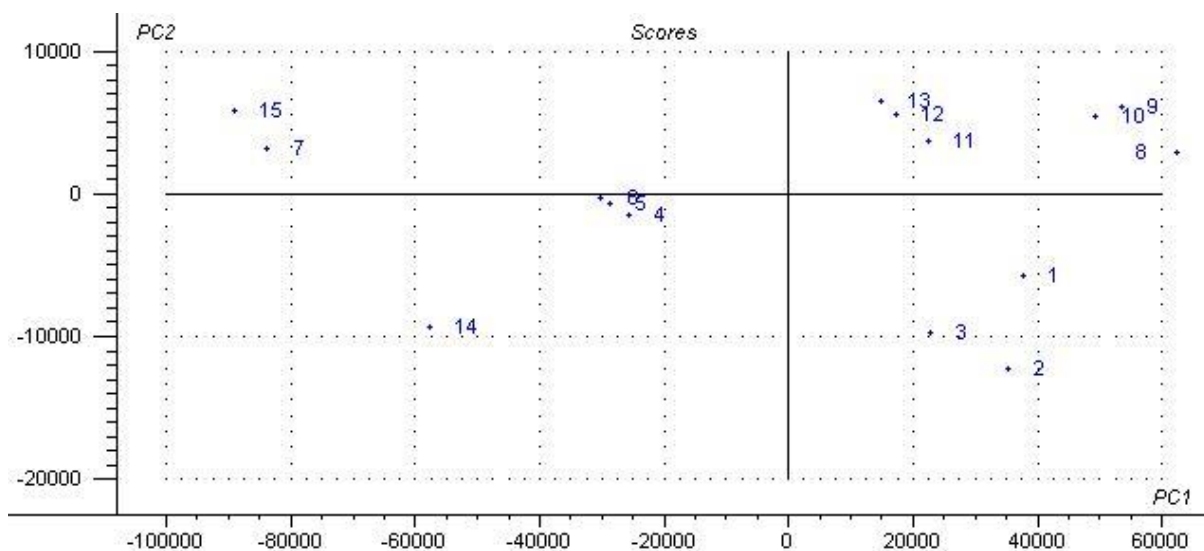


Figure 4.8 PC scores plot of conventional Raman vaccine samples measured using the Horiba XploRA™ PLUS Raman microscope-spectrometer equipped with 532 nm laser and x10 objective across 25-4000 cm^{-1} where PC1 = 98.1% and PC2 = 1.7 %

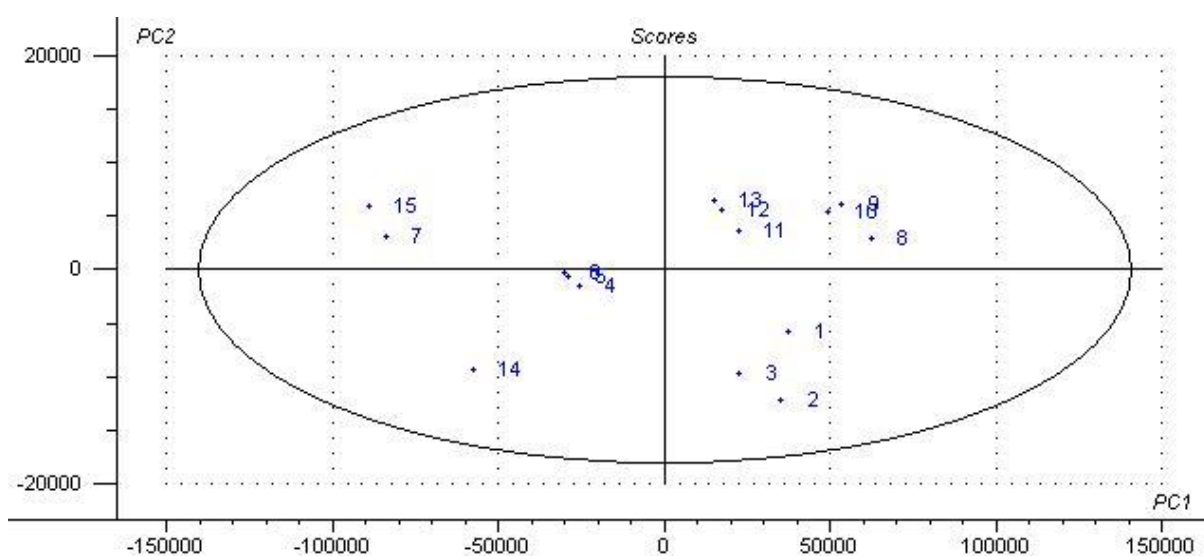


Figure 4.9 PC scores plot with equal frequency ellipsis of conventional Raman vaccine samples measured using the Horiba XploRA™ PLUS Raman microscope-spectrometer equipped with 532 nm laser and x10 objective across 25-4000 cm^{-1} where PC1 = 98.1% and PC2 = 1.7 %

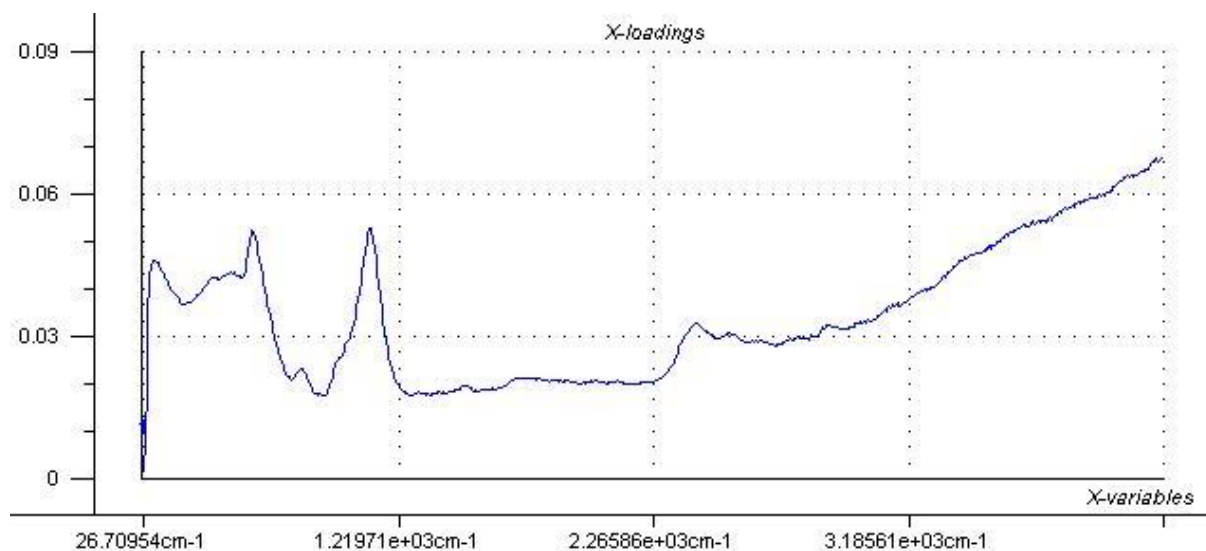


Figure 4.10 PC1 loading graph of conventional Raman vaccine samples measured using the Horiba XploRA™ PLUS Raman microscope-spectrometer equipped with 532 nm laser and x10 objective across 25-4000 cm⁻¹

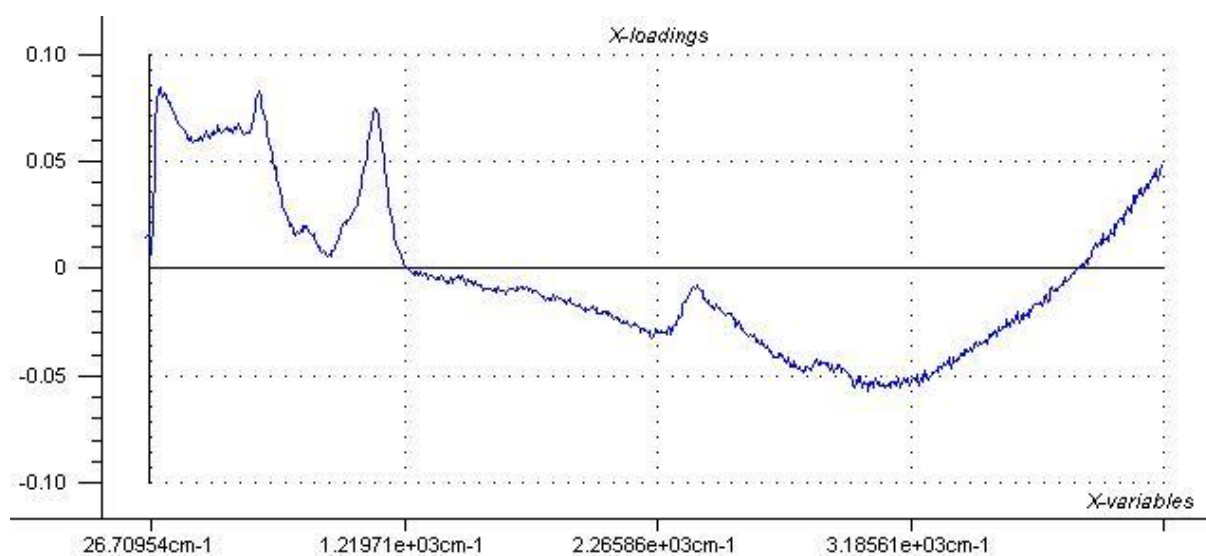


Figure 4.11 PC2 loading graph of conventional Raman vaccine samples measured using the Horiba XploRA™ PLUS Raman microscope-spectrometer equipped with 532 nm laser and x10 objective across 25-4000 cm⁻¹

Different clustering pattern was seen among the vaccines when measured with objective 100 which could be related to the confocality of the 100 objective and the concentration of more energy into a smaller region of the sample i.e. fluorescence quenching (St. Croix, Shand and Watkins, 2005) (Figure 4.12). This improved the focus obtained in objective 100 (Figure 4.15). It is worth noting that the overall spectral quality of vaccines measured with objective 100 were better than objective 10. However, clustering of spectra obtained in objective 100 was related to both fluorescence and the vaccine brand. Hence, three clusters were obtained in this case. The highest variance was seen in cluster one that corresponded to LJMUCV601 (brand 1) that showed the strongest Raman activity (Figure 4.12). This was followed by LJMUCV148 (brand 2) that had strong Raman activity, yet its scores were not clustered together, and this was due to the variations in Raman scattering where noise can interfere in the individual signals, indicating a lack of robustness in the Raman method. This noise could be related to the light source ageing, detector ageing, photon shot noise and/or sample generated noise (Freudiger et al., 2014; Smulko et al., 2014). On the other hand, an overlap was seen between the scores of LJMUCV848 (brand 2), LJMUCV151 (brand 2) and LJMUCV1390 (brand 3) that was related to the fluorescence which was a common interference among these vaccines (Figure 4.16). Yet, fluorescence in these three samples did not have a negative influence on the PCA model where PC1 and PC2 loading plots showed key features to the vaccines' spectra that were analysed (Figure 4.13; Figure 4.14). In this respect, loadings in the range of 600 to 1200 cm^{-1} showed key features corresponding to proteins, amino acids and nucleic acid bases in the formulation of the vaccines. Loadings in the range of 2800-3000 cm^{-1} mainly corresponded to the lipid C-H stretching mechanisms (Kline and Treado, 1997; Koljenović et al., 2005; Krafft et al., 2005; Lazar, 2001).

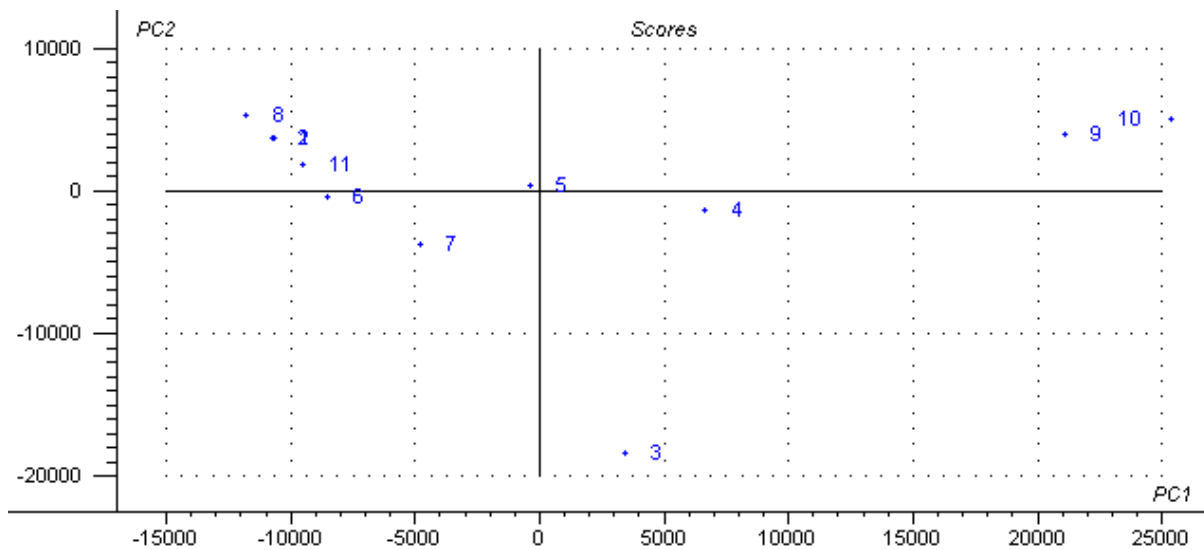


Figure 4.12 PC scores plot of conventional Raman vaccine samples measured using the Horiba XploRA™ PLUS Raman microscope-spectrometer equipped with 532 nm laser and x100 objective across 25-4000 cm^{-1} where PC1 = 77.1% and PC2 = 20.5%

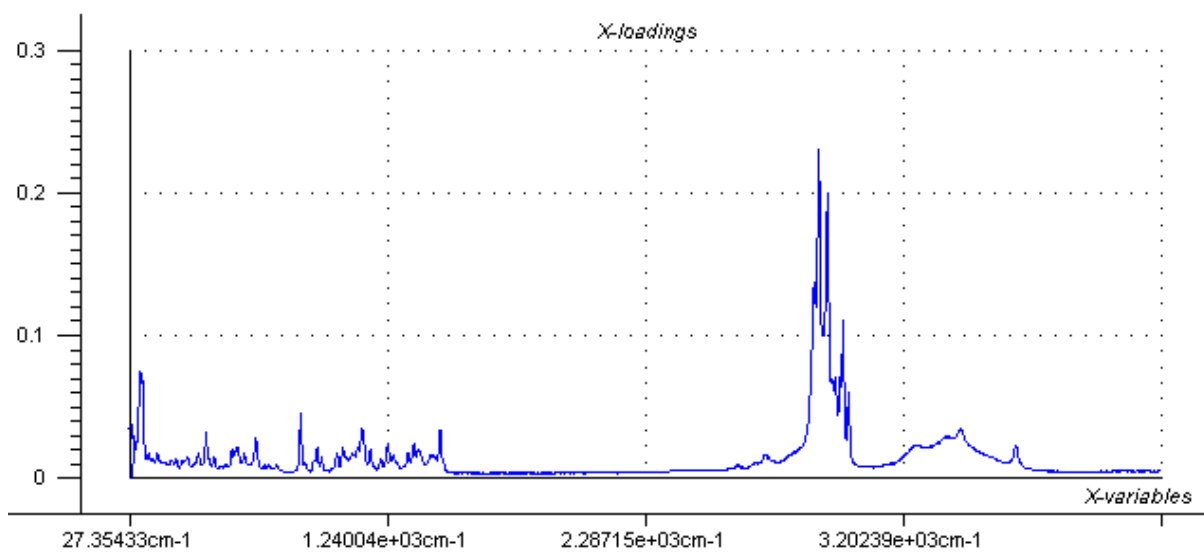


Figure 4.13 PC1 loading graph of conventional Raman vaccine samples measured using the Horiba XploRA™ PLUS Raman microscope-spectrometer equipped with 532 nm laser and x100 objective across 25-4000 cm^{-1}

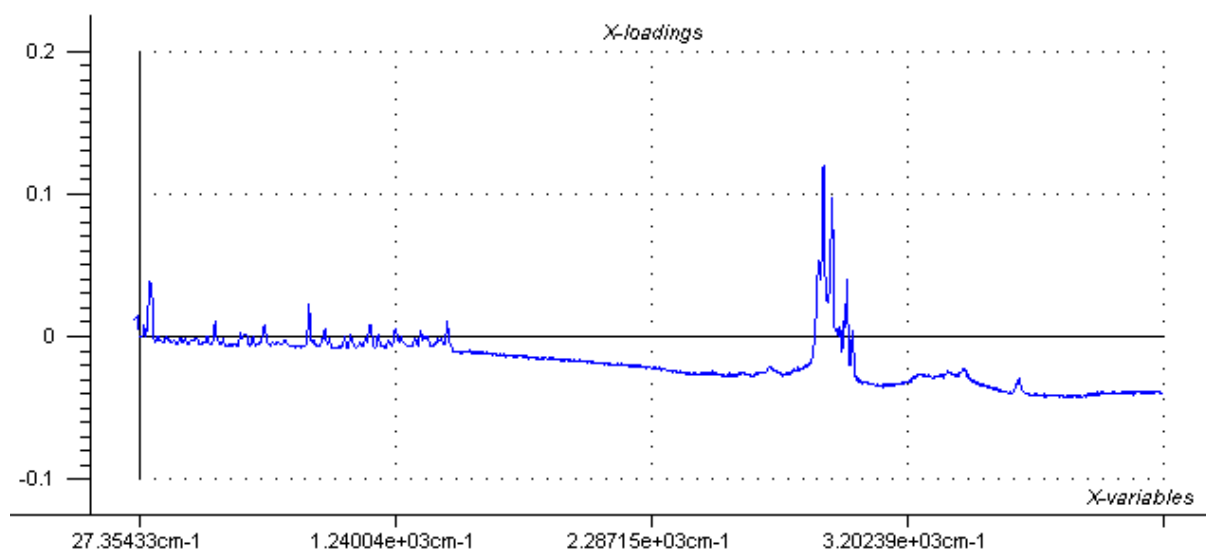


Figure 4.14 PC2 loading graph of conventional Raman vaccine samples measured using the Horiba XploRA™ PLUS Raman microscope-spectrometer equipped with 532 nm laser and x100 objective across 25-4000 cm^{-1}

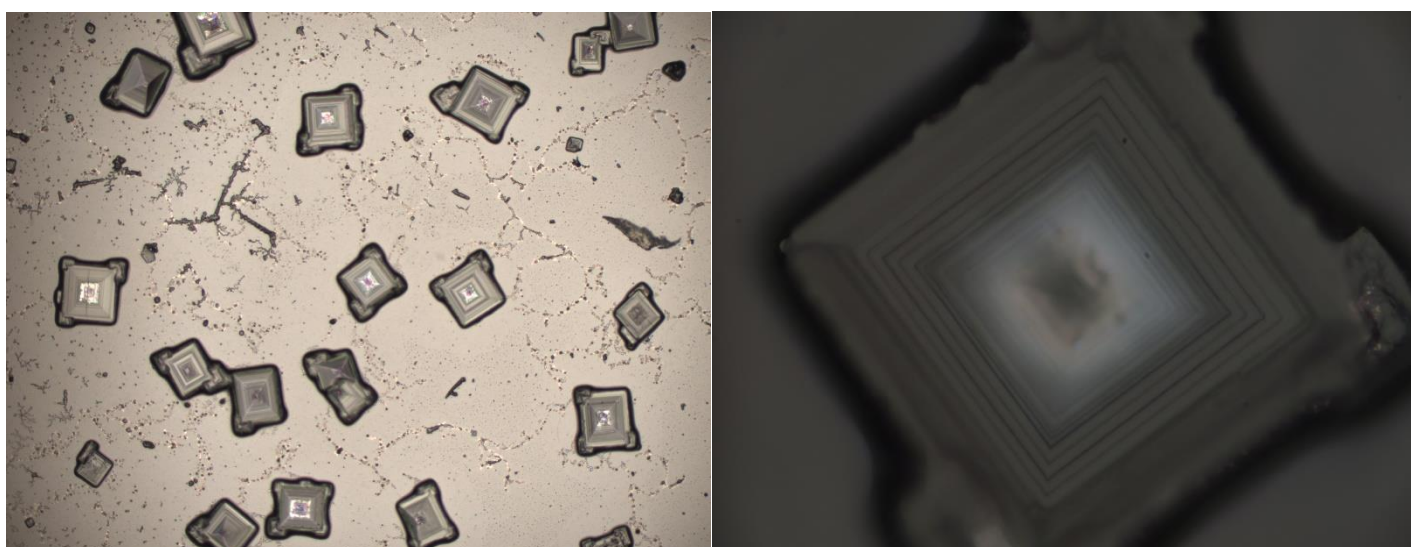


Figure 4.15 Microscope image of brand 2 vaccine SERSLJMUCV159 acquired using the Horiba XploRA™ PLUS Raman microscope-spectrometer equipped with 532 nm laser and x10 objective (left) and x100 objective (right)

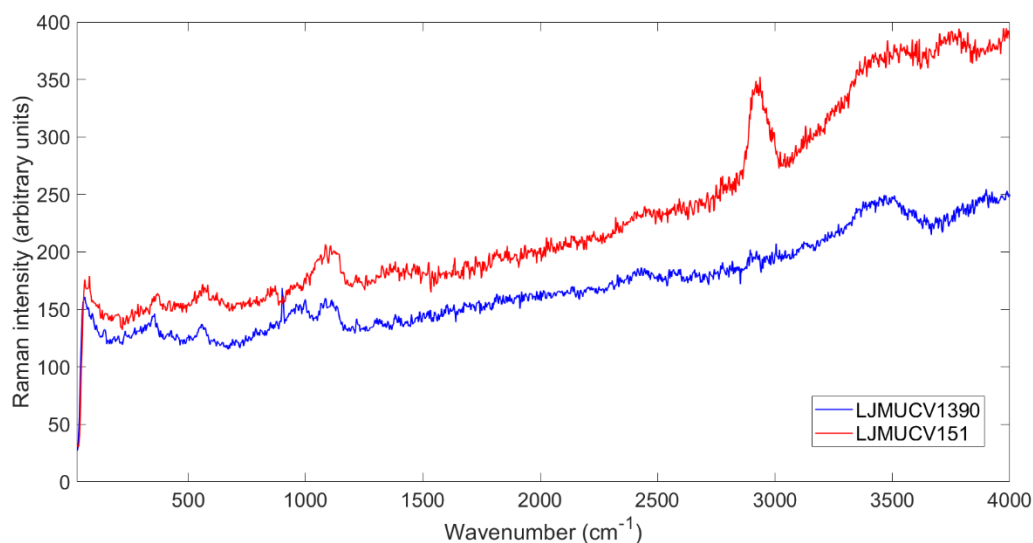


Figure 4.16 Stacked spectra of brand 3 vaccine LJMUCV1390 (blue) and brand 2 vaccine LJMUCV151 (red) measured using the Horiba XploRA™ PLUS Raman microscope-spectrometer equipped with 532 nm laser and x100 objective across 25-4000 cm^{-1}

Considering the differences obtained in both objectives, spectra obtained from both objectives were combined in a PCA model in order to explore the ability of discrimination between the objectives used for the same samples. Accurate clustering was obtained between samples measured with both objectives where fluorescence showed to play a key role in clustering. In this respect, samples measured with objective 10 had higher fluorescence that was of higher variance (samples 12 and 13) and was featured in the positive side of the PC scores (Figure 4.17). Sample 14 was also fluorescent but was scored further down in relation to its Raman activity (Figure 4.17). Conversely, samples measured with objective 100 were clustered separately to the left side of the PCA (Figure 4.17). PC loading confirmed that fluorescence played a more crucial role in the model where its position was featured in PC1 loading (Figure 4.18). On the other hand, PC2 loading reflected spectral features of the vaccine (Figure 4.19). Hence, PCA was successful in classifying both objectives with features from spectra of all the measured vaccines.

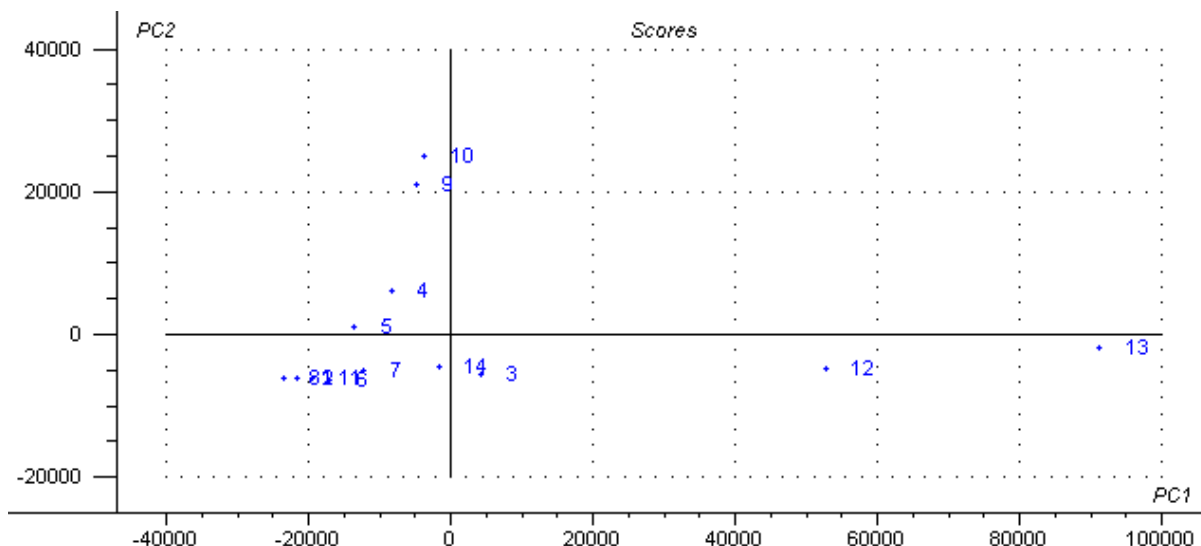


Figure 4.17 PC scores plot of conventional Raman vaccine samples measured using the Horiba XploRA™ PLUS Raman microscope-spectrometer equipped with 532 nm laser and x100 objective, with one sample measured at x10 objective across 25-4000 cm^{-1} where PC1 = 90.2% and PC2 = 9.2%

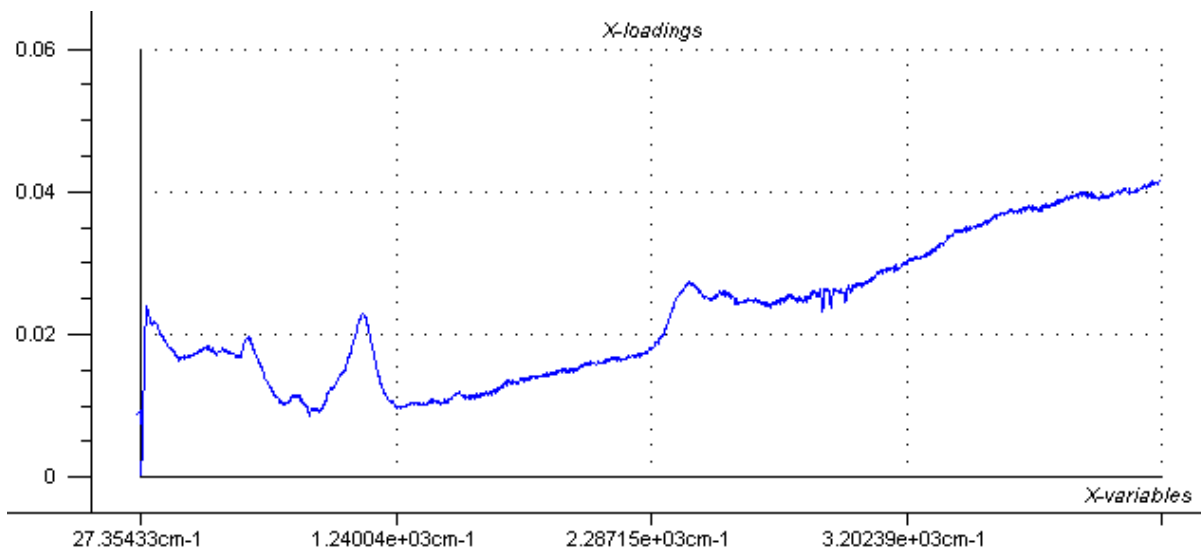


Figure 4.18 PC1 loading graph of conventional Raman vaccine samples measured using the Horiba XploRA™ PLUS Raman microscope-spectrometer equipped with 532 nm laser and x100 objective, with one sample measured at x10 objective across 25-4000 cm^{-1}

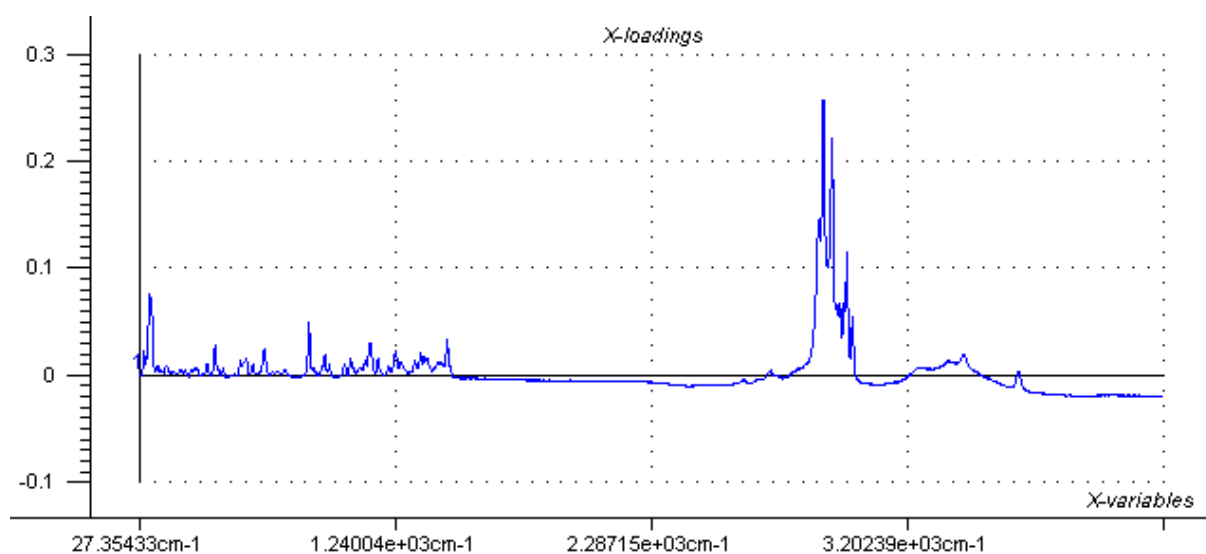


Figure 4.19 PC2 loading graph of conventional Raman vaccine samples measured using the Horiba XploRA™ PLUS Raman microscope-spectrometer equipped with 532 nm laser and x100 objective, with one sample measured at x10 objective across 25-4000 cm^{-1}

CWS was applied to each of the datasets to assess the discrimination potential of Raman microscopy between the different vaccine brands. Figure 4.20 shows the correlation plot of vaccines measured using the x10 objective on the Horiba XploRA™ instrument. All vaccines positively were positively correlated, obtaining an r value of >0.95 when plotted against themselves. All brand 1 vaccines showed an r value of $r>0.95$ when plotted against spectra of the same brand. Brand 1 vaccines demonstrated lower r values, though still exceeding 0.95 against spectra of the brand 2 vaccines, excluding brand 2 vaccines 7, 14 and 15. Vaccine 7 (LJMUCV930) showed an r value of <0.95 against all the vaccines in the dataset excluding 14 and 15 (LJMUCV965). Both vaccines were of the same brand and fluorescence interference featured heavily in both of their spectra, explaining their shared r value of >0.95 . All brand 2 vaccines showed an r value of >0.95 against vaccines of the same brand, excluding vaccines 7, 14 and 15 which scored r values of <0.95 against the other

brand 2 vaccines, demonstrated by the dark blue colour observed in the correlation plot (Figure 4.20).

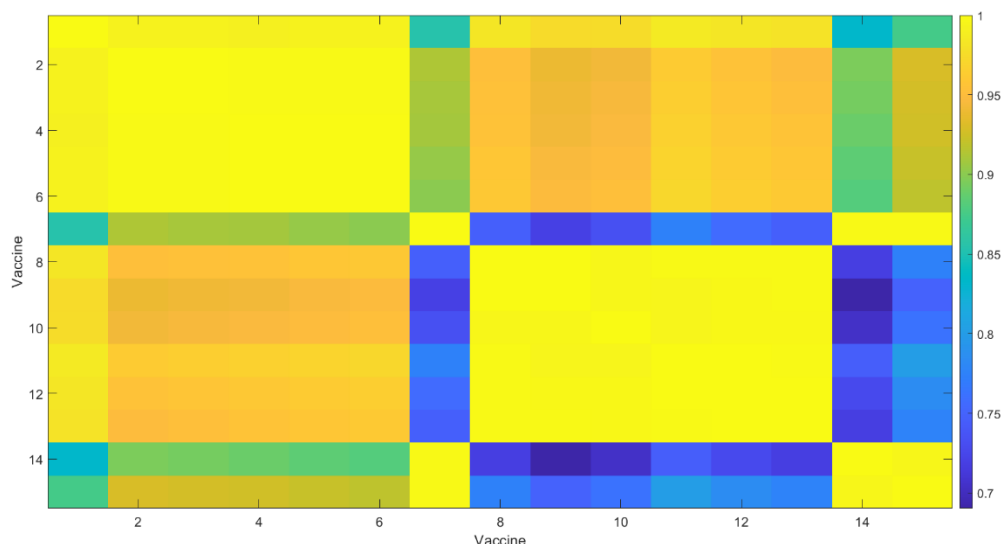


Figure 4.20 CWS of conventional Raman spectra of brand 1 vaccines (1-6) and brand 2 vaccines (7-15) measured using the Horiba XploRA™ PLUS equipped with 532nm laser and x10 objective where dark blue colour represents a minimum r value of 0.75 and a dark yellow colour represents a maximum r value of 0.9999. In between the r values 0.77 – 0.82 correspond to light blue colour, r value of 0.83 – 0.87 correspond to cyan colour, 0.88 – 0.92 correspond to green, 0.93 – 0.97 correspond to greenish yellow colour and 0.98 – 0.99 correspond to orange colour.

Figure 4.21 shows the correlation plot of the spectra acquired from the vaccines measured using the x100 objective with the Horiba Raman instrument. All vaccines were a positive match against themselves as demonstrated by them obtaining an r value of 1 when plotted against themselves. Brand 3 vaccine LJMUCV1390 showed similarities to the spectra of brand 2 vaccines LJMUCV148 scan 1 and LJMUCV151 scan 3 where spectra obtained an r value of >0.8 against each other. Brand 3 vaccine LJMUCV1390 also showed significant similarity to the spectrum of brand 2 vaccine LJMUCV848 with an r value of >0.95 indicating a positive match. Fluorescence

featured heavily in the spectra of both vaccines, suggesting this interference could result in the false correlation of both vaccines against each other. Brand 2 vaccine LJMUCV148 scan 2 and 3 showed negative correlation against the brand 3 vaccines (1-2) and brand 2 vaccine LJMUCV151 (6-8). The spectra of LJMUCV148 was not obscured by major fluorescence, unlike LJMUCV151 and the brand 3 vaccines which spectra were significantly affected by fluorescence. This reinforces that fluorescence has a significant influence on the identification of vaccine spectra and can trigger Type I and II errors in CWS.

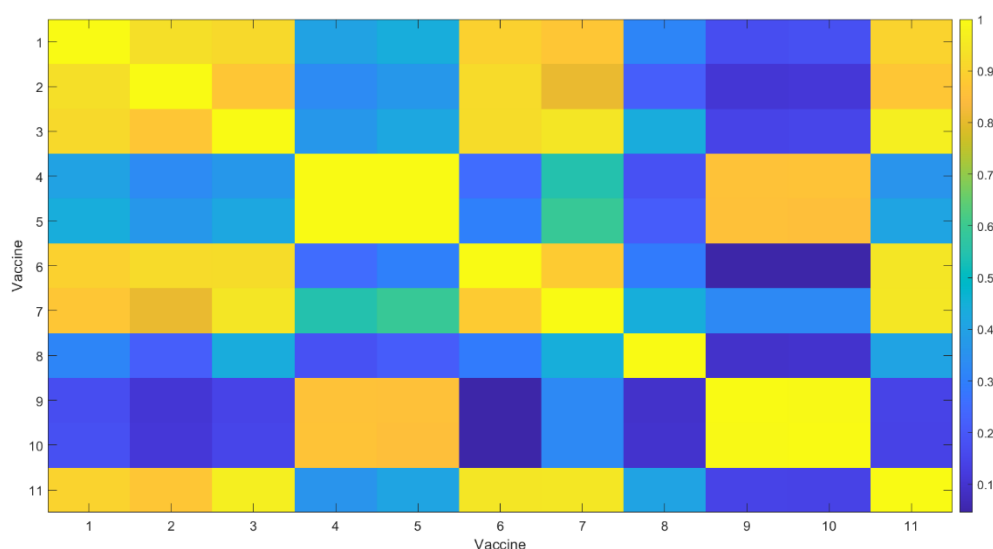


Figure 4.21 CWS of conventional Raman spectra of brand 3 vaccines (1-2), brand 2 vaccines (3-8, 11) and brand 1 vaccine (9-10) measured using the Horiba XploRA™ PLUS equipped with 532nm laser and x100 objective where dark blue colour represents a minimum r value of 0.75 and a dark yellow colour represents a maximum r value of 0.9999. In between the r values 0.0.77 – 0.82 correspond to light blue colour, r value of 0.83 – 0.87 correspond to cyan colour, 0.88 – 0.92 correspond to green, 0.93 – 0.97 correspond to greenish yellow colour and 0.98 – 0.99 correspond to orange colour.

4.4 Conclusion

To conclude, Raman spectrometry-microscopy showed potential as an identification method for substandard and falsified vaccines. This was demonstrated by the spectral quality observed in LJMUCV601, LJMUCV691 and LJMUCV148 spectra which allowed identification of nucleic acid specific bands, alongside identification of the protein and lipid nanoparticle content of the vaccines' formulation. SERS demonstrated strong enhancement of peak intensity for the vaccines measured with the addition of the silver colloid, however, this enhancement was not seen exclusively for vaccine signal. Enhancement of fluorescence in the vaccines' spectra provided misleading results in terms of spectral quality. CWS and PCA demonstrated satisfactory identification potential of the method, where all vaccines obtained an r value of 1 against themselves and clustering of individual vaccines was seen with no type I or type II errors observed in the PC scores plots of the vaccines measured with $\times 100$ objective. However, the method showed limited ability to discriminate between vaccines of different formulations due to shared spectral features related to significant fluorescence interference in their spectra at both $\times 10$ and $\times 100$ objective. Both PCA and CWS revealed that fluorescence was heavily influential on the identification potential of Raman microscopy. The study was limited by the small sample size of Raman active spectra with no fluorescence collected, this could be due to a variety of confounding factors such as varying instrument performance under uncontrolled laboratory conditions; the availability of only one laser source; lack of motor stage that facilitates imaging; and no long working distance objective. Future work would involve the optimisation of system measurement parameters, further exploring the effects of grating and filter on spectral quality to support the fluorescence quenching function of

the confocal 100x objective. The effects of humidity and drying time on fluorescence interference also requires further investigation, as drying can cause variation in spectra due to its effects on the protein content of the liquid pharmaceutical formulation. As discussed in chapter 3, vaccines measured were also pre-diluted with 0.9% NaCl at receipt to increase volume for repeat testing, which significantly reduced the concentration of the vaccine samples. Quantitative analysis of the vaccines could help to establish a limit of detection for the Raman microscopic method outlined in this chapter.

CHAPTER 5. CONCLUSIONS AND FUTURE WORK

5.1 Conclusions

The aim of this thesis was to evaluate the use of vibrational spectroscopic techniques for the rapid, cost-effective and robust analysis of Covid-19 vaccines and subsequent identification of SF Covid-19 vaccines. The methods were applied to both laboratory-based and portable handheld instruments to evaluate their application in both laboratory and field-based settings.

Optimisation of the ATR-FTIR identification method was performed using the Perkin Elmer Spectrum Two FTIR spectrometer equipped with ATR diamond accessory on a standard set of Covid-19 vaccines obtained from the NHS Central Liverpool Primary Care Network. Vaccines were of two brands and consisted of DNA-based and mRNA-based vaccine formulations. System settings including wavenumber range, number of scans and spectral resolution were investigated, and an SOP was composed. Investigation into the effect of drying time on the influence of OH bonding in the vaccines' spectra was also investigated. The resulting optimal method comprised of a total of 16 scans per sample with a resolution of 4 cm^{-1} across a range of $450\text{-}4000\text{ cm}^{-1}$, after liquid vaccine samples had been allowed to dry on the detector for 20-45 minutes. The method yielded promising results in terms of spectral quality, vaccine characterisation and identification potential. Spectral quality showed strong IR activity for the majority of the brand 1 and 2 vaccines with an average of 25 and 22 bands per spectra, respectively. Excipients measured also showed strong IR activity with between 18 and 59 absorption bands, demonstrating reliable performance of the method regardless of physical composition of the sample: excipients ranged from dry

powders to frozen liquids or solids. Brand 1 (DNA-based) and brand 2 (mRNA-based) vaccines produced exceptional SNR values with an average of 397 for brand 1 and 1068 for brand 2. Brand 3 vaccines (live attenuated-inactivated) showed weaker IR activity in terms of number of bands and maximum absorbance with an average of nine bands per spectrum and maximum absorbance of 0.055 absorbance units. Brand 4 vaccines showed medium/strong IR activity with an average of 19 bands per spectrum and max absorbance of 0.08 absorbance units and SNR of 195-1108. Despite brand 1 and 2 vaccines being characterised as strong IR activity, absorbance values were still relatively low in comparison to typical signal for IR. This was attributed to the low concentrations of vaccine remaining after 6 doses had been administered to patients and then samples had been diluted with 0.9% NaCl (normal saline) for improved stability and increased volume for repeat testing.

Spectral interpretation of ATR-FTIR spectra revealed bands corresponding to the constituent nucleic acids of each vaccine brand. Brands were discriminable by their constituent-specific bands, including an additional band in the spectra of brand 2 and 4 (mRNA based) vaccines corresponding to the additional hydroxyl group in ribose (RNA) versus deoxyribose sugar (DNA). Clustering based on PCA also showed accuracy in discrimination between vaccine brands which was further demonstrated by the performance of the Ensemble subspace KNN classification model, yielding 99.7% accuracy in vaccine brand characterisation when presented with spectral features. In this sense, KNN produced better results than PCA despite the imbalance of brand representation in the dataset. High values for accuracy, precision, recall, specificity and F1-score were obtained for the KNN based classification model and the AUC-ROC curve showed faultless separation capacity of the model. These results indicate that portable ATR-FTIR spectroscopy, used in conjunction with the application

of MLAs could serve as a powerful, robust and accurate analytical tool for semi-automated vaccine authentication and identification of SF Covid-19 vaccines.

Optimisation of the conventional Raman and SERS method was performed using the Metrohm MIRA XTR DS handheld Raman spectrometer equipped with orbital raster scattering and involved optimisation of system settings, container, colloid and aggregating salt for SERS. The resulting method was the measurement of vaccines in 2 mL glass vials using the vial holder attachment, with resulting spectra the average of 10 scans across a range of 400 – 2300 cm^{-1} with a laser power of 5 mW, automatic integration time and Metrohm's XTR algorithm applied to every scan. The method yielded positive results in terms of vaccine characterisation, with constituent nucleic acid bands identified in the three brands' vaccine spectra which also showed contribution from the lipid nanoparticle excipients. Similarly to FTIR, discrimination of vaccine brand was possible through the identification of nucleic-acid specific bands in their spectra. Variable results were seen for the enhancement factor of SERS: the application of SERS in the pilot study yielded better performance than was observed in the overall study although this could be the result of numerous factors. Vaccines used in the pilot study were of higher concentration than those used in the final study. The pilot study had been conducted over 12 months prior to the final study, meaning degradation of the vaccines over time, especially related to the instability of their nucleic-acid components could have influenced the enhancement seen in the final study. Finally, the pilot study utilized a hydroxylamine-hydrochloride reduced-silver colloid for SERS measurement whereas the final study used a pre-prepared colloidal silver nanoparticle solution purchased from a chemical supplier for continuity and standardisation of the method. It is possible that the colloid used in the pilot study was a more favourable SERS substrate for the specific formulation of the vaccines.

Regardless, enhancement of up to 498% was still observed for brand 3 vaccines measured with the addition of the silver nanoparticles. The brand 3 vaccines were of sufficient volume at receipt and so were not diluted with 0.95% NaCl, supporting the theory that increased sample concentration yields improved results in terms of SERS enhancement. Clustering by PCA showed some accuracy in vaccine brand discrimination but overall was weaker than in ATR-FTIR with vaccine scores overlapping and both Type I and Type II errors observed, especially for the SERS samples where poor repeatability of the method was indicated by significant variation in vaccine spectra. Similarly to ATR-FTIR, classification outperformed PCA as a measure of identification potential, with 100% accuracy achieved for both validation and test models across various model sub-types. When considering classification, SERS yielded better results than conventional Raman with multiple models obtaining 100% accuracy, precision, recall, specificity and F1-score. It is noteworthy to mention that conventional Raman also produced values of over 90% for all of the aforementioned parameters. AUC demonstrated excellent separation capacity of the high performing classification models.

Optimisation of the Raman microscopic method for identification of Covid-19 vaccines was performed using the Horiba XPIoRA™ PLUS Raman microscope-spectrometer. This included optimisation of objective, grating, filter, acquisition time and number of scans. However, the outcomes of this study did not determine one obvious method that was optimal due to a number of confounding factors, fluorescence interference and time constraints. Instead, results indicated that certain parameters held more significant influence on the spectral quality observed and therefore detailed investigation into each variable on a larger sample size would be recommended as further work before an optimal method can be presented with confidence. Chapter 4

provided proof-of-concept for the use of Raman Microscopy as an analytical tool in the identification of SF Covid-19 vaccines and built a foundation of information for future method optimisation to be further improved and the dataset expanded. Results indicated that the x100 objective produced spectra of improved spectral quality with reduced fluorescence in comparison to those measured using the x10 objective. However, vaccines measured using the x100 objective were also measured using varying grating and filter settings over a small sample size. Insufficient spectra were collected at each grating and filter setting to confidently conclude which of these settings were optimal for vaccine analysis. Three vaccines were exempt from the interference of fluorescence in their spectra and were classified as Raman active. Spectral quality of these vaccines far outperformed the handheld Raman method in terms of number of bands and intensity, suggesting that the confocality offered by Raman microscopy could yield more successful characterisation and accuracy in identification of SF vaccines. However, the limited data (Raman active spectra) that supports this conclusion means the collection of a significantly larger dataset of spectra with no fluorescence interference would be required to fully investigate this claim. Bands corresponding to nucleic acid constituents, proteins, lipids and amino acids could be successfully identified in the spectra of the three vaccines' with no fluorescence. SERS again demonstrated strong enhancement of peak intensity, although this applied to both Raman active spectra and fluorescence, indicating that SERS is only suitable for use where fluorescence interference is insignificant, the enhancement of fluorescence in the vaccines' also produced misleading results in terms of SNR. CWS demonstrated satisfactory results for identification potential of the method where all vaccines obtained an r-value of 1 against themselves and most vaccines of the same brand obtained an r-value of > 0.95 against each other. However,

some type I and II errors were observed for vaccine spectra which were heavily influenced by fluorescence. PCA showed good clustering for vaccines measured using the x100 objective and x10 objective where the two groups of vaccines were clustered away from each other. However, despite spectra of individual vaccines demonstrating good clustering with no overlap of scores, scores of each brand were not clustered together and the presence of fluorescence in the vaccines' spectra appeared to heavily influence the models, causing type I and II errors.

Overall, ATR-FTIR stood out as the most robust and effective analytical approach to rapid, non-destructive identification of SF vaccines as demonstrated by the excellent repeatability of the method, clustering based on PCA and accuracy of classification even at low sample concentration and volume. The results presented in this study support the use of ATR-FTIR spectroscopy for the analysis of complex biologic mixtures like Covid-19 vaccines. While handheld Raman spectroscopy showed positive outcomes in terms of characterisation, identification potential and classification, repeated analysis of a larger sample size is required to determine the validity of these results considering the potential of data overfitting. Though confocal Raman microscopy showed excellent potential as an identification method for Covid-19 vaccines for the spectra acquired without fluorescence interference, the variation observed between spectra and major fluorescence indicated that the methods outlined in this thesis have the potential to produce misleading results and therefore significant method development in terms of optimising system parameters, colloid formulation and measurement of a larger sample size is necessary to truly establish the performance of the technique for this application.

5.2 Outcomes of thesis results/contribution to knowledge

The outcomes of the studies outlined in this thesis were considered in relation to the aim and objectives of the project which are addressed below:

1. Use portable ATR-FTIR spectroscopy for authentication of Covid-19 vaccines surpassing challenges related to water interference.

Based on the results of this study, ATR-FTIR was successfully used as an analytical tool for the characterisation and authentication of Covid-19 vaccines of four different brands. Challenges related to water interference were overcome by method optimisation resulting in the drying of vaccine samples on the detector for 20 – 45 minutes prior to measurement. The results presented in this thesis indicate that the method outlined could be utilised as a repeatable and reproducible method for Covid-19 vaccine authentication of DNA, mRNA and live attenuated inactive viral based Covid-19 vaccines.

2. Compare handheld conventional versus surface enhanced Raman spectroscopic methods for identification DNA and mRNA in vaccines considering challenges in fluorescence and method sensitivity.

Chapter 3 compared the use of conventional versus SERS methods for the identification of nucleic acid constituents of Covid-19 vaccines, although overall the study concludes that conventional Raman is optimal for the analysis of vaccines in very low concentrations. SERS showed improved enhancement of signal when applied to vaccines of an increased concentration, suggesting a potential minimum starting concentration for the effective use of SERS in the authentication of vaccines.

This suggested that the method sensitivity of SERS in this case could be weaker than that of conventional Raman when analysing complex biologic formulations. Successful comparisons were drawn between the two techniques, although quantitative analysis of vaccine samples of varying concentrations would provide more information of method sensitivity and the influence of concentration on Raman activity and fluorescence.

3. Explore the ability of confocal Raman microscopy for authentication of Covid-19 vaccines of different manufacturers in low doses.

The performance of confocal Raman microscopy was explored and evaluated at a relatively basic level of detail due to various confounding factors. Significant interference from fluorescence and the limited acquisition of Raman active spectra prevented reliable conclusions being drawn from the dataset measured in this study. The acquisition of three Raman active spectra with no fluorescence that demonstrated superior spectral quality in comparison to the conventional Raman spectroscopy provided proof-of-principle for the technique as an even greater identification tool for Covid-19 vaccines at very low concentrations, although significant further work is required to support this.

4. Determine the performance of machine learning algorithms in classification of infrared and Raman spectroscopic data.

The performance of MLAs in the classification of data collected using the ATR-FTIR spectrometer, handheld Raman spectrometer and Raman microscope was determined using qualitative evaluation (CWS and PCA) and quantitative evaluation

of performance metrics including accuracy, precision, specificity, recall and F1-score as well as AUC (classification models). Examination of PCA and CWS showed good results in terms of clustering for ATR-FTIR and conventional Raman spectroscopy with varied results for Raman microscopy. It is worth acknowledging that the classification results of the Raman spectroscopy dataset could be at risk of overfitting due to the relatively small sample size, although actions were taken to mitigate this risk including the division of data into a validation and test dataset to prevent the model being tested on data that had been used to train it. Further application of data balancing algorithms such as 'SMOTE' could be employed in the future alongside expansion of the dataset to help mitigate this risk and produce more reliable model evaluation results. Overall, the performance of the classification models trained on each dataset were successfully evaluated through calculation of accuracy, precision, specificity and F1-score. AUC further supported this conclusion.

Considering the above, this research made contributions to knowledge in terms of the successful evaluation of ATR-FTIR spectroscopy as a robust method for SF Covid-19 vaccine authentication, allowing further development and adaptation of the method outlined in this thesis for practical forensic investigations into SF Covid-19 vaccines and analysis of novel complex biologic formulations. The successful implementation of this method could hold particular significance in LMICs if used as an alternative to HPLC, as the method and instrumentation is much more cost effective, and the technique requires less resources and training. ATR-FTIR systems can be sensitive to environmental conditions however, so analysis would still need to be conducted in a controlled environment. Despite this, the use of ATR-FTIR could present a more accessible method of drug authentication in LMICs, increasing the number of SF Covid-19 vaccines identified and therefore reducing exposure to the associated risks.

The research provided a sound foundation of information in terms of method optimisation for Raman spectroscopy as an analytical approach to the identification of SF Covid-19 vaccines and provides proof-of concept for Raman microscopy as a potentially superior analytical method. This information could be used to inform future work in terms of fluorescence and sample concentration awareness and mitigation. Further development of the SERS method could lead to the successful implication of handheld Raman spectroscopy for the rapid, on-site detection of SF Covid-19 vaccines at locations such as airports, borders and hospitals. This would improve the rate of detection of SF vaccines and potentially intercept supply chains before they reach patients, therefore reducing the risk posed to the public by SF vaccines but potentially aiding in the prosecution of those associated with pharmaceutical crimes.

5.3 Limitations

The overarching limitation experienced in this study was the initial volume of brand 1 and 2 vaccines received. After dilution with 0.9% NaCl, low sample concentration was suspected to have significant effects on the Raman activity of vaccines for both conventional Raman and microscopy. Additionally, only four brands of vaccine were measured in this study: for ATR-FTIR spectroscopy to be confidently used as an identification technique in forensic investigations of SF vaccines, the method would require validation for every available brand of Covid-19 vaccine available at the time. Without this, the method is only proved to be suitable for authentication of the four brands outlined in this study. Similarly, no reference standard vaccines were able to be sourced for this project and no further quality control testing was performed on the vaccines acquired. Most limitations of the study relate to the spectral acquisition

difficulties experienced in using the Raman microscope. A series of confounding factors limited the successful acquisition of spectra without fluorescence including variability in instrument performance under uncontrolled laboratory conditions. Only one source of laser was available and there was no motor stage available which would have helped to facilitate imaging due to financial constraints. Additionally, there was no long-distance working objective available which would have aided in image focusing and spectral acquisition from a distance where the objective was not close enough to the sample to risk burning it.

5.4 Further research

Further work would involve the repetition of the ATR-FTIR study on more available vaccine brands to build a spectral library of known Covid-19 vaccine samples. This spectral library would allow comparison of suspected SF vaccines against the spectral fingerprint of a known reference standard vaccine to provide even faster and potentially automated identification of SF Covid-19 vaccines.

Further development of the SERS study would focus on method optimisation related to colloid formulation and aggregating agent, as well as the measurement of a larger sample size of vaccines at increased concentrations. Additionally, this would include quantitative analysis to establish a limit of detection for the method. Expansion of the dataset would help to prevent overfitting in classification models and provide a more reliable accuracy in terms of classification performance.

Repetition of the Raman microscopy chapter, with multiple laser sources available alongside the utilisation of a motor source and long-distance working objective would be preferable. If these adjustments aided in the focussing and hence successful

acquisition of Raman active spectra, variables such as filter and grating could be investigated independently to confidently establish an optimal method for Covid-19 vaccine identification using this technique.

References

Abramczyk, H. and Surmacki, J. (2023). Effect of COVID-19 mRNA Vaccine on Human Lung Carcinoma Cells *In Vitro* by Means of Raman Spectroscopy and Imaging. *ACS Omega*, 8(45), pp.42555–42564. doi:<https://doi.org/10.1021/acsomega.3c05287>.

Abubukar, A., Awosanya, E., Badaru, O., Haladu, S., Nguku, P., Edwards, P., Noe, R., Teran-Maciver, M., Wolkin, A., Lewis, L. and Nguyen, M. (2009). Fatal poisoning among young children from diethylene glycol-contaminated acetaminophen - Nigeria, 2008-2009. *MMWR Morbidity and Mortality Weekly Report*, 58(48), pp.1345–1347.

ACT Consortium Drug Quality Project Team and the IMPACT2 Study Team (2015). Quality of Artemisinin-Containing Antimalarials in Tanzania's Private Sector—Results from a Nationally Representative Outlet Survey. *The American Journal of Tropical Medicine and Hygiene*, [online] 92(6_Suppl), pp.75–86. doi:<https://doi.org/10.4269/ajtmh.14-0544>.

Agarwal, A., Sharma, P., Alshehri, M., Mohamed, A.A. and Alfarraj, O. (2021). Classification model for accuracy and intrusion detection using machine learning approach. *PeerJ Computer Science*, [online] 7, p.e437. doi:<https://doi.org/10.7717/peerj-cs.437>.

Akuse, R.M., Eke, F.U., Ademola, A.D., Fajolu, I.B., Gbelee, H.O., Ihejiahi, U., Bugaje, M.A., Anochie, I.C., Asinobi, A.O., Okafor, H.U., Adeleke, S.I., Audu, L.I., Otuneye, A., Disu, E., Idris, H., Aikhonbare, H., Yakubu, A., Ogala, W., Ogunrinde, O. and Wammanda, R. (2012). Diagnosing renal failure due to diethylene glycol in children in a resource-constrained setting. *Pediatric Nephrology*, [online] 27(6), pp.1021–1028. doi:<https://doi.org/10.1007/s00467-011-2082-8>.

Almehmadi, L.M., Curley, S.M., Tokranova, N.A., Tenenbaum, S.A. and Lednev, I.K. (2019). Surface Enhanced Raman Spectroscopy for Single Molecule Protein Detection. *Scientific Reports*, 9(1). doi:<https://doi.org/10.1038/s41598-019-48650-y>.

Amankwah-Amoah, J. (2022). Covid-19 and Counterfeit Vaccines: Global Implications, New Challenges and Opportunities. *Health Policy and Technology*, 11(2), p.100630. doi:<https://doi.org/10.1016/j.hlpt.2022.100630>.

Amnesty International (2022). *Pharmaceutical companies accused of continuing to profiteer from pandemic - new report*. [online] www.amnesty.org.uk. Available at: <https://www.amnesty.org.uk/press-releases/pharmaceutical-companies-accused-continuing-profiteer-pandemic-new-report>.

Antonio, K.A. and Schultz, Z.D. (2013). Advances in Biomedical Raman Microscopy. *Analytical Chemistry*, [online] 86(1), pp.30–46. doi:<https://doi.org/10.1021/ac403640f>.

Assi, S. (2024). Raman Spectroscopy. *Clarke's Analysis of Drugs and Poisons*. [online] Available at: <https://www.medicinescomplete.com/#!/content/clarke/clk214311?hspl=assi&hspl=35&hspl=raman&hspl=spectroscopy&hspl=S>.

Assi, S., Arafat, B., Lawson-Wood, K. and Robertson, I. (2020). Authentication of Antibiotics Using Portable Near-Infrared Spectroscopy and Multivariate Data Analysis. *Applied Spectroscopy*, 75(4), pp.434–444. doi:<https://doi.org/10.1177/0003702820958081>.

Barhoumi, A., Zhang, D., Tam, F. and Halas, N.J. (2008). Surface-Enhanced Raman Spectroscopy of DNA. *Journal of the American Chemical Society*, 130(16), pp.5523–5529. doi:<https://doi.org/10.1021/ja800023j>.

Barwick, V.J. (1999). Sources of uncertainty in gas chromatography and high-performance liquid chromatography. *Journal of Chromatography A*, [online] 849(1), pp.13–33. doi:[https://doi.org/10.1016/s0021-9673\(99\)00537-3](https://doi.org/10.1016/s0021-9673(99)00537-3).

BBC News (2021). *Coronavirus: Pfizer confirms fake versions of vaccine in Poland and Mexico*. [online] BBC News. Available at: <https://www.bbc.co.uk/news/world-56844149#:~:text=US%20pharmaceutical%20company%20Pfizer%20says%20it%20has%20identified> [Accessed 24 Sep. 2024].

Benevides, J.M. and Thomas, G.J. (1983). Characterization of DNA structures by Raman spectroscopy: high-salt and low-salt forms of double helical poly(dG-dC) in H₂O and D₂O solutions and application to B, Z and A-DNA*. *Nucleic Acids Research*, 11(16), pp.5747–5761. doi:<https://doi.org/10.1093/nar/11.16.5747>.

Berry, M. (2022). How to Reduce Fluorescence in Raman Spectroscopy. [online] Research Gate. doi:<https://doi.org/10.13140/RG.2.2.36208.23048>.

Bhaumik, A., Shearin, A.M., Delong, R., Wanekaya, A. and Ghosh, K. (2014). Probing the Interaction at the Nano–Bio Interface Using Raman Spectroscopy: ZnO Nanoparticles and Adenosine Triphosphate Biomolecules. *The Journal of Physical Chemistry. C, nanomaterials and interfaces*, 118(32), pp.18631–18639. doi:<https://doi.org/10.1021/jp506200a>.

Bidlingmeyer, B.A. (1993). *Practical HPLC Methodology and Applications*. [online] Wiley, pp.1–27. Available at: <https://books.google.co.uk/books?hl=en&lr=&id=iF36W3d2STMC&oi=fnd&pg=PP13&dq=HPLC+made+simple&ots=nRF5H2BMQk&sig=5v4pwrkJcP0t9kFvFXGAeM-dTY8#v=onepage&q=HPLC%20made%20simple&f=false>.

Bieker, L. and Schmidt, H. (1979). Raman spectra of N -formylkynurenine derivatives of lysozyme produced by ozone oxidation. *FEBS Letters*, 106(2), pp.268–270. doi:[https://doi.org/10.1016/0014-5793\(79\)80511-6](https://doi.org/10.1016/0014-5793(79)80511-6).

Blackstone, E.A., Fuhr, Jr, J.P. and Pociask, S. (2014). The health and economic effects of counterfeit drugs. *American health & drug benefits*, [online] 7(4). Available at: <https://pubmed.ncbi.nlm.nih.gov/25126373> [Accessed 25 Sep. 2024].

Brissette, C. and C. Sandorfy (1960). HYDROGEN BONDING IN THE AMINE HYDROHALIDES: II. THE INFRARED SPECTRUM FROM 4000 TO 2200 CM⁻¹. *Canadian Journal of Chemistry*, 38(1), pp.34–44. doi:<https://doi.org/10.1139/v60-003>.

Bruker (2024). *Guide to Raman Microscopy*. [online] Bruker.com. Available at: <https://www.bruker.com/en/products-and-solutions/infrared-and-raman/raman-microscopes/what-is-raman-microscopy.html#:~:text=Raman%20microscopy%20has%20two%20huge%20benefits%3A%20the%20convenience> [Accessed 12 Sep. 2024].

Calvo-Gomez, O., Calvo, H., Cedillo-Barrón, L., Vivanco-Cid, H., Alvarado-Orozco, J.M., Fernandez-Benavides, D.A., Arriaga-Pizano, L., Ferat-Osorio, E., Anda-Garay, J.C., López-Macias, C. and López, M.G. (2022). Potential of ATR-FTIR–Chemometrics in Covid-19: Disease Recognition. *ACS Omega*, 7(35), pp.30756–30767. doi:<https://doi.org/10.1021/acsomega.2c01374>.

Carey, P.R. (2006). RAMAN CRYSTALLOGRAPHY AND OTHER BIOCHEMICAL APPLICATIONS OF RAMAN MICROSCOPY. *Annual Review of Physical Chemistry*, 57(1), pp.527–554. doi:<https://doi.org/10.1146/annurev.physchem.57.032905.104521>.

Carpenter, J.F., Prestrelski, S.J. and Arakawa, T. (1993). Separation of Freezing- and Drying-Induced Denaturation of Lyophilized Proteins Using Stress-Specific Stabilization. *Archives of Biochemistry and Biophysics*, 303(2), pp.456–464. doi:<https://doi.org/10.1006/abbi.1993.1309>.

Cavonius, L., Fink, H., Kiskis, J., Albers, E., Undeland, I. and Enejder, A. (2015). Imaging of Lipids in Microalgae with Coherent Anti-Stokes Raman Scattering Microscopy. *Plant Physiology*, [online] 167(3), pp.603–616. doi:<https://doi.org/10.1104/pp.114.252197>.

Céline, A., Gonçalves, O., Jacquemin, F. and Fréour, S. (2014). Qualitative and quantitative assessment of water sorption in natural fibres using ATR-FTIR spectroscopy. *Carbohydrate Polymers*, [online] 101, pp.163–170. doi:<https://doi.org/10.1016/j.carbpol.2013.09.023>.

Centers for Disease Control and Prevention (CDC) (2021). Acute allergic-type reactions among patients undergoing hemodialysis--multiple states, 2007-2008. *MMWR. Morbidity and mortality weekly report*, [online] 57(5). Available at: <https://pubmed.ncbi.nlm.nih.gov/18256585/#:~:text=Abstract.%20CDC%20is%20investigating%20an%20outbreak%20of%20acute> [Accessed 24 Sep. 2024].

Chan, J.W., Taylor, D.S., Zwerdling, T., Lane, S.M., Ihara, K. and Huser, T. (2006). Micro-Raman Spectroscopy Detects Individual Neoplastic and Normal Hematopoietic Cells. *Biophysical Journal*, 90(2), pp.648–656. doi:<https://doi.org/10.1529/biophysj.105.066761>.

Chen, D., Hu, B., Shao, X. and Su, Q. (2004). Removal of major interference sources in aqueous near-infrared spectroscopy techniques. *Analytical and Bioanalytical Chemistry*, 379(1), pp.143–148. doi:<https://doi.org/10.1007/s00216-004-2569-2>.

Cherry, James.D. (2004). The Chronology of the 2002–2003 SARS Mini Pandemic. *Paediatric Respiratory Reviews*, [online] 5(4), pp.262–269. doi:<https://doi.org/10.1016/j.prrv.2004.07.009>.

Chophi, R., Sharma, S. and Singh, R. (2019). Forensic analysis of red lipsticks using ATR-FTIR spectroscopy and chemometrics. *Forensic Chemistry*, [online] 17. doi:<https://doi.org/10.1016/j.forc.2019.100209>.

Clarke, S.J., Littleford, R.E., Smith, W.E. and Goodacre, R. (2005). Rapid monitoring of antibiotics using Raman and surface enhanced Raman spectroscopy. *The Analyst*, 130(7), p.1019. doi:<https://doi.org/10.1039/b502540k>.

Coates, J.P. (2000). The Interpretation of Infrared Spectra: A Practical Approach. *Encyclopaedia of Analytical Chemistry*, 12, pp.10815–10837. doi:<https://doi.org/10.1080/05704929608000568>.

Coelho Neto, J. and Lisboa, F.L.C. (2017). ATR-FTIR characterization of generic brand-named and counterfeit sildenafil- and tadalafil-based tablets found on the Brazilian market. *Science & Justice*, 57(4), pp.283–295. doi:<https://doi.org/10.1016/j.scijus.2017.04.009>.

Combs, A., McCann, K., Autrey, D., Jaan Laane, Overman, S.A. and Thomas, G.J. (2005). Raman signature of the non-hydrogen-bonded tryptophan side chain in proteins: experimental and ab initio spectra of 3-methylindole in the gas phase. *Journal of Molecular Structure*, [online] 735-736, pp.271–278. doi:<https://doi.org/10.1016/j.molstruc.2004.11.058>.

Cuomo, R.E. and Mackey, T.K. (2014). An exploration of counterfeit medicine surveillance strategies guided by geospatial analysis: lessons learned from counterfeit

Avastin detection in the US drug supply chain. *BMJ Open*, 4(12), p.e006657. doi:<https://doi.org/10.1136/bmjopen-2014-006657>.

Custers, D., Cauwenbergh, T., Bothy, J.L., Courselle, P., De Beer, J.O., Apers, S. and Deconinck, E. (2015). ATR-FTIR spectroscopy and chemometrics: An interesting tool to discriminate and characterize counterfeit medicines. *Journal of Pharmaceutical and Biomedical Analysis*, 112, pp.181–189. doi:<https://doi.org/10.1016/j.jpba.2014.11.007>.

D'Amico, F., Cammisuli, F., Addobbati, R., Rizzardi, C., Gessini, A., Masciovecchio, C., Rossi, B. and Pascolo, L. (2015). Oxidative damage in DNA bases revealed by UV resonant Raman spectroscopy. *The Analyst*, 140(5), pp.1477–1485. doi:<https://doi.org/10.1039/c4an02364a>.

Davis, H.E., McCorkell, L., Vogel, J.M. and Topol, E.J. (2023). Long COVID: Major Findings, Mechanisms and Recommendations. *Nature Reviews Microbiology*, [online] 21(3), pp.1–14. doi:<https://doi.org/10.1038/s41579-022-00846-2>.

De Gelder, J., De Gussem, K., Vandenabeele, P. and Moens, L. (2007). Reference database of Raman spectra of biological molecules. *Journal of Raman Spectroscopy*, [online] 38(9), pp.1133–1147. doi:<https://doi.org/10.1002/jrs.1734>.

de Queiroz, N.M.G.P., Marinho, F.V., Chagas, M.A., Leite, L.C.C., Homan, E.J., de Magalhães, M.T.Q. and Oliveira, S.C. (2020). Vaccines for COVID-19: perspectives from nucleic acid vaccines to BCG as delivery vector system. *Microbes and Infection*, [online] 22(10), pp.515–524. doi:<https://doi.org/10.1016/j.micinf.2020.09.004>.

Delany, I., Rappuoli, R. and De Gregorio, E. (2014). Vaccines for the 21st century. *EMBO molecular medicine*, [online] 6(6), pp.708–720. doi:<https://doi.org/10.1002/emmm.201403876>.

Deluca, M., Hu, H., Popov, M.N., Spitaler, J. and Dieing, T. (2023). Advantages and developments of Raman spectroscopy for electroceramics. *Communications materials*, [online] 4(1). doi:<https://doi.org/10.1038/s43246-023-00400-4>.

Desai, S., Mishra, S.V., Joshi, A., Sarkar, D., Hole, A., Mishra, R., Dutt, S., Chilakapati, M.K., Gupta, S. and Dutt, A. (2020). Raman spectroscopy-based detection of RNA viruses in saliva: A preliminary report. *Journal of Biophotonics*, [online] 13(10). doi:<https://doi.org/10.1002/jbio.202000189>.

Dovbeshko, G.I., Chegel, V.I., Gridina, N.Y., Repnytska, O.P., Shirshov, Y.M., Tryndiak, V.P., Todor, I.M. and Solyanik, G.I. (2002). Surface enhanced IR absorption of nucleic acids from tumor cells: FTIR reflectance study. *Biopolymers*, 67(6), pp.470–486. doi:<https://doi.org/10.1002/bip.10165>.

Downes, A. (2015). Raman Microscopy and Associated Techniques for Label-Free Imaging of Cancer Tissue. *Applied Spectroscopy Reviews*, [online] 50(8), pp.641–653. doi:<https://doi.org/10.1080/05704928.2015.1052817>.

Economist (2012). *Bad medicine*. [online] The Economist. Available at: <https://www.economist.com/international/2012/10/13/bad-medicine> [Accessed 25 Aug. 2020].

Elshout, M., Erckens, R.J., Webers, C.A., Beckers, H.J., Berendschot, T.T., de Brabander, J., Hendrikse, F. and Schouten, J.S. (2011). Detection of Raman Spectra in Ocular Drugs for Potential In Vivo Application of Raman Spectroscopy. *Journal of Ocular Pharmacology and Therapeutics*, 27(5), pp.445–451. doi:<https://doi.org/10.1089/jop.2011.0018>.

Eser, A. (2024). *Intellectual Property Industry Statistics Statistics: Market Data Report 2024*. [online] Worldmetrics.org. Available at: <https://worldmetrics.org/intellectual-property-industry-statistics/> [Accessed 25 Sep. 2024].

European Medicines Agency (2024). *Counterfeit medicine | European Medicines Agency (EMA)*. [online] European Medicines Agency (EMA). Available at: <https://www.ema.europa.eu/en/glossary-terms/counterfeit-medicine> [Accessed 24 Sep. 2024].

Farouk, F., Moussa, B.A. and Azzazy, H.M.E.-S. (2011). Fourier transform infrared spectroscopy for in-process inspection, counterfeit detection and quality control of anti-diabetic drugs. *Journal of Spectroscopy*, [online] 26, pp.297–309. doi:<https://doi.org/10.3233/SPE-2011-0531>.

FDA (2020). *PFIZER-BIONTECH COVID-19 VACCINE (BNT162, PF-07302048) VACCINES AND RELATED BIOLOGICAL PRODUCTS ADVISORY COMMITTEE BRIEFING DOCUMENT*. [online] Available at: <https://www.fda.gov/media/144246/download>.

Fleischmann, M., Hendra, P.J. and McQuillan, A.J. (1974). Raman spectra of pyridine adsorbed at a silver electrode. *Chemical Physics Letters*, [online] 26(2), pp.163–166. doi:[https://doi.org/10.1016/0009-2614\(74\)85388-1](https://doi.org/10.1016/0009-2614(74)85388-1).

Freudiger, C.W., Yang, W., Holtom, G.R., Peyghambarian, N., Sunney Xie, X. and Kieu, K.Q. (2014). Stimulated Raman scattering microscopy with a robust fibre laser source. *Nature Photonics*, 8(2), pp.153–159. doi:<https://doi.org/10.1038/nphoton.2013.360>.

Fung, A.A. and Shi, L. (2020). Mammalian cell and tissue imaging using Raman and coherent Raman microscopy. *WIREs Systems Biology and Medicine*, [online] 12(6). doi:<https://doi.org/10.1002/wsbm.1501>.

Gardner, I.A. and Greiner, M. (2006). Receiver-operating characteristic curves and likelihood ratios: improvements over traditional methods for the evaluation and application of veterinary clinical pathology tests. *Veterinary Clinical Pathology*, 35(1), pp.8–17. doi:<https://doi.org/10.1111/j.1939-165x.2006.tb00082.x>.

Garrone Barauna, V., Singh, M., Rodrigues Barbosa, L., Dantas Marcarini, W., Frizera Vassallo, P., Geraldo Mill, J., Ribeiro-Rodrigues, R., Gastalho, C., Hans-Heinrich Warnke, P. and Martin, F. (2021). Ultrarapid On-Site Detection of SARS-CoV-2 Infection Using Simple ATR-FTIR Spectroscopy and an Analysis Algorithm: High Sensitivity and Specificity. *Analytical Chemistry*, 93(5), pp.2950–2958. doi:<https://doi.org/10.1021/acs.analchem.0c04608>.

Gearheart, L.A., Ploehn, H.J. and Murphy, C.J. (2001). Oligonucleotide Adsorption to Gold Nanoparticles: A Surface-Enhanced Raman Spectroscopy Study of Intrinsically Bent DNA. *Journal of Physical Chemistry B*, 105(50), pp.12609–12615. doi:<https://doi.org/10.1021/jp0106606>.

Ghasemiyeh, P. and Mohammadi-Samani, S. (2020). COVID-19 outbreak: Challenges in pharmacotherapy based on pharmacokinetic and pharmacodynamic aspects of drug therapy in patients with moderate to severe infection. *Heart & Lung*, 49(6), pp.763–773. doi:<https://doi.org/10.1016/j.hrtlng.2020.08.025>.

Gong, B., Chen, J.-H., Yajima, R., Chen, Y., Chase, E., Chadalavada, D.M., Golden, B.L., Carey, P.R. and Bevilacqua, P.C. (2009). Raman crystallography of RNA. *Methods*, [online] 49(2), pp.101–111. doi:<https://doi.org/10.1016/j.ymeth.2009.04.016>.

Graham, D. and Goodacre, R. (2008). Chemical and bioanalytical applications of surface enhanced Raman scattering spectroscopy. *Chemical Society Reviews*, 37(5), p.883. doi:<https://doi.org/10.1039/b804297g>.

Griebenow, K. and Klibanov, A.M. (1995). Lyophilization-induced reversible changes in the secondary structure of proteins. *Proceedings of the National Academy of Sciences*, 92(24), pp.10969–10976. doi:<https://doi.org/10.1073/pnas.92.24.10969>.

Grillet, N., Manchon, D., Cottancin, E., Bertorelle, F., Bonnet, C., Broyer, M., Lermé, J. and Pellarin, M. (2013). Photo-Oxidation of Individual Silver Nanoparticles: A Real-Time Tracking of Optical and Morphological Changes. *Journal of Physical Chemistry C*, 117(5), pp.2274–2282. doi:<https://doi.org/10.1021/jp311502h>.

Gurgula, O. and McDonagh, L. (2023). Access Denied: the Role of Trade Secrets in Preventing Global Equitable Access to COVID-19 Tools. *SSRN Electronic Journal*. [online] doi:<https://doi.org/10.2139/ssrn.4484507>.

Hansen, L., De Beer, T., Pierre, K., Pastoret, S., Bonnegarde-Bernard, A., Daoussi, R., Vervaet, C. and Remon, J.P. (2015). FTIR spectroscopy for the detection and evaluation of live attenuated viruses in freeze dried vaccine formulations. *Biotechnology Progress*, 31(4), pp.1107–1118. doi:<https://doi.org/10.1002/btpr.2100>.

Hernández, B., Coïc, Y.-M., Pflüger, F., Kruglik, S.G. and Ghomi, M. (2015). All characteristic Raman markers of tyrosine and tyrosinate originate from phenol ring fundamental vibrations. *Journal of Raman Spectroscopy*, [online] 47(2), pp.210–220. doi:<https://doi.org/10.1002/jrs.4776>.

Hernández, B., Pflüger, F., Kruglik, S.G. and Ghomi, M. (2013). Characteristic Raman lines of phenylalanine analyzed by a multiconformational approach. *Journal of Raman Spectroscopy*, [online] 44(6), pp.827–833. doi:<https://doi.org/10.1002/jrs.4290>.

Holzgrabe, U. (2018). NMR Spectroscopy, Application—Identification of Counterfeit Drugs and Herbal Medicines. *Encyclopaedia of Analytical Science (Third edition)*, [online] pp.182–185. doi:<https://doi.org/10.1016/b978-0-12-409547-2.14081-8>.

Horiba Scientific (2024). *XploRA™ PLUS*. [online] Horiba.com. Available at: <https://www.horiba.com/int/scientific/products/detail/action/show/Product/xploratm-plus-1528/> [Accessed 16 Sep. 2024].

Huang, J. and Ling, C.X. (2005). Using AUC and accuracy in evaluating learning algorithms. *IEEE Transactions on Knowledge and Data Engineering*, 17(3), pp.299–310. doi:<https://doi.org/10.1109/tkde.2005.50>.

Huang, W.E., Griffiths, R.I., Thompson, I.P., Bailey, M.J. and Whiteley, A.S. (2004). Raman Microscopic Analysis of Single Microbial Cells. *Analytical Chemistry*, [online] 76(15), pp.4452–4458. doi:<https://doi.org/10.1021/ac049753k>.

Huang, Z., McWilliams, A., Lui, H., McLean, D.I., Lam, S. and Zeng, H. (2003). Near-infrared Raman spectroscopy for optical diagnosis of lung cancer. *International Journal of Cancer*, [online] 107(6), pp.1047–1052. doi:<https://doi.org/10.1002/ijc.11500>.

Iconomidou, V.A., Chryssikos, G.D., Gionis, V., Willis, J.H. and Hamodrakas, S.J. (2001). ‘Soft’-cuticle protein secondary structure as revealed by FT-Raman, ATR FT-IR and CD spectroscopy. *Insect Biochemistry and Molecular Biology*, 31(9), pp.877–885. doi:[https://doi.org/10.1016/s0965-1748\(01\)00033-9](https://doi.org/10.1016/s0965-1748(01)00033-9).

Ikeshoji, T. and Sekine, T. (1977). Observation of Concentration Distribution in Diffusion Layer by Focal Cylinder Method and Surface Concentration by Total Reflection Raman Spectroscopy. *Denki Kagaku oyobi Kogyo Butsuri Kagaku*, [online] 45(9), pp.575–579. doi:<https://doi.org/10.5796/kogyobutsurikagaku.45.575>.

INTERPOL (2021). *Fake COVID Vaccine Distribution Network Dismantled after INTERPOL Alert*. [online] www.interpol.int. Available at: <https://www.interpol.int/en/News-and-Events/News/2021/Fake-COVID-vaccine-distribution-network-dismantled-after-INTERPOL-alert>.

INTERPOL (2022). *Pharmaceutical crime operations*. [online] www.interpol.int. Available at: <https://www.interpol.int/en/Crimes/Illicit-goods/Pharmaceutical-crime-operations>.

Ionin, B.I. (2012). *NMR spectroscopy in organic chemistry*. Springer-Verlag New York, pp.2–7.

Ito, T., Koyama, Y. and Otsuka, M. (2010). Analysis of the surface structure of DNA/polycation/hyaluronic acid ternary complex by Raman microscopy. *Journal of Pharmaceutical and Biomedical Analysis*, 51(1), pp.268–272. doi:<https://doi.org/10.1016/j.jpba.2009.07.024>.

Jeanmaire, D.L. and Van Duyne, R.P. (1977). Surface raman spectroelectrochemistry: Part I. Heterocyclic, aromatic, and aliphatic amines adsorbed on the anodized silver electrode. *Journal of Electroanalytical Chemistry and Interfacial Electrochemistry*, [online] 84(1), pp.1–20. doi:[https://doi.org/10.1016/s0022-0728\(77\)80224-6](https://doi.org/10.1016/s0022-0728(77)80224-6).

Jenkins, R.H., Tuma, R., Juuti, J.T., Bamford, D.H. and Thomas, G.J. (1999). A novel Raman spectrophotometric method for quantitative measurement of nucleoside triphosphate hydrolysis. *Biospectroscopy*, 5(1), pp.3–8. doi:[https://doi.org/10.1002/\(sici\)1520-6343\(1999\)5:1%3C3::aid-bspy2%3E3.0.co;2-1](https://doi.org/10.1002/(sici)1520-6343(1999)5:1%3C3::aid-bspy2%3E3.0.co;2-1).

Juba, B. and Le, H.S. (2019). Precision-Recall versus Accuracy and the Role of Large Data Sets. *Proceedings of the AAAI Conference on Artificial Intelligence*, 33(1), pp.4039–4048. doi:<https://doi.org/10.1609/aaai.v33i01.33014039>.

Katainen, E., Elomaa, M., Laakkonen, U.-M., Sippola, E., Niemelä, P., Suhonen, J. and Järvinen, K. (2007). Quantification of the Amphetamine Content in Seized Street Samples by Raman Spectroscopy. *Journal of Forensic Sciences*, 52(1), pp.88–92. doi:<https://doi.org/10.1111/j.1556-4029.2006.00306.x>.

Kaur, H., Green, M.D., Hostetler, D.M., Fernández, F.M. and Newton, P.N. (2010). Antimalarial drug quality: methods to detect suspect drugs. *Therapy*, 7(1), pp.49–57. doi:<https://doi.org/10.2217/thy.09.84>.

Kaur, H., Seifert, K., Hawkes, G.E., Coumbarides, G.S., Alvar, J. and Croft, S.L. (2015). Chemical and Bioassay Techniques to Authenticate Quality of the Anti-Leishmanial Drug Miltefosine. *American Journal of Tropical Medicine and Hygiene*, [online] 92(6), pp.31–38. doi:<https://doi.org/10.4269/ajtmh.14-0586>.

Kimani, M.M., Lanzarotta, A. and Batson, J.S. (2020). Trace level detection of select opioids (fentanyl, hydrocodone, oxycodone, and tramadol) in suspect pharmaceutical tablets using surface-enhanced Raman scattering (SERS) with handheld devices. *Journal of Forensic Sciences*, 66(2), pp.491–504. doi:<https://doi.org/10.1111/1556-4029.14600>.

Kishimoto, T.K., Viswanathan, K., Ganguly, T., Elankumaran, S., Smith, S., Pelzer, K., Lansing, J.C., Sriranganathan, N., Zhao, G., Galcheva-Gargova, Z., Al-Hakim, A., Bailey, G.S., Fraser, B., Roy, S., Rogers-Cotrone, T., Buhse, L., Whary, M., Fox, J., Nasr, M. and Dal Pan, G.J. (2008). Contaminated Heparin Associated with Adverse Clinical Events and Activation of the Contact System. *New England Journal of Medicine*, [online] 358(23), pp.2457–2467. doi:<https://doi.org/10.1056/nejmoa0803200>.

Kline, N.M. and Treado, P.J. (1997). Raman Chemical Imaging of Breast Tissue. *Journal of Raman Spectroscopy*, 28(2-3), pp.119–124.

doi:[https://doi.org/10.1002/\(sici\)1097-4555\(199702\)28:2/3%3C119::aid-](https://doi.org/10.1002/(sici)1097-4555(199702)28:2/3%3C119::aid-jrs73%3E3.0.co;2-3)

[jrs73%3E3.0.co;2-3](https://doi.org/10.1002/(sici)1097-4555(199702)28:2/3%3C119::aid-jrs73%3E3.0.co;2-3).

Kneipp, J. (2022). Chapter 8 - SERS for Sensing and Imaging in Live Cells. *Principles and Clinical Diagnostic Applications of Surface-Enhanced Raman Spectroscopy*, [online] pp.303–325. doi:<https://doi.org/10.1016/b978-0-12-821121-2.00009-3>.

Koljenović, S., Bakker, T.C., Vincent, A., Kros, J.M. and Puppels, G.J. (2005). Detection of Meningioma in Dura Mater by Raman Spectroscopy. *Analytical Chemistry*, 77(24), pp.7958–7965. doi:<https://doi.org/10.1021/ac0512599>.

Krafft, C., Neudert, L., Simat, T. and Salzer, R. (2005). Near infrared Raman spectra of human brain lipids. *Spectrochimica Acta Part A: Molecular and Biomolecular Spectroscopy*, [online] 61(7), pp.1529–1535. doi:<https://doi.org/10.1016/j.saa.2004.11.017>.

Lau, D.P., Huang, Z., Lui, H., Man, C.S., Berean, K., Morrison, M.D. and Zeng, H. (2003). Raman spectroscopy for optical diagnosis in normal and cancerous tissue of the nasopharynx?preliminary findings. *Lasers in Surgery and Medicine*, [online] 32(3), pp.210–214. doi:<https://doi.org/10.1002/lsm.10084>.

Lawson, G., Ogwu, J. and Tanna, S. (2014). Analytical & Bioanalytical Techniques. *Analytical and Bioanalytical Techniques*, 5(214). doi:<https://doi.org/10.4172/2155-9872.1000214>.

Lawson, G., Ogwu, J. and Tanna, S. (2018). Quantitative screening of the pharmaceutical ingredient for the rapid identification of substandard and falsified

medicines using reflectance infrared spectroscopy. *PLOS ONE*, 13(8), p.e0202059. doi:<https://doi.org/10.1371/journal.pone.0202059>.

Lawson, L.S. and Rodriguez, J.D. (2016). Raman Barcode for Counterfeit Drug Product Detection. *Analytical Chemistry*, 88(9), pp.4706–4713. doi:<https://doi.org/10.1021/acs.analchem.5b04636>.

Lazar, G. (2001). Influence of the substrate-electrode applied bias voltage on the properties of sputtered a-C:H thin films. *Journal of Physics: Condensed Matter*, 13(13), pp.3011–3021. doi:<https://doi.org/10.1088/0953-8984/13/13/314>.

Le Ru, E.C. and Etchegoin, P.G. (2006). Rigorous justification of the $|E|^4$ enhancement factor in Surface Enhanced Raman Spectroscopy. *Chemical Physics Letters*, [online] 423(1-3), pp.63–66. doi:<https://doi.org/10.1016/j.cplett.2006.03.042>.

Leonard, J., Haddad, A., Green, O., Birke, R.L., Kubic, T., Kocak, A. and Lombardi, J.R. (2017). SERS, Raman, and DFT analyses of fentanyl and carfentanil: Toward detection of trace samples. *Journal of Raman Spectroscopy*, 48(10), pp.1323–1329. doi:<https://doi.org/10.1002/jrs.5220>.

Leopold, N. and Lendl, B. (2003). A New Method for Fast Preparation of Highly Surface-Enhanced Raman Scattering (SERS) Active Silver Colloids at Room Temperature by Reduction of Silver Nitrate with Hydroxylamine Hydrochloride. *The Journal of Physical Chemistry B*, [online] 107(24), pp.5723–5727. doi:<https://doi.org/10.1021/jp027460u>.

Li, H., Wurrey, C.J. and Thomas, G.J. (1992). Structural studies of viruses by laser Raman spectroscopy. Part XXXVI. Cysteine conformation and sulfhydryl interactions in proteins and viruses. 2. Normal coordinate analysis of the cysteine side chain in

model compounds. *Journal of the American Chemical Society*, [online] 114(19), pp.7463–7469. doi:<https://doi.org/10.1021/ja00045a019>.

Li, Y.-S. and Church, J.S. (2014). Raman spectroscopy in the analysis of food and pharmaceutical nanomaterials. *Journal of Food and Drug Analysis*, 22(1), pp.29–48. doi:<https://doi.org/10.1016/j.jfda.2014.01.003>.

Liu, G.-L. and Kazarian, S. (2022). Recent advances in studies of cultural heritage using ATR-FTIR spectroscopy and ATR-FTIR spectroscopic imaging. *The Analyst*, [online] 147, pp.1777–1797. doi:<https://doi.org/10.1039/d2an00005a>.

Liu, T., Tian, Y., Zheng, A. and Cui, C. (2022). Design Strategies for and Stability of mRNA–Lipid Nanoparticle COVID-19 Vaccines. *Polymers*, [online] 14(19), p.4195. doi:<https://doi.org/10.3390/polym14194195>.

Loethen, Y.L., Kauffman, J.F., Buhse, L.F. and Rodriguez, J.D. (2015). Rapid screening of anti-infective drug products for counterfeits using Raman spectral library-based correlation methods. *The Analyst*, 140(21), pp.7225–7233. doi:<https://doi.org/10.1039/c5an01679g>.

London School of Hygiene & Tropical Medicine (2015). *Fake malaria drugs not as common as previously reported* | LSHTM. [online] LSHTM. Available at: https://www.lshtm.ac.uk/newsevents/news/2015/fake_malaria_drugs_not_as_common_as_previously_reported.html [Accessed 26 Sep. 2024].

Lopes, R.P., Marques, P.M., Valero, R., Tomkinson, J. and Batista, E. (2012). Guanine: A Combined Study Using Vibrational Spectroscopy and Theoretical Methods. *Journal of Spectroscopy*, 27(5-6), pp.273–292. doi:<https://doi.org/10.1155/2012/168286>.

Lopez-Leon, S., Wegman-Ostrosky, T., Perelman, C., Sepulveda, R., Rebolledo, P.A., Cuapio, A. and Villapol, S. (2021). More than 50 long-term effects of COVID-19: a systematic review and meta-analysis. *Scientific Reports*, [online] 11(1), p.16144. doi:<https://doi.org/10.1038/s41598-021-95565-8>.

Lu, X., Liu, Q., Benavides-Montano, J.A., Nicola, A.V., Aston, D.E., Rasco, B.A. and Aguilar, H.C. (2013). Detection of Receptor-Induced Glycoprotein Conformational Changes on Enveloped Virions by Using Confocal Micro-Raman Spectroscopy. *Journal of Virology*, 87(6), pp.3130–3142. doi:<https://doi.org/10.1128/jvi.03220-12>.

Mackey, T.K., Cuomo, R., Guerra, C. and Liang, B.A. (2015). After counterfeit Avastin®—what have we learned and what can be done? *Nature Reviews Clinical Oncology*, [online] 12(5), pp.302–308. doi:<https://doi.org/10.1038/nrclinonc.2015.35>.

Macomber, R.S. (1998). *A complete introduction to modern NMR spectroscopy*. New York: Wiley.

Malini, R., Venkatakrishna, K., Kurien, J., M. Pai, K., Rao, L., Kartha, V.B. and Krishna, C.M. (2006). Discrimination of normal, inflammatory, premalignant, and malignant oral tissue: A Raman spectroscopy study. *Biopolymers*, 81(3), pp.179–193. doi:<https://doi.org/10.1002/bip.20398>.

Mata-Miranda, M.M., Martinez-Cuazitl, A., Gutierrez-Cortes, H., Cordero-Hernandez, L., Guerrero-Ruiz, M., Lopez-Reyes, A., Rodriguez-Baez, A. and Vazquez-Zapien, G.J. (2024). Analysis of the immune response using FTIR spectroscopy in mothers and their newborns with different vaccination schemes for COVID-19. *Scientific Reports*, 14(1). doi:<https://doi.org/10.1038/s41598-024-68340-8>.

Mateen, Z. (2021). *Covishield: WHO flags fake jabs in India, Africa*. [online] BBC News. Available at: <https://www.bbc.co.uk/news/world-asia-india-58253488> [Accessed 24 Sep. 2024].

Mathieu, E., Ritchie, H., Rodés-Guirao, L., Appel, C., Giattino, C., Hasell, J., Macdonald, B., Dattani, S., Beltekian, D., Ortiz-Ospina, E. and Roser, M. (2020) - Coronavirus Pandemic (COVID-19). Published online at OurWorldInData.org. Retrieved from: '<https://ourworldindata.org/coronavirus>' [Online Resource]

Matthäus, C., Bird, B., Miljković, M., Chernenko, T., Romeo, M. and Diem, M. (2008). Infrared and Raman Microscopy in Cell Biology. *Methods in cell biology*, [online] 89, pp.275–308. doi:[https://doi.org/10.1016/S0091-679X\(08\)00610-9](https://doi.org/10.1016/S0091-679X(08)00610-9).

McCreery, R.L. (2000). *Raman Spectroscopy for Chemical Analysis*. John Wiley & Sons. doi:<https://doi.org/10.1002/0471721646>.

Mitra, S. (2003). *Sample Preparation Techniques in Analytical Chemistry*. Hoboken, NJ, USA: John Wiley & Sons, Inc. doi:<https://doi.org/10.1002/0471457817>.

Mittal, M., Sharma, K. and Rathore, A. (2021). Checking counterfeiting of pharmaceutical products by attenuated total reflection mid-infrared spectroscopy. *Spectrochimica Acta Part A: Molecular and Biomolecular Spectroscopy*, [online] 255. doi:<https://doi.org/10.1016/j.saa.2021.119710>.

Mosca, S., Lin, Q., Stokes, R., Bharucha, T., Gangadharan, B., Clarke, R., Fernandez, L.G., Deats, M., Walsby-Tickle, J., Arman, B.Y., Chunekar, S.R., Patil, K.D., Gairola, S., Van Assche, K., Dunachie, S., Merchant, H.A., Kuwana, R., Maes, A., McCullagh, J. and Caillet, C. (2023). Innovative method for rapid detection of falsified COVID-19 vaccines through unopened vials using handheld Spatially Offset Raman

Spectroscopy (SORS). *Vaccine*, [online] 41(47), pp.6960–6968.
doi:<https://doi.org/10.1016/j.vaccine.2023.10.012>.

Mukherjee, D., Maskey, U., Ishak, A., Sarfraz, Z., Sarfraz, A. and Jaiswal, V. (2021). Fake COVID-19 Vaccination in India: an Emerging dilemma? *Postgraduate Medical Journal*, [online] 98(e2). doi:<https://doi.org/10.1136/postgradmedj-2021-141003>.

Müller, M., Torger, B., Bittrich, E., Kaul, E., Ionov, L., Uhlmann, P. and Stamm, M. (2014). In-situ ATR-FTIR for characterization of thin biorelated polymer films. *Thin Solid Films*, 556, pp.1–8. doi:<https://doi.org/10.1016/j.tsf.2013.12.025>.

Napolitano-Tabares, P.I., Negrín-Santamaría, I., Gutiérrez-Serpa, A. and Pino, V. (2021). Recent efforts to increase greenness in chromatography. *Current Opinion in Green and Sustainable Chemistry*, [online] 32, p.100536.
doi:<https://doi.org/10.1016/j.cogsc.2021.100536>.

Ndwandwe, D. and Wiysonge, C.S. (2021). COVID-19 Vaccines. *Current Opinion in Immunology*, [online] 71, pp.111–116. doi:<https://doi.org/10.1016/j.coi.2021.07.003>.

Newton, P.N., Fernández, F.M., Plançon, A., Mildenhall, D.C., Green, M.D., Ziyong, L., Christophel, E.M., Phanouvong, S., Howells, S., McIntosh, E., Laurin, P., Blum, N., Hampton, C.Y., Faure, K., Nyadong, L., Soong, C.W.R., Santoso, B., Zhiguang, W., Newton, J. and Palmer, K. (2008). A Collaborative Epidemiological Investigation into the Criminal Fake Artesunate Trade in South East Asia. *PLoS Medicine*, [online] 5(2), p.e32. doi:<https://doi.org/10.1371/journal.pmed.0050032>.

Ni, Fan., Sheng, Rongsheng. and Cotton, T.M. (1990). Flow-injection analysis and real-time detection of RNA bases by surface-enhanced Raman spectroscopy. *Analytical Chemistry*, 62(18), pp.1958–1963.
doi:<https://doi.org/10.1021/ac00217a012>.

Ochsenkühn, M.A., Jess, P.R.T., Stoquert, H., Dholakia, K. and Campbell, C.J. (2009). Nanoshells for Surface-Enhanced Raman Spectroscopy in Eukaryotic Cells: Cellular Response and Sensor Development. *ACS nano*, 3(11), pp.3613–3621. doi:<https://doi.org/10.1021/nn900681c>.

Okuonghae, H.O., Ighogboja, I.S., Lawson, J.O. and Nwana, E.J. (1992). Diethylene glycol poisoning in Nigerian children. *Annals of Tropical Paediatrics*, [online] 12(3), pp.235–238. doi:<https://doi.org/10.1080/02724936.1992.11747577>.

Orphanou, C.-M., Walton-Williams, L., Mountain, H. and Cassella, J. (2015). The detection and discrimination of human body fluids using ATR FT-IR spectroscopy. *Forensic Science International*, [online] 252, pp.10–16. doi:<https://doi.org/10.1016/j.forsciint.2015.04.020>.

Ortiz, R.S., Mariotti, K. de C., Fank, B., Limberger, R.P., Anzanello, M.J. and Mayorga, P. (2013). Counterfeit Cialis and Viagra fingerprinting by ATR-FTIR spectroscopy with chemometry: Can the same pharmaceutical powder mixture be used to falsify two medicines? *Forensic Science International*, 226(1-3), pp.282–289. doi:<https://doi.org/10.1016/j.forsciint.2013.01.043>.

Otto, C., van den Tweel, T.J.J., de Mul, F.F.M. and Greve, J. (1986). Surface-enhanced Raman spectroscopy of DNA bases. *Journal of Raman Spectroscopy*, 17(3), pp.289–298. doi:<https://doi.org/10.1002/jrs.1250170311>.

Ozawa, S., Evans, D.R., Bessias, S., Haynie, D.G., Yemeke, T.T., Laing, S.K. and Herrington, J.E. (2018). Prevalence and Estimated Economic Burden of Substandard and Falsified Medicines in Low- and Middle-Income Countries. *JAMA Network Open*, [online] 1(4), p.e181662. doi:<https://doi.org/10.1001/jamanetworkopen.2018.1662>.

Pavićević, A., Glumac, S., Sopta, J., Popović-Bijelić, A., Mojović, M. and Bacić, G. (2012). Raman microspectroscopy as a biomarking tool for in vitro diagnosis of cancer: a feasibility study. *Croatian Medical Journal*, [online] 53(6), pp.551–551. doi:<https://doi.org/10.3325/cmj.2012.53.551>.

PerkinElmer (2025). SpectrumTwo FTIR spectrometer. [online] www.perkinelmer.com. Available at: <https://www.perkinelmer.com/uk/product/spectrum-two-ft-ir-sp10-software-l160000a>.

Pham-Tuan, H., Kaskavelis, L., Daykin, C.A. and Janssen, H.-G. (2003). Method development in high-performance liquid chromatography for high-throughput profiling and metabonomic studies of biofluid samples. *Journal of Chromatography B*, 789(2), pp.283–301. doi:[https://doi.org/10.1016/s1570-0232\(03\)00077-1](https://doi.org/10.1016/s1570-0232(03)00077-1).

Pizzo, B., Pecoraro, E., Alves, A., Macchioni, N. and Rodrigues, J.C. (2015). Quantitative evaluation by attenuated total reflectance infrared (ATR-FTIR) spectroscopy of the chemical composition of decayed wood preserved in waterlogged conditions. *Talanta*, 131, pp.14–20. doi:<https://doi.org/10.1016/j.talanta.2014.07.062>.

Platek, S.F., Ranieri, N. and Batson, J. (2016). Applications of the FDA's Counterfeit Detection Device (CD3+) to the Examination of Suspect Counterfeit Pharmaceutical Tablets and Packaging. *Microscopy and Microanalysis*, 22(3), pp.1072–1073. doi:<https://doi.org/10.1017/s1431927616006206>.

Podstawka, E., Ozaki, Y. and Proniewicz, L.M. (2004). Part II: Surface-Enhanced Raman Spectroscopy Investigation of Methionine Containing Heterodipeptides Adsorbed on Colloidal Silver. *Applied Spectroscopy*, 58(5), pp.581–590. doi:<https://doi.org/10.1366/000370204774103417>.

Poole, C.F. (2003). Thin-layer chromatography: challenges and opportunities. *Journal of Chromatography A*, [online] 1000(1-2), pp.963–984. doi:[https://doi.org/10.1016/s0021-9673\(03\)00435-7](https://doi.org/10.1016/s0021-9673(03)00435-7).

Prestrelski, S.J., Tedeschi, N., Arakawa, T. and Carpenter, J.F. (1993). Dehydration-induced conformational transitions in proteins and their inhibition by stabilizers. *Biophysical Journal*, [online] 65(2), pp.661–671. doi:[https://doi.org/10.1016/s0006-3495\(93\)81120-2](https://doi.org/10.1016/s0006-3495(93)81120-2).

Ramer, G. and Lendl, B. (2013). Attenuated Total Reflection Fourier Transform Infrared Spectroscopy. In: *Encyclopedia of Analytical Chemistry*. John Wiley & Sons, Ltd. doi:<https://doi.org/10.1002/9780470027318.a9287>.

Raveendran, A.V., Jayadevan, R. and Sashidharan, S. (2021). Long COVID: an Overview. *Diabetes & Metabolic Syndrome: Clinical Research & Reviews*, [online] 15(3), pp.869–875. doi:<https://doi.org/10.1016/j.dsx.2021.04.007>.

Reuters (2021). China cracks fake COVID-19 vaccine ring, confiscates 3,000 doses: Xinhua. *Reuters*. [online] 2 Feb. Available at: <https://www.reuters.com/article/us-health-coronavirus-china-vaccine-idUSKBN2A2031/>.

Rimai, L., Cole, T., Parsons, J.L., Hickmott, J.T. and Carew, E.B. (1969). Studies of Raman Spectra of Water Solutions of Adenosine Tri-, Di-, and Monophosphate and Some Related Compounds. *Biophysical Journal*, 9(3), pp.320–329. doi:[https://doi.org/10.1016/s0006-3495\(69\)86389-7](https://doi.org/10.1016/s0006-3495(69)86389-7).

Risha, P.G., Msuya, Z., Clark, M., Johnson, K., Ndomondo-Sigonda, M. and Layloff, T. (2008). The use of Minilabs® to improve the testing capacity of regulatory authorities in resource limited settings: Tanzanian experience. *Health Policy*, [online] 87(2), pp.217–222. doi:<https://doi.org/10.1016/j.healthpol.2007.12.010>.

Robichaux Viehoever, A., Anderson, D., Jansen, D. and Mahadevan-Jansen, A. (2003). Organotypic Raft Cultures as an Effective In Vitro Tool for Understanding Raman Spectral Analysis of Tissue¶. *Photochemistry and Photobiology*, 78(5), p.517. doi:[https://doi.org/10.1562/0031-8655\(2003\)078%3C0517:orcaae%3E2.0.co;2](https://doi.org/10.1562/0031-8655(2003)078%3C0517:orcaae%3E2.0.co;2).

Roghayyeh Baghban, Abdolmajid Ghasemian and Mahmoodi, S. (2023). Nucleic acid-based vaccine platforms against the coronavirus disease 19 (COVID-19). *Archives of Microbiology*, 205(4). doi:<https://doi.org/10.1007/s00203-023-03480-5>.

Rule, G.S. and Hitchens, T.K. (2006). Fundamentals of Protein NMR Spectroscopy. *Focus on Structural Biology*, 5, pp.1–27. doi:https://doi.org/10.1007/1-4020-3500-4_1.

Ruokola, P., Dadu, E., Kazmertsuk, A., Häkkänen, H., Marjomäki, V. and Ihalainen, J.A. (2014). Raman Spectroscopic Signatures of Echovirus 1 Uncoating. *Journal of Virology*, 88(15), pp.8504–8513. doi:<https://doi.org/10.1128/jvi.03398-13>.

S. Kulkarni, R. and S. Palled, M. (2024). A Rapid, Sensitive and Cost-Effective RP-HPLC Method for Determination of Loxoprofen Sodium. *Research Journal of Pharmacy and Technology*, pp.2889–2894. doi:<https://doi.org/10.52711/0974-360x.2024.00453>.

Sackmann, M. and Materny, A. (2006). Surface enhanced Raman scattering (SERS)—a quantitative analytical tool? *Journal of Raman Spectroscopy*, 37(1-3), pp.305–310. doi:<https://doi.org/10.1002/jrs.1443>.

Schoenmaker, L., Witzigmann, D., Kulkarni, J.A., Verbeke, R., Kersten, G., Jiskoot, W. and Crommelin, D. (2021). mRNA-lipid nanoparticle COVID-19 vaccines: structure and stability. *International Journal of Pharmaceutics*, [online] 601(120586), p.120586. doi:<https://doi.org/10.1016/j.ijpharm.2021.120586>.

Severcan, F. and Haris, P.I. (2012). *Vibrational Spectroscopy in Diagnosis and Screening*. The Netherlands: IOS Press, pp.12–52.

Shan, F., Zhang, X.-Y., Fu, X.-C., Zhang, L.-J., Su, D., Wang, S.-J., Wu, J.-Y. and Zhang, T. (2017). Investigation of simultaneously existed Raman scattering enhancement and inhibiting fluorescence using surface modified gold nanostars as SERS probes. *Scientific Reports*, 7(1). doi:<https://doi.org/10.1038/s41598-017-07311-8>.

Sharma, B., Frontiera, R.R., Henry, A.-I., Ringe, E. and Van Duyne, R.P. (2012). SERS: Materials, applications, and the future. *Materials Today*, 15(1-2), pp.16–25. doi:[https://doi.org/10.1016/s1369-7021\(12\)70017-2](https://doi.org/10.1016/s1369-7021(12)70017-2).

Sharma, S., Chophi, R., Kaur, H. and Singh, R. (2019). Differentiation of Cosmetic Foundation Creams Using Attenuated Total Reflection Fourier-Transform Infrared Spectroscopy: A Rapid and NonDestructive Approach in Trace Evidence Analysis. *Journal of Forensic Sciences*, [online] 65(3), pp.751–761. doi:<https://doi.org/10.1111/1556-4029.14257>.

Sharma, S. and Singh, R. (2020). Detection of vaginal fluid stains on common substrates via ATR FT-IR spectroscopy. *International Journal of Legal Medicine*, 134(5), pp.1591–1602. doi:<https://doi.org/10.1007/s00414-020-02333-w>.

Sharma, V., Bhardwaj, S. and Kumar, R. (2019). On the spectroscopic investigation of Kohl stains via ATR-FTIR and multivariate analysis: Application in forensic trace evidence. *Vibrational Spectroscopy*, [online] 101, pp.81–91. doi:<https://doi.org/10.1016/j.vibspec.2019.02.006>.

Sheppard, N. (1972). Far Infrared Spectroscopy. *Physics Bulletin*, 23(6), pp.357–359. doi:<https://doi.org/10.1088/0031-9112/23/6/019>.

Sherma, J. and Fried, B. (2003). *Handbook of Thin-Layer Chromatography*. [online] Hoboken: Marcel Dekker Inc., pp.1–62. Available at: <https://books.google.co.uk/books?hl=en&lr=&id=Qc79DwAAQBAJ&oi=fnd&pg=PP1&dq=principles+of+thin+layer+chromatography&ots=68AQ6JxZvy&sig=zsvbWLqzBXWh598c2zQIkHSjmHA#v=onepage&q=principles%20of%20thin%20layer%20chromatography&f=false>.

Shetty, G., Kendall, C., Shepherd, N., Stone, N. and Barr, H. (2006). Raman spectroscopy: elucidation of biochemical changes in carcinogenesis of oesophagus. *British Journal of Cancer*, 94(10), pp.1460–1464. doi:<https://doi.org/10.1038/sj.bjc.6603102>.

Silge, A., Bocklitz, T., Becker, B., Matheis, W., Popp, J. and Bekeredjian-Ding, I. (2018). Raman spectroscopy-based identification of toxoid vaccine products. *npj Vaccines*, 3(1). doi:<https://doi.org/10.1038/s41541-018-0088-y>.

Silge, A., Weber, K., Cialla-May, D., Müller-Böttcher, L., Fischer, D. and Popp, J. (2022). Trends in pharmaceutical analysis and quality control by modern Raman spectroscopic techniques. *TrAC Trends in Analytical Chemistry*, 153, p.116623. doi:<https://doi.org/10.1016/j.trac.2022.116623>.

Smith, B.J. (2011). *Fundamentals of Fourier Transform Infrared Spectroscopy*. 2nd ed. [online] CRC Press eBooks. Informa. doi:<https://doi.org/10.1201/b10777>.

Smulko, J.M., Dingari, N.C., Soares, J.S. and Barman, I. (2014). Anatomy of noise in quantitative biological Raman spectroscopy. *Bioanalysis*, 6(3), pp.411–421. doi:<https://doi.org/10.4155/bio.13.337>.

St. Croix, C.M., Shand, S.H. and Watkins, S.C. (2005). Confocal microscopy: comparisons, applications, and problems. *BioTechniques*, [online] 39(6S), pp.S2–S5. doi:<https://doi.org/10.2144/000112089>.

Stone, N., Kendall, C., Shepherd, N., Crow, P. and Barr, H. (2002). Near-infrared Raman spectroscopy for the classification of epithelial pre-cancers and cancers. *Journal of Raman Spectroscopy*, 33(7), pp.564–573. doi:<https://doi.org/10.1002/jrs.882>.

Stone, N., Kendall, C., Smith, J., Crow, P. and Barr, H. (2004). Raman spectroscopy for identification of epithelial cancers. *Faraday Discussions*, [online] 126. doi:<https://doi.org/10.1039/b304992b>.

Stuart, B.H. (2004a). *Infrared Spectroscopy: Fundamentals and Applications* Stuart/*Infrared Spectroscopy: Fundamentals and Applications*. [online] Chichester, UK John Wiley & Sons, Ltd, pp.1–13. Available at: <https://onlinelibrary.wiley.com/doi/book/10.1002/0470011149>.

Stuart, B.H. (2004b). *Infrared Spectroscopy: Fundamentals and Applications* Stuart/*Infrared Spectroscopy: Fundamentals and Applications*. [online] Chichester, UK John Wiley & Sons, Ltd, pp.71–186. Available at: <https://onlinelibrary.wiley.com/doi/book/10.1002/0470011149>.

Takeuchi, H., Nemoto, Y. and Harada, I. (1990). Environments and conformations of tryptophan side chains of gramicidin A in phospholipid bilayers studied by Raman spectroscopy. *Biochemistry*, 29(6), pp.1572–1579. doi:<https://doi.org/10.1021/bi00458a031>.

Tantra, R., Brown, R.J.C. and Milton, M.J.T. (2007). Strategy to improve the reproducibility of colloidal SERS. *Journal of Raman Spectroscopy*, [online] 38(11), pp.1469–1479. doi:<https://doi.org/10.1002/jrs.1797>.

Teh, S.K., Zheng, W., Ho, K.Y., Teh, M., Yeoh, K.G. and Huang, Z. (2008). Diagnostic potential of near-infrared Raman spectroscopy in the stomach: differentiating dysplasia from normal tissue. *British Journal of Cancer*, 98(2), pp.457–465. doi:<https://doi.org/10.1038/sj.bjc.6604176>.

The Human Medicines Regulations (2013). *The Human Medicines (Amendment) Regulations 2013*. [online] Available at: <https://www.legislation.gov.uk/ukxi/2013/1855/made>.

Thomas, G.J. (1970). Raman spectral studies of nucleic acids. *Biochimica et Biophysica Acta (BBA) - Nucleic Acids and Protein Synthesis*, [online] 213(2), pp.417–423. doi:[https://doi.org/10.1016/0005-2787\(70\)90049-3](https://doi.org/10.1016/0005-2787(70)90049-3).

Thompson, C.A. (2003). Counterfeit drugs arise from various sources. *American Journal of Health-System Pharmacy*, [online] 60(15), pp.1506–1511. doi:<https://doi.org/10.1093/ajhp/60.15.1506>.

Tiernan, H., Byrne, B. and Kazarian, S.G. (2020). ATR-FTIR Spectroscopy and Spectroscopic Imaging for the analysis of biopharmaceuticals. *Spectrochimica Acta Part A: Molecular and Biomolecular Spectroscopy*, [online] 241. doi:<https://doi.org/10.1016/j.saa.2020.118636>.

Tondepu, C., Toth, R., Navin, C.V., Lawson, L.S. and Rodriguez, J.D. (2017). Screening of unapproved drugs using portable Raman spectroscopy. *Analytica Chimica Acta*, 973, pp.75–81. doi:<https://doi.org/10.1016/j.aca.2017.04.016>.

Tuma, R. (2005). Raman spectroscopy of proteins: from peptides to large assemblies. *Journal of Raman Spectroscopy*, [online] 36(4), pp.307–319. doi:<https://doi.org/10.1002/jrs.1323>.

Tuma, R. and Thomas, G.J. (2001). Raman Spectroscopy of Viruses. *Handbook of Vibrational Spectroscopy*. doi:<https://doi.org/10.1002/0470027320.s8207>.

Turrell, G. and Corset, J. (1996). *Raman Microscopy*. Academic Press, pp.27–48.

U.S Government Accountability Office (2022). *Food and Drug Administration: Response to Heparin Contamination Helped Protect Public Health; Controls That Were Needed for Working With External Entities Were Recently Added*. [online] Gao.gov. Available at: [https://www.gao.gov/products/gao-11-95#:~:text=This%20report%20examines%20\(1\)%20how%20FDA%20prevented%20additional](https://www.gao.gov/products/gao-11-95#:~:text=This%20report%20examines%20(1)%20how%20FDA%20prevented%20additional) [Accessed 24 Sep. 2024].

Uddin, M.N. and Roni, M.A. (2021). Challenges of Storage and Stability of mRNA-Based COVID-19 Vaccines. *Vaccines*, [online] 9(9), p.1033. doi:<https://doi.org/10.3390/vaccines9091033>.

United Nations Office On Drugs And Crime (UNODC) (2010). *The globalization of crime : a transnational organized crime threat assessment*. [online] Vienna: United Nations Office On Drugs And Crime. Available at: https://www.unodc.org/documents/data-and-analysis/tocta/TOCTA_Report_2010_low_res.pdf.

Vazquez-Zapien, G.J., Martinez-Cuazitl, A., Sanchez-Brito, M., Delgado-Macuil, R.J., Atriano-Colorado, C., Garibay-Gonzalez, F., Sanchez-Monroy, V., Lopez-Reyes, A. and Mata-Miranda, M.M. (2022). Comparison of the Immune Response in Vaccinated

People Positive and Negative to SARS-CoV-2 Employing FTIR Spectroscopy. *Cells*, 11(23), p.3884. doi:<https://doi.org/10.3390/cells11233884>.

W John Wolfgang (2005). Raman Microscopy as an Aid in Failure Analysis — Examples From the Lab. *Microscopy Today*, [online] 13(3), pp.54–57. doi:<https://doi.org/10.1017/s155192950005166x>.

Wang, W. (2000). Lyophilization and development of solid protein pharmaceuticals. *International Journal of Pharmaceutics*, 203(1-2), pp.1–60. doi:[https://doi.org/10.1016/s0378-5173\(00\)00423-3](https://doi.org/10.1016/s0378-5173(00)00423-3).

Watson, M., Al-Jumeily, D., Birkett, J., Khan, I. and Assi, S. (2023). *Exploring the authentication of COVID-19 vaccines using Surface-enhanced handheld Raman spectroscopy (SERS) equipped with orbital Raster scattering and machine learning*. [online] IEEE Xplore. doi:<https://doi.org/10.1109/DeSE58274.2023.10100028>.

Williamson, R., Raeva, A. and Almirall, J.R. (2016). Characterization of Printing Inks Using DART-Q-TOF-MS and Attenuated Total Reflectance (ATR) FTIR. *Journal of Forensic Sciences*, [online] 61(3), pp.706–714. doi:<https://doi.org/10.1111/1556-4029.13107>.

Wojciechowski, C., Dupuy, N., Ta, C.D., Huvenne, J.P. and Legrand, P. (1998). Quantitative analysis of water-soluble vitamins by ATR-FTIR spectroscopy. *Food Chemistry*, 63(1), pp.133–140. doi:[https://doi.org/10.1016/s0308-8146\(97\)00138-6](https://doi.org/10.1016/s0308-8146(97)00138-6).

World Health Organisation (2017). *WHO Global Surveillance and Monitoring System for Substandard and Falsified Medical Products*. [online] Available at: <https://iris.who.int/bitstream/handle/10665/326708/9789241513425-eng.pdf>.

World Health Organisation (2024). *COVID-19 Cases | WHO COVID-19 Dashboard*. [online] World Health Organisation. Available at: <https://data.who.int/dashboards/covid19/cases?n=c>.

World Health Organisation (WHO) (2021a). *Medical Product Alert N°5/2021: Falsified COVISHIELD vaccine (Update)*. [online] Who.int. Available at: <https://www.who.int/news/item/31-08-2021-medical-product-alert-n-5-2021-falsified-covishield-vaccine> [Accessed 24 Sep. 2024].

World Health Organisation (WHO) (2021b). *Medical Product Alert N°6/2021: Falsified Pfizer-BioNTech COVID-19 Vaccine*. [online] www.who.int. Available at: <https://www.who.int/news/item/04-11-2021-medical-product-alert-n-6-2021-falsified-pfizer-biontech-covid-19-vaccine>.

World Health Organisation (WHO) (2021c). *Medical Product Alert N°7/2021: Falsified COVID-19 Vaccine AstraZeneca*. [online] www.who.int. Available at: <https://www.who.int/news/item/04-11-2021-medical-product-alert-n-7-2021-falsified-covid-19-vaccine-astrazeneca>.

World Health Organisation (WHO) (2024). *COVID-19 cases | WHO COVID-19 dashboard*. [online] Datadot. Available at: <https://data.who.int/dashboards/covid19/cases?n=o>.

World Health Organization (2018). *Substandard and Falsified Medical Products*. [online] Who.int. Available at: <https://www.who.int/news-room/fact-sheets/detail/substandard-and-falsified-medical-products>.

World Intellectual Property Organisation (WIPO) (2024). *WIPO IP Facts and Figures 2023*. [online] WIPO. Available at: <https://www.wipo.int/edocs/pubdocs/en/wipo-pub-943-2023-en-wipo-ip-facts-and-figures-2023.pdf>.

Xu, Y. and Lu, C. (2005). Raman spectroscopic study on structure of human immunodeficiency virus (HIV) and hypericin-induced photosensitive damage of HIV. *Science in China Series C: Life Sciences*, [online] 48(2), pp.117–132. doi:<https://doi.org/10.1007/bf02879664>.

Yacouby, R. and Axman, D. (2020). *Probabilistic Extension of Precision, Recall, and F1 Score for More Thorough Evaluation of Classification Models*. [online] ACLWeb. doi:<https://doi.org/10.18653/v1/2020.eval4nlp-1.9>.

Yamagaki, T. and Yamazaki, T. (2020). Troubleshooting Carry-Over in the LC-MS Analysis of Biomolecules: The Case of Neuropeptide Y. *Mass Spectrometry*, 8(2), pp.S0083–S0083. doi:<https://doi.org/10.5702/massspectrometry.s0083>.

Yeung, S., Lawford, H.L.S., Taberner, P., Nguon, C., van Wyk, A., Malik, N., DeSousa, M., Rada, O., Boravann, M., Dwivedi, P., Hostetler, D.M., Swamidoss, I., Green, M.D., Fernandez, F.M. and Kaur, H. (2015). Quality of Antimalarials at the Epicenter of Antimalarial Drug Resistance: Results from an Overt and Mystery Client Survey in Cambodia. *The American Journal of Tropical Medicine and Hygiene*, [online] 92(6_Suppl), pp.39–50. doi:<https://doi.org/10.4269/ajtmh.14-0391>.

Ying, X. (2019). An Overview of Overfitting and its Solutions. *Journal of Physics: Conference Series*, 1168(2), p.22. doi:<https://doi.org/10.1088/1742-6596/1168/2/022022>.

Young, D. (2004). Counterfeit drugs lawsuit points finger at wholesaler, pharmacy. *American Journal of Health-System Pharmacy*, 61(19), pp.1978–1978. doi:<https://doi.org/10.1093/ajhp/61.19.1978>.

Yu, N.-T., Jo, B.H. and D.C. O'Shea (1973). Laser Raman scattering of cobramine B, a basic protein from cobra venom. *Archives of Biochemistry and Biophysics*, 156(1), pp.71–76. doi:[https://doi.org/10.1016/0003-9861\(73\)90342-1](https://doi.org/10.1016/0003-9861(73)90342-1).

Zhang, K., Guo, Q., Zhao, Q., Wang, F., Wang, H., Zhi, J. and Shan, C. (2021). Photosensitizer Functionalized Nanodiamonds for Raman Imaging and Photodynamic Therapy of Cancer Cells. *Langmuir*, 37(14), pp.4308–4315. doi:<https://doi.org/10.1021/acs.langmuir.1c00292>.

Zhu, G., Zhu, X., Fan, Q. and Wan, X. (2011). Raman spectra of amino acids and their aqueous solutions. *Spectrochimica Acta Part A: Molecular and Biomolecular Spectroscopy*, [online] 78(3), pp.1187–1195. doi:<https://doi.org/10.1016/j.saa.2010.12.079>.

Zhu, T., Chen, X. and Qin, J. (2011). Research progress on mid-IR nonlinear optical crystals with high laser damage threshold in China. *Frontiers of Chemistry in China*, 6(1), pp.1–8. doi:<https://doi.org/10.1007/s11458-011-0224-y>.

Appendices

Appendix I. Details of Covid-19 vaccine samples obtained for the study (manufacturer redacted)

Sample number	Label claim	Expiry	Form	Notes
LJMUCV1	Brand 2	30/08/2021	white liquid	suspension in 0.9% sodium chloride
LJMUCV2	Brand 2	8/30/2021	white liquid	suspension in 0.9% sodium chloride
LJMUCV3	Brand 2	8/30/2021	white liquid	suspension in 0.9% sodium chloride
LJMUCV4	Brand 2	8/30/2021	white liquid	suspension in 0.9% sodium chloride
LJMUCV5	Brand 2	10/30/2021	white liquid	suspension in 0.9% sodium chloride

LJMUCV6	Brand 2	8/30/2021	white liquid	suspension in 0.9% sodium chloride
LJMUCV7	Brand 2	8/30/2021	white liquid	suspension in 0.9% sodium chloride
LJMUCV8	Brand 2	8/30/2021	white liquid	suspension in 0.9% sodium chloride
LJMUCV9	Brand 2	8/30/2021	white liquid	suspension in 0.9% sodium chloride
LJMUCV10	Brand 2	8/30/2021	white liquid	suspension in 0.9% sodium chloride
LJMUCV11	Brand 2	8/30/2021	white liquid	suspension in 0.9% sodium chloride
LJMUCV12	Brand 2	8/30/2021	white liquid	suspension in 0.9% sodium chloride

LJMUCV13	Brand 2	10/30/2021	white liquid	suspension in 0.9% sodium chloride
LJMUCV14	Brand 2	8/30/2021	white liquid	suspension in 0.9% sodium chloride
LJMUCV15	Brand 2	8/30/2021	white liquid	suspension in 0.9% sodium chloride
LJMUCV16	Brand 2	10/30/2021	white liquid	suspension in 0.9% sodium chloride
LJMUCV17	Brand 2	10/30/2021	white liquid	suspension in 0.9% sodium chloride
LJMUCV18	Brand 2	10/30/2021	white liquid	suspension in 0.9% sodium chloride
LJMUCV19	Brand 2	10/30/2021	white liquid	suspension in 0.9% sodium chloride

LJMUCV20	Brand 2	10/30/2021	white liquid	suspension in 0.9% sodium chloride
LJMUCV21	Brand 2	10/30/2021	white liquid	suspension in 0.9% sodium chloride
LJMUCV22	Brand 2	8/30/2021	white liquid	suspension in 0.9% sodium chloride
LJMUCV23	Brand 2	8/30/2021	white liquid	suspension in 0.9% sodium chloride
LJMUCV24	Brand 2	8/30/2021	white liquid	suspension in 0.9% sodium chloride
LJMUCV25	Brand 2	10/30/2021	white liquid	suspension in 0.9% sodium chloride
LJMUCV26	Brand 2	8/30/2021	white liquid	suspension in 0.9% sodium chloride

LJMUCV27	Brand 2	8/30/2021	white liquid	suspension in 0.9% sodium chloride
LJMUCV28	Brand 2	10/30/2021	white liquid	suspension in 0.9% sodium chloride
LJMUCV29	Brand 2	8/30/2021	white liquid	suspension in 0.9% sodium chloride
LJMUCV30	Brand 2	10/30/2021	white liquid	suspension in 0.9% sodium chloride
LJMUCV31	Brand 2	10/30/2021	white liquid	suspension in 0.9% sodium chloride
LJMUCV32	Brand 2	10/30/2021	white liquid	suspension in 0.9% sodium chloride
LJMUCV33	Brand 2	10/30/2021	white liquid	suspension in 0.9% sodium chloride

LJMUCV34	Brand 2	8/30/2021	white liquid	suspension in 0.9% sodium chloride
LJMUCV35	Brand 2	8/30/2021	white liquid	suspension in 0.9% sodium chloride
LJMUCV36	Brand 2	10/30/2021	white liquid	suspension in 0.9% sodium chloride
LJMUCV37	Brand 2	10/30/2021	white liquid	suspension in 0.9% sodium chloride
LJMUCV38	Brand 2	10/30/2021	white liquid	suspension in 0.9% sodium chloride
LJMUCV39	Brand 2	8/30/2021	white liquid	suspension in 0.9% sodium chloride
LJMUCV40	Brand 2	8/30/2021	white liquid	suspension in 0.9% sodium chloride

LJMUCV41	Brand 2	8/30/2021	white liquid	suspension in 0.9% sodium chloride
LJMUCV42	Brand 2	10/30/2021	white liquid	suspension in 0.9% sodium chloride
LJMUCV43	Brand 2	8/30/2021	white liquid	suspension in 0.9% sodium chloride
LJMUCV44	Brand 2	8/30/2021	white liquid	suspension in 0.9% sodium chloride
LJMUCV45	Brand 2	8/30/2021	white liquid	suspension in 0.9% sodium chloride
LJMUCV46	Brand 2	9/30/2021	white liquid	suspension in 0.9% sodium chloride
LJMUCV47	Brand 2	8/30/2021	white liquid	suspension in 0.9% sodium chloride

LJMUCV48	Brand 2	8/30/2021	white liquid	suspension in 0.9% sodium chloride
LJMUCV49	Brand 2	10/30/2021	white liquid	suspension in 0.9% sodium chloride
LJMUCV50	Brand 2	9/30/2021	white liquid	suspension in 0.9% sodium chloride
LJMUCV51	Brand 2	10/30/2021	white liquid	suspension in 0.9% sodium chloride
LJMUCV52	Brand 2	8/30/2021	white liquid	suspension in 0.9% sodium chloride
LJMUCV53	Brand 2	8/30/2021	white liquid	suspension in 0.9% sodium chloride
LJMUCV54	Brand 2	8/30/2021	white liquid	suspension in 0.9% sodium chloride

LJMUCV55	Brand 2	8/30/2021	white liquid	suspension in 0.9% sodium chloride
LJMUCV56	Brand 2	9/30/2021	white liquid	suspension in 0.9% sodium chloride
LJMUCV57	Brand 2	8/30/2021	white liquid	suspension in 0.9% sodium chloride
LJMUCV58	Brand 2	8/30/2021	white liquid	suspension in 0.9% sodium chloride
LJMUCV59	Brand 2	10/30/2021	white liquid	suspension in 0.9% sodium chloride
LJMUCV60	Brand 2	8/30/2021	white liquid	suspension in 0.9% sodium chloride
LJMUCV61	Brand 2	10/30/2021	white liquid	suspension in 0.9% sodium chloride

LJMUCV62	Brand 2	10/30/2021	white liquid	suspension in 0.9% sodium chloride
LJMUCV63	Brand 2	8/30/2021	white liquid	suspension in 0.9% sodium chloride
LJMUCV64	Brand 2	10/30/2021	white liquid	suspension in 0.9% sodium chloride
LJMUCV65	Brand 2	10/30/2021	white liquid	suspension in 0.9% sodium chloride
LJMUCV66	Brand 2	8/30/2021	white liquid	suspension in 0.9% sodium chloride
LJMUCV67	Brand 2	9/30/2021	white liquid	suspension in 0.9% sodium chloride
LJMUCV68	Brand 2	8/30/2021	white liquid	suspension in 0.9% sodium chloride

LJMUCV69	Brand 2	10/30/2021	white liquid	suspension in 0.9% sodium chloride
LJMUCV70	Brand 2	10/30/2021	white liquid	suspension in 0.9% sodium chloride
LJMUCV71	Brand 2	10/30/2021	white liquid	suspension in 0.9% sodium chloride
LJMUCV72	Brand 2	10/30/2021	white liquid	suspension in 0.9% sodium chloride
LJMUCV73	Brand 2	10/30/2021	white liquid	suspension in 0.9% sodium chloride
LJMUCV74	Brand 2	8/30/2021	white liquid	suspension in 0.9% sodium chloride
LJMUCV75	Brand 2	10/30/2021	white liquid	suspension in 0.9% sodium chloride

LJMUCV76	Brand 2	8/30/2021	white liquid	suspension in 0.9% sodium chloride
LJMUCV77	Brand 2	8/30/2021	white liquid	suspension in 0.9% sodium chloride
LJMUCV78	Brand 2	8/30/2021	white liquid	suspension in 0.9% sodium chloride
LJMUCV79	Brand 2	8/30/2021	white liquid	suspension in 0.9% sodium chloride
LJMUCV80	Brand 2	10/30/2021	white liquid	suspension in 0.9% sodium chloride
LJMUCV81	Brand 2	8/30/2021	white liquid	suspension in 0.9% sodium chloride
LJMUCV82	Brand 2	9/30/2021	white liquid	suspension in 0.9% sodium chloride

LJMUCV83	Brand 2	9/30/2021	white liquid	suspension in 0.9% sodium chloride
LJMUCV84	Brand 2	10/30/2021	white liquid	suspension in 0.9% sodium chloride
LJMUCV85	Brand 2	10/30/2021	white liquid	suspension in 0.9% sodium chloride
LJMUCV86	Brand 2	10/30/2021	white liquid	suspension in 0.9% sodium chloride
LJMUCV87	Brand 2	10/30/2021	white liquid	suspension in 0.9% sodium chloride
LJMUCV88	Brand 2	10/30/2021	white liquid	suspension in 0.9% sodium chloride
LJMUCV89	Brand 2	9/30/2021	white liquid	suspension in 0.9% sodium chloride

LJMUCV90	Brand 2	8/30/2021	white liquid	suspension in 0.9% sodium chloride
LJMUCV91	Brand 2	10/30/2021	white liquid	suspension in 0.9% sodium chloride
LJMUCV92	Brand 2	8/30/2021	white liquid	suspension in 0.9% sodium chloride
LJMUCV93	Brand 2	10/30/2021	white liquid	suspension in 0.9% sodium chloride
LJMUCV94	Brand 2	8/30/2021	white liquid	suspension in 0.9% sodium chloride
LJMUCV95	Brand 2	8/30/2021	white liquid	suspension in 0.9% sodium chloride
LJMUCV96	Brand 2	10/30/2021	white liquid	suspension in 0.9% sodium chloride

LJMUCV97	Brand 2	8/30/2021	white liquid	suspension in 0.9% sodium chloride
LJMUCV98	Brand 2	9/30/2021	white liquid	suspension in 0.9% sodium chloride
LJMUCV99	Brand 2	8/30/2021	white liquid	suspension in 0.9% sodium chloride
LJMUCV100	Brand 2	10/30/2021	white liquid	suspension in 0.9% sodium chloride
LJMUCV101	Brand 2	10/30/2021	white liquid	suspension in 0.9% sodium chloride
LJMUCV102	Brand 2	8/30/2021	white liquid	suspension in 0.9% sodium chloride
LJMUCV103	Brand 2	9/30/2021	white liquid	suspension in 0.9% sodium chloride

LJMUCV104	Brand 2	10/30/2021	white liquid	suspension in 0.9% sodium chloride
LJMUCV105	Brand 2	10/30/2021	white liquid	suspension in 0.9% sodium chloride
LJMUCV106	Brand 2	10/30/2021	white liquid	suspension in 0.9% sodium chloride
LJMUCV107	Brand 2	8/30/2021	white liquid	suspension in 0.9% sodium chloride
LJMUCV108	Brand 2	10/30/2021	white liquid	suspension in 0.9% sodium chloride
LJMUCV109	Brand 2	9/30/2021	white liquid	suspension in 0.9% sodium chloride
LJMUCV110	Brand 2	10/30/2021	white liquid	suspension in 0.9% sodium chloride

LJMUCV111	Brand 2	10/30/2021	white liquid	suspension in 0.9% sodium chloride
LJMUCV112	Brand 2	8/30/2021	white liquid	suspension in 0.9% sodium chloride
LJMUCV113	Brand 2	10/30/2021	white liquid	suspension in 0.9% sodium chloride
LJMUCV114	Brand 2	10/30/2021	white liquid	suspension in 0.9% sodium chloride
LJMUCV115	Brand 2	8/30/2021	white liquid	suspension in 0.9% sodium chloride
LJMUCV116	Brand 2	10/30/2021	white liquid	suspension in 0.9% sodium chloride
LJMUCV117	Brand 2	10/30/2021	white liquid	suspension in 0.9% sodium chloride

LJMUCV118	Brand 2	8/30/2021	white liquid	suspension in 0.9% sodium chloride
LJMUCV119	Brand 2	8/30/2021	white liquid	suspension in 0.9% sodium chloride
LJMUCV120	Brand 2	8/30/2021	white liquid	suspension in 0.9% sodium chloride
LJMUCV121	Brand 2	9/30/2021	white liquid	suspension in 0.9% sodium chloride
LJMUCV122	Brand 2	9/30/2021	white liquid	suspension in 0.9% sodium chloride
LJMUCV123	Brand 2	9/30/2021	white liquid	suspension in 0.9% sodium chloride
LJMUCV124	Brand 2	9/30/2021	white liquid	suspension in 0.9% sodium chloride

LJMUCV125	Brand 2	9/30/2021	white liquid	suspension in 0.9% sodium chloride
LJMUCV126	Brand 2	9/30/2021	white liquid	suspension in 0.9% sodium chloride
LJMUCV127	Brand 2	9/30/2021	white liquid	suspension in 0.9% sodium chloride
LJMUCV128	Brand 2	9/30/2021	white liquid	suspension in 0.9% sodium chloride
LJMUCV129	Brand 2	9/30/2021	white liquid	suspension in 0.9% sodium chloride
LJMUCV130	Brand 2	9/30/2021	white liquid	suspension in 0.9% sodium chloride
LJMUCV131	Brand 2	9/30/2021	white liquid	suspension in 0.9% sodium chloride

LJMUCV132	Brand 2	9/30/2021	white liquid	suspension in 0.9% sodium chloride
LJMUCV133	Brand 2	9/30/2021	white liquid	suspension in 0.9% sodium chloride
LJMUCV134	Brand 2	9/30/2021	white liquid	suspension in 0.9% sodium chloride
LJMUCV135	Brand 2	9/30/2021	white liquid	suspension in 0.9% sodium chloride
LJMUCV136	Brand 2	9/30/2021	white liquid	suspension in 0.9% sodium chloride
LJMUCV137	Brand 2	9/30/2021	white liquid	suspension in 0.9% sodium chloride
LJMUCV138	Brand 2	9/30/2021	white liquid	suspension in 0.9% sodium chloride

LJMUCV139	Brand 2	9/30/2021	white liquid	suspension in 0.9% sodium chloride
LJMUCV140	Brand 2	9/30/2021	white liquid	suspension in 0.9% sodium chloride
LJMUCV141	Brand 2	9/30/2021	white liquid	suspension in 0.9% sodium chloride
LJMUCV142	Brand 2	9/30/2021	white liquid	suspension in 0.9% sodium chloride
LJMUCV143	Brand 2	10/30/2021	white liquid	suspension in 0.9% sodium chloride
LJMUCV144	Brand 2	9/30/2021	white liquid	suspension in 0.9% sodium chloride
LJMUCV145	Brand 2	10/30/2021	white liquid	suspension in 0.9% sodium chloride

LJMUCV146	Brand 2	9/30/2021	white liquid	suspension in 0.9% sodium chloride
LJMUCV147	Brand 2	9/30/2021	white liquid	suspension in 0.9% sodium chloride
LJMUCV148	Brand 2	9/30/2021	white liquid	suspension in 0.9% sodium chloride
LJMUCV149	Brand 2	9/30/2021	white liquid	suspension in 0.9% sodium chloride
LJMUCV150	Brand 2	9/30/2021	white liquid	suspension in 0.9% sodium chloride
LJMUCV151	Brand 2	9/30/2021	white liquid	suspension in 0.9% sodium chloride
LJMUCV152	Brand 2	9/30/2021	white liquid	suspension in 0.9% sodium chloride

LJMUCV153	Brand 2	9/30/2021	white liquid	suspension in 0.9% sodium chloride
LJMUCV154	Brand 2	9/30/2021	white liquid	suspension in 0.9% sodium chloride
LJMUCV155	Brand 2	9/30/2021	white liquid	suspension in 0.9% sodium chloride
LJMUCV156	Brand 2	9/30/2021	white liquid	suspension in 0.9% sodium chloride
LJMUCV157	Brand 2	9/30/2021	white liquid	suspension in 0.9% sodium chloride
LJMUCV158	Brand 2	9/30/2021	white liquid	suspension in 0.9% sodium chloride
LJMUCV159	Brand 2	9/30/2021	white liquid	suspension in 0.9% sodium chloride

LJMUCV160	Brand 2	9/30/2021	white liquid	suspension in 0.9% sodium chloride
LJMUCV161	Brand 2	9/30/2021	white liquid	suspension in 0.9% sodium chloride
LJMUCV162	Brand 2	9/30/2021	white liquid	suspension in 0.9% sodium chloride
LJMUCV163	Brand 2	9/30/2021	white liquid	suspension in 0.9% sodium chloride
LJMUCV164	Brand 2	8/30/2021	white liquid	suspension in 0.9% sodium chloride
LJMUCV165	Brand 2	9/30/2021	white liquid	suspension in 0.9% sodium chloride
LJMUCV166	Brand 2	9/30/2021	white liquid	suspension in 0.9% sodium chloride

LJMUCV167	Brand 2	9/30/2021	white liquid	suspension in 0.9% sodium chloride
LJMUCV168	Brand 2	9/30/2021	white liquid	suspension in 0.9% sodium chloride
LJMUCV169	Brand 2	9/30/2021	white liquid	suspension in 0.9% sodium chloride
LJMUCV170	Brand 2	9/30/2021	white liquid	suspension in 0.9% sodium chloride
LJMUCV171	Brand 2	9/30/2021	white liquid	suspension in 0.9% sodium chloride
LJMUCV172	Brand 2	10/30/2021	white liquid	suspension in 0.9% sodium chloride
LJMUCV173	Brand 2	9/30/2021	white liquid	suspension in 0.9% sodium chloride

LJMUCV174	Brand 2	9/30/2021	white liquid	suspension in 0.9% sodium chloride
LJMUCV175	Brand 2	9/30/2021	white liquid	suspension in 0.9% sodium chloride
LJMUCV176	Brand 2	9/30/2021	white liquid	suspension in 0.9% sodium chloride
LJMUCV177	Brand 2	8/30/2021	white liquid	suspension in 0.9% sodium chloride
LJMUCV178	Brand 2	9/30/2021	white liquid	suspension in 0.9% sodium chloride
LJMUCV179	Brand 2	9/30/2021	white liquid	suspension in 0.9% sodium chloride
LJMUCV180	Brand 2	9/30/2021	white liquid	suspension in 0.9% sodium chloride

LJMUCV181	Brand 1	7/30/2021	transparent liquid	recombinant
LJMUCV182	Brand 1	6/30/2021	transparent liquid	recombinant
LJMUCV183	Brand 1	6/30/2021	transparent liquid	recombinant
LJMUCV184	Brand 1	6/30/2021	transparent liquid	recombinant
LJMUCV185	Brand 1	6/30/2021	transparent liquid	recombinant
LJMUCV186	Brand 1	6/30/2021	transparent liquid	recombinant
LJMUCV187	Brand 1	8/30/2021	transparent liquid	recombinant

LJMUCV188	Brand 1	10/30/2021	transparent liquid	recombinant
LJMUCV189	Brand 1	9/30/2021	transparent liquid	recombinant
LJMUCV190	Brand 2	9/30/2021	white liquid	suspension in 0.9% sodium chloride
LJMUCV191	Brand 2	9/30/2021	white liquid	suspension in 0.9% sodium chloride
LJMUCV192	Brand 2	9/30/2021	white liquid	suspension in 0.9% sodium chloride
LJMUCV193	Brand 2	9/30/2021	white liquid	suspension in 0.9% sodium chloride
LJMUCV194	Brand 2	9/30/2021	white liquid	suspension in 0.9% sodium chloride

LJMUCV195	Brand 2	9/30/2021	white liquid	suspension in 0.9% sodium chloride
LJMUCV196	Brand 2	10/30/2021	white liquid	suspension in 0.9% sodium chloride
LJMUCV197	Brand 2	9/30/2021	white liquid	suspension in 0.9% sodium chloride
LJMUCV198	Brand 2	10/30/2021	white liquid	suspension in 0.9% sodium chloride
LJMUCV199	Brand 2	9/30/2021	white liquid	suspension in 0.9% sodium chloride
LJMUCV200	Brand 2	9/30/2021	white liquid	suspension in 0.9% sodium chloride
LJMUCV201	Brand 2	10/30/2021	white liquid	suspension in 0.9% sodium chloride

LJMUCV202	Brand 2	10/30/2021	white liquid	suspension in 0.9% sodium chloride
LJMUCV203	Brand 2	10/30/2021	white liquid	suspension in 0.9% sodium chloride
LJMUCV204	Brand 2	9/30/2021	white liquid	suspension in 0.9% sodium chloride
LJMUCV205	Brand 2	10/30/2021	white liquid	suspension in 0.9% sodium chloride
LJMUCV206	Brand 2	9/30/2021	white liquid	suspension in 0.9% sodium chloride
LJMUCV207	Brand 2	10/30/2021	white liquid	suspension in 0.9% sodium chloride
LJMUCV208	Brand 2	9/30/2021	white liquid	suspension in 0.9% sodium chloride

LJMUCV209	Brand 2	9/30/2021	white liquid	suspension in 0.9% sodium chloride
LJMUCV210	Brand 2	10/30/2021	white liquid	suspension in 0.9% sodium chloride
LJMUCV211	Brand 2	9/30/2021	white liquid	suspension in 0.9% sodium chloride
LJMUCV212	Brand 2	10/30/2021	white liquid	suspension in 0.9% sodium chloride
LJMUCV213	Brand 2	9/30/2021	white liquid	suspension in 0.9% sodium chloride
LJMUCV214	Brand 2	10/30/2021	white liquid	suspension in 0.9% sodium chloride
LJMUCV215	Brand 2	9/30/2021	white liquid	suspension in 0.9% sodium chloride

LJMUCV216	Brand 2	9/30/2021	white liquid	suspension in 0.9% sodium chloride
LJMUCV217	Brand 2	10/30/2021	white liquid	suspension in 0.9% sodium chloride
LJMUCV218	Brand 2	10/30/2021	white liquid	suspension in 0.9% sodium chloride
LJMUCV219	Brand 2	9/30/2021	white liquid	suspension in 0.9% sodium chloride
LJMUCV220	Brand 2	10/30/2021	white liquid	suspension in 0.9% sodium chloride
LJMUCV221	Brand 2	9/30/2021	white liquid	suspension in 0.9% sodium chloride
LJMUCV222	Brand 2	9/30/2021	white liquid	suspension in 0.9% sodium chloride

LJMUCV223	Brand 2	10/30/2021	white liquid	suspension in 0.9% sodium chloride
LJMUCV224	Brand 2	9/30/2021	white liquid	suspension in 0.9% sodium chloride
LJMUCV225	Brand 2	9/30/2021	white liquid	suspension in 0.9% sodium chloride
LJMUCV226	Brand 2	10/30/2021	white liquid	suspension in 0.9% sodium chloride
LJMUCV227	Brand 2	10/30/2021	white liquid	suspension in 0.9% sodium chloride
LJMUCV228	Brand 2	10/30/2021	white liquid	suspension in 0.9% sodium chloride
LJMUCV229	Brand 2	10/30/2021	white liquid	suspension in 0.9% sodium chloride

LJMUCV230	Brand 2	9/30/2021	white liquid	suspension in 0.9% sodium chloride
LJMUCV231	Brand 2	9/30/2021	white liquid	suspension in 0.9% sodium chloride
LJMUCV232	Brand 2	9/30/2021	white liquid	suspension in 0.9% sodium chloride
LJMUCV233	Brand 2	9/30/2021	white liquid	suspension in 0.9% sodium chloride
LJMUCV234	Brand 2	9/30/2021	white liquid	suspension in 0.9% sodium chloride
LJMUCV235	Brand 2	9/30/2021	white liquid	suspension in 0.9% sodium chloride
LJMUCV236	Brand 2	10/30/2021	white liquid	suspension in 0.9% sodium chloride

LJMUCV237	Brand 2	9/30/2021	white liquid	suspension in 0.9% sodium chloride
LJMUCV238	Brand 2	10/30/2021	white liquid	suspension in 0.9% sodium chloride
LJMUCV239	Brand 2	10/30/2021	white liquid	suspension in 0.9% sodium chloride
LJMUCV240	Brand 2	9/30/2021	white liquid	suspension in 0.9% sodium chloride
LJMUCV241	Brand 2	9/30/2021	white liquid	suspension in 0.9% sodium chloride
LJMUCV242	Brand 2	9/30/2021	white liquid	suspension in 0.9% sodium chloride
LJMUCV243	Brand 2	9/30/2021	white liquid	suspension in 0.9% sodium chloride

LJMUCV244	Brand 2	10/30/2021	white liquid	suspension in 0.9% sodium chloride
LJMUCV245	Brand 2	9/30/2021	white liquid	suspension in 0.9% sodium chloride
LJMUCV246	Brand 2	10/30/2021	white liquid	suspension in 0.9% sodium chloride
LJMUCV247	Brand 2	9/30/2021	white liquid	suspension in 0.9% sodium chloride
LJMUCV248	Brand 2	10/30/2021	white liquid	suspension in 0.9% sodium chloride
LJMUCV249	Brand 2	10/30/2021	white liquid	suspension in 0.9% sodium chloride
LJMUCV250	Brand 2	10/30/2021	white liquid	suspension in 0.9% sodium chloride

LJMUCV251	Brand 2	9/30/2021	white liquid	suspension in 0.9% sodium chloride
LJMUCV252	Brand 2	10/30/2021	white liquid	suspension in 0.9% sodium chloride
LJMUCV253	Brand 2	9/30/2021	white liquid	suspension in 0.9% sodium chloride
LJMUCV254	Brand 2	10/30/2021	white liquid	suspension in 0.9% sodium chloride
LJMUCV255	Brand 2	9/30/2021	white liquid	suspension in 0.9% sodium chloride
LJMUCV256	Brand 2	10/30/2021	white liquid	suspension in 0.9% sodium chloride
LJMUCV257	Brand 2	10/30/2021	white liquid	suspension in 0.9% sodium chloride

LJMUCV258	Brand 2	9/30/2021	white liquid	suspension in 0.9% sodium chloride
LJMUCV259	Brand 2	10/30/2021	white liquid	suspension in 0.9% sodium chloride
LJMUCV260	Brand 2	9/30/2021	white liquid	suspension in 0.9% sodium chloride
LJMUCV261	Brand 2	9/30/2021	white liquid	suspension in 0.9% sodium chloride
LJMUCV262	Brand 2	9/30/2021	white liquid	suspension in 0.9% sodium chloride
LJMUCV263	Brand 2	9/30/2021	white liquid	suspension in 0.9% sodium chloride
LJMUCV264	Brand 2	10/30/2021	white liquid	suspension in 0.9% sodium chloride

LJMUCV265	Brand 2	9/30/2021	white liquid	suspension in 0.9% sodium chloride
LJMUCV266	Brand 2	9/30/2021	white liquid	suspension in 0.9% sodium chloride
LJMUCV267	Brand 2	9/30/2021	white liquid	suspension in 0.9% sodium chloride
LJMUCV268	Brand 2	10/30/2021	white liquid	suspension in 0.9% sodium chloride
LJMUCV269	Brand 2	10/30/2021	white liquid	suspension in 0.9% sodium chloride
LJMUCV270	Brand 2	9/30/2021	white liquid	suspension in 0.9% sodium chloride
LJMUCV271	Brand 2	9/30/2021	white liquid	suspension in 0.9% sodium chloride

LJMUCV272	Brand 2	9/30/2021	white liquid	suspension in 0.9% sodium chloride
LJMUCV273	Brand 2	9/30/2021	white liquid	suspension in 0.9% sodium chloride
LJMUCV274	Brand 2	10/30/2021	white liquid	suspension in 0.9% sodium chloride
LJMUCV275	Brand 2	10/30/2021	white liquid	suspension in 0.9% sodium chloride
LJMUCV276	Brand 2	10/30/2021	white liquid	suspension in 0.9% sodium chloride
LJMUCV277	Brand 2	9/30/2021	white liquid	suspension in 0.9% sodium chloride
LJMUCV278	Brand 2	10/30/2021	white liquid	suspension in 0.9% sodium chloride

LJMUCV279	Brand 2	9/30/2021	white liquid	suspension in 0.9% sodium chloride
LJMUCV280	Brand 2	10/30/2021	white liquid	suspension in 0.9% sodium chloride
LJMUCV281	Brand 2	9/30/2021	white liquid	suspension in 0.9% sodium chloride
LJMUCV282	Brand 2	10/30/2021	white liquid	suspension in 0.9% sodium chloride
LJMUCV283	Brand 2	9/30/2021	white liquid	suspension in 0.9% sodium chloride
LJMUCV284	Brand 2	10/30/2021	white liquid	suspension in 0.9% sodium chloride
LJMUCV285	Brand 2	10/30/2021	white liquid	suspension in 0.9% sodium chloride

LJMUCV286	Brand 2	10/30/2021	white liquid	suspension in 0.9% sodium chloride
LJMUCV287	Brand 2	10/30/2021	white liquid	suspension in 0.9% sodium chloride
LJMUCV288	Brand 2	9/30/2021	white liquid	suspension in 0.9% sodium chloride
LJMUCV289	Brand 2	9/30/2021	white liquid	suspension in 0.9% sodium chloride
LJMUCV290	Brand 2	10/30/2021	white liquid	suspension in 0.9% sodium chloride
LJMUCV291	Brand 2	10/30/2021	white liquid	suspension in 0.9% sodium chloride
LJMUCV292	Brand 2	10/30/2021	white liquid	suspension in 0.9% sodium chloride

LJMUCV293	Brand 2	9/30/2021	white liquid	suspension in 0.9% sodium chloride
LJMUCV294	Brand 2	10/30/2021	white liquid	suspension in 0.9% sodium chloride
LJMUCV295	Brand 2	9/30/2021	white liquid	suspension in 0.9% sodium chloride
LJMUCV296	Brand 2	10/30/2021	white liquid	suspension in 0.9% sodium chloride
LJMUCV297	Brand 2	9/30/2021	white liquid	suspension in 0.9% sodium chloride
LJMUCV298	Brand 2	9/30/2021	white liquid	suspension in 0.9% sodium chloride
LJMUCV299	Brand 1	8/30/2021	transparent liquid	recombinant

LJMUCV300	Brand 1	8/30/2021	transparent liquid	recombinant
LJMUCV301	Brand 1	8/30/2021	transparent liquid	recombinant
LJMUCV302	Brand 1	7/30/2021	transparent liquid	recombinant
LJMUCV303	Brand 1	8/30/2021	transparent liquid	recombinant
LJMUCV304	Brand 1	8/30/2021	transparent liquid	recombinant
LJMUCV305	Brand 1	8/30/2021	transparent liquid	recombinant
LJMUCV306	Brand 1	7/30/2021	transparent liquid	recombinant

LJMUCV307	Brand 1	8/30/2021	transparent liquid	recombinant
LJMUCV308	Brand 1	8/30/2021	transparent liquid	recombinant
LJMUCV309	Brand 1	8/30/2021	transparent liquid	recombinant
LJMUCV310	Brand 1	8/30/2021	transparent liquid	recombinant
LJMUCV311	Brand 1	8/30/2021	transparent liquid	recombinant
LJMUCV312	Brand 1	8/30/2021	transparent liquid	recombinant
LJMUCV313	Brand 1	7/30/2021	transparent liquid	recombinant

LJMUCV314	Brand 1	8/30/2021	transparent liquid	recombinant
LJMUCV315	Brand 1	8/30/2021	transparent liquid	recombinant
LJMUCV316	Brand 1	8/30/2021	transparent liquid	recombinant
LJMUCV317	Brand 1	8/30/2021	transparent liquid	recombinant
LJMUCV318	Brand 1	8/30/2021	transparent liquid	recombinant
LJMUCV319	Brand 1	8/30/2021	transparent liquid	recombinant
LJMUCV320	Brand 1	8/30/2021	transparent liquid	recombinant

LJMUCV321	Brand 1	8/30/2021	transparent liquid	recombinant
LJMUCV322	Brand 1	8/30/2021	transparent liquid	recombinant
LJMUCV323	Brand 1	8/30/2021	transparent liquid	recombinant
LJMUCV324	Brand 1	8/30/2021	transparent liquid	recombinant
LJMUCV325	Brand 1	8/30/2021	transparent liquid	recombinant
LJMUCV326	Brand 1	7/30/2021	transparent liquid	recombinant
LJMUCV327	Brand 1	8/30/2021	transparent liquid	recombinant

LJMUCV328	Brand 1	8/30/2021	transparent liquid	recombinant
LJMUCV329	Brand 1	8/30/2021	transparent liquid	recombinant
LJMUCV330	Brand 1	8/30/2021	transparent liquid	recombinant
LJMUCV331	Brand 1	8/30/2021	transparent liquid	recombinant
LJMUCV332	Brand 1	7/30/2021	transparent liquid	recombinant
LJMUCV333	Brand 1	8/30/2021	transparent liquid	recombinant
LJMUCV334	Brand 1	8/30/2021	transparent liquid	recombinant

LJMUCV335	Brand 1	7/30/2021	transparent liquid	recombinant
LJMUCV336	Brand 1	8/30/2021	transparent liquid	recombinant
LJMUCV337	Brand 1	8/30/2021	transparent liquid	recombinant
LJMUCV338	Brand 1	8/30/2021	transparent liquid	recombinant
LJMUCV339	Brand 1	8/30/2021	transparent liquid	recombinant
LJMUCV340	Brand 1	8/30/2021	transparent liquid	recombinant
LJMUCV341	Brand 1	8/30/2021	transparent liquid	recombinant

LJMUCV342	Brand 1	8/30/2021	transparent liquid	recombinant
LJMUCV343	Brand 1	8/30/2021	transparent liquid	recombinant
LJMUCV344	Brand 1	8/30/2021	transparent liquid	recombinant
LJMUCV345	Brand 2	9/30/2021	white liquid	suspension in 0.9% sodium chloride
LJMUCV346	Brand 2	9/30/2021	white liquid	suspension in 0.9% sodium chloride
LJMUCV347	Brand 2	9/30/2021	white liquid	suspension in 0.9% sodium chloride
LJMUCV348	Brand 2	9/30/2021	white liquid	suspension in 0.9% sodium chloride

LJMUCV349	Brand 2	9/30/2021	white liquid	suspension in 0.9% sodium chloride
LJMUCV350	Brand 2	9/30/2021	white liquid	suspension in 0.9% sodium chloride
LJMUCV351	Brand 2	10/30/2021	white liquid	suspension in 0.9% sodium chloride
LJMUCV352	Brand 2	9/30/2021	white liquid	suspension in 0.9% sodium chloride
LJMUCV353	Brand 2	9/30/2021	white liquid	suspension in 0.9% sodium chloride
LJMUCV354	Brand 2	9/30/2021	white liquid	suspension in 0.9% sodium chloride
LJMUCV355	Brand 2	9/30/2021	white liquid	suspension in 0.9% sodium chloride

LJMUCV356	Brand 2	9/30/2021	white liquid	suspension in 0.9% sodium chloride
LJMUCV357	Brand 2	9/30/2021	white liquid	suspension in 0.9% sodium chloride
LJMUCV358	Brand 2	9/30/2021	white liquid	suspension in 0.9% sodium chloride
LJMUCV359	Brand 2	9/30/2021	white liquid	suspension in 0.9% sodium chloride
LJMUCV360	Brand 2	9/30/2021	white liquid	suspension in 0.9% sodium chloride
LJMUCV361	Brand 2	9/30/2021	white liquid	suspension in 0.9% sodium chloride
LJMUCV362	Brand 2	9/30/2021	white liquid	suspension in 0.9% sodium chloride

LJMUCV363	Brand 2	9/30/2021	white liquid	suspension in 0.9% sodium chloride
LJMUCV364	Brand 2	9/30/2021	white liquid	suspension in 0.9% sodium chloride
LJMUCV365	Brand 2	9/30/2021	white liquid	suspension in 0.9% sodium chloride
LJMUCV366	Brand 2	9/30/2021	white liquid	suspension in 0.9% sodium chloride
LJMUCV367	Brand 2	9/30/2021	white liquid	suspension in 0.9% sodium chloride
LJMUCV368	Brand 2	9/30/2021	white liquid	suspension in 0.9% sodium chloride
LJMUCV369	Brand 2	9/30/2021	white liquid	suspension in 0.9% sodium chloride

LJMUCV370	Brand 2	9/30/2021	white liquid	suspension in 0.9% sodium chloride
LJMUCV371	Brand 2	9/30/2021	white liquid	suspension in 0.9% sodium chloride
LJMUCV372	Brand 2	9/30/2021	white liquid	suspension in 0.9% sodium chloride
LJMUCV373	Brand 2	9/30/2021	white liquid	suspension in 0.9% sodium chloride
LJMUCV374	Brand 2	9/30/2021	white liquid	suspension in 0.9% sodium chloride
LJMUCV375	Brand 2	9/30/2021	white liquid	suspension in 0.9% sodium chloride
LJMUCV376	Brand 2	9/30/2021	white liquid	suspension in 0.9% sodium chloride

LJMUCV377	Brand 2	9/30/2021	white liquid	suspension in 0.9% sodium chloride
LJMUCV378	Brand 2	9/30/2021	white liquid	suspension in 0.9% sodium chloride
LJMUCV379	Brand 2	9/30/2021	white liquid	suspension in 0.9% sodium chloride
LJMUCV380	Brand 2	9/30/2021	white liquid	suspension in 0.9% sodium chloride
LJMUCV381	Brand 2	9/30/2021	white liquid	suspension in 0.9% sodium chloride
LJMUCV382	Brand 2	9/30/2021	white liquid	suspension in 0.9% sodium chloride
LJMUCV383	Brand 2	9/30/2021	white liquid	suspension in 0.9% sodium chloride

LJMUCV384	Brand 2	9/30/2021	white liquid	suspension in 0.9% sodium chloride
LJMUCV385	Brand 2	9/30/2021	white liquid	suspension in 0.9% sodium chloride
LJMUCV386	Brand 2	9/30/2021	white liquid	suspension in 0.9% sodium chloride
LJMUCV387	Brand 2	9/30/2021	white liquid	suspension in 0.9% sodium chloride
LJMUCV388	Brand 2	9/30/2021	white liquid	suspension in 0.9% sodium chloride
LJMUCV389	Brand 2	9/30/2021	white liquid	suspension in 0.9% sodium chloride
LJMUCV390	Brand 2	9/30/2021	white liquid	suspension in 0.9% sodium chloride

LJMUCV391	Brand 2	9/30/2021	white liquid	suspension in 0.9% sodium chloride
LJMUCV392	Brand 2	9/30/2021	white liquid	suspension in 0.9% sodium chloride
LJMUCV393	Brand 2	9/30/2021	white liquid	suspension in 0.9% sodium chloride
LJMUCV394	Brand 2	9/30/2021	white liquid	suspension in 0.9% sodium chloride
LJMUCV395	Brand 2	9/30/2021	white liquid	suspension in 0.9% sodium chloride
LJMUCV396	Brand 2	9/30/2021	white liquid	suspension in 0.9% sodium chloride
LJMUCV397	Brand 2	9/30/2021	white liquid	suspension in 0.9% sodium chloride

LJMUCV398	Brand 2	9/30/2021	white liquid	suspension in 0.9% sodium chloride
LJMUCV399	Brand 2	9/30/2021	white liquid	suspension in 0.9% sodium chloride
LJMUCV400	Brand 2	9/30/2021	white liquid	suspension in 0.9% sodium chloride
LJMUCV401	Brand 2	9/30/2021	white liquid	suspension in 0.9% sodium chloride
LJMUCV402	Brand 2	10/30/2021	white liquid	suspension in 0.9% sodium chloride
LJMUCV403	Brand 2	9/30/2021	white liquid	suspension in 0.9% sodium chloride
LJMUCV404	Brand 2	9/30/2021	white liquid	suspension in 0.9% sodium chloride

LJMUCV405	Brand 2	9/30/2021	white liquid	suspension in 0.9% sodium chloride
LJMUCV406	Brand 2	9/30/2021	white liquid	suspension in 0.9% sodium chloride
LJMUCV407	Brand 2	9/30/2021	white liquid	suspension in 0.9% sodium chloride
LJMUCV408	Brand 2	9/30/2021	white liquid	suspension in 0.9% sodium chloride
LJMUCV409	Brand 2	9/30/2021	white liquid	suspension in 0.9% sodium chloride
LJMUCV410	Brand 2	10/30/2021	white liquid	suspension in 0.9% sodium chloride
LJMUCV411	Brand 2	10/30/2021	white liquid	suspension in 0.9% sodium chloride

LJMUCV412	Brand 2	10/30/2021	white liquid	suspension in 0.9% sodium chloride
LJMUCV413	Brand 2	8/30/2021	white liquid	suspension in 0.9% sodium chloride
LJMUCV414	Brand 2	8/30/2021	white liquid	suspension in 0.9% sodium chloride
LJMUCV415	Brand 2	9/30/2021	white liquid	suspension in 0.9% sodium chloride
LJMUCV416	Brand 2	9/30/2021	white liquid	suspension in 0.9% sodium chloride
LJMUCV417	Brand 2	9/30/2021	white liquid	suspension in 0.9% sodium chloride
LJMUCV418	Brand 2	9/30/2021	white liquid	suspension in 0.9% sodium chloride

LJMUCV419	Brand 2	9/30/2021	white liquid	suspension in 0.9% sodium chloride
LJMUCV420	Brand 2	9/30/2021	white liquid	suspension in 0.9% sodium chloride
LJMUCV421	Brand 2	9/30/2021	white liquid	suspension in 0.9% sodium chloride
LJMUCV422	Brand 2	9/30/2021	white liquid	suspension in 0.9% sodium chloride
LJMUCV423	Brand 2	9/30/2021	white liquid	suspension in 0.9% sodium chloride
LJMUCV424	Brand 2	9/30/2021	white liquid	suspension in 0.9% sodium chloride
LJMUCV425	Brand 2	10/30/2021	white liquid	suspension in 0.9% sodium chloride

LJMUCV426	Brand 2	9/30/2021	white liquid	suspension in 0.9% sodium chloride
LJMUCV427	Brand 2	9/30/2021	white liquid	suspension in 0.9% sodium chloride
LJMUCV428	Brand 2	9/30/2021	white liquid	suspension in 0.9% sodium chloride
LJMUCV429	Brand 2	9/30/2021	white liquid	suspension in 0.9% sodium chloride
LJMUCV430	Brand 2	9/30/2021	white liquid	suspension in 0.9% sodium chloride
LJMUCV431	Brand 2	9/30/2021	white liquid	suspension in 0.9% sodium chloride
LJMUCV432	Brand 2	9/30/2021	white liquid	suspension in 0.9% sodium chloride

LJMUCV433	Brand 2	9/30/2021	white liquid	suspension in 0.9% sodium chloride
LJMUCV434	Brand 2	9/30/2021	white liquid	suspension in 0.9% sodium chloride
LJMUCV435	Brand 2	9/30/2021	white liquid	suspension in 0.9% sodium chloride
LJMUCV436	Brand 2	9/30/2021	white liquid	suspension in 0.9% sodium chloride
LJMUCV437	Brand 2	9/30/2021	white liquid	suspension in 0.9% sodium chloride
LJMUCV438	Brand 2	9/30/2021	white liquid	suspension in 0.9% sodium chloride
LJMUCV439	Brand 2	9/30/2021	white liquid	suspension in 0.9% sodium chloride

LJMUCV440	Brand 2	9/30/2021	white liquid	suspension in 0.9% sodium chloride
LJMUCV441	Brand 2	9/30/2021	white liquid	suspension in 0.9% sodium chloride
LJMUCV442	Brand 2	10/30/2021	white liquid	suspension in 0.9% sodium chloride
LJMUCV443	Brand 2	10/30/2021	white liquid	suspension in 0.9% sodium chloride
LJMUCV444	Brand 2	10/30/2021	white liquid	suspension in 0.9% sodium chloride
LJMUCV445	Brand 2	9/30/2021	white liquid	suspension in 0.9% sodium chloride
LJMUCV446	Brand 2	9/30/2021	white liquid	suspension in 0.9% sodium chloride

LJMUCV447	Brand 2	9/30/2021	white liquid	suspension in 0.9% sodium chloride
LJMUCV448	Brand 2	9/30/2021	white liquid	suspension in 0.9% sodium chloride
LJMUCV449	Brand 2	9/30/2021	white liquid	suspension in 0.9% sodium chloride
LJMUCV450	Brand 2	9/30/2021	white liquid	suspension in 0.9% sodium chloride
LJMUCV451	Brand 2	9/30/2021	white liquid	suspension in 0.9% sodium chloride
LJMUCV452	Brand 2	9/30/2021	white liquid	suspension in 0.9% sodium chloride
LJMUCV453	Brand 2	9/30/2021	white liquid	suspension in 0.9% sodium chloride

LJMUCV454	Brand 2	10/30/2021	white liquid	suspension in 0.9% sodium chloride
LJMUCV455	Brand 2	10/30/2021	white liquid	suspension in 0.9% sodium chloride
LJMUCV456	Brand 2	9/30/2021	white liquid	suspension in 0.9% sodium chloride
LJMUCV457	Brand 2	9/30/2021	white liquid	suspension in 0.9% sodium chloride
LJMUCV458	Brand 2	9/30/2021	white liquid	suspension in 0.9% sodium chloride
LJMUCV459	Brand 1	6/30/2021	transparent liquid	recombinant
LJMUCV460	Brand 1	6/30/2021	transparent liquid	recombinant

LJMUCV461	Brand 1	6/30/2021	transparent liquid	recombinant
LJMUCV462	Brand 1	6/30/2021	transparent liquid	recombinant
LJMUCV463	Brand 1	6/30/2021	transparent liquid	recombinant
LJMUCV464	Brand 1	6/30/2021	transparent liquid	recombinant
LJMUCV465	Brand 1	6/30/2021	transparent liquid	recombinant
LJMUCV466	Brand 1	6/30/2021	transparent liquid	recombinant
LJMUCV467	Brand 1	6/30/2021	transparent liquid	recombinant

LJMUCV468	Brand 1	6/30/2021	transparent liquid	recombinant
LJMUCV469	Brand 1	6/30/2021	transparent liquid	recombinant
LJMUCV470	Brand 1	6/30/2021	transparent liquid	recombinant
LJMUCV471	Brand 1	6/30/2021	transparent liquid	recombinant
LJMUCV472	Brand 1	6/30/2021	transparent liquid	recombinant
LJMUCV473	Brand 1	6/30/2021	transparent liquid	recombinant
LJMUCV474	Brand 1	6/30/2021	transparent liquid	recombinant

LJMUCV475	Brand 1	6/30/2021	transparent liquid	recombinant
LJMUCV476	Brand 1	6/30/2021	transparent liquid	recombinant
LJMUCV477	Brand 1	6/30/2021	transparent liquid	recombinant
LJMUCV478	Brand 1	6/30/2021	transparent liquid	recombinant
LJMUCV479	Brand 1	6/30/2021	transparent liquid	recombinant
LJMUCV480	Brand 1	6/30/2021	transparent liquid	recombinant
LJMUCV481	Brand 1	6/30/2021	transparent liquid	recombinant

LJMUCV482	Brand 1	6/30/2021	transparent liquid	recombinant
LJMUCV483	Brand 1	6/30/2021	transparent liquid	recombinant
LJMUCV484	Brand 1	6/30/2021	transparent liquid	recombinant
LJMUCV485	Brand 1	6/30/2021	transparent liquid	recombinant
LJMUCV486	Brand 1	6/30/2021	transparent liquid	recombinant
LJMUCV487	Brand 1	6/30/2021	transparent liquid	recombinant
LJMUCV488	Brand 1	6/30/2021	transparent liquid	recombinant

LJMUCV489	Brand 1	6/30/2021	transparent liquid	recombinant
LJMUCV490	Brand 1	6/30/2021	transparent liquid	recombinant
LJMUCV491	Brand 1	6/30/2021	transparent liquid	recombinant
LJMUCV492	Brand 1	6/30/2021	transparent liquid	recombinant
LJMUCV493	Brand 1	6/30/2021	transparent liquid	recombinant
LJMUCV494	Brand 1	6/30/2021	transparent liquid	recombinant
LJMUCV495	Brand 1	6/30/2021	transparent liquid	recombinant

LJMUCV496	Brand 1	6/30/2021	transparent liquid	recombinant
LJMUCV497	Brand 1	6/30/2021	transparent liquid	recombinant
LJMUCV498	Brand 1	6/30/2021	transparent liquid	recombinant
LJMUCV499	Brand 1	6/30/2021	transparent liquid	recombinant
LJMUCV500	Brand 1	6/30/2021	transparent liquid	recombinant
LJMUCV501	Brand 1	6/30/2021	transparent liquid	recombinant
LJMUCV502	Brand 1	6/30/2021	transparent liquid	recombinant

LJMUCV503	Brand 1	6/30/2021	transparent liquid	recombinant
LJMUCV504	Brand 1	6/30/2021	transparent liquid	recombinant
LJMUCV505	Brand 1	6/30/2021	transparent liquid	recombinant
LJMUCV506	Brand 1	6/30/2021	transparent liquid	recombinant
LJMUCV507	Brand 1	6/30/2021	transparent liquid	recombinant
LJMUCV508	Brand 1	6/30/2021	transparent liquid	recombinant
LJMUCV509	Brand 1	6/30/2021	transparent liquid	recombinant

LJMUCV510	Brand 1	6/30/2021	transparent liquid	recombinant
LJMUCV511	Brand 1	6/30/2021	transparent liquid	recombinant
LJMUCV512	Brand 1	6/30/2021	transparent liquid	recombinant
LJMUCV513	Brand 1	6/30/2021	transparent liquid	recombinant
LJMUCV514	Brand 1	6/30/2021	transparent liquid	recombinant
LJMUCV515	Brand 1	6/30/2021	transparent liquid	recombinant
LJMUCV516	Brand 1	6/30/2021	transparent liquid	recombinant

LJMUCV517	Brand 1	6/30/2021	transparent liquid	recombinant
LJMUCV518	Brand 1	6/30/2021	transparent liquid	recombinant
LJMUCV519	Brand 1	6/30/2021	transparent liquid	recombinant
LJMUCV520	Brand 1	6/30/2021	transparent liquid	recombinant
LJMUCV521	Brand 1	6/30/2021	transparent liquid	recombinant
LJMUCV522	Brand 1	6/30/2021	transparent liquid	recombinant
LJMUCV523	Brand 1	6/30/2021	transparent liquid	recombinant

LJMUCV524	Brand 1	6/30/2021	transparent liquid	recombinant
LJMUCV525	Brand 1	6/30/2021	transparent liquid	recombinant
LJMUCV526	Brand 1	6/30/2021	transparent liquid	recombinant
LJMUCV527	Brand 1	6/30/2021	transparent liquid	recombinant
LJMUCV528	Brand 1	6/30/2021	transparent liquid	recombinant
LJMUCV529	Brand 1	6/30/2021	transparent liquid	recombinant
LJMUCV530	Brand 1	6/30/2021	transparent liquid	recombinant

LJMUCV531	Brand 1	6/30/2021	transparent liquid	recombinant
LJMUCV532	Brand 1	6/30/2021	transparent liquid	recombinant
LJMUCV533	Brand 1	6/30/2021	transparent liquid	recombinant
LJMUCV534	Brand 1	6/30/2021	transparent liquid	recombinant
LJMUCV535	Brand 1	6/30/2021	transparent liquid	recombinant
LJMUCV536	Brand 1	6/30/2021	transparent liquid	recombinant
LJMUCV537	Brand 1	6/30/2021	transparent liquid	recombinant

LJMUCV538	Brand 1	6/30/2021	transparent liquid	recombinant
LJMUCV539	Brand 1	6/30/2021	transparent liquid	recombinant
LJMUCV540	Brand 1	6/30/2021	transparent liquid	recombinant
LJMUCV541	Brand 1	6/30/2021	transparent liquid	recombinant
LJMUCV542	Brand 1	6/30/2021	transparent liquid	recombinant
LJMUCV543	Brand 1	6/30/2021	transparent liquid	recombinant
LJMUCV544	Brand 1	6/30/2021	transparent liquid	recombinant

LJMUCV545	Brand 1	6/30/2021	transparent liquid	recombinant
LJMUCV546	Brand 1	6/30/2021	transparent liquid	recombinant
LJMUCV547	Brand 1	6/30/2021	transparent liquid	recombinant
LJMUCV548	Brand 1	6/30/2021	transparent liquid	recombinant
LJMUCV549	Brand 1	6/30/2021	transparent liquid	recombinant
LJMUCV550	Brand 1	6/30/2021	transparent liquid	recombinant
LJMUCV551	Brand 1	6/30/2021	transparent liquid	recombinant

LJMUCV552	Brand 1	6/30/2021	transparent liquid	recombinant
LJMUCV553	Brand 1	6/30/2021	transparent liquid	recombinant
LJMUCV554	Brand 1	6/30/2021	transparent liquid	recombinant
LJMUCV555	Brand 1	6/30/2021	transparent liquid	recombinant
LJMUCV556	Brand 1	6/30/2021	transparent liquid	recombinant
LJMUCV557	Brand 1	6/30/2021	transparent liquid	recombinant
LJMUCV558	Brand 1	6/30/2021	transparent liquid	recombinant

LJMUCV559	Brand 1	6/30/2021	transparent liquid	recombinant
LJMUCV560	Brand 1	6/30/2021	transparent liquid	recombinant
LJMUCV561	Brand 1	6/30/2021	transparent liquid	recombinant
LJMUCV562	Brand 1	6/30/2021	transparent liquid	recombinant
LJMUCV563	Brand 1	6/30/2021	transparent liquid	recombinant
LJMUCV564	Brand 1	6/30/2021	transparent liquid	recombinant
LJMUCV565	Brand 1	6/30/2021	transparent liquid	recombinant

LJMUCV566	Brand 1	6/30/2021	transparent liquid	recombinant
LJMUCV567	Brand 1	6/30/2021	transparent liquid	recombinant
LJMUCV568	Brand 1	6/30/2021	transparent liquid	recombinant
LJMUCV569	Brand 1	6/30/2021	transparent liquid	recombinant
LJMUCV570	Brand 1	6/30/2021	transparent liquid	recombinant
LJMUCV571	Brand 1	6/30/2021	transparent liquid	recombinant
LJMUCV572	Brand 1	6/30/2021	transparent liquid	recombinant

LJMUCV573	Brand 1	6/30/2021	transparent liquid	recombinant
LJMUCV574	Brand 1	6/30/2021	transparent liquid	recombinant
LJMUCV575	Brand 1	6/30/2021	transparent liquid	recombinant
LJMUCV576	Brand 1	7/30/2021	transparent liquid	recombinant
LJMUCV577	Brand 1	7/30/2021	transparent liquid	recombinant
LJMUCV578	Brand 1	7/30/2021	transparent liquid	recombinant
LJMUCV579	Brand 1	7/30/2021	transparent liquid	recombinant

LJMUCV580	Brand 1	7/30/2021	transparent liquid	recombinant
LJMUCV581	Brand 1	7/30/2021	transparent liquid	recombinant
LJMUCV582	Brand 1	7/30/2021	transparent liquid	recombinant
LJMUCV583	Brand 1	7/30/2021	transparent liquid	recombinant
LJMUCV584	Brand 1	7/30/2021	transparent liquid	recombinant
LJMUCV585	Brand 1	7/30/2021	transparent liquid	recombinant
LJMUCV586	Brand 1	7/30/2021	transparent liquid	recombinant

LJMUCV587	Brand 1	7/30/2021	transparent liquid	recombinant
LJMUCV588	Brand 1	7/30/2021	transparent liquid	recombinant
LJMUCV589	Brand 1	7/30/2021	transparent liquid	recombinant
LJMUCV590	Brand 1	7/30/2021	transparent liquid	recombinant
LJMUCV591	Brand 1	7/30/2021	transparent liquid	recombinant
LJMUCV592	Brand 1	7/30/2021	transparent liquid	recombinant
LJMUCV593	Brand 1	7/30/2021	transparent liquid	recombinant

LJMUCV594	Brand 1	7/30/2021	transparent liquid	recombinant
LJMUCV595	Brand 1	7/30/2021	transparent liquid	recombinant
LJMUCV596	Brand 1	7/30/2021	transparent liquid	recombinant
LJMUCV597	Brand 1	7/30/2021	transparent liquid	recombinant
LJMUCV598	Brand 1	7/30/2021	transparent liquid	recombinant
LJMUCV599	Brand 1	7/30/2021	transparent liquid	recombinant
LJMUCV600	Brand 1	7/30/2021	transparent liquid	recombinant

LJMUCV601	Brand 1	7/30/2021	transparent liquid	recombinant
LJMUCV602	Brand 1	7/30/2021	transparent liquid	recombinant
LJMUCV603	Brand 1	7/30/2021	transparent liquid	recombinant
LJMUCV604	Brand 1	7/30/2021	transparent liquid	recombinant
LJMUCV605	Brand 1	7/30/2021	transparent liquid	recombinant
LJMUCV606	Brand 1	7/30/2021	transparent liquid	recombinant
LJMUCV607	Brand 1	7/30/2021	transparent liquid	recombinant

LJMUCV608	Brand 1	7/30/2021	transparent liquid	recombinant
LJMUCV609	Brand 1	7/30/2021	transparent liquid	recombinant
LJMUCV610	Brand 1	7/30/2021	transparent liquid	recombinant
LJMUCV611	Brand 1	7/30/2021	transparent liquid	recombinant
LJMUCV612	Brand 1	7/30/2021	transparent liquid	recombinant
LJMUCV613	Brand 1	7/30/2021	transparent liquid	recombinant
LJMUCV614	Brand 1	7/30/2021	transparent liquid	recombinant

LJMUCV615	Brand 1	7/30/2021	transparent liquid	recombinant
LJMUCV616	Brand 1	7/30/2021	transparent liquid	recombinant
LJMUCV617	Brand 1	7/30/2021	transparent liquid	recombinant
LJMUCV618	Brand 1	7/30/2021	transparent liquid	recombinant
LJMUCV619	Brand 1	7/30/2021	transparent liquid	recombinant
LJMUCV620	Brand 1	7/30/2021	transparent liquid	recombinant
LJMUCV621	Brand 1	7/30/2021	transparent liquid	recombinant

LJMUCV622	Brand 1	7/30/2021	transparent liquid	recombinant
LJMUCV623	Brand 1	7/30/2021	transparent liquid	recombinant
LJMUCV624	Brand 1	7/30/2021	transparent liquid	recombinant
LJMUCV625	Brand 1	7/30/2021	transparent liquid	recombinant
LJMUCV626	Brand 1	7/30/2021	transparent liquid	recombinant
LJMUCV627	Brand 1	7/30/2021	transparent liquid	recombinant
LJMUCV628	Brand 1	7/30/2021	transparent liquid	recombinant

LJMUCV629	Brand 1	7/30/2021	transparent liquid	recombinant
LJMUCV630	Brand 1	7/30/2021	transparent liquid	recombinant
LJMUCV631	Brand 1	7/30/2021	transparent liquid	recombinant
LJMUCV632	Brand 1	7/30/2021	transparent liquid	recombinant
LJMUCV633	Brand 1	7/30/2021	transparent liquid	recombinant
LJMUCV634	Brand 1	7/30/2021	transparent liquid	recombinant
LJMUCV635	Brand 1	7/30/2021	transparent liquid	recombinant

LJMUCV636	Brand 1	7/30/2021	transparent liquid	recombinant
LJMUCV637	Brand 1	7/30/2021	transparent liquid	recombinant
LJMUCV638	Brand 1	7/30/2021	transparent liquid	recombinant
LJMUCV639	Brand 1	7/30/2021	transparent liquid	recombinant
LJMUCV640	Brand 1	7/30/2021	transparent liquid	recombinant
LJMUCV641	Brand 1	7/30/2021	transparent liquid	recombinant
LJMUCV642	Brand 1	7/30/2021	transparent liquid	recombinant

LJMUCV643	Brand 1	7/30/2021	transparent liquid	recombinant
LJMUCV644	Brand 1	7/30/2021	transparent liquid	recombinant
LJMUCV645	Brand 1	7/30/2021	transparent liquid	recombinant
LJMUCV646	Brand 1	7/30/2021	transparent liquid	recombinant
LJMUCV647	Brand 1	7/30/2021	transparent liquid	recombinant
LJMUCV648	Brand 1	7/30/2021	transparent liquid	recombinant
LJMUCV649	Brand 1	7/30/2021	transparent liquid	recombinant

LJMUCV650	Brand 1	7/30/2021	transparent liquid	recombinant
LJMUCV651	Brand 1	7/30/2021	transparent liquid	recombinant
LJMUCV652	Brand 1	7/30/2021	transparent liquid	recombinant
LJMUCV653	Brand 1	7/30/2021	transparent liquid	recombinant
LJMUCV654	Brand 1	7/30/2021	transparent liquid	recombinant
LJMUCV655	Brand 1	7/30/2021	transparent liquid	recombinant
LJMUCV656	Brand 1	7/30/2021	transparent liquid	recombinant

LJMUCV657	Brand 1	7/30/2021	transparent liquid	recombinant
LJMUCV658	Brand 1	7/30/2021	transparent liquid	recombinant
LJMUCV659	Brand 1	7/30/2021	transparent liquid	recombinant
LJMUCV660	Brand 1	7/30/2021	transparent liquid	recombinant
LJMUCV661	Brand 1	7/30/2021	transparent liquid	recombinant
LJMUCV662	Brand 1	7/30/2021	transparent liquid	recombinant
LJMUCV663	Brand 1	7/30/2021	transparent liquid	recombinant

LJMUCV664	Brand 1	7/30/2021	transparent liquid	recombinant
LJMUCV665	Brand 1	7/30/2021	transparent liquid	recombinant
LJMUCV666	Brand 1	7/30/2021	transparent liquid	recombinant
LJMUCV667	Brand 1	7/30/2021	transparent liquid	recombinant
LJMUCV668	Brand 1	7/30/2021	transparent liquid	recombinant
LJMUCV669	Brand 1	7/30/2021	transparent liquid	recombinant
LJMUCV670	Brand 1	7/30/2021	transparent liquid	recombinant

LJMUCV671	Brand 1	7/30/2021	transparent liquid	recombinant
LJMUCV672	Brand 1	7/30/2021	transparent liquid	recombinant
LJMUCV673	Brand 1	7/30/2021	transparent liquid	recombinant
LJMUCV674	Brand 1	7/30/2021	transparent liquid	recombinant
LJMUCV675	Brand 1	7/30/2021	transparent liquid	recombinant
LJMUCV676	Brand 1	7/30/2021	transparent liquid	recombinant
LJMUCV677	Brand 1	7/30/2021	transparent liquid	recombinant

LJMUCV678	Brand 1	7/30/2021	transparent liquid	recombinant
LJMUCV679	Brand 1	7/30/2021	transparent liquid	recombinant
LJMUCV680	Brand 1	7/30/2021	transparent liquid	recombinant
LJMUCV681	Brand 1	7/30/2021	transparent liquid	recombinant
LJMUCV682	Brand 1	7/30/2021	transparent liquid	recombinant
LJMUCV683	Brand 1	7/30/2021	transparent liquid	recombinant
LJMUCV684	Brand 1	7/30/2021	transparent liquid	recombinant

LJMUCV685	Brand 1	7/30/2021	transparent liquid	recombinant
LJMUCV686	Brand 1	7/30/2021	transparent liquid	recombinant
LJMUCV687	Brand 1	7/30/2021	transparent liquid	recombinant
LJMUCV688	Brand 1	7/30/2021	transparent liquid	recombinant
LJMUCV689	Brand 1	7/30/2021	transparent liquid	recombinant
LJMUCV690	Brand 1	7/30/2021	transparent liquid	recombinant
LJMUCV691	Brand 1	7/30/2021	transparent liquid	recombinant

LJMUCV692	Brand 1	7/30/2021	transparent liquid	recombinant
LJMUCV693	Brand 1	7/30/2021	transparent liquid	recombinant
LJMUCV694	Brand 1	7/30/2021	transparent liquid	recombinant
LJMUCV695	Brand 1	7/30/2021	transparent liquid	recombinant
LJMUCV696	Brand 1	7/30/2021	transparent liquid	recombinant
LJMUCV697	Brand 1	7/30/2021	transparent liquid	recombinant
LJMUCV698	Brand 1	7/30/2021	transparent liquid	recombinant

LJMUCV699	Brand 1	7/30/2021	transparent liquid	recombinant
LJMUCV700	Brand 1	7/30/2021	transparent liquid	recombinant
LJMUCV701	Brand 1	7/30/2021	transparent liquid	recombinant
LJMUCV702	Brand 1	7/30/2021	transparent liquid	recombinant
LJMUCV703	Brand 1	7/30/2021	transparent liquid	recombinant
LJMUCV704	Brand 1	7/30/2021	transparent liquid	recombinant
LJMUCV705	Brand 1	7/30/2021	transparent liquid	recombinant

LJMUCV706	Brand 1	7/30/2021	transparent liquid	recombinant
LJMUCV707	Brand 1	7/30/2021	transparent liquid	recombinant
LJMUCV708	Brand 1	7/30/2021	transparent liquid	recombinant
LJMUCV709	Brand 1	7/30/2021	transparent liquid	recombinant
LJMUCV710	Brand 1	7/30/2021	transparent liquid	recombinant
LJMUCV711	Brand 1	7/30/2021	transparent liquid	recombinant
LJMUCV712	Brand 1	7/30/2021	transparent liquid	recombinant

LJMUCV713	Brand 1	7/30/2021	transparent liquid	recombinant
LJMUCV714	Brand 1	7/30/2021	transparent liquid	recombinant
LJMUCV715	Brand 1	7/30/2021	transparent liquid	recombinant
LJMUCV716	Brand 1	7/30/2021	transparent liquid	recombinant
LJMUCV717	Brand 1	7/30/2021	transparent liquid	recombinant
LJMUCV718	Brand 1	7/30/2021	transparent liquid	recombinant
LJMUCV719	Brand 1	7/30/2021	transparent liquid	recombinant

LJMUCV720	Brand 1	7/30/2021	transparent liquid	recombinant
LJMUCV721	Brand 1	7/30/2021	transparent liquid	recombinant
LJMUCV722	Brand 1	7/30/2021	transparent liquid	recombinant
LJMUCV723	Brand 1	7/30/2021	transparent liquid	recombinant
LJMUCV724	Brand 1	7/30/2021	transparent liquid	recombinant
LJMUCV725	Brand 1	7/30/2021	transparent liquid	recombinant
LJMUCV726	Brand 1	7/30/2021	transparent liquid	recombinant

LJMUCV727	Brand 1	7/30/2021	transparent liquid	recombinant
LJMUCV728	Brand 1	7/30/2021	transparent liquid	recombinant
LJMUCV729	Brand 1	7/30/2021	transparent liquid	recombinant
LJMUCV730	Brand 1	7/30/2021	transparent liquid	recombinant
LJMUCV731	Brand 1	7/30/2021	transparent liquid	recombinant
LJMUCV732	Brand 1	7/30/2021	transparent liquid	recombinant
LJMUCV733	Brand 1	7/30/2021	transparent liquid	recombinant

LJMUCV734	Brand 1	7/30/2021	transparent liquid	recombinant
LJMUCV735	Brand 1	7/30/2021	transparent liquid	recombinant
LJMUCV736	Brand 1	7/30/2021	transparent liquid	recombinant
LJMUCV737	Brand 1	7/30/2021	transparent liquid	recombinant
LJMUCV738	Brand 1	7/30/2021	transparent liquid	recombinant
LJMUCV739	Brand 1	7/30/2021	transparent liquid	recombinant
LJMUCV740	Brand 1	7/30/2021	transparent liquid	recombinant

LJMUCV741	Brand 1	7/30/2021	transparent liquid	recombinant
LJMUCV742	Brand 1	7/30/2021	transparent liquid	recombinant
LJMUCV743	Brand 1	7/30/2021	transparent liquid	recombinant
LJMUCV744	Brand 1	7/30/2021	transparent liquid	recombinant
LJMUCV745	Brand 1	7/30/2021	transparent liquid	recombinant
LJMUCV746	Brand 1	7/30/2021	transparent liquid	recombinant
LJMUCV747	Brand 1	7/30/2021	transparent liquid	recombinant

LJMUCV748	Brand 1	7/30/2021	transparent liquid	recombinant
LJMUCV749	Brand 1	7/30/2021	transparent liquid	recombinant
LJMUCV750	Brand 1	7/30/2021	transparent liquid	recombinant
LJMUCV751	Brand 1	7/30/2021	transparent liquid	recombinant
LJMUCV752	Brand 1	7/30/2021	transparent liquid	recombinant
LJMUCV753	Brand 1	7/30/2021	transparent liquid	recombinant
LJMUCV754	Brand 1	7/30/2021	transparent liquid	recombinant

LJMUCV755	Brand 1	7/30/2021	transparent liquid	recombinant
LJMUCV756	Brand 1	7/30/2021	transparent liquid	recombinant
LJMUCV757	Brand 1	7/30/2021	transparent liquid	recombinant
LJMUCV758	Brand 1	7/30/2021	transparent liquid	recombinant
LJMUCV759	Brand 1	7/30/2021	transparent liquid	recombinant
LJMUCV760	Brand 1	7/30/2021	transparent liquid	recombinant
LJMUCV761	Brand 1	7/30/2021	transparent liquid	recombinant

LJMUCV762	Brand 1	7/30/2021	transparent liquid	recombinant
LJMUCV763	Brand 1	7/30/2021	transparent liquid	recombinant
LJMUCV764	Brand 1	7/30/2021	transparent liquid	recombinant
LJMUCV765	Brand 1	7/30/2021	transparent liquid	recombinant
LJMUCV766	Brand 1	7/30/2021	transparent liquid	recombinant
LJMUCV767	Brand 1	7/30/2021	transparent liquid	recombinant
LJMUCV768	Brand 1	7/30/2021	transparent liquid	recombinant

LJMUCV769	Brand 1	7/30/2021	transparent liquid	recombinant
LJMUCV770	Brand 1	7/30/2021	transparent liquid	recombinant
LJMUCV771	Brand 1	7/30/2021	transparent liquid	recombinant
LJMUCV772	Brand 1	7/30/2021	transparent liquid	recombinant
LJMUCV773	Brand 1	7/30/2021	transparent liquid	recombinant
LJMUCV774	Brand 1	7/30/2021	transparent liquid	recombinant
LJMUCV775	Brand 1	7/30/2021	transparent liquid	recombinant

LJMUCV776	Brand 1	8/30/2021	transparent liquid	recombinant
LJMUCV777	Brand 2	10/30/2021	white liquid	suspension in 0.9% sodium chloride
LJMUCV778	Brand 2	10/30/2021	white liquid	suspension in 0.9% sodium chloride
LJMUCV779	Brand 2	10/30/2021	white liquid	suspension in 0.9% sodium chloride
LJMUCV780	Brand 2	10/30/2021	white liquid	suspension in 0.9% sodium chloride
LJMUCV781	Brand 2	10/30/2021	white liquid	suspension in 0.9% sodium chloride
LJMUCV782	Brand 2	10/30/2021	white liquid	suspension in 0.9% sodium chloride

LJMUCV783	Brand 2	10/30/2021	white liquid	suspension in 0.9% sodium chloride
LJMUCV784	Brand 2	10/30/2021	white liquid	suspension in 0.9% sodium chloride
LJMUCV785	Brand 2	10/30/2021	white liquid	suspension in 0.9% sodium chloride
LJMUCV786	Brand 2	10/30/2021	white liquid	suspension in 0.9% sodium chloride
LJMUCV787	Brand 2	10/30/2021	white liquid	suspension in 0.9% sodium chloride
LJMUCV788	Brand 2	10/30/2021	white liquid	suspension in 0.9% sodium chloride
LJMUCV789	Brand 2	10/30/2021	white liquid	suspension in 0.9% sodium chloride

LJMUCV790	Brand 2	10/30/2021	white liquid	suspension in 0.9% sodium chloride
LJMUCV791	Brand 2	10/30/2021	white liquid	suspension in 0.9% sodium chloride
LJMUCV792	Brand 2	10/30/2021	white liquid	suspension in 0.9% sodium chloride
LJMUCV793	Brand 2	10/30/2021	white liquid	suspension in 0.9% sodium chloride
LJMUCV794	Brand 2	10/30/2021	white liquid	suspension in 0.9% sodium chloride
LJMUCV795	Brand 2	10/30/2021	white liquid	suspension in 0.9% sodium chloride
LJMUCV796	Brand 2	10/30/2021	white liquid	suspension in 0.9% sodium chloride

LJMUCV797	Brand 2	10/30/2021	white liquid	suspension in 0.9% sodium chloride
LJMUCV798	Brand 2	10/30/2021	white liquid	suspension in 0.9% sodium chloride
LJMUCV799	Brand 2	10/30/2021	white liquid	suspension in 0.9% sodium chloride
LJMUCV800	Brand 2	10/30/2021	white liquid	suspension in 0.9% sodium chloride
LJMUCV801	Brand 2	10/30/2021	white liquid	suspension in 0.9% sodium chloride
LJMUCV802	Brand 2	10/30/2021	white liquid	suspension in 0.9% sodium chloride
LJMUCV803	Brand 2	10/30/2021	white liquid	suspension in 0.9% sodium chloride

LJMUCV804	Brand 2	10/30/2021	white liquid	suspension in 0.9% sodium chloride
LJMUCV805	Brand 2	10/30/2021	white liquid	suspension in 0.9% sodium chloride
LJMUCV806	Brand 2	10/30/2021	white liquid	suspension in 0.9% sodium chloride
LJMUCV807	Brand 2	10/30/2021	white liquid	suspension in 0.9% sodium chloride
LJMUCV808	Brand 2	10/30/2021	white liquid	suspension in 0.9% sodium chloride
LJMUCV809	Brand 2	10/30/2021	white liquid	suspension in 0.9% sodium chloride
LJMUCV810	Brand 2	10/30/2021	white liquid	suspension in 0.9% sodium chloride

LJMUCV811	Brand 2	10/30/2021	white liquid	suspension in 0.9% sodium chloride
LJMUCV812	Brand 2	10/30/2021	white liquid	suspension in 0.9% sodium chloride
LJMUCV813	Brand 2	10/30/2021	white liquid	suspension in 0.9% sodium chloride
LJMUCV814	Brand 2	10/30/2021	white liquid	suspension in 0.9% sodium chloride
LJMUCV815	Brand 2	10/30/2021	white liquid	suspension in 0.9% sodium chloride
LJMUCV816	Brand 2	10/30/2021	white liquid	suspension in 0.9% sodium chloride
LJMUCV817	Brand 2	10/30/2021	white liquid	suspension in 0.9% sodium chloride

LJMUCV818	Brand 2	10/30/2021	white liquid	suspension in 0.9% sodium chloride
LJMUCV819	Brand 2	10/30/2021	white liquid	suspension in 0.9% sodium chloride
LJMUCV820	Brand 2	10/30/2021	white liquid	suspension in 0.9% sodium chloride
LJMUCV821	Brand 2	10/30/2021	white liquid	suspension in 0.9% sodium chloride
LJMUCV822	Brand 2	10/30/2021	white liquid	suspension in 0.9% sodium chloride
LJMUCV823	Brand 2	10/30/2021	white liquid	suspension in 0.9% sodium chloride
LJMUCV824	Brand 2	10/30/2021	white liquid	suspension in 0.9% sodium chloride

LJMUCV825	Brand 2	10/30/2021	white liquid	suspension in 0.9% sodium chloride
LJMUCV826	Brand 2	10/30/2021	white liquid	suspension in 0.9% sodium chloride
LJMUCV827	Brand 2	10/30/2021	white liquid	suspension in 0.9% sodium chloride
LJMUCV828	Brand 2	10/30/2021	white liquid	suspension in 0.9% sodium chloride
LJMUCV829	Brand 2	10/30/2021	white liquid	suspension in 0.9% sodium chloride
LJMUCV830	Brand 2	10/30/2021	white liquid	suspension in 0.9% sodium chloride
LJMUCV831	Brand 2	10/30/2021	white liquid	suspension in 0.9% sodium chloride

LJMUCV832	Brand 2	10/30/2021	white liquid	suspension in 0.9% sodium chloride
LJMUCV833	Brand 2	10/30/2021	white liquid	suspension in 0.9% sodium chloride
LJMUCV834	Brand 2	10/30/2021	white liquid	suspension in 0.9% sodium chloride
LJMUCV835	Brand 2	10/30/2021	white liquid	suspension in 0.9% sodium chloride
LJMUCV836	Brand 2	10/30/2021	white liquid	suspension in 0.9% sodium chloride
LJMUCV837	Brand 2	10/30/2021	white liquid	suspension in 0.9% sodium chloride
LJMUCV838	Brand 2	10/30/2021	white liquid	suspension in 0.9% sodium chloride

LJMUCV839	Brand 2	10/30/2021	white liquid	suspension in 0.9% sodium chloride
LJMUCV840	Brand 2	10/30/2021	white liquid	suspension in 0.9% sodium chloride
LJMUCV841	Brand 2	10/30/2021	white liquid	suspension in 0.9% sodium chloride
LJMUCV842	Brand 2	10/30/2021	white liquid	suspension in 0.9% sodium chloride
LJMUCV843	Brand 2	10/30/2021	white liquid	suspension in 0.9% sodium chloride
LJMUCV844	Brand 2	10/30/2021	white liquid	suspension in 0.9% sodium chloride
LJMUCV845	Brand 2	10/30/2021	white liquid	suspension in 0.9% sodium chloride

LJMUCV846	Brand 2	10/30/2021	white liquid	suspension in 0.9% sodium chloride
LJMUCV847	Brand 2	10/30/2021	white liquid	suspension in 0.9% sodium chloride
LJMUCV848	Brand 2	10/30/2021	white liquid	suspension in 0.9% sodium chloride
LJMUCV849	Brand 2	10/30/2021	white liquid	suspension in 0.9% sodium chloride
LJMUCV850	Brand 2	10/30/2021	white liquid	suspension in 0.9% sodium chloride
LJMUCV851	Brand 2	10/30/2021	white liquid	suspension in 0.9% sodium chloride
LJMUCV852	Brand 2	10/30/2021	white liquid	suspension in 0.9% sodium chloride

LJMUCV853	Brand 2	10/30/2021	white liquid	suspension in 0.9% sodium chloride
LJMUCV854	Brand 2	10/30/2021	white liquid	suspension in 0.9% sodium chloride
LJMUCV855	Brand 2	10/30/2021	white liquid	suspension in 0.9% sodium chloride
LJMUCV856	Brand 2	10/30/2021	white liquid	suspension in 0.9% sodium chloride
LJMUCV857	Brand 2	10/30/2021	white liquid	suspension in 0.9% sodium chloride
LJMUCV858	Brand 2	10/30/2021	white liquid	suspension in 0.9% sodium chloride
LJMUCV859	Brand 2	10/30/2021	white liquid	suspension in 0.9% sodium chloride

LJMUCV860	Brand 2	10/30/2021	white liquid	suspension in 0.9% sodium chloride
LJMUCV861	Brand 2	10/30/2021	white liquid	suspension in 0.9% sodium chloride
LJMUCV862	Brand 2	10/30/2021	white liquid	suspension in 0.9% sodium chloride
LJMUCV863	Brand 2	10/30/2021	white liquid	suspension in 0.9% sodium chloride
LJMUCV864	Brand 2	10/30/2021	white liquid	suspension in 0.9% sodium chloride
LJMUCV865	Brand 2	10/30/2021	white liquid	suspension in 0.9% sodium chloride
LJMUCV866	Brand 2	10/30/2021	white liquid	suspension in 0.9% sodium chloride

LJMUCV867	Brand 2	10/30/2021	white liquid	suspension in 0.9% sodium chloride
LJMUCV868	Brand 2	10/30/2021	white liquid	suspension in 0.9% sodium chloride
LJMUCV869	Brand 2	10/30/2021	white liquid	suspension in 0.9% sodium chloride
LJMUCV870	Brand 2	10/30/2021	white liquid	suspension in 0.9% sodium chloride
LJMUCV871	Brand 2	10/30/2021	white liquid	suspension in 0.9% sodium chloride
LJMUCV872	Brand 2	10/30/2021	white liquid	suspension in 0.9% sodium chloride
LJMUCV873	Brand 2	10/30/2021	white liquid	suspension in 0.9% sodium chloride

LJMUCV874	Brand 2	10/30/2021	white liquid	suspension in 0.9% sodium chloride
LJMUCV875	Brand 2	10/30/2021	white liquid	suspension in 0.9% sodium chloride
LJMUCV876	Brand 2	10/30/2021	white liquid	suspension in 0.9% sodium chloride
LJMUCV877	Brand 2	10/30/2021	white liquid	suspension in 0.9% sodium chloride
LJMUCV878	Brand 2	10/30/2021	white liquid	suspension in 0.9% sodium chloride
LJMUCV879	Brand 2	10/30/2021	white liquid	suspension in 0.9% sodium chloride
LJMUCV880	Brand 2	10/30/2021	white liquid	suspension in 0.9% sodium chloride

LJMUCV881	Brand 2	10/30/2021	white liquid	suspension in 0.9% sodium chloride
LJMUCV882	Brand 2	10/30/2021	white liquid	suspension in 0.9% sodium chloride
LJMUCV883	Brand 2	10/30/2021	white liquid	suspension in 0.9% sodium chloride
LJMUCV884	Brand 2	10/30/2021	white liquid	suspension in 0.9% sodium chloride
LJMUCV885	Brand 2	10/30/2021	white liquid	suspension in 0.9% sodium chloride
LJMUCV886	Brand 2	10/30/2021	white liquid	suspension in 0.9% sodium chloride
LJMUCV887	Brand 2	10/30/2021	white liquid	suspension in 0.9% sodium chloride

LJMUCV888	Brand 2	10/30/2021	white liquid	suspension in 0.9% sodium chloride
LJMUCV889	Brand 2	10/30/2021	white liquid	suspension in 0.9% sodium chloride
LJMUCV890	Brand 2	10/30/2021	white liquid	suspension in 0.9% sodium chloride
LJMUCV891	Brand 2	10/30/2021	white liquid	suspension in 0.9% sodium chloride
LJMUCV892	Brand 2	10/30/2021	white liquid	suspension in 0.9% sodium chloride
LJMUCV893	Brand 2	10/30/2021	white liquid	suspension in 0.9% sodium chloride
LJMUCV894	Brand 2	10/30/2021	white liquid	suspension in 0.9% sodium chloride

LJMUCV895	Brand 2	10/30/2021	white liquid	suspension in 0.9% sodium chloride
LJMUCV896	Brand 2	10/30/2021	white liquid	suspension in 0.9% sodium chloride
LJMUCV897	Brand 2	10/30/2021	white liquid	suspension in 0.9% sodium chloride
LJMUCV898	Brand 2	10/30/2021	white liquid	suspension in 0.9% sodium chloride
LJMUCV899	Brand 2	10/30/2021	white liquid	suspension in 0.9% sodium chloride
LJMUCV900	Brand 2	10/30/2021	white liquid	suspension in 0.9% sodium chloride
LJMUCV901	Brand 2	10/30/2021	white liquid	suspension in 0.9% sodium chloride

LJMUCV902	Brand 2	10/30/2021	white liquid	suspension in 0.9% sodium chloride
LJMUCV903	Brand 2	10/30/2021	white liquid	suspension in 0.9% sodium chloride
LJMUCV904	Brand 2	10/30/2021	white liquid	suspension in 0.9% sodium chloride
LJMUCV905	Brand 2	10/30/2021	white liquid	suspension in 0.9% sodium chloride
LJMUCV906	Brand 2	10/30/2021	white liquid	suspension in 0.9% sodium chloride
LJMUCV907	Brand 2	10/30/2021	white liquid	suspension in 0.9% sodium chloride
LJMUCV908	Brand 2	10/30/2021	white liquid	suspension in 0.9% sodium chloride

LJMUCV909	Brand 2	10/30/2021	white liquid	suspension in 0.9% sodium chloride
LJMUCV910	Brand 2	10/30/2021	white liquid	suspension in 0.9% sodium chloride
LJMUCV911	Brand 2	10/30/2021	white liquid	suspension in 0.9% sodium chloride
LJMUCV912	Brand 2	10/30/2021	white liquid	suspension in 0.9% sodium chloride
LJMUCV913	Brand 2	10/30/2021	white liquid	suspension in 0.9% sodium chloride
LJMUCV914	Brand 2	10/30/2021	white liquid	suspension in 0.9% sodium chloride
LJMUCV915	Brand 2	10/30/2021	white liquid	suspension in 0.9% sodium chloride

LJMUCV916	Brand 2	10/30/2021	white liquid	suspension in 0.9% sodium chloride
LJMUCV917	Brand 2	10/30/2021	white liquid	suspension in 0.9% sodium chloride
LJMUCV918	Brand 2	10/30/2021	white liquid	suspension in 0.9% sodium chloride
LJMUCV919	Brand 2	10/30/2021	white liquid	suspension in 0.9% sodium chloride
LJMUCV920	Brand 2	10/30/2021	white liquid	suspension in 0.9% sodium chloride
LJMUCV921	Brand 2	10/30/2021	white liquid	suspension in 0.9% sodium chloride
LJMUCV922	Brand 2	10/30/2021	white liquid	suspension in 0.9% sodium chloride

LJMUCV923	Brand 2	10/30/2021	white liquid	suspension in 0.9% sodium chloride
LJMUCV924	Brand 2	10/30/2021	white liquid	suspension in 0.9% sodium chloride
LJMUCV925	Brand 2	10/30/2021	white liquid	suspension in 0.9% sodium chloride
LJMUCV926	Brand 2	10/30/2021	white liquid	suspension in 0.9% sodium chloride
LJMUCV927	Brand 2	10/30/2021	white liquid	suspension in 0.9% sodium chloride
LJMUCV928	Brand 2	10/30/2021	white liquid	suspension in 0.9% sodium chloride
LJMUCV929	Brand 2	10/30/2021	white liquid	suspension in 0.9% sodium chloride

LJMUCV930	Brand 2	10/30/2021	white liquid	suspension in 0.9% sodium chloride
LJMUCV931	Brand 2	10/30/2021	white liquid	suspension in 0.9% sodium chloride
LJMUCV932	Brand 2	10/30/2021	white liquid	suspension in 0.9% sodium chloride
LJMUCV933	Brand 2	10/30/2021	white liquid	suspension in 0.9% sodium chloride
LJMUCV934	Brand 2	10/30/2021	white liquid	suspension in 0.9% sodium chloride
LJMUCV935	Brand 2	10/30/2021	white liquid	suspension in 0.9% sodium chloride
LJMUCV936	Brand 2	10/30/2021	white liquid	suspension in 0.9% sodium chloride

LJMUCV937	Brand 2	10/30/2021	white liquid	suspension in 0.9% sodium chloride
LJMUCV938	Brand 2	10/30/2021	white liquid	suspension in 0.9% sodium chloride
LJMUCV939	Brand 2	10/30/2021	white liquid	suspension in 0.9% sodium chloride
LJMUCV940	Brand 2	10/30/2021	white liquid	suspension in 0.9% sodium chloride
LJMUCV941	Brand 2	10/30/2021	white liquid	suspension in 0.9% sodium chloride
LJMUCV942	Brand 2	10/30/2021	white liquid	suspension in 0.9% sodium chloride
LJMUCV943	Brand 2	10/30/2021	white liquid	suspension in 0.9% sodium chloride

LJMUCV944	Brand 2	10/30/2021	white liquid	suspension in 0.9% sodium chloride
LJMUCV945	Brand 2	10/30/2021	white liquid	suspension in 0.9% sodium chloride
LJMUCV946	Brand 2	10/30/2021	white liquid	suspension in 0.9% sodium chloride
LJMUCV947	Brand 2	10/30/2021	white liquid	suspension in 0.9% sodium chloride
LJMUCV948	Brand 2	10/30/2021	white liquid	suspension in 0.9% sodium chloride
LJMUCV949	Brand 2	10/30/2021	white liquid	suspension in 0.9% sodium chloride
LJMUCV950	Brand 2	10/30/2021	white liquid	suspension in 0.9% sodium chloride

LJMUCV951	Brand 2	10/30/2021	white liquid	suspension in 0.9% sodium chloride
LJMUCV952	Brand 2	10/30/2021	white liquid	suspension in 0.9% sodium chloride
LJMUCV953	Brand 2	10/30/2021	white liquid	suspension in 0.9% sodium chloride
LJMUCV954	Brand 2	10/30/2021	white liquid	suspension in 0.9% sodium chloride
LJMUCV955	Brand 2	10/30/2021	white liquid	suspension in 0.9% sodium chloride
LJMUCV956	Brand 2	10/30/2021	white liquid	suspension in 0.9% sodium chloride
LJMUCV957	Brand 2	10/30/2021	white liquid	suspension in 0.9% sodium chloride

LJMUCV958	Brand 2	10/30/2021	white liquid	suspension in 0.9% sodium chloride
LJMUCV959	Brand 2	10/30/2021	white liquid	suspension in 0.9% sodium chloride
LJMUCV960	Brand 2	10/30/2021	white liquid	suspension in 0.9% sodium chloride
LJMUCV961	Brand 2	10/30/2021	white liquid	suspension in 0.9% sodium chloride
LJMUCV962	Brand 2	10/30/2021	white liquid	suspension in 0.9% sodium chloride
LJMUCV963	Brand 2	10/30/2021	white liquid	suspension in 0.9% sodium chloride
LJMUCV964	Brand 2	10/30/2021	white liquid	suspension in 0.9% sodium chloride

LJMUCV965	Brand 2	10/30/2021	white liquid	suspension in 0.9% sodium chloride
LJMUCV966	Brand 2	10/30/2021	white liquid	suspension in 0.9% sodium chloride
LJMUCV967	Brand 2	10/30/2021	white liquid	suspension in 0.9% sodium chloride
LJMUCV968	Brand 2	10/30/2021	white liquid	suspension in 0.9% sodium chloride
LJMUCV969	Brand 2	10/30/2021	white liquid	suspension in 0.9% sodium chloride
LJMUCV970	Brand 2	10/30/2021	white liquid	suspension in 0.9% sodium chloride
LJMUCV971	Brand 2	10/30/2021	white liquid	suspension in 0.9% sodium chloride

LJMUCV972	Brand 2	10/30/2021	white liquid	suspension in 0.9% sodium chloride
LJMUCV973	Brand 2	10/30/2021	white liquid	suspension in 0.9% sodium chloride
LJMUCV974	Brand 2	10/30/2021	white liquid	suspension in 0.9% sodium chloride
LJMUCV975	Brand 2	10/30/2021	white liquid	suspension in 0.9% sodium chloride
LJMUCV976	Brand 2	10/30/2021	white liquid	suspension in 0.9% sodium chloride
LJMUCV977	Brand 2	10/30/2021	white liquid	suspension in 0.9% sodium chloride
LJMUCV978	Brand 2	10/30/2021	white liquid	suspension in 0.9% sodium chloride

LJMUCV979	Brand 2	10/30/2021	white liquid	suspension in 0.9% sodium chloride
LJMUCV980	Brand 2	10/30/2021	white liquid	suspension in 0.9% sodium chloride
LJMUCV981	Brand 2	10/30/2021	white liquid	suspension in 0.9% sodium chloride
LJMUCV982	Brand 2	10/30/2021	white liquid	suspension in 0.9% sodium chloride
LJMUCV983	Brand 2	10/30/2021	white liquid	suspension in 0.9% sodium chloride
LJMUCV984	Brand 2	10/30/2021	white liquid	suspension in 0.9% sodium chloride
LJMUCV985	Brand 2	10/30/2021	white liquid	suspension in 0.9% sodium chloride

LJMUCV986	Brand 2	10/30/2021	white liquid	suspension in 0.9% sodium chloride
LJMUCV987	Brand 2	10/30/2021	white liquid	suspension in 0.9% sodium chloride
LJMUCV988	Brand 2	10/30/2021	white liquid	suspension in 0.9% sodium chloride
LJMUCV989	Brand 2	10/30/2021	white liquid	suspension in 0.9% sodium chloride
LJMUCV990	Brand 2	10/30/2021	white liquid	suspension in 0.9% sodium chloride
LJMUCV991	Brand 2	10/30/2021	white liquid	suspension in 0.9% sodium chloride
LJMUCV992	Brand 2	10/30/2021	white liquid	suspension in 0.9% sodium chloride

LJMUCV993	Brand 2	10/30/2021	white liquid	suspension in 0.9% sodium chloride
LJMUCV994	Brand 2	10/30/2021	white liquid	suspension in 0.9% sodium chloride
LJMUCV995	Brand 2	10/30/2021	white liquid	suspension in 0.9% sodium chloride
LJMUCV996	Brand 2	10/30/2021	white liquid	suspension in 0.9% sodium chloride
LJMUCV997	Brand 2	10/30/2021	white liquid	suspension in 0.9% sodium chloride
LJMUCV998	Brand 2	10/30/2021	white liquid	suspension in 0.9% sodium chloride
LJMUCV999	Brand 2	10/30/2021	white liquid	suspension in 0.9% sodium chloride

LJMUCV1000	Brand 2	10/30/2021	white liquid	suspension in 0.9% sodium chloride
LJMUCV1001	Brand 2	10/30/2021	white liquid	suspension in 0.9% sodium chloride
LJMUCV1002	Brand 2	10/30/2021	white liquid	suspension in 0.9% sodium chloride
LJMUCV1003	Brand 2	10/30/2021	white liquid	suspension in 0.9% sodium chloride
LJMUCV1004	Brand 2	10/30/2021	white liquid	suspension in 0.9% sodium chloride
LJMUCV1005	Brand 2	10/30/2021	white liquid	suspension in 0.9% sodium chloride
LJMUCV1006	Brand 2	10/30/2021	white liquid	suspension in 0.9% sodium chloride

LJMUCV1007	Brand 2	10/30/2021	white liquid	suspension in 0.9% sodium chloride
LJMUCV1008	Brand 2	10/30/2021	white liquid	suspension in 0.9% sodium chloride
LJMUCV1009	Brand 2	10/30/2021	white liquid	suspension in 0.9% sodium chloride
LJMUCV1010	Brand 2	10/30/2021	white liquid	suspension in 0.9% sodium chloride
LJMUCV1011	Brand 2	10/30/2021	white liquid	suspension in 0.9% sodium chloride
LJMUCV1012	Brand 2	10/30/2021	white liquid	suspension in 0.9% sodium chloride
LJMUCV1013	Brand 2	10/30/2021	white liquid	suspension in 0.9% sodium chloride

LJMUCV1014	Brand 2	10/30/2021	white liquid	suspension in 0.9% sodium chloride
LJMUCV1015	Brand 2	10/30/2021	white liquid	suspension in 0.9% sodium chloride
LJMUCV1016	Brand 2	10/30/2021	white liquid	suspension in 0.9% sodium chloride
LJMUCV1017	Brand 2	10/30/2021	white liquid	suspension in 0.9% sodium chloride
LJMUCV1018	Brand 2	10/30/2021	white liquid	suspension in 0.9% sodium chloride
LJMUCV1019	Brand 2	10/30/2021	white liquid	suspension in 0.9% sodium chloride
LJMUCV1020	Brand 2	10/30/2021	white liquid	suspension in 0.9% sodium chloride

LJMUCV1021	Brand 2	10/30/2021	white liquid	suspension in 0.9% sodium chloride
LJMUCV1022	Brand 2	10/30/2021	white liquid	suspension in 0.9% sodium chloride
LJMUCV1023	Brand 2	10/30/2021	white liquid	suspension in 0.9% sodium chloride
LJMUCV1024	Brand 2	10/30/2021	white liquid	suspension in 0.9% sodium chloride
LJMUCV1025	Brand 2	10/30/2021	white liquid	suspension in 0.9% sodium chloride
LJMUCV1026	Brand 2	10/30/2021	white liquid	suspension in 0.9% sodium chloride
LJMUCV1027	Brand 2	10/30/2021	white liquid	suspension in 0.9% sodium chloride

LJMUCV1028	Brand 2	10/30/2021	white liquid	suspension in 0.9% sodium chloride
LJMUCV1029	Brand 2	10/30/2021	white liquid	suspension in 0.9% sodium chloride
LJMUCV1030	Brand 2	10/30/2021	white liquid	suspension in 0.9% sodium chloride
LJMUCV1031	Brand 2	10/30/2021	white liquid	suspension in 0.9% sodium chloride
LJMUCV1032	Brand 2	10/30/2021	white liquid	suspension in 0.9% sodium chloride
LJMUCV1033	Brand 2	10/30/2021	white liquid	suspension in 0.9% sodium chloride
LJMUCV1034	Brand 2	9/30/2021	white liquid	suspension in 0.9% sodium chloride

LJMUCV1035	Brand 2	10/30/2021	white liquid	suspension in 0.9% sodium chloride
LJMUCV1036	Brand 2	10/30/2021	white liquid	suspension in 0.9% sodium chloride
LJMUCV1037	Brand 2	10/30/2021	white liquid	suspension in 0.9% sodium chloride
LJMUCV1038	Brand 2	10/30/2021	white liquid	suspension in 0.9% sodium chloride
LJMUCV1039	Brand 2	10/30/2021	white liquid	suspension in 0.9% sodium chloride
LJMUCV1040	Brand 2	10/30/2021	white liquid	suspension in 0.9% sodium chloride
LJMUCV1041	Brand 2	10/30/2021	white liquid	suspension in 0.9% sodium chloride

LJMUCV1042	Brand 2	10/30/2021	white liquid	suspension in 0.9% sodium chloride
LJMUCV1043	Brand 2	10/30/2021	white liquid	suspension in 0.9% sodium chloride
LJMUCV1044	Brand 2	10/30/2021	white liquid	suspension in 0.9% sodium chloride
LJMUCV1045	Brand 2	10/30/2021	white liquid	suspension in 0.9% sodium chloride
LJMUCV1046	Brand 2	10/30/2021	white liquid	suspension in 0.9% sodium chloride
LJMUCV1047	Brand 2	10/30/2021	white liquid	suspension in 0.9% sodium chloride
LJMUCV1048	Brand 2	10/30/2021	white liquid	suspension in 0.9% sodium chloride

LJMUCV1049	Brand 2	10/30/2021	white liquid	suspension in 0.9% sodium chloride
LJMUCV1050	Brand 2	10/30/2021	white liquid	suspension in 0.9% sodium chloride
LJMUCV1051	Brand 2	10/30/2021	white liquid	suspension in 0.9% sodium chloride
LJMUCV1052	Brand 2	10/30/2021	white liquid	suspension in 0.9% sodium chloride
LJMUCV1053	Brand 2	9/30/2021	white liquid	suspension in 0.9% sodium chloride
LJMUCV1054	Brand 2	10/30/2021	white liquid	suspension in 0.9% sodium chloride
LJMUCV1055	Brand 2	10/30/2021	white liquid	suspension in 0.9% sodium chloride

LJMUCV1056	Brand 2	10/30/2021	white liquid	suspension in 0.9% sodium chloride
LJMUCV1057	Brand 2	10/30/2021	white liquid	suspension in 0.9% sodium chloride
LJMUCV1058	Brand 2	10/30/2021	white liquid	suspension in 0.9% sodium chloride
LJMUCV1059	Brand 2	10/30/2021	white liquid	suspension in 0.9% sodium chloride
LJMUCV1060	Brand 2	10/30/2021	white liquid	suspension in 0.9% sodium chloride
LJMUCV1061	Brand 2	10/30/2021	white liquid	suspension in 0.9% sodium chloride
LJMUCV1062	Brand 2	10/30/2021	white liquid	suspension in 0.9% sodium chloride

LJMUCV1063	Brand 2	10/30/2021	white liquid	suspension in 0.9% sodium chloride
LJMUCV1064	Brand 2	10/30/2021	white liquid	suspension in 0.9% sodium chloride
LJMUCV1065	Brand 2	10/30/2021	white liquid	suspension in 0.9% sodium chloride
LJMUCV1066	Brand 2	10/30/2021	white liquid	suspension in 0.9% sodium chloride
LJMUCV1067	Brand 2	10/30/2021	white liquid	suspension in 0.9% sodium chloride
LJMUCV1068	Brand 2	10/30/2021	white liquid	suspension in 0.9% sodium chloride
LJMUCV1069	Brand 2	10/30/2021	white liquid	suspension in 0.9% sodium chloride

LJMUCV1070	Brand 2	10/30/2021	white liquid	suspension in 0.9% sodium chloride
LJMUCV1071	Brand 2	10/30/2021	white liquid	suspension in 0.9% sodium chloride
LJMUCV1072	Brand 2	10/30/2021	white liquid	suspension in 0.9% sodium chloride
LJMUCV1073	Brand 2	10/30/2021	white liquid	suspension in 0.9% sodium chloride
LJMUCV1074	Brand 2	10/30/2021	white liquid	suspension in 0.9% sodium chloride
LJMUCV1075	Brand 2	10/30/2021	white liquid	suspension in 0.9% sodium chloride
LJMUCV1076	Brand 2	10/30/2021	white liquid	suspension in 0.9% sodium chloride

LJMUCV1077	Brand 2	10/30/2021	white liquid	suspension in 0.9% sodium chloride
LJMUCV1078	Brand 2	10/30/2021	white liquid	suspension in 0.9% sodium chloride
LJMUCV1079	Brand 2	10/30/2021	white liquid	suspension in 0.9% sodium chloride
LJMUCV1080	Brand 2	10/30/2021	white liquid	suspension in 0.9% sodium chloride
LJMUCV1081	Brand 2	10/30/2021	white liquid	suspension in 0.9% sodium chloride
LJMUCV1082	Brand 2	10/30/2021	white liquid	suspension in 0.9% sodium chloride
LJMUCV1083	Brand 2	10/30/2021	white liquid	suspension in 0.9% sodium chloride

LJMUCV1084	Brand 2	9/30/2021	white liquid	suspension in 0.9% sodium chloride
LJMUCV1085	Brand 2	10/30/2021	white liquid	suspension in 0.9% sodium chloride
LJMUCV1086	Brand 2	10/30/2021	white liquid	suspension in 0.9% sodium chloride
LJMUCV1087	Brand 2	9/30/2021	white liquid	suspension in 0.9% sodium chloride
LJMUCV1088	Brand 2	9/30/2021	white liquid	suspension in 0.9% sodium chloride
LJMUCV1089	Brand 2	9/30/2021	white liquid	suspension in 0.9% sodium chloride
LJMUCV1090	Brand 2	10/30/2021	white liquid	suspension in 0.9% sodium chloride

LJMUCV1091	Brand 2	10/30/2021	white liquid	suspension in 0.9% sodium chloride
LJMUCV1092	Brand 2	10/30/2021	white liquid	suspension in 0.9% sodium chloride
LJMUCV1093	Brand 2	10/30/2021	white liquid	suspension in 0.9% sodium chloride
LJMUCV1094	Brand 2	10/30/2021	white liquid	suspension in 0.9% sodium chloride
LJMUCV1095	Brand 2	10/30/2021	white liquid	suspension in 0.9% sodium chloride
LJMUCV1096	Brand 2	10/30/2021	white liquid	suspension in 0.9% sodium chloride
LJMUCV1097	Brand 2	10/30/2021	white liquid	suspension in 0.9% sodium chloride

LJMUCV1098	Brand 2	10/30/2021	white liquid	suspension in 0.9% sodium chloride
LJMUCV1099	Brand 2	10/30/2021	white liquid	suspension in 0.9% sodium chloride
LJMUCV1100	Brand 2	10/30/2021	white liquid	suspension in 0.9% sodium chloride
LJMUCV1101	Brand 2	9/30/2021	white liquid	suspension in 0.9% sodium chloride
LJMUCV1102	Brand 2	10/30/2021	white liquid	suspension in 0.9% sodium chloride
LJMUCV1103	Brand 2	10/30/2021	white liquid	suspension in 0.9% sodium chloride
LJMUCV1104	Brand 2	10/30/2021	white liquid	suspension in 0.9% sodium chloride

LJMUCV1105	Brand 2	9/30/2021	white liquid	suspension in 0.9% sodium chloride
LJMUCV1106	Brand 2	10/30/2021	white liquid	suspension in 0.9% sodium chloride
LJMUCV1107	Brand 2	10/30/2021	white liquid	suspension in 0.9% sodium chloride
LJMUCV1108	Brand 2	9/30/2021	white liquid	suspension in 0.9% sodium chloride
LJMUCV1109	Brand 2	10/30/2021	white liquid	suspension in 0.9% sodium chloride
LJMUCV1110	Brand 2	10/30/2021	white liquid	suspension in 0.9% sodium chloride
LJMUCV1111	Brand 2	10/30/2021	white liquid	suspension in 0.9% sodium chloride

LJMUCV1112	Brand 2	10/30/2021	white liquid	suspension in 0.9% sodium chloride
LJMUCV1113	Brand 2	10/30/2021	white liquid	suspension in 0.9% sodium chloride
LJMUCV1114	Brand 2	10/30/2021	white liquid	suspension in 0.9% sodium chloride
LJMUCV1115	Brand 2	10/30/2021	white liquid	suspension in 0.9% sodium chloride
LJMUCV1116	Brand 2	9/30/2021	white liquid	suspension in 0.9% sodium chloride
LJMUCV1117	Brand 2	9/30/2021	white liquid	suspension in 0.9% sodium chloride
LJMUCV1118	Brand 2	10/30/2021	white liquid	suspension in 0.9% sodium chloride

LJMUCV1119	Brand 2	9/30/2021	white liquid	suspension in 0.9% sodium chloride
LJMUCV1120	Brand 2	10/30/2021	white liquid	suspension in 0.9% sodium chloride
LJMUCV1121	Brand 2	10/30/2021	white liquid	suspension in 0.9% sodium chloride
LJMUCV1122	Brand 2	9/30/2021	white liquid	suspension in 0.9% sodium chloride
LJMUCV1123	Brand 2	10/30/2021	white liquid	suspension in 0.9% sodium chloride
LJMUCV1124	Brand 2	10/30/2021	white liquid	suspension in 0.9% sodium chloride
LJMUCV1125	Brand 2	10/30/2021	white liquid	suspension in 0.9% sodium chloride

LJMUCV1126	Brand 2	10/30/2021	white liquid	suspension in 0.9% sodium chloride
LJMUCV1127	Brand 2	10/30/2021	white liquid	suspension in 0.9% sodium chloride
LJMUCV1128	Brand 2	10/30/2021	white liquid	suspension in 0.9% sodium chloride
LJMUCV1129	Brand 2	9/30/2021	white liquid	suspension in 0.9% sodium chloride
LJMUCV1130	Brand 2	10/30/2021	white liquid	suspension in 0.9% sodium chloride
LJMUCV1131	Brand 2	10/30/2021	white liquid	suspension in 0.9% sodium chloride
LJMUCV1132	Brand 2	10/30/2021	white liquid	suspension in 0.9% sodium chloride

LJMUCV1133	Brand 2	10/30/2021	white liquid	suspension in 0.9% sodium chloride
LJMUCV1134	Brand 2	10/30/2021	white liquid	suspension in 0.9% sodium chloride
LJMUCV1135	Brand 2	10/30/2021	white liquid	suspension in 0.9% sodium chloride
LJMUCV1136	Brand 2	10/30/2021	white liquid	suspension in 0.9% sodium chloride
LJMUCV1137	Brand 2	10/30/2021	white liquid	suspension in 0.9% sodium chloride
LJMUCV1138	Brand 2	10/30/2021	white liquid	suspension in 0.9% sodium chloride
LJMUCV1139	Brand 2	10/30/2021	white liquid	suspension in 0.9% sodium chloride

LJMUCV1140	Brand 2	10/30/2021	white liquid	suspension in 0.9% sodium chloride
LJMUCV1141	Brand 2	10/30/2021	white liquid	suspension in 0.9% sodium chloride
LJMUCV1142	Brand 2	10/30/2021	white liquid	suspension in 0.9% sodium chloride
LJMUCV1143	Brand 2	9/30/2021	white liquid	suspension in 0.9% sodium chloride
LJMUCV1144	Brand 2	10/30/2021	white liquid	suspension in 0.9% sodium chloride
LJMUCV1145	Brand 2	10/30/2021	white liquid	suspension in 0.9% sodium chloride
LJMUCV1146	Brand 2	10/30/2021	white liquid	suspension in 0.9% sodium chloride

LJMUCV1147	Brand 2	10/30/2021	white liquid	suspension in 0.9% sodium chloride
LJMUCV1148	Brand 2	10/30/2021	white liquid	suspension in 0.9% sodium chloride
LJMUCV1149	Brand 2	10/30/2021	white liquid	suspension in 0.9% sodium chloride
LJMUCV1150	Brand 2	10/30/2021	white liquid	suspension in 0.9% sodium chloride
LJMUCV1151	Brand 2	10/30/2021	white liquid	suspension in 0.9% sodium chloride
LJMUCV1152	Brand 2	10/30/2021	white liquid	suspension in 0.9% sodium chloride
LJMUCV1153	Brand 2	10/30/2021	white liquid	suspension in 0.9% sodium chloride

LJMUCV1154	Brand 2	10/30/2021	white liquid	suspension in 0.9% sodium chloride
LJMUCV1155	Brand 2	10/30/2021	white liquid	suspension in 0.9% sodium chloride
LJMUCV1156	Brand 2	10/30/2021	white liquid	suspension in 0.9% sodium chloride
LJMUCV1157	Brand 2	10/30/2021	white liquid	suspension in 0.9% sodium chloride
LJMUCV1158	Brand 2	10/30/2021	white liquid	suspension in 0.9% sodium chloride
LJMUCV1159	Brand 2	10/30/2021	white liquid	suspension in 0.9% sodium chloride
LJMUCV1160	Brand 2	10/30/2021	white liquid	suspension in 0.9% sodium chloride

LJMUCV1161	Brand 2	9/30/2021	white liquid	suspension in 0.9% sodium chloride
LJMUCV1162	Brand 2	10/30/2021	white liquid	suspension in 0.9% sodium chloride
LJMUCV1163	Brand 2	9/30/2021	white liquid	suspension in 0.9% sodium chloride
LJMUCV1164	Brand 2	10/30/2021	white liquid	suspension in 0.9% sodium chloride
LJMUCV1165	Brand 2	10/30/2021	white liquid	suspension in 0.9% sodium chloride
LJMUCV1166	Brand 2	10/30/2021	white liquid	suspension in 0.9% sodium chloride
LJMUCV1167	Brand 2	10/30/2021	white liquid	suspension in 0.9% sodium chloride

LJMUCV1168	Brand 2	10/30/2021	white liquid	suspension in 0.9% sodium chloride
LJMUCV1169	Brand 2	10/30/2021	white liquid	suspension in 0.9% sodium chloride
LJMUCV1170	Brand 2	10/30/2021	white liquid	suspension in 0.9% sodium chloride
LJMUCV1171	Brand 2	10/30/2021	white liquid	suspension in 0.9% sodium chloride
LJMUCV1172	Brand 2	10/30/2021	white liquid	suspension in 0.9% sodium chloride
LJMUCV1173	Brand 2	9/30/2021	white liquid	suspension in 0.9% sodium chloride
LJMUCV1174	Brand 2	10/30/2021	white liquid	suspension in 0.9% sodium chloride

LJMUCV1175	Brand 2	9/30/2021	white liquid	suspension in 0.9% sodium chloride
LJMUCV1176	Brand 2	9/30/2021	white liquid	suspension in 0.9% sodium chloride
LJMUCV1177	Brand 2	10/30/2021	white liquid	suspension in 0.9% sodium chloride
LJMUCV1178	Brand 2	10/30/2021	white liquid	suspension in 0.9% sodium chloride
LJMUCV1179	Brand 2	10/30/2021	white liquid	suspension in 0.9% sodium chloride
LJMUCV1180	Brand 2	10/30/2021	white liquid	suspension in 0.9% sodium chloride
LJMUCV1181	Brand 2	10/30/2021	white liquid	suspension in 0.9% sodium chloride

LJMUCV1182	Brand 2	9/30/2021	white liquid	suspension in 0.9% sodium chloride
LJMUCV1183	Brand 2	10/30/2021	white liquid	suspension in 0.9% sodium chloride
LJMUCV1184	Brand 2	9/30/2021	white liquid	suspension in 0.9% sodium chloride
LJMUCV1185	Brand 2	10/30/2021	white liquid	suspension in 0.9% sodium chloride
LJMUCV1186	Brand 2	10/30/2021	white liquid	suspension in 0.9% sodium chloride
LJMUCV1187	Brand 2	10/30/2021	white liquid	suspension in 0.9% sodium chloride
LJMUCV1188	Brand 2	10/30/2021	white liquid	suspension in 0.9% sodium chloride

LJMUCV1189	Brand 2	10/30/2021	white liquid	suspension in 0.9% sodium chloride
LJMUCV1190	Brand 2	9/30/2021	white liquid	suspension in 0.9% sodium chloride
LJMUCV1191	Brand 2	10/30/2021	white liquid	suspension in 0.9% sodium chloride
LJMUCV1192	Brand 2	10/30/2021	white liquid	suspension in 0.9% sodium chloride
LJMUCV1193	Brand 2	10/30/2021	white liquid	suspension in 0.9% sodium chloride
LJMUCV1194	Brand 2	10/30/2021	white liquid	suspension in 0.9% sodium chloride
LJMUCV1195	Brand 2	9/30/2021	white liquid	suspension in 0.9% sodium chloride

LJMUCV1196	Brand 2	10/30/2021	white liquid	suspension in 0.9% sodium chloride
LJMUCV1197	Brand 2	10/30/2021	white liquid	suspension in 0.9% sodium chloride
LJMUCV1198	Brand 2	10/30/2021	white liquid	suspension in 0.9% sodium chloride
LJMUCV1199	Brand 2	10/30/2021	white liquid	suspension in 0.9% sodium chloride
LJMUCV1200	Brand 2	9/30/2021	white liquid	suspension in 0.9% sodium chloride
LJMUCV1201	Brand 2	10/30/2021	white liquid	suspension in 0.9% sodium chloride
LJMUCV1202	Brand 2	9/30/2021	white liquid	suspension in 0.9% sodium chloride

LJMUCV1203	Brand 2	9/30/2021	white liquid	suspension in 0.9% sodium chloride
LJMUCV1204	Brand 2	10/30/2021	white liquid	suspension in 0.9% sodium chloride
LJMUCV1205	Brand 2	10/30/2021	white liquid	suspension in 0.9% sodium chloride
LJMUCV1206	Brand 2	9/30/2021	white liquid	suspension in 0.9% sodium chloride
LJMUCV1207	Brand 2	10/30/2021	white liquid	suspension in 0.9% sodium chloride
LJMUCV1208	Brand 2	10/30/2021	white liquid	suspension in 0.9% sodium chloride
LJMUCV1209	Brand 2	10/30/2021	white liquid	suspension in 0.9% sodium chloride

LJMUCV1210	Brand 2	9/30/2021	white liquid	suspension in 0.9% sodium chloride
LJMUCV1211	Brand 2	10/30/2021	white liquid	suspension in 0.9% sodium chloride
LJMUCV1212	Brand 2	9/30/2021	white liquid	suspension in 0.9% sodium chloride
LJMUCV1213	Brand 2	9/30/2021	white liquid	suspension in 0.9% sodium chloride
LJMUCV1214	Brand 2	10/30/2021	white liquid	suspension in 0.9% sodium chloride
LJMUCV1215	Brand 2	10/30/2021	white liquid	suspension in 0.9% sodium chloride
LJMUCV1216	Brand 2	9/30/2021	white liquid	suspension in 0.9% sodium chloride

LJMUCV1217	Brand 2	10/30/2021	white liquid	suspension in 0.9% sodium chloride
LJMUCV1218	Brand 2	10/30/2021	white liquid	suspension in 0.9% sodium chloride
LJMUCV1219	Brand 2	10/30/2021	white liquid	suspension in 0.9% sodium chloride
LJMUCV1220	Brand 2	10/30/2021	white liquid	suspension in 0.9% sodium chloride
LJMUCV1221	Brand 2	9/30/2021	white liquid	suspension in 0.9% sodium chloride
LJMUCV1222	Brand 2	10/30/2021	white liquid	suspension in 0.9% sodium chloride
LJMUCV1223	Brand 2	10/30/2021	white liquid	suspension in 0.9% sodium chloride

LJMUCV1224	Brand 2	9/30/2021	white liquid	suspension in 0.9% sodium chloride
LJMUCV1225	Brand 2	10/30/2021	white liquid	suspension in 0.9% sodium chloride
LJMUCV1226	Brand 2	10/30/2021	white liquid	suspension in 0.9% sodium chloride
LJMUCV1227	Brand 2	10/30/2021	white liquid	suspension in 0.9% sodium chloride
LJMUCV1228	Brand 2	10/30/2021	white liquid	suspension in 0.9% sodium chloride
LJMUCV1229	Brand 2	10/30/2021	white liquid	suspension in 0.9% sodium chloride
LJMUCV1230	Brand 2	10/30/2021	white liquid	suspension in 0.9% sodium chloride

LJMUCV1231	Brand 2	10/30/2021	white liquid	suspension in 0.9% sodium chloride
LJMUCV1232	Brand 2	10/30/2021	white liquid	suspension in 0.9% sodium chloride
LJMUCV1233	Brand 2	10/30/2021	white liquid	suspension in 0.9% sodium chloride
LJMUCV1234	Brand 2	10/30/2021	white liquid	suspension in 0.9% sodium chloride
LJMUCV1235	Brand 2	9/30/2021	white liquid	suspension in 0.9% sodium chloride
LJMUCV1236	Brand 2	10/30/2021	white liquid	suspension in 0.9% sodium chloride
LJMUCV1237	Brand 2	10/30/2021	white liquid	suspension in 0.9% sodium chloride

LJMUCV1238	Brand 2	10/30/2021	white liquid	suspension in 0.9% sodium chloride
LJMUCV1239	Brand 2	10/30/2021	white liquid	suspension in 0.9% sodium chloride
LJMUCV1240	Brand 2	10/30/2021	white liquid	suspension in 0.9% sodium chloride
LJMUCV1241	Brand 2	10/30/2021	white liquid	suspension in 0.9% sodium chloride
LJMUCV1242	Brand 2	10/30/2021	white liquid	suspension in 0.9% sodium chloride
LJMUCV1243	Brand 2	10/30/2021	white liquid	suspension in 0.9% sodium chloride
LJMUCV1244	Brand 2	10/30/2021	white liquid	suspension in 0.9% sodium chloride

LJMUCV1245	Brand 2	9/30/2021	white liquid	suspension in 0.9% sodium chloride
LJMUCV1246	Brand 2	10/30/2021	white liquid	suspension in 0.9% sodium chloride
LJMUCV1247	Brand 2	9/30/2021	white liquid	suspension in 0.9% sodium chloride
LJMUCV1248	Brand 2	10/30/2021	white liquid	suspension in 0.9% sodium chloride
LJMUCV1249	Brand 2	10/30/2021	white liquid	suspension in 0.9% sodium chloride
LJMUCV1250	Brand 2	10/30/2021	white liquid	suspension in 0.9% sodium chloride
LJMUCV1251	Brand 2	9/30/2021	white liquid	suspension in 0.9% sodium chloride

LJMUCV1252	Brand 2	9/30/2021	white liquid	suspension in 0.9% sodium chloride
LJMUCV1253	Brand 2	9/30/2021	white liquid	suspension in 0.9% sodium chloride
LJMUCV1254	Brand 2	10/30/2021	white liquid	suspension in 0.9% sodium chloride
LJMUCV1255	Brand 2	10/30/2021	white liquid	suspension in 0.9% sodium chloride
LJMUCV1256	Brand 2	10/30/2021	white liquid	suspension in 0.9% sodium chloride
LJMUCV1257	Brand 2	10/30/2021	white liquid	suspension in 0.9% sodium chloride
LJMUCV1258	Brand 2	10/30/2021	white liquid	suspension in 0.9% sodium chloride

LJMUCV1259	Brand 2	9/30/2021	white liquid	suspension in 0.9% sodium chloride
LJMUCV1260	Brand 2	10/30/2021	white liquid	suspension in 0.9% sodium chloride
LJMUCV1261	Brand 2	10/30/2021	white liquid	suspension in 0.9% sodium chloride
LJMUCV1262	Brand 2	9/30/2021	white liquid	suspension in 0.9% sodium chloride
LJMUCV1263	Brand 2	9/30/2021	white liquid	suspension in 0.9% sodium chloride
LJMUCV1264	Brand 2	10/30/2021	white liquid	suspension in 0.9% sodium chloride
LJMUCV1265	Brand 2	10/30/2021	white liquid	suspension in 0.9% sodium chloride

LJMUCV1266	Brand 2	9/30/2021	white liquid	suspension in 0.9% sodium chloride
LJMUCV1267	Brand 2	10/30/2021	white liquid	suspension in 0.9% sodium chloride
LJMUCV1268	Brand 2	10/30/2021	white liquid	suspension in 0.9% sodium chloride
LJMUCV1269	Brand 2	10/30/2021	white liquid	suspension in 0.9% sodium chloride
LJMUCV1270	Brand 2	9/30/2021	white liquid	suspension in 0.9% sodium chloride
LJMUCV1271	Brand 2	9/30/2021	white liquid	suspension in 0.9% sodium chloride
LJMUCV1272	Brand 2	10/30/2021	white liquid	suspension in 0.9% sodium chloride

LJMUCV1273	Brand 2	9/30/2021	white liquid	suspension in 0.9% sodium chloride
LJMUCV1274	Brand 2	9/30/2021	white liquid	suspension in 0.9% sodium chloride
LJMUCV1275	Brand 2	9/30/2021	white liquid	suspension in 0.9% sodium chloride
LJMUCV1276	Brand 2	10/30/2021	white liquid	suspension in 0.9% sodium chloride
LJMUCV1277	Brand 2	10/30/2021	white liquid	suspension in 0.9% sodium chloride
LJMUCV1278	Brand 2	10/30/2021	white liquid	suspension in 0.9% sodium chloride
LJMUCV1279	Brand 2	10/30/2021	white liquid	suspension in 0.9% sodium chloride

LJMUCV1280	Brand 2	9/30/2021	white liquid	suspension in 0.9% sodium chloride
LJMUCV1281	Brand 2	10/30/2021	white liquid	suspension in 0.9% sodium chloride
LJMUCV1282	Brand 2	9/30/2021	white liquid	suspension in 0.9% sodium chloride
LJMUCV1283	Brand 2	10/30/2021	white liquid	suspension in 0.9% sodium chloride
LJMUCV1284	Brand 2	10/30/2021	white liquid	suspension in 0.9% sodium chloride
LJMUCV1285	Brand 2	10/30/2021	white liquid	suspension in 0.9% sodium chloride
LJMUCV1286	Brand 2	9/30/2021	white liquid	suspension in 0.9% sodium chloride

LJMUCV1287	Brand 2	10/30/2021	white liquid	suspension in 0.9% sodium chloride
LJMUCV1288	Brand 2	10/30/2021	white liquid	suspension in 0.9% sodium chloride
LJMUCV1289	Brand 2	10/30/2021	white liquid	suspension in 0.9% sodium chloride
LJMUCV1290	Brand 2	9/30/2021	white liquid	suspension in 0.9% sodium chloride
LJMUCV1291	Brand 2	10/30/2021	white liquid	suspension in 0.9% sodium chloride
LJMUCV1292	Brand 2	10/30/2021	white liquid	suspension in 0.9% sodium chloride
LJMUCV1293	Brand 2	10/30/2021	white liquid	suspension in 0.9% sodium chloride

LJMUCV1294	Brand 2	9/30/2021	white liquid	suspension in 0.9% sodium chloride
LJMUCV1295	Brand 2	10/30/2021	white liquid	suspension in 0.9% sodium chloride
LJMUCV1296	Brand 2	10/30/2021	white liquid	suspension in 0.9% sodium chloride
LJMUCV1297	Brand 2	10/30/2021	white liquid	suspension in 0.9% sodium chloride
LJMUCV1298	Brand 2	10/30/2021	white liquid	suspension in 0.9% sodium chloride
LJMUCV1299	Brand 2	9/30/2021	white liquid	suspension in 0.9% sodium chloride
LJMUCV1300	Brand 2	10/30/2021	white liquid	suspension in 0.9% sodium chloride

LJMUCV1301	Brand 2	10/30/2021	white liquid	suspension in 0.9% sodium chloride
LJMUCV1302	Brand 2	10/30/2021	white liquid	suspension in 0.9% sodium chloride
LJMUCV1303	Brand 2	10/30/2021	white liquid	suspension in 0.9% sodium chloride
LJMUCV1304	Brand 2	10/30/2021	white liquid	suspension in 0.9% sodium chloride
LJMUCV1305	Brand 2	10/30/2021	white liquid	suspension in 0.9% sodium chloride
LJMUCV1306	Brand 2	10/30/2021	white liquid	suspension in 0.9% sodium chloride
LJMUCV1307	Brand 2	9/30/2021	white liquid	suspension in 0.9% sodium chloride

LJMUCV1308	Brand 2	9/30/2021	white liquid	suspension in 0.9% sodium chloride
LJMUCV1309	Brand 2	10/30/2021	white liquid	suspension in 0.9% sodium chloride
LJMUCV1310	Brand 2	9/30/2021	white liquid	suspension in 0.9% sodium chloride
LJMUCV1311	Brand 2	10/30/2021	white liquid	suspension in 0.9% sodium chloride
LJMUCV1312	Brand 2	9/30/2021	white liquid	suspension in 0.9% sodium chloride
LJMUCV1313	Brand 2	10/30/2021	white liquid	suspension in 0.9% sodium chloride
LJMUCV1314	Brand 2	10/30/2021	white liquid	suspension in 0.9% sodium chloride

LJMUCV1315	Brand 2	10/30/2021	white liquid	suspension in 0.9% sodium chloride
LJMUCV1316	Brand 2	9/30/2021	white liquid	suspension in 0.9% sodium chloride
LJMUCV1317	Brand 1	7/30/2021	transparent liquid	recombinant
LJMUCV1318	Brand 1	8/30/2021	transparent liquid	recombinant
LJMUCV1319	Brand 1	7/30/2021	transparent liquid	recombinant
LJMUCV1320	Brand 1	8/30/2021	transparent liquid	recombinant
LJMUCV1321	Brand 1	8/30/2021	transparent liquid	recombinant

LJMUCV1322	Brand 1	8/30/2021	transparent liquid	recombinant
LJMUCV1323	Brand 1	8/30/2021	transparent liquid	recombinant
LJMUCV1324	Brand 1	7/30/2021	transparent liquid	recombinant
LJMUCV1325	Brand 1	7/30/2021	transparent liquid	recombinant
LJMUCV1326	Brand 1	8/30/2021	transparent liquid	recombinant
LJMUCV1327	Brand 1	8/30/2021	transparent liquid	recombinant
LJMUCV1328	Brand 1	8/30/2021	transparent liquid	recombinant

LJMUCV1329	Brand 1	8/30/2021	transparent liquid	recombinant
LJMUCV1330	Brand 1	7/30/2021	transparent liquid	recombinant
LJMUCV1331	Brand 1	7/30/2021	transparent liquid	recombinant
LJMUCV1332	Brand 1	8/30/2021	transparent liquid	recombinant
LJMUCV1333	Brand 1	8/30/2021	transparent liquid	recombinant
LJMUCV1334	Brand 1	8/30/2021	transparent liquid	recombinant
LJMUCV1335	Brand 1	8/30/2021	transparent liquid	recombinant

LJMUCV1336	Brand 1	8/30/2021	transparent liquid	recombinant
LJMUCV1337	Brand 1	8/30/2021	transparent liquid	recombinant
LJMUCV1338	Brand 1	8/30/2021	transparent liquid	recombinant
LJMUCV1339	Brand 1	7/30/2021	transparent liquid	recombinant
LJMUCV1340	Brand 1	8/30/2021	transparent liquid	recombinant
LJMUCV1341	Brand 1	8/30/2021	transparent liquid	recombinant
LJMUCV1342	Brand 1	7/30/2021	transparent liquid	recombinant

LJMUCV1343	Brand 1	7/30/2021	transparent liquid	recombinant
LJMUCV1344	Brand 1	8/30/2021	transparent liquid	recombinant
LJMUCV1345	Brand 1	8/30/2021	transparent liquid	recombinant
LJMUCV1346	Brand 1	8/30/2021	transparent liquid	recombinant
LJMUCV1347	Brand 1	7/30/2021	transparent liquid	recombinant
LJMUCV1348	Brand 3	07/10/2023	white liquid	
LJMUCV1349	Brand 3	07/10/2023	white liquid	

LJMUCV1350	Brand 2		white liquid	suspension in 0.9% sodium chloride
LJMUCV1351	Brand 2		white liquid	suspension in 0.9% sodium chloride
LJMUCV1352	Brand 3	07/10/2023	white liquid	
LJMUCV1353	Brand 3	07/10/2023	white liquid	
LJMUCV1354	Brand 2		white liquid	suspension in 0.9% sodium chloride
LJMUCV1355	Brand 2		white liquid	suspension in 0.9% sodium chloride
LJMUCV1356	Brand 3	07/10/2023	transparent liquid	suspension in 0.9% sodium chloride

LJMUCV1357	Brand 3	07/10/2023	transparent liquid	suspension in 0.9% sodium chloride
LJMUCV1358	Brand 3	07/10/2023	transparent liquid	suspension in 0.9% sodium chloride
LJMUCV1359	Brand 3	07/10/2023	transparent liquid	suspension in 0.9% sodium chloride
LJMUCV1360	Brand 3	07/10/2023	transparent liquid	suspension in 0.9% sodium chloride
LJMUCV1361	Brand 3	07/10/2023	transparent liquid	suspension in 0.9% sodium chloride
LJMUCV1362	Brand 3	07/10/2023	transparent liquid	suspension in 0.9% sodium chloride
LJMUCV1363	Brand 3	07/10/2023	transparent liquid	suspension in 0.9% sodium chloride

LJMUCV1364	Brand 3	07/10/2023	transparent liquid	suspension in 0.9% sodium chloride
LJMUCV1365	Brand 3	07/10/2023	transparent liquid	suspension in 0.9% sodium chloride
LJMUCV1366	Brand 2		white liquid	suspension in 0.9% sodium chloride
LJMUCV1367	Brand 2		white liquid	suspension in 0.9% sodium chloride
LJMUCV1368	Brand 2		white liquid	suspension in 0.9% sodium chloride
LJMUCV1369	Brand 2		white liquid	suspension in 0.9% sodium chloride
LJMUCV1370	Brand 2		white liquid	suspension in 0.9% sodium chloride

LJMUCV1371	Brand 3	10/07/2023	transparent liquid	suspension in 0.9% sodium chloride
LJMUCV1372	Brand 3	10/07/2023	transparent liquid	suspension in 0.9% sodium chloride
LJMUCV1373	Brand 3	10/07/2023	transparent liquid	suspension in 0.9% sodium chloride
LJMUCV1374	Brand 3	10/07/2023	transparent liquid	suspension in 0.9% sodium chloride
LJMUCV1375	Brand 3	10/07/2023	transparent liquid	suspension in 0.9% sodium chloride
LJMUCV1376	Brand 3	10/07/2023	transparent liquid	suspension in 0.9% sodium chloride
LJMUCV1377	Brand 3	10/07/2023	transparent liquid	suspension in 0.9% sodium chloride

LJMUCV1378	Brand 3	10/07/2023	transparent liquid	suspension in 0.9% sodium chloride
LJMUCV1379	Brand 3	10/07/2023	transparent liquid	suspension in 0.9% sodium chloride
LJMUCV1380	Brand 3	10/07/2023	transparent liquid	suspension in 0.9% sodium chloride
LJMUCV1381	Brand 3	10/07/2023	transparent liquid	suspension in 0.9% sodium chloride
LJMUCV1382	Brand 3	10/07/2023	transparent liquid	suspension in 0.9% sodium chloride
LJMUCV1383	Brand 3	10/07/2023	transparent liquid	suspension in 0.9% sodium chloride
LJMUCV1384	Brand 3	10/07/2023	transparent liquid	suspension in 0.9% sodium chloride

LJMUCV1385	Brand 3	10/07/2023	transparent liquid	suspension in 0.9% sodium chloride
LJMUCV1386	Brand 3	10/07/2023	transparent liquid	suspension in 0.9% sodium chloride
LJMUCV1387	Brand 3	10/07/2023	transparent liquid	suspension in 0.9% sodium chloride
LJMUCV1388	Brand 3	10/07/2023	transparent liquid	suspension in 0.9% sodium chloride
LJMUCV1389	Brand 3	10/07/2023	transparent liquid	suspension in 0.9% sodium chloride
LJMUCV1390	Brand 3	10/07/2023	transparent liquid	suspension in 0.9% sodium chloride
LJMUCV1391	Brand 3	10/07/2023	transparent liquid	suspension in 0.9% sodium chloride

LJMUCV1392	Brand 3	10/07/2023	transparent liquid	suspension in 0.9% sodium chloride
LJMUCV1393	Brand 3	10/07/2023	transparent liquid	suspension in 0.9% sodium chloride
LJMUCV1394	Brand 3	10/07/2023	transparent liquid	suspension in 0.9% sodium chloride
LJMUCV1395	Brand 3	10/07/2023	transparent liquid	suspension in 0.9% sodium chloride
LJMUCV1396	Brand 3	10/07/2023	transparent liquid	suspension in 0.9% sodium chloride
LJMUCV1397	Brand 3	10/07/2023	transparent liquid	suspension in 0.9% sodium chloride
LJMUCV1398	Brand 3	10/07/2023	transparent liquid	suspension in 0.9% sodium chloride

LJMUCV1399	Brand 3	10/07/2023	transparent liquid	suspension in 0.9% sodium chloride
LJMUCV1400	Brand 3	10/07/2023	transparent liquid	suspension in 0.9% sodium chloride
LJMUCV1401	Brand 3	10/07/2023	transparent liquid	suspension in 0.9% sodium chloride
LJMUCV1402	Brand 3	10/07/2023	transparent liquid	suspension in 0.9% sodium chloride
LJMUCV1403	Brand 3	10/07/2023	transparent liquid	suspension in 0.9% sodium chloride
LJMUCV1404	Brand 3	10/07/2023	transparent liquid	suspension in 0.9% sodium chloride
LJMUCV1405	Brand 3	10/07/2023	transparent liquid	suspension in 0.9% sodium chloride

LJMUCV1406	Brand 3	10/07/2023	transparent liquid	suspension in 0.9% sodium chloride
LJMUCV1407	Brand 3	10/07/2023	transparent liquid	suspension in 0.9% sodium chloride
LJMUCV1408	Brand 3	10/07/2023	transparent liquid	suspension in 0.9% sodium chloride
LJMUCV1409	Brand 3	10/07/2023	transparent liquid	suspension in 0.9% sodium chloride
LJMUCV1410	Brand 3	10/07/2023	transparent liquid	suspension in 0.9% sodium chloride
LJMUCV1411	Brand 3	10/07/2023	transparent liquid	suspension in 0.9% sodium chloride
LJMUCV1412	Brand 3	10/07/2023	transparent liquid	suspension in 0.9% sodium chloride

LJMUCV1413	Brand 3	10/07/2023	transparent liquid	suspension in 0.9% sodium chloride
LJMUCV1414	Brand 3	10/07/2023	transparent liquid	suspension in 0.9% sodium chloride
LJMUCV1415	Brand 3	10/07/2023	transparent liquid	suspension in 0.9% sodium chloride
LJMUCV1416	Brand 3	10/07/2023	transparent liquid	suspension in 0.9% sodium chloride
LJMUCV1417	Brand 3	10/07/2023	transparent liquid	suspension in 0.9% sodium chloride
LJMUCV1418	Brand 3	10/07/2023	transparent liquid	suspension in 0.9% sodium chloride
LJMUCV1419	Brand 3	10/07/2023	transparent liquid	suspension in 0.9% sodium chloride

LJMUCV1420	Brand 3	10/07/2023	transparent liquid	suspension in 0.9% sodium chloride
LJMUCV1421	Brand 3	10/07/2023	transparent liquid	suspension in 0.9% sodium chloride
LJMUCV1422	Brand 4	10/30/2022	white liquid	
LJMUCV1423	Brand 4	10/30/2022	white liquid	
LJMUCV1424	Brand 4	10/30/2022	white liquid	
LJMUCV1425	Brand 4	10/30/2022	white liquid	
LJMUCV1426	Brand 4	10/30/2022	white liquid	
LJMUCV1427	Brand 4	10/30/2022	white liquid	
LJMUCV1428	Brand 4	10/30/2022	white liquid	

Appendix II. Risk Assessment



James Parsons PBS

COSHH Risk Assessment Form

Title of Protocol/Procedure: Conventional and surface enhanced handheld spectroscopic methods for medicines and vaccines

Name of Faculty: Science		Name of School/Dept. School of Pharmacy and Biomolecular Science	
Date of assessment: 03/10/2022		Site/Location/Room No. James Parsons 8.11, 6.41, 4.03, 4.06, 4.07 and 3.33	
Name of person(s) carrying out procedure: Megan Watson	Signature of person(s) carrying out procedure: 	Tel No: 07885830063 E-mail: M.Watson@2019.ljmu.ac.uk	
Name of supervisor: Sulaf Assi	Signature 	Tel No. 0151 231 6144 E-mail S.Assi@ljmu.ac.uk	
Persons at Risk (Staff/Students/Others?) Any visitors or contractors must be informed of risks if access required.		Total number of people in lab Variable but up to 10 people depending on researchers and laboratory location	
Is Health Surveillance Required? No		Duration of Exposure: mins/hrs	
Health Surveillance is required if the procedure involves substances which are respiratory sensitisers or skin sensitisers. If other substances with potential health effects are used and if		Maximum 8 hours a day	
		Are there any Ethical Issues? (Attach Consents)	

<p>any health effects are observed that is believed to have resulted from its use then Occupational Health should be contacted. Consideration should be made of the existing health status of the user of hazardous substances. Are special arrangements required? E.g. for types of PPE.</p>	None
<p>Emergency Contact Names: Joanna Watson Low risk activity, General Security services in case of emergency as per laboratory guidelines</p>	<p>07894078489 Tel No Ext 2222 as per normal laboratory guidelines</p>
<p>Description of Experimental Methods and Procedures:</p> <p><u>Development of conventional and surface enhanced handheld spectroscopic methods for the authentication of anti-infective medicines and vaccines</u></p> <p>The aim of the experiment will be to utilise handheld conventional and enhanced spectroscopic techniques (including FTIR, NIR and Raman) for identification of counterfeit anti-infective medicines and vaccines. The specific precautions for handling raw materials and avoiding accidents are listed in the tables below.</p> <ol style="list-style-type: none"> 1. The experiments will be done in laboratory 8.11, 4.03, 4.06, 4.07 and 3.33 which are secure. 2. All chemicals and samples will be labelled clearly. 3. The details of each sample provided on the label claim will be logged in an Excel sheet that is stored on LJMU onedrive and not accessed outside the project researchers. 4. When not measured chemicals will be stored in cupboards. 5. Masks, safety glasses and double gloves will be worn during analysis. 6. IR and Raman spectra will be collected non-destructively or through glass vials. 7. Three to five spectra will be taken from each sample depending on the signal to noise ratio 8. Though the techniques are non-destructive, any waste of material will be disposed as per the SDS sheets provided by the manufacturer e.g. Sigma Aldrich. 9. Spectral data will be stored securely on LJMU one drive and only accessed to researcher partners at LJMU, PerkinElmer and Agilent. <p>Spectroscopic collection procedure involves:</p> <ol style="list-style-type: none"> 1. Taking a background measurement 2. Positioning the vial (in case of solids). 3. Taking spectra 4. Repositioning the vial 5. Spectra will be backed up on a USB memory device daily to prevent data loss as spc, jcampdx or csv. <p>In the case of IR Spectroscopy, samples will be transferred from the vial to the crystal plate using either a spatula (solids) or syringe (liquids).</p>	
<p>Description of Waste Disposal Methods: In accordance with Faculty Research Laboratory Guideline Booklet and SOPs for lab No.s JP206, JP208, JP209/211, JP414 HPLC lab</p>	

General Waste disposal procedure:

Emergency Action Procedures (spillages/ leaks, first aid, fire & explosion,)

No expected actions required as a result of the experiment.

Evacuate lab in the event of fire or similar emergency.

If there is a fire use appropriate extinguisher as detailed in COSHH forms – no specific fire extinguisher is required

Turn off electrical equipment at the switch or push the Laboratory Emergency Off Button if necessary.

Spill: Be aware of spillage procedures detailed in the COSHH section and add any specific information here.

General procedure for minor spillage: Absorb with an inert dry material such as blue roll or chemical absorbents in spillage kits or dilute with water if appropriate and mop up, then place in an appropriate waste disposal container consistent with the hazardous nature of the chemical that has been cleaned (if unsure check COSHH before cleaning). If substance is flammable keep away from sources of ignition.

For spillage of vaccine in solutions, it will be collected in sponge and disposed in the clinical/biological waste bin.

Refer to Faculty Chemical Spillage Procedure for further details.

Does the experiment run overnight or at weekends unattended? Has the appropriate form been completed? (see SCP 22)

No . Spectroscopy is rapid and each spectrum collection should take 1-2 min.

Training/Direct Supervision Requirements

NA. All researchers are well experienced in spectroscopic analysis.

Any additional training/supervision will be provided by Dr Sulaf Assi as necessary.

Business Interruption (e.g. power shutdown, fire, flood) What are the Contingency Procedures for work and waste?

No expected contingency plans required for the experiment.

In case of any interruption: Evacuation; return when safe to do so as instructed by local health and safety/fire evacuation staff.

In case of fire or explosion: Raise alarm, immediately evacuate area, call security on ext 2222 (0151 231 2222 from an external line) and inform them of the location and source of the fire, they will contact Merseyside Fire and Rescue Service. Inform fire warden on site of the location and source of the fire.

Contingency for waste: Assess effect of interruption/shutdown on the experiment and products and dispose of any spoiled starting materials, synthesised products and hazardous intermediate products that may have been formed and need disposal, following COSHH guidance.

Risk Evaluation Comments

Hazards/Risks Identified:

- The uses of chemical which are hazardous in case of ingestion, inhalation, skin
- Handling of flammable, combustible, skin and eye irritating and other potentially dangerous chemicals.
- Handling of biologic pharmaceuticals (anti-infectives, anti-malarials, vaccines etc.)
- **COVID-19:** Other individuals in the lab, labware and equipment which may have been handled by others

What procedures are in place to minimise risks:

All researchers will wear lab safety spectacles, fastened lab coat, gloves following COSHH and try to be as careful as possible.

- Ensuring essential training procedures are completed and researchers are competent in the procedures and familiar with all SOPs listed above.
- Using the flammable and organic solvents under hood, ensure everything is appropriately labelled, including cautions and warning signs for hazardous materials.
- Applying all health and safety instructions and follow good lab practice and Faculty Laboratory Guidelines Booklet
- Using personal protective equipment (e.g. clothing, footwear, goggles etc.)
- Follow all precautions when working with glassware and do not use any broken or damaged vessels.

To minimise risks to other lab users, samples will be prepared in the fume hood in 406. Continued adherence to rules of good laboratory practice.

COVID-19:

1. Keeping the activity time involved as short as possible
2. Using screens or barriers to separate people from each other
3. Using back-to-back or side-to-side working (rather than face-to-face) whenever possible
4. Reducing the number of people each person has contact with by using 'fixed teams or partnering' (so each person works with only a few others)
5. Increasing the frequency of hand washing and surface cleaning.
6. Staggering arrival and departure times at work to reduce crowding into and out of the workplace, taking account of the impact on those with protected characteristics.
7. Wear gloves when working in the lab and wipe down commonly used equipment with 70% ethanol

Summary: The risk associated with the experimental part of the present form has been identified as Low.

Low risk: No additional controls are required.

COVID-19: Review the UK government guidelines regarding working safely in labs during COVID-19. (<https://www.gov.uk/guidance/working-safely-during-coronavirus-covid-19/labs-and-research-facilities>).

COSHH MATERIAL SAFETY DATA

TECHNIQUE/METHOD TITLE:

Hazardous Substance and equipment	Hazard Type	State e.g. solid, liquid, gas	Quantity used	Route of entry & Target Organs	WEL	Controls and Precautions	Disposal Route Spillage procedure Emergency procedures
ALC-0315 (CAS: 2036272-55-4)	Irritant	Liquid	1 g	Skin corrosion/ Irritation, Serious eye damage/eye irritation	n/a	<ul style="list-style-type: none"> • Skin Contact: Immediately wash skin with soap and plenty of water for at least 20 minutes. Remove contaminated clothing. Get medical attention if symptoms occur. Wash clothing before reuse - Use of gloves • Eye Contact: Hold eyelids apart and flush eyes with plenty of water for at least 20 minutes. Have eyes examined and tested by medical personnel – Use of safety glasses • Immediately relocate self or casualty to fresh air. If breathing is difficult, give cardiopulmonary resuscitation (CPR). Avoid mouth-to-mouth resuscitation– Use of N95 or P1 dust masks if desired • If swallowed: Wash out mouth with water provided person is conscious. Never give anything by mouth to an unconscious person. Get medical attention. Do NOT induce vomiting unless directed to do so by medical personnel. 	<p>Keep container tightly sealed in cool, well-ventilated area. Keep away from direct sunlight and sources of ignition.</p> <p>Must be disposed of an incinerator.</p> <p>Extinguishing with use of water spray, alcohol-resistant foam, dry chemical or carbon dioxide.</p>

Hazardous Substance and equipment	Hazard Type	State e.g. solid, liquid, gas	Quantity used	Route of entry & Target Organs	WEL	Controls and Precautions	Disposal Route Spillage procedure Emergency procedures
ALC-0159 (CAS: 1849616-42-7)	Not a hazardous substance	Solid	1 g	Eye irritation, skin irritation, respiratory and digestive tract irritation	n/a	<ul style="list-style-type: none"> • Skin Contact: Immediately wash with water and soap and rinse thoroughly - Use of gloves • Eye Contact: Rinse opened eye for several minutes under running water. If symptoms persist, consult a doctor – Use of safety glasses • If inhaled: Supply fresh air; consult a doctor in case of complaint • If swallowed: Seek immediate medical advice 	<p>Keep container tightly sealed in cool, well-ventilated area. Keep away from direct sunlight and sources of ignition. Should be stored at -20 °C as powder and -80°C when in solution.</p> <p>Must be disposed of an incinerator.</p> <p>Extinguishing with use of carbon dioxide, sand or extinguishing powder; do not use water</p>
DSPC (CAS: 816-94-4)	Not a hazardous substance	Solid	1 g	Eye irritation, skin irritation, respiratory and digestive tract irritation	n/a	<ul style="list-style-type: none"> • Skin Contact: Wash off with soap and plenty of water - Use of gloves • Eye Contact: Flush eyes with water as a precaution – Use of safety glasses • If inhaled: If breathed in, move person into fresh air. If not breathing, give artificial respiration – Use of N95 of P1 dust masks if desired • If swallowed: Never give anything by mouth to an unconscious person. Rinse mouth with water • 	<p>Store in cool place. Keep container tightly closed in a dry and well-ventilated place.</p> <p>Allocated solid waste disposal. Do not let product enter drains.</p> <p>Extinguishing with use of water spray, alcohol-resistant foam, dry chemical or carbon dioxide.</p>
Cholesterol	Not a hazardous substance	Solid	1g	Eye irritation, skin irritation, respiratory and digestive tract irritation	n/a	<ul style="list-style-type: none"> • Skin Contact: Immediately wash with water and soap and rinse thoroughly - Use of gloves • Eye Contact: Rinse opened eye for several minutes under running water. If symptoms persist, consult a doctor – Use of safety glasses • If inhaled: Supply fresh air; consult a doctor in case of complaint • If swallowed: Seek immediate medical advice 	<p>Store the product in its original packaging sealed tightly, protected from light and moisture.</p> <p>Allocated solid waste disposal. Do not let product enter drains.</p> <p>Extinguishing with use of carbon dioxide, sand or extinguishing powder; do not use water</p>

Hazardous Substance and equipment	Hazard Type	State e.g. solid, liquid, gas	Quantity used	Route of entry & Target Organs	WEL	Controls and Precautions	Disposal Route Spillage procedure Emergency procedures
SM-102 (CAS: 2089251-47-6)	Irritant	Solid	1g	Eye irritation, skin irritation, respiratory and digestive tract irritation	n/a	<ul style="list-style-type: none"> • Skin Contact: Immediately wash with water and soap and rinse thoroughly. Consult a physician - Use of gloves • Eye Contact: Rinse opened eye for at least 15 minutes under running water and consult a physician – Use of safety glasses • If inhaled: Immediately relocate self or casualty to fresh air. If breathing is difficult, give cardiopulmonary resuscitation (CPR). Avoid mouth-to-mouth resuscitation – Use Mask • If swallowed: Wash out mouth with water; Do NOT induce vomiting; call a physician. 	<p>Store the product in its original packaging sealed tightly, in a dry, cool and well-ventilated place. Store at -20°C as solid or -80°C if in solution.</p> <p>Allocated solid waste disposal. Do not let product enter drains.</p> <p>Extinguishing with use of water spray, alcohol-resistant foam, dry chemical or carbon dioxide.</p>
PEG-2000DMG (CAS: 160743-62-4)	Not a hazardous substance	Solid	1g	Eye irritation, skin irritation, respiratory and digestive tract irritation	n/a	<ul style="list-style-type: none"> • Skin Contact: Immediately wash with water for at least 15 minutes. Get medical attention if symptoms occur • Eye Contact: Rinse opened eye for at least 15 minutes under running water. Get medical attention – Use of safety glasses • If inhaled: Supply fresh air; consult a doctor in case of complaint • If swallowed: Clean mouth with water and drink afterwards plenty of water. Get medical attention if symptoms occur. 	<p>Store the product in its original packaging sealed tightly, in a dry, cool and well-ventilated place.</p> <p>Allocated solid waste disposal. Do not let product enter drains.</p> <p>Extinguishing with use of water spray, alcohol-resistant foam, dry chemical or carbon dioxide.</p>

Hazardous Substance and equipment	Hazard Type	State e.g. solid, liquid, gas	Quantity used	Route of entry & Target Organs	WEL	Controls and Precautions	Disposal Route Spillage procedure Emergency procedures
2-Hydroxypropyl-β-cyclodextrin (CAS: 128446-35-5)	Not a hazardous substance or mixture. Not classified in accordance with international standards for workplace safety.	Solid	1g	Eyes, ingestion, inhalation		<ul style="list-style-type: none"> • Skin Contact: Immediately wash with water for at least 15 minutes. Get medical attention if symptoms occur – Use of gloves • Eye Contact: Rinse opened eye for at least 15 minutes under running water. Get medical attention – Use of safety glasses • If inhaled: Supply fresh air; consult a doctor in case of complaint <p>If swallowed: Clean mouth with water and drink afterwards plenty of water. Get medical attention if symptoms occur.</p> <p>Storage: Tightly closed container in a dry environment.</p>	<p>Allocated solid waste disposal. Do not let product enter drains.</p> <p>Extinguishing with use of carbon dioxide, sand or extinguishing powder; do not use water</p>
2-phenoxyethanol (CAS: 122-99-6)	Harmful if swallowed, Causes serious eye irritation	Liquid	100 mL	Eyes, skin, inhalation, ingestion		<ul style="list-style-type: none"> • Skin Contact: Immediately wash with water for at least 15 minutes. Get medical attention – Use of gloves • Eye Contact: Rinse opened eye for at least 15 minutes under running water. Get medical attention – Use of safety glasses • If inhaled: Immediately relocate self or casualty to fresh air. Avoid mouth-to-mouth resuscitation <p>If swallowed: Clean mouth with water and drink afterwards plenty of water. Get medical attention if symptoms occur.</p>	<p>Keep container tightly sealed in cool, well-ventilated area. Keep away from direct sunlight and sources of ignition.</p> <p>Must be disposed of an incinerator.</p> <p>Extinguishing with use of water spray, alcohol-resistant foam, dry chemical or carbon dioxide.</p>

Hazardous Substance and equipment	Hazard Type	State e.g. solid, liquid, gas	Quantity used	Route of entry & Target Organs	WEL	Controls and Precautions	Disposal Route Spillage procedure Emergency procedures
Acetic acid (CAS: 64-19-7)	Flammable liquid and vapour, causes severe skin burns and eye damage	Liquid	100 mL	Ingestion, Eyes, Inhalation, Skin		<ul style="list-style-type: none"> • Skin Contact: Take off immediately all contaminated clothing. Rinse skin with water or shower – Wear Gloves • Eye Contact: Rinse cautiously with water for several minutes. Remove contact lenses, if present and easy to do. Continue rinsing –Wear Safety Goggles • If swallowed: Rinse mouth. Do NOT induce vomiting • If inhaled: Immediately relocate self or casualty to fresh air. Avoid mouth-to-mouth resuscitation – use in fume hood 	<p>Keep container tightly sealed in cool, well-ventilated area. Keep away from direct sunlight and sources of ignition.</p> <p>Must be disposed of an incinerator.</p> <p>Extinguishing with use of water spray, alcohol-resistant foam, dry chemical or carbon dioxide.</p>
Aluminium Hydroxide (CAS: 21645-51-2)	Not classified for physical or health hazards, Combustible dust	Solid	1 g	N/A		<ul style="list-style-type: none"> • Skin Contact: Take off immediately all contaminated clothing. Rinse skin with water or shower – Wear Gloves • Eye Contact: Rinse cautiously with water for several minutes. Remove contact lenses, if present and easy to do. Continue rinsing –Wear Safety Goggles • If swallowed: Rinse mouth. Do NOT induce vomiting • If inhaled: Immediately relocate self or casualty to fresh air. <p>Storage: Tightly closed container in a dry environment.</p>	<p>Allocated solid waste disposal. Do not let product enter drains.</p> <p>Extinguishing with use of carbon dioxide, sand or extinguishing powder; do not use water</p>

Hazardous Substance and equipment	Hazard Type	State e.g. solid, liquid, gas	Quantity used	Route of entry & Target Organs	WEL	Controls and Precautions	Disposal Route Spillage procedure Emergency procedures
Citric acid monohydrate (CAS: 5949-29-1)	Causes serious eye irritation	Solid	1g	Eyes		<ul style="list-style-type: none"> • Skin Contact: Take off immediately all contaminated clothing. Rinse skin with water or shower – Wear Gloves • Eye Contact: Rinse cautiously with water for several minutes. Remove contact lenses, if present and easy to do. Continue rinsing –Wear Safety Goggles • If swallowed: Rinse mouth. Do NOT induce vomiting • If inhaled: Immediately relocate self or casualty to fresh air. Give artificial respiration if not breathing and seek medical attention. <p>Storage: Tightly closed container in a dry environment</p>	<p>Must be disposed of an incinerator.</p> <p>Extinguishing with use of water spray, alcohol-resistant foam, dry chemical or carbon dioxide.</p>
Disodium edetate dihydrate (CAS: 6381-92-6)	Harmful if inhaled, may cause damage to respiratory tract through prolonged exposure, harmful to aquatic life	Solid	1g	Respiratory tract		<ul style="list-style-type: none"> • Skin Contact: Take off immediately all contaminated clothing. Rinse skin with water or shower – Wear Gloves • Eye Contact: Rinse cautiously with water for several minutes. Remove contact lenses, if present and easy to do. Continue rinsing –Wear Safety Goggles • If swallowed: Rinse mouth. Do NOT induce vomiting • If inhaled: Immediately relocate self or casualty to fresh air. Give artificial respiration (if necessary also oxygen) if not breathing and seek medical attention. <p>Storage: Tightly closed container in a dry environment</p>	<p>Must be disposed of an incinerator.</p> <p>Extinguishing with use of water spray, alcohol-resistant foam, dry chemical or carbon dioxide.</p>

Hazardous Substance and equipment	Hazard Type	State e.g. solid, liquid, gas	Quantity used	Route of entry & Target Organs	WEL	Controls and Precautions	Disposal Route Spillage procedure Emergency procedures
L-histidine (CAS: 71-00-1)	Not classified for physical or health hazards	Solid	1g	N/A		<ul style="list-style-type: none"> • Skin Contact: Take off immediately all contaminated clothing. Rinse skin with water or shower – Wear Gloves • Eye Contact: Rinse cautiously with water for several minutes. Remove contact lenses, if present and easy to do. Continue rinsing –Wear Safety Goggles • If swallowed: Rinse mouth. Do NOT induce vomiting – consult a doctor if feeling unwell • If inhaled: Immediately relocate self or casualty to fresh air. <p>Storage: Tightly closed container in a dry environment.</p>	<p>Allocated solid waste disposal. Do not let product enter drains.</p> <p>Extinguishing with use of carbon dioxide, sand or extinguishing powder; do not use water</p>
L-histidine HCl monohydrate (CAS: 5934-19-2)	Causes serious eye irritation	Solid	1g	Eyes		<ul style="list-style-type: none"> • Skin Contact: Take off immediately all contaminated clothing. Rinse skin with water or shower – Wear Gloves • Eye Contact: Rinse cautiously with water for several minutes. Remove contact lenses, if present and easy to do. Call ophthalmologist. Continue rinsing –Wear Safety Goggles • If swallowed: Rinse mouth. Do NOT induce vomiting – consult a doctor if feeling unwell • If inhaled: Immediately relocate self or casualty to fresh air. <p>Storage: Tightly closed container in a dry environment.</p>	<p>Allocated solid waste disposal. Do not let product enter drains.</p> <p>Extinguishing with use of carbon dioxide, sand or extinguishing powder; do not use water</p>

Hazardous Substance and equipment	Hazard Type	State e.g. solid, liquid, gas	Quantity used	Route of entry & Target Organs	WEL	Controls and Precautions	Disposal Route Spillage procedure Emergency procedures
Magnesium chloride hexahydrate (CAS: 7791-18-6)	Not classified for physical or health hazards	Solid	1g	N/A		<ul style="list-style-type: none"> • Skin Contact: Take off immediately all contaminated clothing. Rinse skin with water or shower – Wear Gloves • Eye Contact: Rinse cautiously with water for several minutes. Remove contact lenses, if present and easy to do. Continue rinsing –Wear Safety Goggles • If swallowed: Rinse mouth. Do NOT induce vomiting – consult a doctor if feeling unwell • If inhaled: Immediately relocate self or casualty to fresh air. <p>Storage: Tightly closed container in a dry environment.</p>	<p>Allocated solid waste disposal. Do not let product enter drains.</p> <p>Extinguishing with use of carbon dioxide, sand or extinguishing powder; do not use water</p>
Polysorbate 80 (CAS: 9005-65-6)	Not classified for physical or health hazards	Solid	1g	N/A		<ul style="list-style-type: none"> • Skin Contact: Take off immediately all contaminated clothing. Rinse skin with water or shower – Wear Gloves • Eye Contact: Rinse cautiously with water for several minutes. Remove contact lenses, if present and easy to do. Continue rinsing –Wear Safety Goggles • If swallowed: Rinse mouth. Do NOT induce vomiting – consult a doctor if feeling unwell • If inhaled: Immediately relocate self or casualty to fresh air. <p>Storage: Tightly closed container in a dry environment.</p>	<p>Allocated solid waste disposal. Do not let product enter drains.</p> <p>Extinguishing with use of carbon dioxide, sand or extinguishing powder; do not use water</p>

Hazardous Substance and equipment	Hazard Type	State e.g. solid, liquid, gas	Quantity used	Route of entry & Target Organs	WEL	Controls and Precautions	Disposal Route Spillage procedure Emergency procedures
Sodium acetate trihydrate (CAS: 6131-90-4)	Not classified for physical or health hazards	Solid	1g	N/A		<ul style="list-style-type: none"> • Skin Contact: Take off immediately all contaminated clothing. Rinse skin with water or shower – Wear Gloves • Eye Contact: Rinse cautiously with water for several minutes. Remove contact lenses, if present and easy to do. Continue rinsing –Wear Safety Goggles • If swallowed: Rinse mouth. Do NOT induce vomiting – consult a doctor if feeling unwell • If inhaled: Immediately relocate self or casualty to fresh air. <p>Storage: Tightly closed container in a dry environment.</p>	<p>Allocated solid waste disposal. Do not let product enter drains.</p> <p>Extinguishing with use of carbon dioxide, sand or extinguishing powder; do not use water</p>
Sucrose (CAS: 57-50-1)	Not classified for physical or health hazards	Solid	1g	N/A		<ul style="list-style-type: none"> • Skin Contact: Take off immediately all contaminated clothing. Rinse skin with water or shower – Wear Gloves • Eye Contact: Rinse cautiously with water for several minutes. Remove contact lenses, if present and easy to do. Continue rinsing –Wear Safety Goggles • If swallowed: Rinse mouth. Do NOT induce vomiting – consult a doctor if feeling unwell • If inhaled: Immediately relocate self or casualty to fresh air. <p>Storage: Tightly closed container in a dry environment.</p>	<p>Allocated solid waste disposal. Do not let product enter drains.</p> <p>Extinguishing with use of carbon dioxide, sand or extinguishing powder; do not use water</p>

Hazardous Substance and equipment	Hazard Type	State e.g. solid, liquid, gas	Quantity used	Route of entry & Target Organs	WEL	Controls and Precautions	Disposal Route Spillage procedure Emergency procedures
Trisodium citrate dihydrate (CAS: 6132-04-3)	Not classified for physical or health hazards	Solid	1g	N/A		<ul style="list-style-type: none"> • Skin Contact: Take off immediately all contaminated clothing. Rinse skin with water or shower – Wear Gloves • Eye Contact: Rinse cautiously with water for several minutes. Remove contact lenses, if present and easy to do. Continue rinsing –Wear Safety Goggles • If swallowed: Rinse mouth. Do NOT induce vomiting – consult a doctor if feeling unwell • If inhaled: Immediately relocate self or casualty to fresh air. • Storage: Tightly closed container in a dry environment. 	<p>Allocated solid waste disposal. Do not let product enter drains.</p> <p>Extinguishing with use of carbon dioxide, sand or extinguishing powder; do not use water</p>
Water for Injection (CAS: 7732-18-5)	Not classified for physical or health hazards	Liquid	100 mL	N/A		<ul style="list-style-type: none"> • Skin Contact: Take off immediately all contaminated clothing. Rinse skin with water or shower – Wear Gloves • Eye Contact: Rinse cautiously with water for several minutes. Remove contact lenses, if present and easy to do. Continue rinsing –Wear Safety Goggles • If swallowed: Rinse mouth. Do NOT induce vomiting – consult a doctor if feeling unwell • If inhaled: Immediately relocate self or casualty to fresh air. • Storage: Tightly closed container in a dry environment. 	<p>Must be disposed of an incinerator.</p> <p>Use extinguishing measures that are appropriate to local circumstances and the surrounding environment.</p>

Hazardous Substance and equipment	Hazard Type	State e.g. solid, liquid, gas	Quantity used	Route of entry & Target Organs	WEL	Controls and Precautions	Disposal Route Spillage procedure Emergency procedures
Enalapril Maleate	H361 - Suspected of damaging fertility or the unborn child Reproductive toxicity Category 2 Warning	Solid	50 mgs	N/A		<ul style="list-style-type: none"> • P261 Avoid breathing dust/fume/gas/mist/vapours/spray. • P280 Wear protective gloves/protective clothing/eye protection/face protection. • P305+P351+P338 IF IN EYES: Rinse cautiously with water for several minutes. Remove contact lenses, if present and easy to do. Continue rinsing. • P321 Specific treatment (see on this label). • P405 Store locked up. • P501 Dispose of contents/container in accordance with local/regional/national/international regulations. 	<ul style="list-style-type: none"> • Waste treatment methods • Recommendation Must not be disposed of together with household garbage. Do not allow product to reach sewage system. • European waste catalogue Waste disposal key numbers from EWC have to be assigned depending on origin and processing. • Uncleaned packaging: • Recommendation: Dispose of in accordance with national regulations. • Recommended cleansing agents: Water, if necessary together with cleansing agents.
Stearic acid	No warning	Solid	500 mg	N/A		<ul style="list-style-type: none"> • Substance is not considered persistent, bioaccumulative and toxic (PBT) / very persistent and very bioaccumulative (vPvB) 	<p>Waste from Residues/Unused Products</p> <p>Chemical waste generators must determine whether a discarded chemical is classified as a hazardous waste. Consult local, regional, and national hazardous waste regulations to ensure complete and accurate classification. Contaminated Packaging Empty remaining contents. Dispose of in accordance with local regulations. Do not re-use empty containers. European Waste Catalogue (EWC) According to the European Waste Catalog, Waste Codes are not product specific, but application specific. Other Information Waste codes</p>

Hazardous Substance and equipment	Hazard Type	State e.g. solid, liquid, gas	Quantity used	Route of entry & Target Organs	WEL	Controls and Precautions	Disposal Route Spillage procedure Emergency procedures
Brand 1 Vaccine	Not a hazardous substance or mixture The product does not meet the definition of a hazardous chemical. Based on the replication deficient nature of the adenovirus vector, there is no risk of pathogenicity and virulence in case of an incidental occupational exposure.	Liquid/reconstituted	0-2ml per vial	All routes		<ul style="list-style-type: none"> • If inhaled: Remove patient from exposure, keep warm and at rest. Obtain medical attention if ill effects occur. • In case of skin contact: Wash skin with soap and water for at least 15 minutes. Seek medical attention for cuts, abrasions, punctures or material contact with broken skin. • In case of eye contact: Irrigate with eyewash solution or clean water, holding the eyelids apart, for at least 15 minutes. Obtain medical attention if ill effects remain. • If swallowed: Wash out mouth with water and give 200-300ml of water to drink. Do NOT induce vomiting as a First-Aid measure. Obtain medical attention if ill effects occur. <p>Storage: Long term storage of the bulk vaccine vector solutions should be stored frozen at ≤ -65 °C. Short-term use, bulk vaccine vector solution may be thawed and refrigerated at 2 - 8 °C.</p> <p>Handle at Biosafety Level 1 (BSL1). Where there may be a risk of aerosol generation a Biosafety Level 2 (BSL2) is recommended. Prevent entry into drains unless inactivated or denatured.</p>	Dispose of liquid and any material used to absorb liquid in yellow hazardous waste container

Brand 2 Vaccine	Not a hazardous substance or mixture. Not classified in accordance with international standards for workplace safety.	Liquid	0-2ml per vial	All routes		<ul style="list-style-type: none"> • If inhaled: Remove patient from exposure, keep warm and at rest. Obtain medical attention if ill effects occur. • In case of skin contact: Wash skin with soap and water for at least 15 minutes. Seek medical attention for cuts, abrasions, punctures or material contact with broken skin. • In case of eye contact: Irrigate with eyewash solution or clean water, holding the eyelids apart, for at least 15 minutes. Obtain medical attention if ill effects remain. • If swallowed: Wash out mouth with water and give 200-300ml of water to drink. Do NOT induce vomiting as a First-Aid measure. Obtain medical attention if ill effects occur. <p>Storage: Store at < -70 °C in properly labelled containers.</p> <p>Handling: Restrict access to work area. No open handling permitted. Minimize generating airborne mists and vapors. If solvent based liquid, consideration. A change area to facilitate 'good laboratory/manufacturing' decontamination practices is recommended. Avoid inhalation and contact with skin, eye, and clothing. When handling, use appropriate personal protective equipment. Wash hands and any exposed skin after removal of PPE.</p> <ul style="list-style-type: none"> • ground and bond all bulk transfer equipment. 	Dispose of liquid and any material used to absorb liquid in yellow hazardous waste container
Hydroxylamine Hydrochloride (CAS: 5470-11-1)	Corrosive, irritant, toxic to aquatic life	Solid	1g			Wear protective gloves/ protective clothing/ eye protection/ face protection/ hearing protection.	Avoid inhalation of dusts. Avoid substance contact.

Hazardous Substance and equipment	Hazard Type	State e.g. solid, liquid, gas	Quantity used	Route of entry & Target Organs	WEL	Controls and Precautions	Disposal Route Spillage procedure Emergency procedures
						<p>IF SWALLOWED: Call a POISON CENTER/ doctor if you feel unwell.</p> <p>IF ON SKIN: Wash with plenty of water. Call a Poison Centre/doctor if you feel unwell.</p> <p>If in eyes: Rinse cautiously with water for several minutes.</p> <p>Remove contact lenses, if present and easy to do. Continue rinsing.</p> <p>If exposed or concerned: Get medical advice/ attention.</p>	<p>Ensure adequate ventilation. Evacuate the danger area, observe emergency procedures, consult an expert.</p> <p>Do not let product enter drains. Cover drains. Collect, bind, and pump off spills. Take up dry. Dispose of properly. Clean up affected area. Avoid generation of dusts.</p> <p>Waste material must be disposed of in accordance with the national and local regulations. Leave chemicals in original containers. No mixing with other waste. Handle uncleaned containers like the product itself.</p>
Silver Nitrate (CAS: 7761-88-8)	Corrosive to metals, skin, eyes, aquatic hazard	Solid	1g			<p>Keep away from heat, hot surfaces, sparks, open flames and other ignition sources. No smoking.</p> <p>Wear protective gloves/ protective clothing/ eye protection/ face protection/ hearing protection.</p> <p>IF ON SKIN (or hair): Take off immediately all contaminated clothing. Rinse skin with water.</p> <p>IF IN EYES: Rinse cautiously with water for several minutes. Remove contact lenses, if present and easy to do. Continue rinsing.</p>	<p>Avoid inhalation of dusts. Avoid substance contact.</p> <p>Ensure adequate ventilation. Evacuate the danger area, observe emergency procedures, consult an expert.</p> <p>Do not let product enter drains. Cover drains. Collect, bind, and pump off spills. Take up dry. Dispose of properly. Clean up affected area. Avoid generation of dusts.</p>

Hazardous Substance and equipment	Hazard Type	State e.g. solid, liquid, gas	Quantity used	Route of entry & Target Organs	WEL	Controls and Precautions	Disposal Route Spillage procedure Emergency procedures
Potassium Bromide (CAS: 7758-02-3)	No physical hazards classified, causes serious eye irritation, Toxicity to Soil Dwelling Organisms Toxic to terrestrial vertebrates	solid	500mg	Oral, dermal, inhalation		Use personal protective equipment as required. Ensure adequate ventilation. Avoid dust formation. Eye Contact: Rinse immediately with plenty of water, also under the eyelids, for at least 15 minutes. Get medical attention. Skin Contact: Wash off immediately with plenty of water for at least 15 minutes. Get medical attention. Ingestion: Clean mouth with water and drink afterwards plenty of water. Get medical attention if symptoms occur. Inhalation: Remove to fresh air. If breathing is difficult, give oxygen. Get medical attention.	Should not be released into the environment. Do not flush into surface water or sanitary sewer system. Sweep up and shovel into suitable containers for disposal. Keep in suitable, closed containers for disposal.
Nitric acid (CAS: 7697-37-2)	Oxidizing liquids, Corrosive to Metals, Acute toxicity, Inhalation, Skin corrosion, Serious eye damage	liquid	20ml	Oral, dermal, inhalation, eyes. Material is extremely destructive to tissue of the mucous membranes and upper respiratory tract, eyes, and skin.		Keep away from heat, hot surfaces, sparks, open flames and other ignition sources. No smoking. Keep away from clothing and other combustible materials. Wear protective gloves/ protective clothing/ eye protection/ face protection. IF ON SKIN (or hair): Take off immediately all contaminated clothing. Rinse skin with water. IF INHALED: Remove person to fresh air and keep comfortable for breathing. Immediately call a POISON CENTER/ doctor. IF IN EYES: Rinse cautiously with water for several minutes. Remove contact lenses, if present and easy to do. Continue rinsing.	Waste material must be disposed of in accordance with the national and local regulations. Leave chemicals in original containers. No mixing with other waste. Handle uncleaned containers like the product itself. Do not let product enter drains. Cover drains. Collect, bind, and pump off spills. Observe possible material restrictions. Take up carefully with liquid-absorbent material. Dispose of properly. Clean up affected area.

Hazardous Substance and equipment	Hazard Type	State e.g. solid, liquid, gas	Quantity used	Route of entry & Target Organs	WEL	Controls and Precautions	Disposal Route Spillage procedure Emergency procedures
Hydrochloric acid (CAS: 7647-01-0)	Corrosive to Metals, Skin corrosion, Serious eye damage, Specific target organ toxicity - single exposure, Respiratory system,	liquid	60ml	Oral, dermal, inhalation, eyes. Classified as specific target organ toxicant, single exposure, category 3 with respiratory tract irritation. Acute inhalation toxicity - mucosal irritations, Cough, Shortness of breath, Inhalation may lead to the formation of oedemas in the respiratory tract.		Wear protective gloves/ protective clothing/ eye protection/ face protection. IF ON SKIN (or hair): Take off immediately all contaminated clothing. Rinse skin with water. IF IN EYES: Rinse cautiously with water for several minutes. Remove contact lenses, if present and easy to do. Continue rinsing. If swallowed: After swallowing make victim drink water (two glasses at most), avoid vomiting (risk of perforation). Call a physician immediately. Do not attempt to neutralise.	Waste material must be disposed of in accordance with the national and local regulations. Leave chemicals in original containers. No mixing with other waste. Handle uncleaned containers like the product itself. Do not let product enter drains. Cover drains. Collect, bind, and pump off spills. Observe possible material restrictions. Take up carefully with liquid-absorbent material. Dispose of properly. Clean up affected area.

Hazardous Substance and equipment	Hazard Type	State e.g. solid, liquid, gas	Quantity used	Route of entry & Target Organs	WEL	Controls and Precautions	Disposal Route Spillage procedure Emergency procedures
Aqua Regia (CAS: NA to mixtures)	Acute toxicity – Gases, Oxidizing liquids, Serious eye damage, Skin corrosion / irritation, Specific target organ systemic toxicity (single exposure)	Liquid	<100ml	Oral, dermal, inhalation, eyes. Classified as specific target organ toxicant, single exposure, Category 3 with respiratory tract irritation. Inhalation of vapors can cause breathing difficulties and lead to pneumonia and pulmonary edema, which may be fatal. Other symptoms may include coughing, choking, and irritation of the nose, throat, and respiratory tract.		A system of local and / or general exhaust is recommended to keep exposures below the Airborne Exposure Limits. Store in a cool, dry, ventilated storage area with acid resistant floors and good drainage. Protect from physical damage. Keep out of direct sunlight and away from heat, water, and incompatible materials. Do not wash out container and use it for other purposes. When diluting, the acid should always be added slowly to water and in small amounts. Never use hot water and never add water to the acid. Water added to acid can cause uncontrolled boiling and splashing. Containers of this material may be hazardous when empty since they retain product residues (vapours, liquid.)	Waste material must be disposed of in accordance with the national and local regulations. Leave chemicals in original containers. No mixing with other waste. Handle uncleaned containers like the product itself. Do not let product enter drains. Personal Precautions, Protective Equipment and Emergency Procedures: Ventilate area of leak or spill. Wear appropriate personal protective equipment. Isolate hazard area. Keep unnecessary and unprotected personnel from entering. Environmental Precautions and Methods and Materials for Containment and Cleaning Up: Contain and recover liquid when possible. Do not let product enter drains. Neutralize with alkaline material (sodium bicarbonate) then absorb with an inert material (e. g., vermiculite, dry sand, earth,) and place in a chemical waste container. Do not use combustible materials, such as saw dust.

Hazardous Substance and equipment	Hazard Type	State e.g. solid, liquid, gas	Quantity used	Route of entry & Target Organs	WEL	Controls and Precautions	Disposal Route Spillage procedure Emergency procedures
PerkinElmer Spectrum Two w/ UATR	Not classified for physical or health hazards					<ul style="list-style-type: none"> Do not scratch the plate Do not look directly into the sources 	n/a
PerkinElmer Spectrum Two N w/ NIRM	Potential damage to eye if the person looked directly through the light.					<ul style="list-style-type: none"> Do not look in the source 	NA
Agilent Raman spectrometer	Potential damage to eye if the person looked directly through the light.					<ul style="list-style-type: none"> Do not look in the source Do not point the source to an individual Wear laser specs where required 	NA
Agilent portable infrared spectrometer	Not classified for physical or health hazards					<ul style="list-style-type: none"> Do not scratch the plate Do not look directly into the sources 	n/a
BW Tek handheld Raman Spectrometer	Potential damage to eye if the person looked directly through the light.					<ul style="list-style-type: none"> Do not look in the source 	NA
Metrohm MIRA XTR DS handheld Raman Spectrometer	Potential damage to eye if the person looked directly through the light.					<ul style="list-style-type: none"> Do not look in the source 	NA

COMMENTS: Attach any additional hazard data, consider any substance with an allocated WEL. Use EH40 Guidance HSE

Appendix III. Standard Operating Procedures

PerkinElmer Spectrum Two ATR-FTIR spectrometer

FTIR SOP

Daily memos:

- Record room temperature.
- Record room humidity.
- Do a performance validation test: PQ test or Performance Qualification and save it everyday. DO NOT start work without doing PQ test.
- If in doubt on any procedures read Bruker IR introduction.
- Back up data everyday.
- Always clean ATR-Diamond accessory before using it. Always assume is not clean.

Turn on computer:

- UserID: [REDACTED]
- Password [REDACTED]

Opus 7.5.18:

- Double click on Opus link on desktop
- **UserID:** Administrator
- **Password:** OPUS
- A box will appear with the software information: print screen when using it for the first time for future reference

FTIR spectra:

- X-axis: wavenumbers 6500 to 500
- Y-axis: absorbance
- FTIR is more specific to functional groups whereas NIR is more specific to overtones

Quick Opus screen guide:

- **Acquire:** button on the on the top left of the spectral screen. Used for acquiring spectral readings.
- **Orange numbers:** present on the top right of the spectral graph area. They are coordinate for the spectral area. It is an interactive screen, therefore as the cursor is moved around the area the coordinates change.
- **Opus browser:** column on the top right of screen. Shows the spectra being analysed.
- **Bottom middle:** shows what is happening in the software in real time.
- **Bottom right:** shows the following options: CAP, NUM, SCRL and red or green circle.

What to do if the bottom right circle is red:

- Double click on red circle, it opens and instrument status window.
- Anything that is highlighted in green is working.
- ATR-Diamond accessory is highlighted in red and labelled as failed
- First clean ATR-Diamond accessory with a methylated spirit and some tissue.
- Double click on the ATR-Diamond button which is highlighted in red
- Run a PQ test by clicking on Run Test
- Once test is done a window will open with the status of the PQ test. Save this document. At the end of the document it will be written in green writing if the procedure was successful or not.

What does the PQ test analyse:

- **Signal noise test:** verifies that the signal-to-noise ratio is better than specified limit which in this case has to be bigger than 125.
- **Line test:** verifies that the 100% line does not shift on long term. Maximum line deviation allowed is 2.0.
- **Wavenumber accuracy test:** verifies the absolute x-axis accuracy of the instrument. Tests the polystyrene in the instrument.

Tobacco sample preparation and weighing:

- Turn on scale and press tare (always press tare in-between readings).
- Make sure that the bubble in the spirit level/bubble level on the scale is centred.
- Weight an empty vile (W1) and record it.
- Weight the vial containing the entirety of the sample (W2) and record it. From this value obtained subtract the value obtained for the empty vial ($W2 - W1$), the resulting value will be the quantity of the whole sample.
- Extract the amount of sample needed for the FTIR analysis and place it in a mortar.
- Weigh the vial containing the sample again (W3). From the value obtained before W2 subtract W3 ($W2 - W3$). The resulting value will give you the amount of sample being used in the FTIR analysis.
- Crush the sample placed in the mortar until it becomes a fairly homogeneous powder.

How to perform a FTIR spectral reading:

- Make sure ATR-Diamond accessory is clean.
- Click on Acquire on the left hand side of the screen.
- Click on advanced test on the left hand side of the screen. A window will open up.
- Go to the advance tab:
 1. Change path to save the spectra to the wanted file by clicking on the three dots next to the path box and choosing the wanted destination file;
 2. Write the sample name in the appropriate box;
 3. Change sample scan time to 16 scans;
 4. Change background scan time to 16 scans;
 5. Save data from 4000 cm^{-1} to 400 cm^{-1} ;
 6. Set up resolution to 4 for powders or 2 for liquids;
 7. Save method if required.
- Go back to first tab. Make sure that the ATR-Diamond accessory is fully open (put pressure tower to the side).
- Click on the Background Single Channel button and wait until the background scan is done.
- Once this is done click on Run Spectra. The previously open window will close and the spectral graph area will appear again.
- Once peaks or lines start showing on the spectral graph are click on Run Measurement at the bottom of the page.
- The spectra name (sample name) will appear in the Opus Browser column.
- To save it click on the AB button just underneath the sample name.
- Go to File and chose Save as. A window will open up.
- Click on the mode tab. Choose the wanted modes to save the spectra. In this case it will be: data point table (.dpt), Opus (1.0) and JCAMP DX (.dx).

How to measure the S/N ratio:

- Print the screen with the spectra wanted. Do it once for every sample batch.
- Paste pressing ctrl+v into Word. Zoom the picture if wanted.
- Draw top and bottom lines on the noise part of spectra (noise power), measure distance between lines with a ruler (N).
- Draw a top and bottom line on highest peak (signal power), measure distance between lines with a ruler (S).
- Divide S by N and get the ratio between the two, which is unitless number.

Operating Procedure for Metrohm MIRA XTR DS handheld Raman spectrometer

Metrohm Mira XTR handheld Raman SOP

- Turn the button from the side of the instrument.
- Enter the password.
- A calibration screen will appear, and the software will ask whether calibrate the device or not and then place calibration standard.
- Click on Calibrate.
- The instrument will start calibration. Once it did, whether it was successful or not.
- If it passes, this will appear on the screen (System suitability test passed, wavenumber, intensity, performance, voltage)
- Click next then the display will show the current procedure in the instrument.
- If you want to change the procedure, click on change procedure; otherwise, click on arm Laser.
- Place the suitable measurement accessory.
- For vials, -> place the vial inside the holder
- For the tablets and the powders in a transparent bag, -> use the pointer.
- Click on arm laser followed by acquire.
- The screen will show the spectra. Please do not note the scan number on the left top of the screen.

- When the Raman measurement, Raman extraction will show. Then the result will be displayed on the screen with a mixture tab and percentage match against the substances in the library. The number displayed alongside the mixture is the spectrum number.
- To know the correlation coefficient value or the hit quality index (HQI), click on the identification tab and note the substance correlation coefficient on the lab notebook.
- To visualise the spectrum, click on the spectrum button on the lower right of the screen.
- To measure the next sample, click on the arrow on the bottom left of the screen and repeat the procedure described above.

Raman spectra

- X-axis-> wavenumber
- Y-axis-> Raman scatter